

Understanding Correlations between Secondary Relaxations and Thermal Behaviour of Biologically Relevant Molecules

BY

SAMUEL OWUSU-WARE [B.Sc. (Hons)]

A thesis submitted in partial fulfilment of the requirements of the University of Greenwich for the degree of Doctor of Philosophy

May, 2013

School of Science

University of Greenwich (Medway Campus)

Chatham Maritime, Kent ME4 4TB, UK



DECLARATION

“I certify that this work has not been accepted in substance for any degree, and is not concurrently being submitted for any degree other than that of Doctor of Philosophy being studied at the University of Greenwich. I also declare that this work is the result of my own investigations except where otherwise identified by references and that I have not plagiarised another’s work”.

Mr S. Owusu-Ware (Candidate)

.....

PhD Thesis Supervisors

Dr. M.D. Antonijevic (1st Supervisor)

Prof. B.Z. Chowdhry (2nd Supervisor)

May, 2013

ACKNOWLEDGEMENTS

My greatest thanks and appreciation, first and foremost, goes to my God for his mercies and divine intervention(s) throughout this postgraduate programme. It is my strong belief that the work completed in this thesis has not been by my will, power or own intellect, but by the spirit of my Lord and personal saviour Jesus Christ.

I cannot thank my partner (Samantha Happy) enough. Before embarking on this PhD programme, I did not understand the real meaning of the saying “Behind every successful man is a strong woman”. Samantha has been a rock that has supported me emotionally throughout this PhD. My mother and father have been a source of inspiration for my tireless hardworking attitude. They are both incredibly hard working people and have always encouraged me to be of the same character no matter what the circumstance. My younger brother (Kingsley Owusu-Ware) has also been a driving force for me in seeing this PhD through to completion. I hope I have demonstrated to him that with hard work and self-belief he can achieve whatever he sets his mind to.

The support I have received from staff members, particularly, Steve Williams, Link-lab technicians, Diviani and Ian slipper has been exceptional. They have been a great source of motivation and technical support. I am indebted to Dr Milan Antonijevic for his confidence in my scientific ability to pursue a PhD and for inspiring me throughout the journey, the University of Greenwich for sponsoring my research, but most importantly to Professor Babur Z. Chowdhry and Professor Stephen Leharne for their tireless support and belief in me that I can always do better.

I dedicate this PhD to my late uncle Kwami Adu, who was the first of all my relatives to have embarked on a post-graduate study but passed away before completing his studies. He was a hardworking and highly intellectual individual with an insatiable appetite for knowledge. He has and always will be my inspiration.

ABSTRACT

Understanding correlations between secondary relaxations and thermal behaviour of biologically relevant molecules

The research presented in this doctoral thesis examines the application of thermally stimulated depolarisation current (TSDC) spectroscopy as a probe of molecular mobility in the solid (powdered) state. TSDC spectroscopy has proved useful in understanding the molecular mobility of amorphous materials. However, few investigations have been undertaken in order to understand molecular mobility in crystalline and semi-crystalline solid-state (powder) materials and how mobility in such systems can be related to stability. Differential scanning calorimetry (DSC), including - where applicable - temperature modulated differential scanning calorimetry (TMDSC), and thermal gravimetric analyses (TGA) were employed to study the thermal behaviour/stability of the different molecular systems under scrutiny.

Experiments on crystalline butyric acids, γ -aminobutyric acid (GABA), DL- α -aminobutyric acid (AABA) and DL- β -aminobutyric acid (BABA), were undertaken in order to examine the influence of positional isomerism on molecular mobility and stability. These molecules differ in the position of the amine group relative to the carboxyl functionality. GABA, DL-BABA and DL-AABA were found to undergo localised non-cooperative rotational motions at $77 \pm 2^\circ\text{C}$ and $114 \pm 2^\circ\text{C}$, $104 \pm 1^\circ\text{C}$ and $109 \pm 1^\circ\text{C}$, respectively, prior to the higher temperature thermal events detected via DSC and TGA. The carbon chain length between the amino and the carboxyl moiety is found to be a key contributor to solid-state molecular mobility. Molecular relaxation frequency was found to correlate to thermal stability of the materials investigated i.e. the lower the relaxation frequency the greater the thermal stability.

The molecular mobility of a homologous series of semi-crystalline phosphatidylcholines: 1,2-dilauryl-*sn*-glycero-3-phosphocholine (DLPC), 1,2-dimyristoyl-*sn*-glycero-3-phosphocholine (DMPC), 1,2-dipalmitoyl-*sn*-glycero-3-phosphocholine (DPPC) and 1,2-distearoyl-*sn*-glycero-3-phosphocholine (DSPC) with acyl chain lengths of 12, 14, 16 and 18, respectively has been examined at temperatures below the chain melting transition temperature (T_m). The results show that increasing the acyl chain length increases the temperature at which molecular mobility is observed i.e. the temperature maxima (T_{max}) of the global relaxation processes occur at 41 ± 2 , 47 ± 2 , 57 ± 2 and 67 ± 3 °C for DLPC, DMPC, DPPC and DSPC, respectively. The molecular mobilities of the phosphatidylcholines are hypothesized to involve both inter- and intra-molecular co-operation and originate from the segmental motion of the diacyl backbone. The relaxation times (21 ± 2 , 19 ± 3 , 25 ± 1 and 32 ± 4 s for DLPC, DMPC, DPPC and DSPC, respectively) are shown to correlate with the apparent activation energy (E_a) and T_m values of the phosphatidylcholines.

Studies of lyophilized peptide/proteins namely insulin, lysozyme and myoglobin were investigated in the hydrated and dehydrated state in the temperature range -150 to 150 °C. This body of work attempts to understand if and how moisture and/or parameters associated with structure influence molecular mobility of lyophilized peptide/proteins. The results show that the presence of low levels of moisture content (<10%) facilitates molecular mobility at sub-zero temperatures; no mobility is observed in the sub-zero temperature regions after dehydration. The temperature locations of the relaxation processes in the proteins containing moisture are -95 ± 3 , -102 ± 3 and 111 ± 2 °C for insulin, lysozyme and myoglobin, respectively. Whilst the temperature location of the relaxation processes in the dehydrated protein samples are 96 ± 3 , 72 ± 4 and 82 ± 3 °C for insulin, lysozyme and myoglobin, respectively. It was found that the temperature order in which molecular mobility occurs correlates with the temperature order at which denaturation-decomposition processes occur for the three peptide/protein systems investigated.

The work presented herein demonstrates the capability of TSDC spectroscopy to detect and characterise low energy transitions (secondary relaxations) that are inaccessible by conventional DSC methods. In addition, the ability to relate molecular mobility to thermal stability of materials examined has been established.

SAMUEL OWUSU-WARE [B.Sc. (Hons)]

CONTENTS

DECLARATION	ii
ACKNOWLEDGEMENTS	iii
ABSTRACT	iv
CONTENTS	vii
LIST OF FIGURES	x
LIST OF TABLES	xiv
ABBREVIATIONS	xvi
LIST OF PUBLICATIONS/PRESENTATIONS	xix
Chapter 1 : Introduction	1
1.1. Solid Phases	1
1.1.1. Crystalline Solids	2
1.1.2. Amorphous Solids	3
1.2. Solid-State Reactivity	3
1.2.1. Chemical Reactivity	3
1.2.2. Physical Reactivity	4
1.2.2.1. Crystalline	4
1.2.2.2. Amorphous	6
1.3. Molecular Mobility	8
1.3.1. Primary and Secondary Relaxations: Amorphous Systems	9
1.3.2. Secondary Relaxations in Crystalline Solids	12
1.4. Solid-State Characterisation Methods	13
1.5. Thermally Stimulated Current (TSC) Spectroscopy	20
1.5.1. Dipoles and Polarisation Processes	22
1.5.2. Theoretical Background	24
1.6. Thermal Gravimetric Analysis (TGA)	27
1.7. Differential Scanning Calorimetry (DSC)	30
1.8. Aims of Project	34
Chapter 2 : Materials and Instrumentation	35
2.1. Materials	35
2.1.1. Aminobutyric Acids	35
2.1.2. Phosphatidylcholines	41
2.1.3. Proteins	45
2.2. Instrumentation	46
2.2.1. Thermogravimetric Analyser (TGA)	46

2.2.2	Differential scanning calorimetry (DSC)	47
2.2.3	Thermally Stimulated Current (TSC) spectroscopy.....	48
Chapter 3 : Influence of Positional Isomerism on Solid-state Molecular Mobility and Thermal Stability of Aminobutyric Acids		50
3.1	Introduction.....	50
3.2	Methods.....	51
3.2.1	TGA	51
3.2.2	DSC.....	52
3.2.3	TSDC	52
3.3	Results and Discussion	52
3.3.1	TGA and DSC.....	52
3.3.2	Global TSDC	57
3.3.3	Thermal Windowing.....	60
3.3.4	Compensation Analysis.....	66
3.4.	Conclusions.....	71
Chapter 4 : Influence of Carbon Chain Length on Solid-State Mobility and Thermal Stability of Phosphatidylcholines		73
4.1	Introduction.....	73
4.2	Methods.....	76
4.2.1	DSC.....	76
4.2.2	XRPD.....	77
4.2.3	TSDC	77
4.3	Results and Discussion	79
4.3.1	DSC.....	79
4.3.2	Global TSDC Results.....	91
4.3.3	Thermal Windowing Results	100
4.4	Conclusions.....	114
Chapter 5 : Influence of Molecular Size on Solid-State Mobility and Thermal Stability of a Peptide and Proteins.....		117
5.1	Introduction.....	117
5.2	Methods.....	120
5.2.1	TGA	120
5.2.2	DSC.....	120
5.2.3	TSDC	120
5.3	Results and Discussions	121
5.3.1	TGA and DSC.....	121

5.3.2	Hydrated States	125
5.3.3	Dehydrated Samples	140
5.3.4	Comparison of Hydrated and Dehydrated Samples	150
5.4	Conclusions.....	152
Chapter 6 : Summary and General Conclusions		154
Chapter 7 : Future Work		157
REFERENCES		159

LIST OF FIGURES

CHAPTER 1

- Fig. 1.1 The different sub-states of solids observed in pharmaceutical development..... 2
- Fig. 1.2 Gibbs free energy phase diagram as a function of temperature showing stability relationships between two crystalline forms I and II, (a) shows the monotropic relationship between the two forms and (b) shows enantiotropic relationships. T_m is the melting temperature, T_t is the point where the Gibbs free energies of the two forms are the same and L is the liquid phase (Zhang et al., 2004). 5
- Fig. 1.3 The relative differences in volume (V), enthalpy (H) and entropy (S) between crystalline and amorphous solids as function of temperature. T_K is the Kauzmann temperature, T_g is the glass transition temperature and T_m is the melting temperature (Chawla and Bansal, 2009). 7
- Fig. 1.4 Schematic of the response of molecules during a typical TSC spectroscopy experiment. 20
- Fig. 1.5 Typical TSC output obtained during TSDC experiments. 21
- Fig. 1. 6 Schematic of the response of molecules during a TW experiment. 22
- Fig. 1.7 Typical TGA output showing the thermal gravimetric or TG curve (navy plot) and the derivative thermal gravimetric or DTG curve (red plot) of chlorogenic acid hemihydrate. 28
- Fig. 1.8 A typical DSC output of the main thermal transitions of pharmaceutical interest during a heating scan. 32

CHAPTER 2

- Fig. 2.1 FTIR spectra obtained for DL-AABA, DL-BABA and GABA. 37
- Fig. 2.2 NMR spectra of DL-AABA, DL-BABA and GABA acid obtained at 400 MHz. 39
- Fig. 2.3 X-ray powder diffractogram of DL-AABA, DL-BABA and GABA. 41
- Fig. 2.4 FT-IR spectra of DLPC, DMPC, DPPC and DSPC. 44
- Fig. 2.5 Overlay of HSDSC thermograms for insulin (blue), lysozyme (red) and myoglobin (green) heated from 10°C to 95°C at a heating rate of 1°C/min. Concentrations used: 3, 5 and 3 mg/ml of insulin, lysozyme and myoglobin, respectively. The pH employed was 6.6 for insulin and myoglobin, and 2.4 for lysozyme. 45
- Fig. 2.6 SETARAM TSC II calibration kit set up (SETERAM TSC II manual). 48
- Fig. 2.7 Calibration results showing the onset of crystallisation and melting processes (SETERAM TSC II manual). 49

CHAPTER 3

- Fig. 3.1** Chemical structures of (a) α -aminobutyric acid (AABA), (b) β -aminobutyric acid (BABA) and (c) γ -aminobutyric acid (GABA). 51

Fig. 3.2 TGA curve overlay of DL-AABA, DL-BABA and GABA heated from ambient temperature to 340°C at 2°C/min. (a) Thermogravimetric (TG) curves and (b) derivative thermogravimetric (DTG) curves.	54
Fig. 3.3 Overlay of the thermograms observed for DL-AABA, DL-BABA and GABA heated from -90 to 350°C at 2°C/min.	56
Fig. 3.4 Global TSDC obtained using different electrical field strengths (V/mm) for (a) DL-AABA, (b) DL-BABA and (c) GABA.	58
Fig. 3.5 A linear regression plot of current intensity at T_{max} vs applied electrical field strength (E_p) for the aminobutyric acids.	59
Fig. 3.6 Global TSDC curve overlay of DL-AABA, DL-BABA and GABA polarized at 100°C with a polarizing field of 120 V/mm for GABA and 160 V/mm for DL-AABA and DL- BABA.	60
Fig. 3.7 The discrete relaxation modes of the global relaxation processes for (a) DL-AABA, (b) DL-BABA and (c) GABA obtained by the partial polarisation method.	62
Fig. 3.8 Distribution of relaxation time as a function of temperature determined for each elementary relaxation obtained using the Bucci method.	63
Fig. 3.9 Plot of log pre-exponential factor (τ_0) vs T_m for all processes observed for the amino butyric acids.	64
Fig. 3.10 “Compensation search” plots of the intercept vs slope of the Arrhenius plots for the TW experiments performed for DL-AABA and DL-BABA	67
Fig. 3.11 Relaxation map analysis of the compensation point obtained for the lower 23 and 17 polarisation temperatures for DL-AABA and DL-BABA, respectively.	68

CHAPTER 4

Fig. 4.1 Homologous series of phosphatidylcholines: 1,2-dilauryl-sn-glycero-3-phosphocholine (DLPC), 1,2-dimyristoyl-sn-glycero-3-phosphocholine (DMPC), 1,2-dipalmitoyl-sn-glycero-3-phosphocholine (DPPC) and 1,2-distearoyl-sn-glycero-3-phosphocholine (DSPC) with carbon chain lengths of 12, 14, 16 and 18, respectively.	75
Fig. 4.2 Illustration of custom made sample holder and electrode arrangement employed to study the phosphatidylcholines.	78
Fig. 4.3 Schematic of the change in the appearance of a phosphatidylcholine samples after the initial heat treatment and after all TSDC experiments were performed.	78
Fig. 4.4 Overlay of the thermograms observed for DLPC, DMPC, DPPC and DSPC heated from -50 to 240°C at 10°C/min after removal of moisture from the samples.	80
Fig. 4.5 Representation of a typical multi-layered arrangement of phospholipids (reproduced from Doxastakis et al., 2007).	82

Fig. 4.6 XRPD results for the phosphatidylcholines after heating to 140°C and cooling to ambient temperature (3 times).	86
Fig. 4.7 Total, reversing and non-reversing TMDSC curves obtained for (a) DLPC, (b) DMPC, (c) DPPC and (d) DSPC. Data were obtained at an underlying heating rate of 2°C/min and temperature amplitude of 1.5°C every 60 s, using a sample size of 8.5 ± 0.4 mg.	88
Fig. 4.8 Plots of activation energy (E_a) vs the degree of conversion (α) for the chain melting transition (T_m) of DLPC, DMPC, DPPC and DSPC.	90
Fig. 4.9 Global depolarisation current as a function of temperature observed for (a) DLPC, (b) DMPC, (c) DPPC and (d) DSPC, obtained using different E_p strength at a T_p of 90°C.	94
Fig. 4.10 A plot of current intensity at T_{max} vs applied electrical field strength (E_p) for the phospholipids.	95
Fig. 4.11 Global TSDC curve overlay for the phosphatidylcholines polarized at 90°C with a polarizing field of 350 V/mm.	96
Fig. 4.12 A regression plot showing the relationship between T_m and acyl chain length for the phosphatidylcholines.	96
Fig. 4.13 Overlay of DSC curve and TSDCS profiles obtained after polarising the sample at 90°C using electrical field strength of 350 V/mm for (a) DLPC, (b) DMPC, (c) DPPC and (d) DSPC.	99
Fig. 4.14 The discrete relaxation modes observed under the global relaxation processes for (a) DLPC, (b) DMPC, (c) DPPC and (d) DSPC.	102
Fig. 4.15 Plot of distribution of relaxation time as a function of temperature (relaxation map analysis) for each elementary relaxation obtained using the Bucci method.	105
Fig. 4.16 Plot of activation enthalpy vs T_m of the discrete relaxation components for (a) DLPC, (b) DMPC, (c) DPPC and (d) DSPC.	108
Fig. 4.17 Plots of relaxation times (τ) at the T_{max} of the discrete relaxation component with the highest current intensity against carbon chain length.	112
Fig. 4.18 Plots of the relaxation times (τ) obtained at the T_{max} of the main depolarisation processes observed for DMPC, DPPC and DSPC versus the apparent activation energies obtained at 30, 40 and 50% α of the chain melting transition observed in DSC and the peak temperatures of the chain melting transition (T_m).	114

CHAPTER 5

Fig. 5. 1 Timescale of dynamic processes observed in hydrated proteins (reproduced from: Henzler-Wildman and Kern, 2007).	117
Fig. 5.2 TGA curve overlay of the proteins heated from ambient temperature to 600°C at 10°C/min. (a) Thermogravimetric (TG) curves and (b) derivative thermogravimetric (DTG) curves.	122
Fig. 5.3 Overlay of DSC thermograms observed for the proteins obtained using a heating rate of 10°C/min.	124

Fig. 5.4 Global depolarisation current as a function of temperature observed using varying polarising field strength for (a) insulin polarised at -50°C , (b) lysozyme polarised at -100°C and (c) myoglobin polarised at -50°C showing two processes (P1 and P2).....	127
Fig. 5.6 Plots of current intensity at T_{max} against applied electrical field strength (E_p) for (a) insulin, (b) lysozyme and (c) myoglobin.	130
Fig. 5.7 Global depolarisation current observed for the proteins when polarised with an E_p of 400 V/mm before and after dehydration, (a) insulin polarised at -75°C , (b) lysozyme polarised at -100°C and (c) myoglobin polarised at -50°C	132
Fig. 5.8 The discrete relaxation mode observed under the global relaxation processes for (a) insulin, (b) lysozyme and (d) myoglobin obtained with a polarising field of 400 V/mm.	134
Fig. 5.9 Plots of the distribution of relaxation time as a function of temperature obtained for each elementary relaxation process for (a) insulin, (b) lysozyme and (c) myoglobin.....	136
Fig. 5.10 Plot of activation enthalpies against T_{max} of the discrete relaxation components for protein containing water molecules.....	137
Fig. 5.11 Global depolarisation current as a function of temperature observed using varying polarising field strength for (a) insulin, (b) lysozyme, and (c) myoglobin, all polarised at 100°C	142
Fig. 5.12 Plots of current intensity at T_{max} against applied electrical field strength (E_p) for (a) insulin, (b) lysozyme, and (c) myoglobin.	143
Fig. 5.13 The discrete relaxation mode observed under the global relaxation processes for (a) insulin, (b) lysozyme and (c) myoglobin obtained with a polarising field of 400 V/mm.	146
Fig. 5.14 Plots of the distribution of relaxation time as a function of temperature obtained for each elementary relaxation process for (a) insulin, (b) lysozyme, and (c) myoglobin.....	147
Fig. 5.15 Plot of activation enthalpies against T_{max} of the discrete relaxation components for dehydrated protein samples.....	149
Fig. 5.16 Plots of relaxation times vs T_{max} for the discrete relaxation processes observed for hydrated (below 0°C) and dehydrated (above 0°C) protein samples.....	151

LIST OF TABLES

CHAPTER 1

Table 1.1 Analytical techniques used for the study of solid-state pharmaceuticals (modified from Chieng et al., 2011). 15

Table 1.2 Techniques used to characterise relaxation process in order of their sensitivity (S) to and resolution power (R) of secondary relaxations. 19

CHAPTER 2

Table 2.1 CHN composition analysis of the aminobutyric acids ($n=3$). 35

Table 2.2 CHN composition analysis of the phosphatidylcholines ($n=3$). 42

CHAPTER 3

Table 3.1 The temperatures and weight changes associated with the processes observed in TGA studies for the butyric acids. 55

Table 3.2 Temperatures and heat changes observed for the endothermic processes observed for DL-AABA, DL-BABA and GABA ($n=3$). 56

Table 3.3 Arrhenius parameters for the aminobutyric acids and the relaxation times observed at the peak maxima. 65

CHAPTER 4

Table 4. 1. Mean temperatures at the peak maxima and enthalpies associated with the mesomorphic transitions of the homologous series of phosphatidylcholines ($n=3$). 81

Table 4.2 Temperatures at the peak maxima of the pre-transition and chain melting transition processes. 83

Table 4.3 Calculated mean apparent activation energies of the chain melting transition (T_m) at each α for DLP, DMPC, DPPC and DSPC ($n=3$). 91

Table 4.4 Temperatures and activation enthalpy values obtained at the enthalpy maxima for DLPC, DMPC, DPPC and DSPC 110

Table 4.5 Relaxation times obtained at the T_{max} of the discrete components corresponding to the main relaxation process observed for homologous series of the phosphatidylcholine studied ($n=3$). 112

CHAPTER 5

Table 5.1 The temperatures and weight changes associated with the processes observed in TGA studies for the proteins. 123

Table 5.2 The “glass transition” temperatures observed for the proteins investigated. 124

Table 5.3 Global depolarisation temperature maxima observed for the proteins and the moisture contents observed in TGA studies.	128
Table 5.4 The relaxation times obtained at the T_{\max} of the discrete component with the highest depolarisation current intensity and at the T_{\max} of the discrete component with the highest ΔH^\ddagger	139
Table 5.5 The current intensity observed for the protein samples when polarised at 100°C using polarising electrical field strength of 350 V/mm	144
Table 5.6 Activation enthalpies and the relaxation times obtained at the T_{\max} of the discrete relaxation components with the greatest current intensity.	149

ABBREVIATIONS

Abbreviation	Meaning
DLPC	1,2-dilauryl- <i>sn</i> -glycero-3-phosphocholine
DMPC	1,2-dimyristoyl- <i>sn</i> -glycero-3-phosphocholine
DPPC	1,2-dipalmitoyl- <i>sn</i> -glycero-3-phosphocholine
DSPC	1,2-distearoyl- <i>sn</i> -glycero-3-phosphocholine
ΔH^\ddagger	Activation enthalpy change
ΔS^\ddagger	Activation entropy change
ΔG^\ddagger	Activation Gibbs free energy change
API	Active pharmaceutical ingredient
θ	Angle between incident X-rays and reflecting planes
E_a	Apparent activation energy
AUC	Area under curve
ATIR-FT-IR	Attenuated internal reflectance -Fourier transform infrared
k_B	Boltzmann constant
ΔH	Change in enthalpy
ΔS	Change in entropy
ΔG	Change in Gibbs free energy
ΔQ	Change in heat
I	Current density
α	Degree of conversion/ fraction reacted
F	Degrees of freedom
DTG	Derivative thermogram
DETA	Dielectric thermal analysis
$f(\alpha)$	Differential form of reaction model
DSC	Differential scanning calorimetry
μ	Electric dipole moment
Pe	Equilibrium polarisation
E_p	External polarisation field
W_∞	Final sample weight
T_f	Final temperature
T_g	Glass transition temperature
β	Heating/Scanning rate ($^\circ/\text{min}$)

HSM	Hot-stage microscopy
W₀	Initial sample weight
T₀	Initial temperature
G(α)	Integral form of reaction model
g(α)	Integral form of reaction model
T_K	Kauzmann temperature
T_m	Chain melting temperature
P	Number of phases existing at equilibrium
P	Polarisation
P	Polarisation
t_p	Polarisation time
A	Pre-exponential factor
τ_0	Relaxation pre-exponential factor
τ	Relaxation time
WT	Sample weight at temperature (T)
Wt	Sample weight at time (t)
SS-NMR	Solid-state nuclear magnetic resonance
SDC	Spontaneous depolarisation current
D	Strength parameter
T	Temperature
T_{max}	Temperature at peak maxima
k(T)	Temperature dependent rate constant
T_p	Temperature of polarisation
T_w	Temperature window
TGA	Thermal gravimetric analysis
TW	Thermal windowing
TSC	Thermally stimulated calorimetry
TSDC	Thermally stimulated depolarisation current
TSPC	Thermally stimulated polarisation current
TG	Thermogram
t	Time
t_f	Time at final temperature
t₀	Time at initial temperature
R	Universal gas constant; 8.314 J K ⁻¹ mol ⁻¹
V	Volume

λ	Wavelength of incident x-rays
t_w	Windowing time
AABA	α -aminobutyric acid
BABA	β -aminobutyric acid
GABA	γ -aminobutyric acid

LIST OF PUBLICATIONS/PRESENTATIONS

Full manuscripts

- Title:** Quantitative analysis of overlapping processes in the non-isothermal decomposition of chlorogenic acid by peak fitting
Authors: S. Owusu-Ware, B. Z. Chowdhry, S. A. Leharne, M. D. Antonijevic
Year: 2013
Journal: *Thermochimica Acta*, 565, 27–33
Status: Published
- Title:** Sirolimus encapsulated liposomes for cancer therapy: physicochemical and mechanical characterization of sirolimus distribution within liposome bilayers
Authors: I. Onyesom, D. Lamprou, L. Sygellou, S. Owusu-Ware, M. Antonijevic, B. Z. Chowdhry, D. Douroumis
Year: 2013
Journal: *Molecular Pharmaceutics*
Status: In Press (October, 2013)
- Title:** Novel analytical approaches for the study of mobility and relaxation phenomena in positional isomers of GABA
Authors: S. Owusu-Ware, B. Z. Chowdhry, S. A. Leharne, M. D. Antonijevic.
Year: 2013
Journal: *Phys.Chem.Chem.Phys.*
Status: In Press (October, 2013)
- Title:** Application of Thermally Stimulated Current (TSC) to understand relationship between molecular mobility and physical stability of phosphatidylcholines
Authors: S. Owusu-Ware, B. Z. Chowdhry, S. A. Leharne, M. D. Antonijevic
Year: 2013
Journal: *Materials Chemistry (B)*
Status: To be submitted, 2013
- Title:** Application of Thermally Stimulated Current (TSC) study of partially hydrated and dehydrated peptides and proteins
Authors: S. Owusu-Ware, B. Z. Chowdhry, S. A. Leharne, M. D. Antonijevic
Year: 2013
Journal: *Phys.Chem.Chem.Phys.*
Status: In progress, 2013

Abstracts in Refereed Journals and Proceedings

- Title:** Studies of the relationship between molecular mobility and the thermal stability of the isomers of aminobutyric acid
Authors: S. Owusu-Ware, S. Leharne, B. Chowdhry, M. Antonijevic.
Year: 2011

- Journal:** *AAPS Journal*; 13(S2)
- Title:** Thermal stability implication of positional isomerism of novel biphenyl derivatives
- Authors:** S. Owusu-Ware, M. Masud, C. Baltus, J. Spencer, M. Antonijevic.
- Year:** 2011
- Journal:** *AAPS Journal*, 13(S2),
- Title:** Thermal Studies of the Structural Isomers of Aminobutyric acid
- Authors:** Samuel K. Owusu-Ware, Babur Z. Chowdhry, Stephen A. Leharne and Milan D. Antonijevic.
- Year:** 2010
- Journal:** *AAPS Journal*,12(S2), 2353
- Title:** Thermal decomposition of chlorogenic acid in different atmospheres
- Authors:** Samuel K. Owusu-Ware, Babur Z. Chowdhry, Stephen A. Leharne and Milan D. Antonijevic.
- Year:** 2010
- Journal:** *Journal of Pharmacy and Pharmacology* – UK PharmSci 2010 –Special Issue, Vol. 62, 1357.
- Title:** HPLC-ESI-MS method development for the elucidation of nicardipine degradation products
- Authors:** Owusu-Ware, S.K. and MD Antonijevic, M.D.
- Year:** 2009
- Journal:** *AAPS Journal*; 11(S2), 3311
- Presentations**
- Title:** Applications of TSDC to investigate molecular mobility and its relationship with thermal stability
- Conference:** Thermal Analysis and Calorimetry (TAC) 2013, 9-10 Apr-2013, University of Greenwich, Chatham, UK
- Type:** Oral Presentation
- Title:** Thermally Stimulated Depolarisation Current Spectroscopy (TSDC) study of γ -butyric acid and its isomers
- Conference:** ICTAC 15th International Conference on Thermal Analysis and Calorimetry, August 20th-24th, 2012, Osaka, Japan
- Type:** Poster Presentation
- Title:** Thermally Stimulated Depolarisation Current Spectroscopy (TSDC) study of γ -butyric acid and its isomers
- Conference:** ICTAC 15th International Conference on Thermal Analysis and Calorimetry, August 20th-24th, 2012, Osaka, Japan
- Type:** Poster Presentation

- Title:** Studies of the relationship between molecular mobility and the thermal stability of the isomers of aminobutyric acid
- Conference:** **AAPS:** American Association of Pharmaceutical Scientists Annual Meeting and Exposition, October 23rd to 27th, 2011, Washington, DC, USA.
- Type:** Poster Presentation
- Title:** Thermal stability implication of positional isomerism of novel biphenyl derivatives
- Conference:** **AAPS:** American Association of Pharmaceutical Scientists Annual Meeting and Exposition, October 23rd to 27th, 2011, Washington, DC, USA.
- Type:** Poster Presentation
- Title:** Thermal Kinetic studies of the isomers of aminobutyric acid
- Conference:** **TMG TAC:** Thermal Methods Group of the Royal Society of Chemistry - Thermal Analysis Conference “The Use of Thermal Methods in the Investigation of Biomaterials”, November 24th, 2010, Manchester, UK.
- Type:** Poster Presentation
- Title:** Thermal Studies of the Structural Isomers of Aminobutyric acid
- Conference:** **PSWC (AAPS):** American Association of Pharmaceutical Scientists Annual Meeting and Exposition, November 14th to 18th, 2010, New Orleans, Louisiana, USA.
- Type:** Poster Presentation
- Title:** Deconvolution of complex TG-DTG data: applications in pharmaceutical systems
- Conference:** **5th Congress of Pharmacists of Serbia**
Belgrade, 13th-17th October 2010
- Type:** Poster Presentation
- Title:** Thermal decomposition of chlorogenic acid in different atmospheres
- Conference:** **“The Science of Medicine” - APS 2010**
UK PharmSci, 1st – 3rd September 2010, Nottingham, UK
- Type:** Poster Presentation
- Title:** Chlorogenic Acid: Thermal Decomposition Studies
- Conference:** **TMG TAC March 2010**
Thermal Methods Group of the Royal Society of Chemistry - Thermal Analysis Conference, March 30th to 31st, 2010, Aldermaston, UK.
- Type:** Poster Presentation

Title: HPLC-ESI-MS method development for the elucidation of nicardipine degradation products

Conference: **AAPS 2009**
American Association of Pharmaceutical Scientists Annual Meeting and Exposition, November 8th to 12th, 2009, Los Angeles, California, USA.

Type: Poster Presentation

Chapter 1 : Introduction

Solid state dosage forms (SSDFs) have been estimated to contribute more than 66% of all pharmaceutical products on the market (GBI, 2011). They are the preferred state for pharmaceutical development because they exhibit superior stability compared to their liquid and gaseous counterparts. As such, SSDFs are easier to handle and offer lower manufacturing and storage costs (Zhang et al., 2004). The development of solid (i.e. powdered) pharmaceuticals, however, is not without stability challenges.

“Stability” has been defined as the capacity of a drug substance or product to remain within established specifications (Lucas et al., 2004). In the solid-state, this refers to the capacity of the solid substance to preserve its physical and chemical characteristics. Changes to these characteristics can have major implications for the quality and performance of the pharmaceutical under development (Chen et al., 2002, Chen et al., 2009). Therefore, it is in the interest of drug developers to acquire a comprehensive understanding of the physico-chemical properties of solid materials. Such knowledge facilitates better control over the behaviour of solid state pharmaceuticals and enables manipulation of their properties in order to enhance clinical performance.

1.1. Solid Phases

The stability of solids in a given application is governed, in part, by the properties of the solid phase (Qiu et al., 2009). Solid phases are classified into two major groups: (1) crystalline and (2) amorphous (Fig. 1.1).

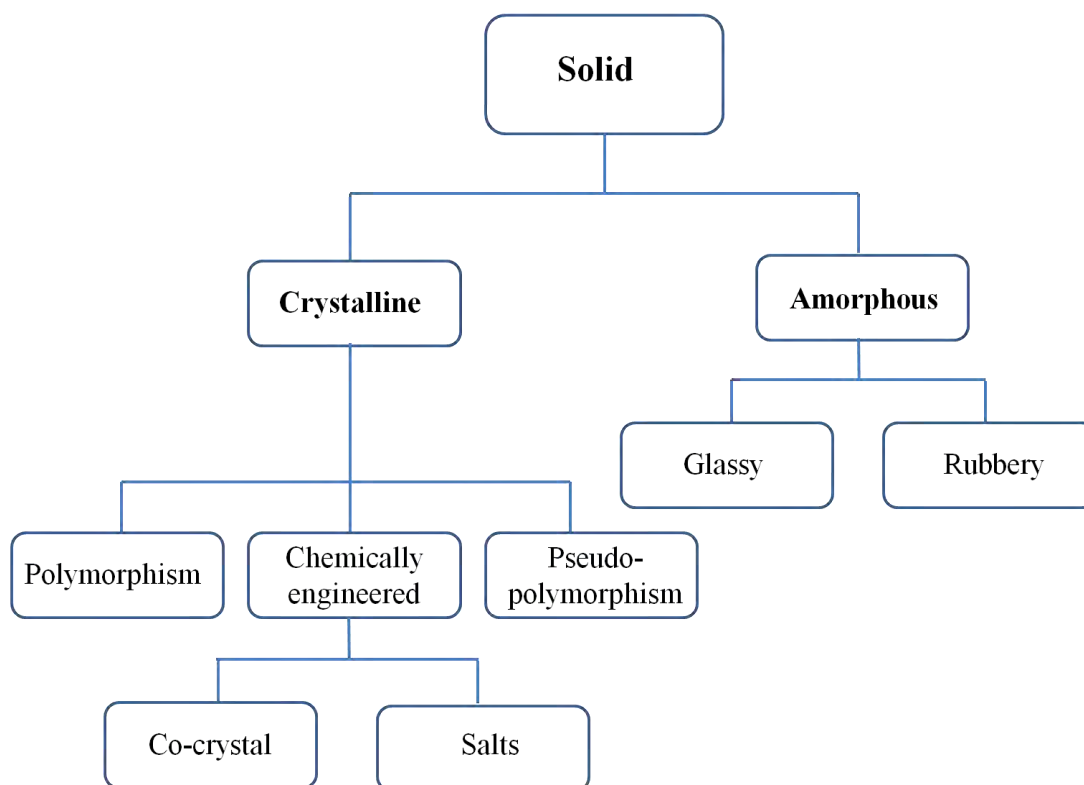


Fig. 1.1 The different sub-states of solids observed in pharmaceutical development.

1.1.1. Crystalline Solids

An ideal crystal is one that has infinite, three-dimensional and regularly repeating unit cells and is free from impurities and crystalline defects. The unit cells represent the spatial arrangements of molecules with defined coordinates of translational vectors (a , b , and c) and angles (α , β and γ) (Vippagunta et al., 2001). Hence, crystalline systems have defined orientation, shape and volume. From a thermodynamic perspective, crystalline solids generally have a lower potential energy and therefore greater stability compared to their amorphous forms. This is due to the highly ordered arrangement of their molecules. Furthermore, different unit cell arrangements of the same compound can exhibit different Gibbs free energy and therefore stabilities i.e. the monoclinic form (I) of paracetamol melts at 167°C, whilst the orthorhombic form (II) melts at 156°C (Rengarajan et al., 2007). This ability of a single homogeneous compound to exhibit different crystalline structures with different properties is termed polymorphism. As shown in Fig.1.1 different crystal structures can also be chemically engineered, by the incorporation of other chemical species or the

modification of the chemical properties of the compound. Pseudo-polymorphism is the incorporation of solvent/water molecules into the crystal system.

1.1.2 Amorphous Solids

Amorphous solids, on the other hand, are solid systems that have short-range molecular order, but lack the periodicity of the translational symmetry that characterises crystalline systems, and are therefore referred to as disordered solids (Cui, 2007). The macroscopic properties of amorphous solids are characterised by high thermodynamic energies and they, therefore, have lower stability in comparison to their crystalline counterparts. Amorphous solids can either exist in the glassy vitrified state or in the rubbery (super-cooled liquid) state. These two states exhibit distinct thermodynamic quantities i.e. free energy and volume, and therefore differences in stability. These differences in solid-state chemistry contribute to the overall complexity of solid-state pharmaceuticals.

1.2 Solid-State Reactivity

Solid-state reactions of pharmaceutical compounds include chemical reactions and physical transformations (Morissette et al., 2004). Both types of reactions are important, as they can result in dire consequences, if they are not controlled (Gardner et al., 2004). For example, one major consequence of chemical changes is increased toxicity of the drug, while physical changes can drastically alter the dissolution rate and chemical reactivity. Hence, from a regulatory/clinical point of view, the importance of understanding solid-state physical and chemical stability is unquestionable.

1.2.1 Chemical Reactivity

Chemical reactions in the solid-state are akin to those observed in solution (Oliyai et al., 1994, Costantino, 1995, Lai and Topp, 1999, Byrn et al., 2001). However, due to the non-homogenous nature of solids, these reactions are much more difficult to interpret. It is quite

evident from the scientific literature that different solid phases have a significant impact on the chemical reactivity of a particular compound (Shalaev et al., 1997).

The mechanism by which chemical reactions occur in the solid-state can be classified as topochemical or non-topochemical reactions (Qiu et al., 2009). Topochemical reactions involve the formation of new bonds or bond exchange, and are determined by the lattice arrangement of molecules in the solid material (Atwood and Steed, 2004, Shalaev et al., 1997). In this case, the reaction requires minimum mobility of molecules and the rate of the reaction is dictated - in part - by molecular packing. In other words, the reaction occurs because the reacting moieties are held in favourable orientations and positions in the lattice arrangement. This mechanism of degradation is not commonly observed in pharmaceutical research. Non-topochemical reactions, on the other hand, are the most common mechanism observed in solid-state pharmaceuticals (Qiu et al., 2009). This type of reactions is not a true solid-state reaction as it requires significant mobility of reacting molecules. The rate at which non-topochemical reactions occur is determined by the nature of the solid phase i.e. amorphous or crystalline and factors that modulate molecular mobility in the solid-state, such as temperature and moisture.

1.2.2 Physical Reactivity

Physical transformations are of considerable concern, as the products of these reactions have major implications on the development, quality, performance and safety of the pharmaceutical substance or product (Chieng et al., 2011). It is therefore important to understand the stability relationships between the different solid forms of pharmaceutically relevant molecules.

1.2.2.1 Crystalline

The tendency for solids to convert into another state, whether it is a solid-solid, solid-liquid or solid-gas transition is governed by the differences in the Gibbs free energy between the

initial and the final state at a given temperature (Eq.1.1). It follows that the transition from the initial to the final state will occur spontaneously if the change in Gibbs free energy is negative. However, the rate at which the conversion occurs depends on the kinetic properties of the initial state. In other words, for the conversion to occur, an appropriate level of mobility is required, and this will require a certain activation barrier to be overcome for the reaction to progress.

$$\Delta G_{I-II} = (H_{II} - TS_{II}) - (H_I - TS_I) \quad (1.1)$$

I and *II* denote the different crystalline forms of a drug.

When considering transitions from one crystalline state to another the stability relationships between the different phases are described as monotropic or enantiotropic (Fig. 1.2a and b).

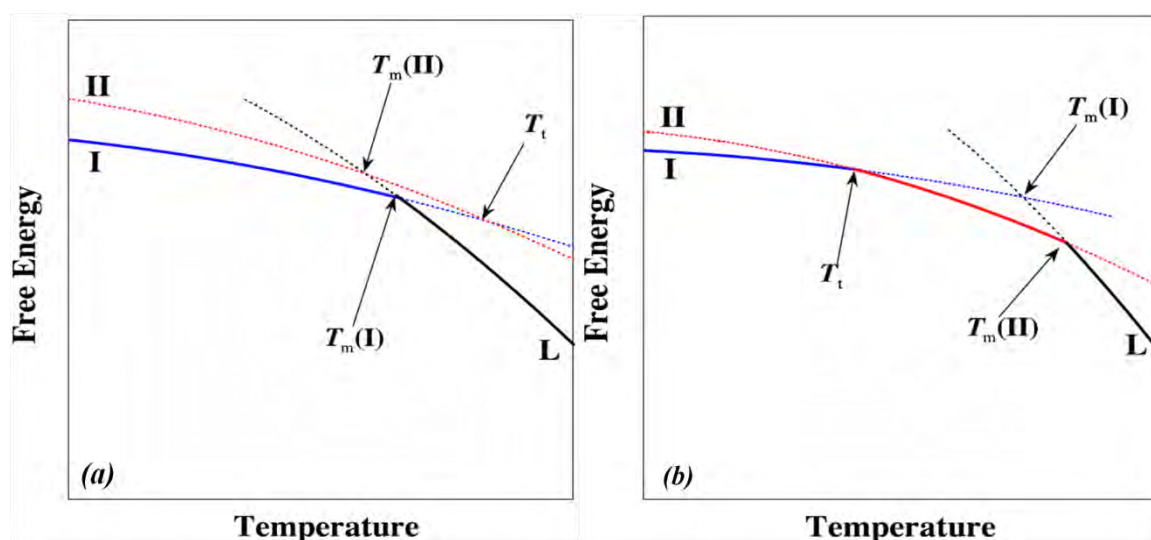


Fig. 1.2 Gibbs free energy phase diagram as a function of temperature showing stability relationships between two crystalline forms I and II, (a) shows the monotropic relationship between the two forms and (b) shows enantiotropic relationships. T_m is the melting temperature, T_t is the point where the Gibbs free energies of the two forms are the same and L is the liquid phase (Zhang et al., 2004).

For a fully characterised pharmaceutical substance or product, in which all crystalline phases are known, a monotropic relationship between phases is preferred. This is because in monotropically related polymorphism only one form (the higher melting form) is stable at all temperatures. This is because the Gibbs free energy cross-over/transition temperature (T_t) for monotropic polymorphs are above melting temperature (see Fig 1.2). As such the behaviour of the form during development can be more easily controlled. However, in enantiotropic polymorphism there exist unique temperatures below the melting point of both forms, where the Gibbs free energies meet and cross-over (see Fig 1.2). This “crossing-over” of free energies indicates that there are two domains of stabilities i.e. the lower melting form is more thermodynamically stable at temperatures below the transition point (T_t), and the higher melting form is more stable at temperatures above this point (Barbas et al., 2007). This suggests, for example, that if form I (in Fig. 1.2) is kept at a temperature above the T_t then it is metastable and can convert to the more thermodynamically stable form II via a solid-solid transition.

1.2.2.2 Amorphous

Amorphous solids have the greatest tendency, of all solid forms, to undergo both physical and chemical transformations, as they exhibit higher thermodynamic quantities (free energy and free volume relative to the crystalline forms). This means that at all temperatures below the melting point, the amorphous phase is metastable. Hence, the formation of amorphates must be avoided if it is not the intended form. Furthermore, if the amorphous state is the intended form, the stability must be fully understood so as to avoid/prevent crystallization, which will result in the loss of solubility advantages of the formulation.

The relative difference in thermodynamic stability between the crystalline and amorphous phases of the same compound is shown in Fig. 1.3.

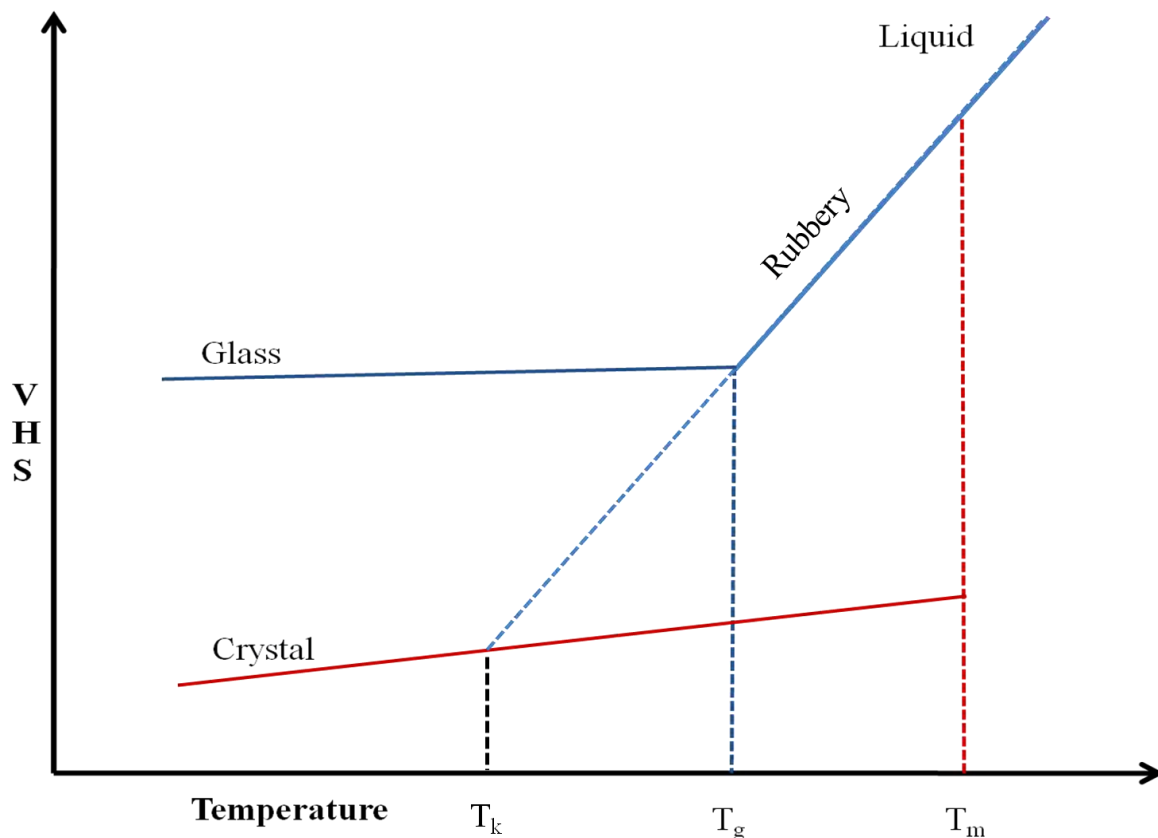


Fig. 1.3 The relative differences in volume (V), enthalpy (H) and entropy (S) between crystalline and amorphous solids as function of temperature. T_K is the Kauzmann temperature, T_g is the glass transition temperature and T_m is the melting temperature (Chawla and Bansal, 2009).

When a liquid is cooled to below the melting temperature (T_m) without crystallising, it is said to be in the super-cooled or rubbery amorphous phase (Chawla and Bansal, 2009). This phase is characterised by a more sluggish mobility in comparison to the liquid state due to reduced free volume and free energy, but exhibits greater mobility (by several orders of magnitude) when compared to the crystalline state. Reducing the temperature of the rubbery phase results in a further decrease of the thermodynamic quantities and equilibrium is lost when the time-scale of molecular motions coincide with experimental time scales (Cui, 2007, Wunderlich, 1999). At this point molecules are moving so slowly, that there is not enough time to undergo the rearrangements necessary to find the equilibrium thermodynamic state at that temperature, before a further reduction in temperature occurs. The deviation from the

equilibrium point results in the formation of the highly viscous glassy amorphous phase, in which mobility appears trapped (relaxation time is increased well above the observational time frame), but which still exhibits higher thermodynamic quantities in comparison to the crystalline form. The temperature at which this occurs is the glass transition temperature (T_g).

Crystallization, and in fact chemical reactions in amorphous solids, is driven- in part- by molecular mobility. When considering the thermodynamic quantities in Fig. 1.3 it is clearly observed that the rubbery amorphous phase, with higher thermodynamic quantities, is more likely to exhibit greater molecular mobility amongst the solid phases and therefore have greater tendency to undergo physical and chemical reactions. For this reason a great deal of research effort in the pharmaceutical industry has been undertaken into understanding glass transitions and the influence of molecular mobility on physical and chemical stability.

1.3 Molecular Mobility

Molecular mobility can increase solid-state reactivity (Yoshioka and Aso, 2005, Yoshioka and Aso, 2007, Chawla and Bansal, 2009). However, the significance of mobility in enhancing reaction rates is not always clear. For example, a comparative study of storage stability of amorphous and crystalline insulin demonstrated that the crystalline state (which in theory should have lower degree of motional freedom compared to the amorphous state) exhibits inferior stability when subjected to different storage conditions (Pikal and Rigsbee, 1997). This suggests that the generalised view of the influence of mobility on stability does not hold for all compounds; in this case for larger molecular weight compounds such as proteins. It can therefore be inferred that amongst other factors, the influence of mobility on solid-state stability may also be molecular weight dependent. In addition, motional freedom or molecular mobility may, likewise, be dependent on molecular weight (You and Ludescher, 2010). It has also become apparent that the T_g and therefore the mobility, with characteristic relaxation times, associated with the T_g is not always a reliable predictor of either physical or

chemical stability (Chang et al., 2005a, Chang et al., 2005b, Bhattacharya and Suryanarayanan, 2009).

In order to fully understand the relationship between molecular mobility and stability of pharmaceutical solids, greater insight into the molecular mobility of solids prior to any thermo-physical and thermo-chemical changes (observed macroscopically) need to be acquired. A relationship, if any, needs to be drawn between the lower temperature mobility states, such as rotational/orientational and localised segmental mobilities, and the higher temperature thermal events such as the glass transition, crystallisation, melting and degradation processes.

1.3.1 Primary and Secondary Relaxations: Amorphous Systems

The assignment of primary and secondary relaxation phenomena is based on the location of the relaxation processes in dielectric relaxation profiles, usually observed for amorphous materials. These molecular relaxation processes are categorised in accordance with the frequencies at which they are observed i.e. the primary relaxations are so named because they typically appear at the lower frequencies in dielectric profiles. The temperature location of the relaxation processes in the dielectric profile can also be used to differentiate primary and secondary relaxation modes (Vyazovkin and Dranca, 2006). For example, secondary relaxation processes occur at lower temperatures, while primary relaxations occur at higher temperatures.

The primary (or α -relaxation) processes are molecular relaxations that are responsible for the manifestation of the glass transition process. This relaxation is structural and it is characterised by a relaxation time of <100 s. A major problem in amorphous systems is the generally non-Arrhenius temperature dependence in the glass transition region (Bhattacharya and Suryanarayanan, 2009), which makes their physico-chemical behaviour very unpredictable. As a result of the significantly reduced free volume in the system at the T_g (as

the sample is being cooled), the mobility of the molecules require the cooperation of neighbouring molecules in order to change their relative positions. As such, α -relaxation processes are cooperative in nature (Jimenez-Ruiz et al., 1999).

For an ideal glass forming liquid, the temperature dependent average relaxation time ($\tau(T)$) of the glass transition is thought to obey Arrhenius behaviour (Dyre, 1998) and relaxation time can therefore be expressed as:

$$\tau(T) = \tau_0 \exp\left(\frac{E_a}{k_B T}\right) \quad (1.2)$$

Where τ_0 is the pre-exponential constant, E_a the apparent activation energy, k_B the Boltzmann constant and T is temperature (K).

As stated previously, amorphous systems almost never obey/display Arrhenius dependent relaxation time, because at the glass transition a small change in temperature is compensated for by a large change in relaxation time (or other properties of the amorphous system such as volume and viscosity). This non-Arrhenius temperature dependence relaxation time in the glass transition region is commonly described by the Vogel-Tammann-Fulcher (Eq.1.3; also known as the VTF) relationship (Crowley and Zografi, 2001):

$$\tau(T) = \tau_0 \exp\left[\frac{DT_0}{T - T_0}\right] \quad (1.3)$$

Where D is the strength parameter i.e. it indicates whether the glass former is strong or fragile. D values >30 suggest a strong glass forming behaviour whilst values <10 represent fragile glass formers. T_0 represents the temperature at which molecular relaxation time is infinite and is proposed to be equivalent to the Kauzmann temperature (T_K) (Angell, 1991).

Secondary relaxation processes, on the other hand, are localised, faster processes (typically $<10^{-1}$ s) that are non-cooperative. Furthermore, these relaxation processes generally exhibit Arrhenius type temperature dependence (Bhattacharya and Suryanarayanan, 2009). There are two types of secondary relaxation processes typically observed in amorphous solids: β -relaxations and γ -relaxations, named in order of increasing frequency or decreasing temperature.

Different molecular mechanisms can give rise to the secondary relaxation processes in glassy amorphous materials. Both γ - and β -relaxation processes involve intra-molecular mobility in which part of the molecule i.e. polymer side chain(s), undergo rotational motion. In addition to intra-molecular mobility, β -relaxations can also originate from inter-molecular motions i.e. movement of the molecular backbone/entire molecule (Smith and Bedrov, 2007). As such a “completely rigid molecule” with “no degrees of freedom” can undergo secondary β -relaxation. β -relaxations of this kind were first reported by Johari and Goldstein in their study on “simple” rigid molecules (Johari and Goldstein, 1970).

Secondary relaxation phenomena are considered to be the precursor of the α -relaxation process (Kaminska et al., 2006, Kaminski et al., 2010) i.e. the molecular dynamic model of super-cooled liquids described by Ngai (Ngai, 2003) suggests that β -relaxations gradually increase in cooperativity due to mutual interactions with neighbouring molecules. This view of non-cooperative β -relaxation manifesting into the cooperative α -relaxation process was also expressed by Goldstein (Matheson et al., 1972), who initially suggested that intermolecular β -relaxations involve the same type of rearrangements observed in α -relaxations.

The potential influence of secondary relaxations on physical and chemical stability has been the driving force for the investigation of these processes in amorphous materials. It has been reported that crystallisation in some amorphous systems could be controlled by β -relaxation

processes. For example it has been demonstrated that the nucleation growth rate observed experimentally can only be simulated when the β -relaxation time of the material under study is considered as opposed to the α -relaxation time (Hikima et al., 1999). In addition, work by Alie and colleagues (Alie et al., 2004) also suggests that intra-molecular β -relaxations are responsible for the crystallisation of pharmaceutical drug substances.

The influence of chemical stability upon secondary relaxation is more pronounced for larger molecular weight compounds such as proteins. As reported by Yoshioka and colleagues (Yoshioka et al., 2007), β -galactosidase aggregation is controlled by intra-molecular rotational β -relaxation processes. This conclusion was based on the fact that the order of the ability of sugar excipients, used to freeze-dry β -galactosidase, to decrease β -relaxations was the same as the rank order in which the sugars were able to decrease aggregation rates. A similar conclusion on the role of secondary relaxations on the stability of proteins has been reported (Chang et al., 2005a, Chang et al., 2005b) and a recent review of the correlation between secondary relaxations and protein stability has been published (Cicerone and Douglas, 2012).

1.3.2 Secondary Relaxations in Crystalline Solids

Due to the low energetic state of crystalline solids, mobility is greatly limited. As such molecular motions or relaxation processes in crystalline materials and their influence on stability have been the subject of little consideration. It must be stated that it is unlikely that a Johari-Goldstein type secondary relaxation in crystalline solids occurs due to the limitations imposed on molecules by the crystal lattice. However, as stated previously, not all secondary relaxations observed in amorphous solids are of the Johari-Goldstein type i.e. intra-molecular motions observed for γ - and some β -relaxations can be localised relaxation processes. Such intra-molecular motions can indeed occur in crystalline solids.

Studies using thermally stimulated current spectroscopy (TSCS) have shown the existence of localised relaxation processes in crystalline solids at temperatures below their melting points (Diogo and Ramos, 2008, Pinto et al., 2010, Jain et al., 2010). These processes are characterised by a lack of cooperativity and negligible influence of molecular orientations on the entropy of the whole system (Ramos and Mano, 1997). Discussion on the significance of these relaxations processes, with regard to the stability of crystalline solids, is often scarce. However, as demonstrated by Yoshioka and colleagues (Yoshioka et al., 2007), localised mobility in the solid-state can have a significant influence on chemical stability, particularly in proteins. The interesting fact about these mobility states in crystalline solids is that they are almost universal i.e. these activated relaxation processes exist below the melting points of the solids studied in all the literature reviewed. In most cases, when two or more molecules are compared with different melting temperatures, the order of melting temperature is the same as the order of the temperatures at which the “secondary relaxation” processes are observed in TSCS studies. These findings indicate the possible existence of some relationship between the relaxation processes observed by TSCS and the thermal behaviour of crystalline solids. It is important to investigate the possibility of such a relationship, even in crystalline solids; as such knowledge can enhance understanding of solid-state stability and formulation development.

For the purpose of this study secondary relaxation processes observed in solid systems other than the amorphous will be denoted β' - and γ' - relaxations depending on the temperature location of the process.

1.4 Solid-State Characterisation Methods

There are a large number of techniques available that can be used to probe the different properties of solid materials. Table 1.1 provides a list of some of the major and most generally employed techniques in pharmaceutical research. The interested reader is referred to the work of Storey and Yman, (2011). The content of Table.1.2 compares the major

techniques currently used to probe secondary relaxation processes in solid systems, introducing the least used technique (TSC), which has gained growing interest in solid-state characterisation of molecular mobility in recent years, due to its high sensitivity and resolving power in detecting secondary relaxations.

Table 1.1 Analytical techniques used for the study of solid-state pharmaceuticals (modified from Chieng et al., 2011).

Analytical Technique	Basic principal	Information	Advantages	Disadvantages	
Spectroscopy techniques					
X-ray diffraction					
Powder X-ray diffraction (PXRD)	Generated single beam X-ray is directed onto the sample. The atoms in the sample absorb some energy and coherently scatter this energy with the same λ as the incident x-radiation. The diffraction of the x-rays are described by the Bragg equation $n\lambda = 2 d \sin\theta$ where λ is the wavelength, d is the distance between diffracting planes and θ is diffraction angle, The measurement output is the distance between diffracting planes against 2θ	<ul style="list-style-type: none"> Identifies polymorphic forms: unique diffraction patterns Amorphous forms: no diffraction patter Amorphous or crystalline contents 	<ul style="list-style-type: none"> Non-destructive Gold standard for phase identification Qualitative and quantitative 	<ul style="list-style-type: none"> Relatively large sample size Preferred orientation 	
Single crystal X-ray diffraction (SCXRD)		<ul style="list-style-type: none"> Determines the unit cell lattice parameters 	<ul style="list-style-type: none"> Provides in depth understanding of crystalline forms 	<ul style="list-style-type: none"> Requires a high purity single crystal that is $>0.1\text{mm}$ which may be difficult to prepare 	
Vibrational spectroscopy					
Mid-Infrared (MIR)	Infrared (IR) spectroscopy measures radiations absorbed by molecules undergoing vibrational motions that results in a change in dipole moment. Frequencies absorbed correspond to vibrational frequencies of chemical bonds in the molecule.	<ul style="list-style-type: none"> Intra-molecular vibrations corresponding to specific functional groups Hydrogen bonding polymorphic forms: determined due to unique bands and peak shifting identification of amorphous forms: peak broadening 	<ul style="list-style-type: none"> Small sample size Fast data acquisition Availability of spectral libraries No sample preparation for ATR Ability to penetrate through containers Polymorphic transitions can be monitored in DRIFT in the variable-temperature mode 	<ul style="list-style-type: none"> IR cannot be used to analyse primary and secondary relaxations Some sample preparation methods may induce phase change 	
Near-Infrared (NIR)	IR data is acquired by the generation of an interferogram, which is converted into IR spectra by Fourier transform	<ul style="list-style-type: none"> Overtones Combinations of vibrations in the MIR regions Sensitive to different water state 			<ul style="list-style-type: none"> Low sensitivity and selectivity Baseline slope Difficult to interpret
Terahertz pulse spectroscopy (TPS)	Generated pulsed terahertz radiation is directed onto the sample. Lattice vibrations in the crystalline sample cause a change in the electric field of the incident radiation, as a result of absorption and dispersion. The ratio between the incident and transmitted field strengths are then calculated and converted into absorption spectra	<ul style="list-style-type: none"> Intra-molecular and lattice vibrations Differentiate between crystalline forms: unique peaks/bands Differentiation of amorphous from crystalline: amorphous solids exhibit no spectral features 			<ul style="list-style-type: none"> Spectrum is significantly affected by water content Pellet compression could result in phase transformations

Table 1.1 continued

Analytical Technique	Basic principal	Information	Advantages	Disadvantages
Raman spectroscopy	Measures the inelastic scattering of an intense single wavelength of incident radiation, caused by bond vibrations that result in a change in polarizability.	<ul style="list-style-type: none"> • Intra-molecular and lattice vibrations • polymorphic forms: determined due to unique bands and peak shifting • identification of amorphous forms: peak broadening complimentary to IR spectroscopy 	<ul style="list-style-type: none"> • Small sample size • Non-destructive method • No sample preparation required • Can analyse lattice vibrations at lower frequencies 	<ul style="list-style-type: none"> • Can be destructive: local heating of samples, photo-degradation • Sample fluorescence
Solid-state NMR	<p>For atoms to be a NMR active, they must possess a nucleus with overall magnetic spin moment i.e. the nucleus must have an odd sum of protons and neutrons, or odd number of protons and neutrons.</p> <p>During experiments the sample is held in a strong magnetic field. The different spin states favourably separate into low-energy (α) state (parallel with the applied field), and high- energy (β) states (anti-parallel to the field) establishing an equilibrium spin moment. Irradiation of the sample with a radio frequency pulse results in absorption energy that promotes some spin-states from α to β. These promoted spin states relax and emits radio frequency proportional to the energy separation between α and β states.</p>	<ul style="list-style-type: none"> • Nuclei and chemical environment of an atom in a molecule leads to the elucidation of molecular formula • Determination of molecular conformation and arrangements • Able to provide detailed information on secondary relaxation processes 	<ul style="list-style-type: none"> • Non-destructive • Qualitative and quantitative • Negligible influence of particle size of materials • Determination of the origin of molecular motions 	<ul style="list-style-type: none"> • Relatively expensive • Long data acquisition time • High level of expertise is required for experimental setup and data interpretation
Time-of-flight secondary ion mass spectrometry (TOF-SIMS)	Pulsed particle beam is focused onto the sample and the impact removes chemical species from the surfaces of the material surfaces. Generated species at the impact sites are positive and negative ions (primary ions) and those generated farther from site of impact are parent or molecular ions (secondary ions). These species are accelerated into a flight path to the detector. The time taken from the impact to the detector is recorded.	<ul style="list-style-type: none"> • Provides chemical image of specific components over a two-dimensional area of the sample 	<ul style="list-style-type: none"> • Provides information about the chemical distribution on a solid surface • Qualitative and quantitative information 	<ul style="list-style-type: none"> • Cannot differentiate between solid forms • Irradiation may cause sample degradation


Table 1.1 continued

Analytical Technique	Basic principal	Information	Advantages	Disadvantages
Microscopy techniques				
Scanning Electron Microscopy (SEM)	High energy electron beam is focused onto the sample. Electron-sample interaction results in the dissipation of this energy, generating secondary ions. These secondary ions are detected and information generates SEM image of the sample.	<ul style="list-style-type: none"> • Topographical properties 	<ul style="list-style-type: none"> • Small sample size • Higher resolution of solid morphology than microscope 	<ul style="list-style-type: none"> • Sample preparation and stage condition set up (vacuum settings) is required • Large and expensive
Atomic Force Microscopy (AFM)	Measures the forces acting between a fine tip and a samples surface. During experiments a tip attached to the free end of a cantilever is brought very close to the surface of the sample (distance between the probe and sample surfaces is usually in the order of angstroms). Positive or negative bending of the cantilever is realised when the interaction of the fine tip of the cantilever with the sample results in repulsive or attractive forces. The bending of the cantilever is detected by a laser beam reflected from the backside of the cantilever.	<ul style="list-style-type: none"> • Topographical map of sample surfaces • Interaction forces and mechanical properties at the nanoscale 	<ul style="list-style-type: none"> • Wide range of materials can be analysed • Provides a 3-dimensional image of the sample surface • Does not require any special pre-treatment as in SEM • Possible to achieve atomic level resolution of sample surfaces 	<ul style="list-style-type: none"> • Relatively slower scan speed • Forces on sample can cause distortion, tip wear and sample damage
Thermal Analytical techniques				
Hot-stage microscopy (HSM)	A beam of visible light is passed through a condenser onto the sample. Transmission, refraction and reflection of the light by the sample is then magnified and focused onto the ocular. The attached heating block heats the sample at a controlled rate, allowing the assessment of the optical properties of the sample as a function of temperature or time. The attachment of cross- polarisers below and above the sample, which rotates the plane of a polarised light, allows the analysis of the birefringence of crystalline solids due to their anisotropic properties.	<ul style="list-style-type: none"> • Birefringent properties (crystallinity) • Crystal habits • Morphology 	<ul style="list-style-type: none"> • Small sample mass • Easy to use • Very little sample preparations • Temperature variability 	<ul style="list-style-type: none"> • Destructive method • Does not provide quantitative information
Dynamic Vapour Sorption (DVS)	The sample and empty reference in their respective chambers, held in a temperature-controlled incubator, are subjected to varying relative humidity and temperatures and the sample response is measured gravimetrically.	<ul style="list-style-type: none"> • Sorption and desorption properties of solid materials 	<ul style="list-style-type: none"> • Determines moisture content at specific conditions • Small sample size 	<ul style="list-style-type: none"> • Destructive method • Not suitable for samples that decompose at low temperatures • Only suitable for sorption/desorption studies

Table 1.1 continued

Analytical Technique	Basic principal	Information	Advantages	Disadvantages
Thermal Gravimetric Analysis (TGA)	Sample in a crucible is heated in an enclosed furnace under inert or oxidative atmosphere suspended on a highly sensitive balance. The weight of the sample is measured as a function of temperature or time.	<ul style="list-style-type: none"> • Thermally activated processes associated with weight change i.e. decomposition, sublimation and evaporation 	<ul style="list-style-type: none"> • Small sample mass • Easy to use • Very little sample preparations • Temperature variability 	<ul style="list-style-type: none"> • Destructive • Limited to transitions with associated weight change
Differential Scanning Calorimetry (DSC)	The instrument measures the heat flow into and out of a sample and an empty reference pan in a single furnace, as a function of temperature or time. The sample and the reference are heated at a controlled rate or held isothermally for a time period.	<ul style="list-style-type: none"> • Thermally activated processes associated heat exchange i.e. melting, evaporation, decomposition sublimation and, Glass transition (T_g) 	<ul style="list-style-type: none"> • Small sample mass • Easy to use • Very little sample preparations • Temperature variability • Various sample types can be analysed 	<ul style="list-style-type: none"> • Cannot capture transitions that are associated small changes in energy • No gold standard for baseline type to use for integration
Dielectric Thermal Analysis (DETA)	A sample is placed between two electrodes to form a capacitor. An alternating electric field is then applied simultaneously with a controlled heating programme. This results in the movement of dipoles and/or charge species, which generates current. The current is measured as a function of temperature or time.	<ul style="list-style-type: none"> • Conductive and capacitive properties of dielectric materials • Glass transition • Pre-glass transition molecular mobility • Viscoelastic properties 	<ul style="list-style-type: none"> • Can be non-destructive • Small sample size • Ability to characterize low energy transitions that are inaccessible to other techniques 	<ul style="list-style-type: none"> • Requires dedicated expert to develop method • Difficulty in interpreting data
Dynamic mechanical analysis (DMA)	A sample of known geometry is subjected to controlled sinusoidal stress/strain and the displacement response of the sample i.e. the ability of the sample to deform, to this force is recorded. This is measured in terms of stiffness (modulus) and damping (dissipation of energy, which is given by the ratio between in-phase and out of phase components in respect to the sinusoidal force. This is reported as tan delta) as a function to time, temperature or frequency.	<ul style="list-style-type: none"> • Viscoelastic properties • Glass transition • Can probe secondary relaxations 	<ul style="list-style-type: none"> • Non-destructive • Small sample size • Highly sensitivity to low energy transitions: weak glass transitions 	<ul style="list-style-type: none"> • Requires dedicated expert to develop method • Difficulty in interpreting data

Table 1.2 Techniques used to characterise relaxation process in order of their sensitivity (S) to and resolution power (R) of secondary relaxations.

Decreasing (S/R)	NMR	TSC	DEA	DMA	DSC
 Measurement principle	Measures the emission of absorbed radio frequency radiation by nuclei in presence of an external magnetic field. The common approach for determining mobility is through the analysis of spin-lattice relaxation time measurements (T_1) in solid systems	Measures the current generated by the orientation/reorientation of dipoles under the influence of static electrical field. Secondary relaxations appear at temperatures below primary processes	Measures current generated by the orientation/reorientation of dipoles and charged species under the influence of electrical field of various frequencies. Secondary relaxations are detected at lower frequencies and temperatures with respect to the glass transition	Changes in storage modulus and tan delta are indication of phase transitions. Secondary relaxations are characterised by relatively small drop in storage modulus when compared with the T_g at lower frequencies and temperatures	Measures heat flow associated with thermally induced transitions i.e. glass transitions. Characterisation of secondary relaxations is usually undertaken by measuring enthalpic relaxation as a function of annealing temperature and time. Primary process can also be assessed using scanning rate dependence of the ΔC_p .
Usefulness	<ul style="list-style-type: none"> • Very sensitive to secondary relaxation processes. • Can resolve individual relaxation process at an atomic level. • Has been used to correlate molecular mobility with stability. • Can analysis mobility in crystalline as well as amorphous systems 	<ul style="list-style-type: none"> • Direct determination of relaxation times and their distribution • Able to distinguish between primary and secondary relaxation process • Highest sensitivity to secondary relaxation in comparison to DEA, DMA and DSC • Provides better resolution in comparison to DEA and DMA 	<ul style="list-style-type: none"> • Direct determination of distribution of relaxation time • Able to distinguish between primary and secondary (β and γ) relaxation processes above and below main transition 	<ul style="list-style-type: none"> • Able to distinguish between primary and secondary relaxations • Very flexible sample preparation methods 	<ul style="list-style-type: none"> • Easiest technique and fastest data acquisition time. • Possible to simultaneously study secondary and primary relaxation processes including the eventual crystallisation
Limitations	<ul style="list-style-type: none"> • Longest data acquisition time of the techniques • Most expensive of the techniques listed here. • Requires specialized and dedicated expertise for experimental design. • Distinguish between primary and secondary relaxation events 	<ul style="list-style-type: none"> • Problems with reproducibility 	<ul style="list-style-type: none"> • Inability to separate overlapping relaxation events • Interference form electrical conductivity at low frequencies • Greater number of experiments needs to be performed in comparison to TSC 	<ul style="list-style-type: none"> • Inability to separate overlapping relaxation events • Sensitivity to secondary relaxation processes not as good as TSC • Great number of experiments need to be performed in comparison to TSC 	<ul style="list-style-type: none"> • Cannot separate individual relaxation modes • Insensitive to secondary relaxations (which is of low activation enthalpy) • Can only provide indirect and limited information on secondary relaxation processes
References	(Wu et al., 2002, Masuda et al., 2005, Margulies et al., 2000, Luthra et al., 2008, Miura et al., 2011)	(Saffell et al., 1991, Grein et al., 2004, Ramos et al., 2004, Barker and Antonijeivic, 2011)	(Saffell et al., 1991, Kriptomou et al., 2003, Kaminska et al., 2006, Kaminski et al., 2010)	(Saffell et al., 1991, Alves et al., 2002, Andronis and Zografí, 1997, Pinheiro and Mano, 2009)	(Saffell et al., 1991, Alves et al., 2002, Vyazovkin and Dranca, 2006, Dranca et al., 2009)

1.5 Thermally Stimulated Current (TSC) Spectroscopy

TSC spectroscopy is used to measure the changes in dipole orientation in response to an externally applied static electric field, as a function of temperature or time. The primary output of the technique is current, which is generated by the movement of dipoles and/or any charged species. The movement of dipoles measured in TSC spectroscopy usually results from localised rotational motion of parts or the whole molecule (Diogo and Ramos, 2008). As such, the technique is extremely useful in directly probing molecular mobility of solid systems. There are several experimental modes of TSC spectroscopy; the most common are the thermally stimulated depolarisation current (TSDC) and thermal windowing (TW) methods. The behaviour of dipoles during a TSDC experiment is shown in Fig.1.4.

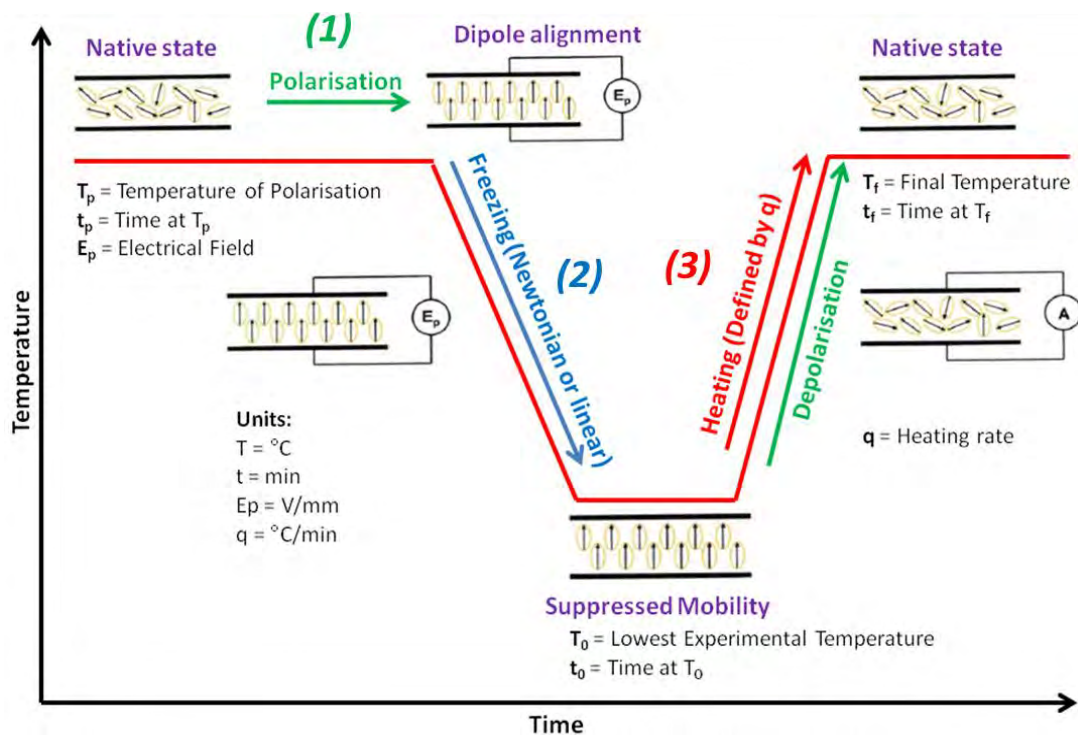


Fig. 1.4 Schematic of the response of molecules during a typical TSC spectroscopy experiment.

The application of a static electric field (E_p) for a time (t_p) orients dipoles in the sample and aligns them to their respective opposite charges (1). By quench cooling the sample to a

temperature (T_0) that is substantially lower than the T_p , the dipoles are frozen in their polarised position (2) i.e. dipole relaxation time (τ) at T_0 is significantly greater than that at T_p . Hence, the polarisation will remain in the material even when the external electric field is removed. When the sample is heated the relaxation time decreases, inducing movement of dipoles back to equilibrium (3). This relaxation process generates current that is measured as function of temperature (Fig. 1.5) using a sensitive electrometer.

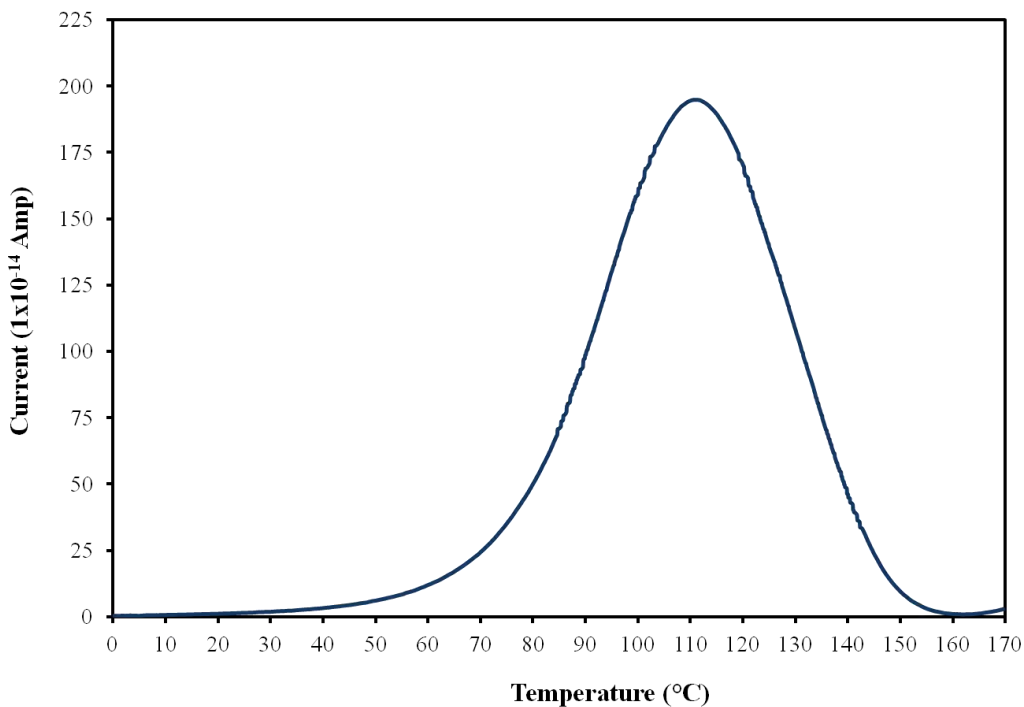


Fig. 1.5 Typical TSC output obtained during TSDC experiments.

It is also possible to deconvolute the complex global relaxation process obtained using the TSDC method by the application of thermal windowing (TW) experiments described in Fig. 1.6. This is achieved by employing narrow polarisation windows i.e. an electric field is applied over a narrow range of temperatures. Typically the procedure involves polarisation of the sample at T_p for a short period (t_p), which is then cooled by a few degrees (T_w) below the initial T_p . At this temperature (T_d), which is given by $T_p - T_w$, the electric field is switched off and the sample is held for a brief period (t_w) allowing all fast relaxation processes to complete. The sample is then quench cooled to T_0 and the depolarisation current is measured

as the sample is heated to the T_f at a controlled rate. This procedure permits analysis of relaxation processes that have different relaxation times thereby facilitating the calculation of activation energies for each independent relaxation process.

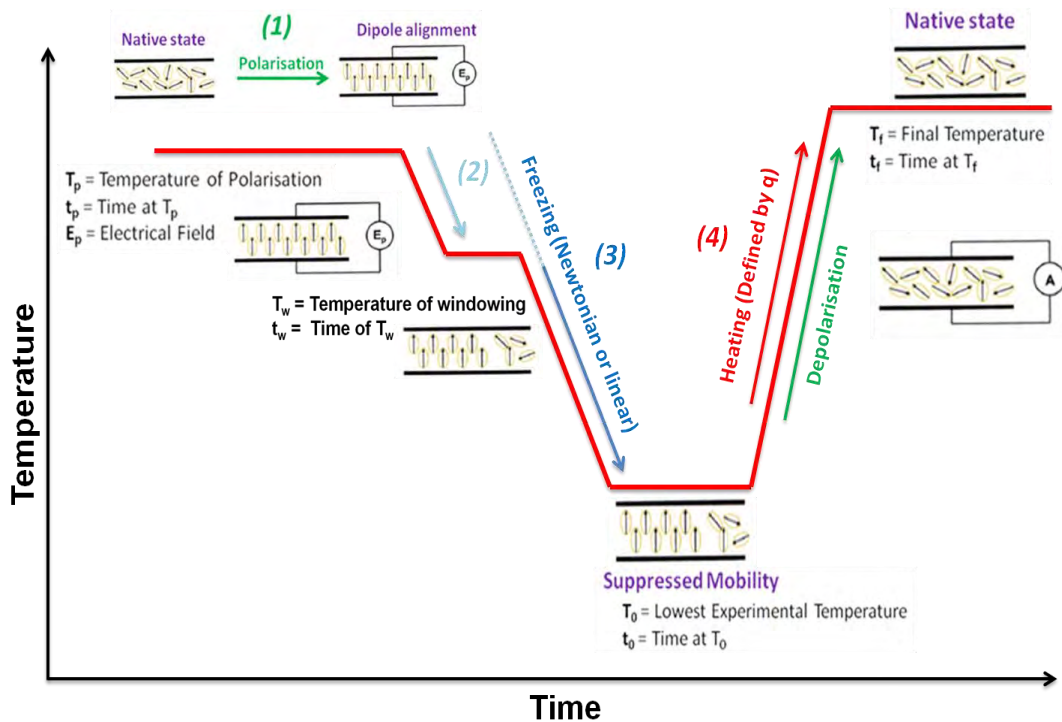


Fig.1. 6 Schematic of the response of molecules during a TW experiment.

1.5.1 Dipoles and Polarisation Processes

A dipole arises from the existence of partial positive (δ^+) and negative (δ^-) regions in a polar bond, which result from differences in the electronegativity of the bonding atoms in the molecule. An electric dipole moment exists in the molecule when the δ^+ and δ^- charge centres do not coincide. The electric dipole moment (μ) is therefore defined as the difference in the magnitude of the charge (e) at either end of the electric poles, multiplied by the separation distance (d) between the charge centres (Tripathy and De, 2008).

Upon the application of external electric field, several polarisation mechanisms may occur. The polarisation may be electronic, atomic, space charge, interfacial or orientational.

- ***Electronic polarisation***

This involves the distortion of an electron shell and is the fastest ($\leq 10^{-15}$ s), due to the very small distances required for electronic displacement in atoms.

- ***Atomic polarisation***

This polarisation results from atomic displacement in a molecule with hetero-polar bonds. Homo-polar bonds do not exhibit atomic polarisation due to the homogeneous nature. The atomic polarisation is similar to electronic polarisation and it is the second fastest polarisation ($10^{-14} - 10^{-12}$ s)

- ***Space charge polarisation***

This type of polarisation results from excess charge carriers (ionic /electronics) caused by high voltage field and insufficient contact between electrodes and sample. As a result there is a macroscopic charge transfer towards the electrodes. These charges can have different origins. For example it can arise from ion migration which generates hetero-charges (opposite polarity of nearest electrode) or from the injection of homo-charges (same polarity to nearest electrode) by the electrodes with breakdown which takes place in air inclusion. The hetero-charge is intrinsic to the material and results from the application of high voltage. It is also known as Townsend breakdown. The homo-charge is extrinsic and results more from insufficient contact between the material and electrodes. The homo-charge always give a negative peak; it can therefore be distinguished from the hetero-charge and removed by improving the contact between electrodes and material.

- ***Interfacial polarisation***

This can be considered a space charge via a different mechanism. In this polarisation charges accumulate near the interface of the different phases. This occurs because the different phases have different ohmic conductivity. This phenomenon is also known as the Maxwell-Wagner-Sillars effect (MWS).

- ***Orientational/or dipole polarisation***

This polarisation is due to the orientation of permanent or induced molecular or ionic dipoles. The time required for these polarisations is generally in the region of 10^{-12} s. This polarisation is attributed to the restricted rotation of parts of the molecule or the whole molecule and therefore limited by viscous forces.

The orientational polarisation is the most important in TSC experiments as it provides information about rotational freedom of molecules or molecular segments and also viscous forces in the material. The faster polarisations - such as the electronic and atomic polarisations - are too fast to be measured in the experimental time-frames used. On the other hand, all precautions must be taken to minimize/or remove completely the effect of space charge and interfacial polarisations. In TSC experiments, orientational polarisations can easily be distinguished from space charge and interfacial polarisations by assessing the relationship between the depolarisation current intensity and the strength of the external electric field. Orientational polarisation will exhibit depolarisation current intensity that is proportional to the strength of the applied electric field.

1.5.2 Theoretical Background

Detailed consideration of the theory pertaining to TSC spectroscopy is provided elsewhere (Turnhout, 1975). A summary of the most important characteristics of the outputs of the technique has been provided by Correia and colleagues (2000).

The widely accepted model describing the TSDC relaxation process is Debye's theory of dipole relaxation. This theory makes three major assumptions: (1) that polarisation of dielectric materials is homogeneous, (2) dipoles have a single relaxation time, and (3) that there are no interactions between dipoles during the polarisation processes. The decay of polarisation is therefore generally expressed as:

$$P(t) = P_e \left[\exp \left(- \int_0^t \frac{dt}{\tau} \right) \right] \quad (1.4)$$

Where $P(t)$ is the remaining polarization at time t , P_e is equilibrium polarisation at infinite time and τ is the relaxation time.

Assuming that depolarisation is the direct opposite of the polarising process i.e. dipoles exhibit the same relaxation time and no interactions between dipoles occur, then the rate of depolarisation in TSDC experiments is given by:

$$\frac{dP(t)}{dt} = - \frac{P(t)}{\tau(T)} \quad (1.5)$$

During experiments, depolarisation is induced by the application of a constant heating rate (β); hence there is a well-defined relationship between temperature and time so that $T(t) = T_i + \beta t$, where T_i is the initial temperature. Incorporation of the heating rate into Eq.1.5 gives:

$$\frac{dP(T)}{dT} = - \frac{1}{\beta} \frac{P(T)}{\tau(T)} \quad (1.6)$$

The depolarisation current ($I(T)$), which is the experimental output, is therefore given by:

$$I(T) = - \frac{dP(t)}{dt} = - \beta \frac{dP(T)}{dT} \quad (1.7)$$

Values for the polarisation in the samples are given by taking the integral of Eq. 1.6 to give Eq.1.8:

$$P(T) = \frac{1}{\beta} \int_T^{T_f} I(T') dT' \quad (1.8)$$

Where T_f is the final temperature i.e. the temperature at which the sample is completely depolarised.

The temperature dependent relaxation time is therefore given by the expression:

$$\tau(T) = \frac{\frac{1}{\beta} \int_T^{T_f} I(T') dT'}{I(T)} \quad (1.9)$$

The TSDC output of the distribution of relaxation time is usually presented in the logarithmic form, hence Eq.1.9 is usually expressed as:

$$\ln[\tau(T)] = \ln \left[\frac{1}{\beta} \int_T^{T_f} I(T') dT' \right] - \ln I(T) \quad (1.10)$$

This is the widely accepted approach for analysing the temperature dependent distribution of relaxation time for an “elementary” relaxation process, obtained using the thermal windowing experimental setup. The approach is often referred to as the Bucci method.

It is assumed that the elementary relaxation curves observed are those that are sufficiently temperature dependent. The TSDC curve can therefore be described as a continuous depolarisation process that is induced by a linear heating program exhibiting Debye exponential behaviour and a relaxation time that is temperature dependent (Correia et al., 2000).

A plot of $\ln[\tau(T)]$ vs $1/T$ for an elementary relaxation process is generally expected to generate a linear relationship. This is based on the notion that the relaxation times are characterised by narrow energy distributions i.e. a small change in temperature is compensated for by a small change in relaxation time. As such the activation parameters

associated with the relaxation process can be obtained by fitting the plot of $\ln[\tau(T)]$ vs $1/T$ to the Arrhenius (Eq.1.2) or Eyring equation (Eq.1.11).

$$\tau(T) = \frac{h}{k_B T} \exp\left(-\frac{\Delta S}{k_B}\right) \exp\left(\frac{\Delta H}{k_B T}\right) = \frac{h}{k_B T} \exp\left(\frac{\Delta G}{k_B T}\right) \quad (1.11)$$

Where h is Plank's constant, k_B the Boltzmann constant, ΔS is the entropy and ΔH and ΔG the enthalpy and Gibbs free energy, respectively.

1.6 Thermal Gravimetric Analysis (TGA)

TGA is used to measure sample weight as a function of time or temperature. This provides information about chemical reactions, such as decomposition and oxidative processes, and some physical processes, such as sublimation and evaporation. A typical curve of a TGA output is displayed in Fig.1. 7. The derivative curve (DTG) is the 1st derivative of the weight as a function of temperature. This curve is used to identify more clearly, the onset, peaks and endpoint of poorly resolved processes. DTG characteristics can also be used qualitatively.

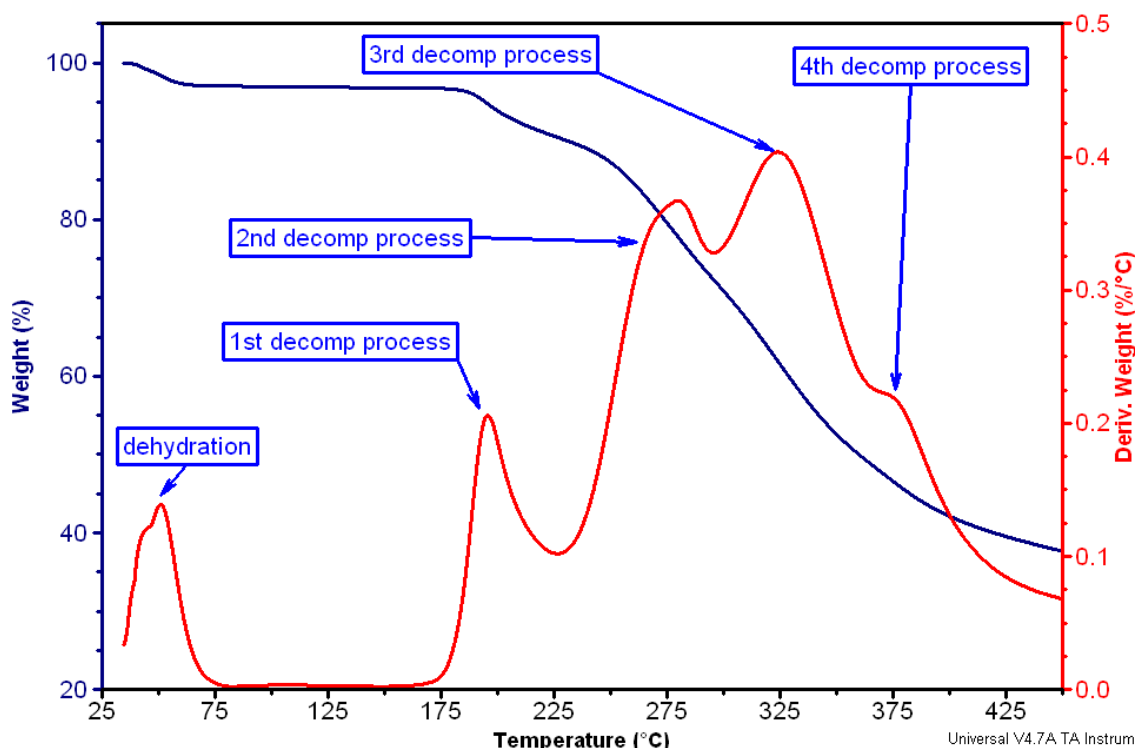


Fig. 1.7 Typical TGA output showing the thermal gravimetric or TG curve (navy plot) and the derivative thermal gravimetric or DTG curve (red plot) of chlorogenic acid hemihydrate.

It is rare to find TGA studies dealing with the decomposition of materials in the pharmaceutical literature. The main application of TGA has been in the determination of moisture contents of samples (Craig and Reading, 2007, Hulse et al., 2009). However, undertaking decomposition studies can reveal important information about pharmaceutical formulation conditions and the nature of excipient-drug interactions (Rus et al., 2012). The capability of TGA is further increased when hyphenated with evolved gas analysis (Craig and Reading, 2007).

In addition to compositional analysis, TGA is one of the most important techniques for the assessment of solid-state kinetic behaviour (Vyazovkin et al., 2011). This provides insight into the dehydration/hydration kinetics (Alkhamis et al., 2006), as well as the influence of solid forms and excipients on the stability of the system under scrutiny (Roeder et al., 2005, Vecchio et al., 2008, Reyes-Labarta et al., 2006, Bal and Murthy, 2012).

In the assessment of solid-state kinetics, TGA outputs are normalised to the degree of conversion (α), which range from 0-1. This serves as a quantitative measure of the progression of a reaction as a function of time or temperature (Eq.1.12 and 1.13):

$$\alpha = \frac{w_0 - w_t}{w_0 - w_\infty} \quad (1.12)$$

$$\alpha = \frac{w_0 - w_T}{w_0 - w_\infty} \quad (1.13)$$

Where w_0 is the initial sample weight, w_t is the weight at time (t), w_T is the weight at temperature (T) and w_∞ is the weight at the end point of the reaction.

The calculated value of α is used to extract activation energy (E_a), pre-exponential factor (A) and reaction mechanism parameters using modified forms of the generalised solid-state Arrhenius equation e.g:

$$\frac{d\alpha}{dt} = A \exp\left(-\frac{E_a}{RT}\right) f(\alpha) \quad (1.14)$$

For non-isothermal experiments, where the heating rate β is equal to dT/dt , the variation in the degree of conversion can be analysed as a function of temperature instead of time. Substitution of the heating rate into Eq.1.14 gives:

$$\beta \frac{d\alpha}{dT} = A \exp\left(-\frac{E_a}{RT}\right) f(\alpha) \quad (1.15)$$

For solid-state reactions, several steps, with different apparent activation energies may be exhibited. Hence the relative contribution of the different reaction steps to the overall reaction

rate will vary with temperature and the degree of conversion. As such the activation energy will vary significantly if the reaction involves multiple steps.

Iso-conversion is a solid-state kinetic computational approach that enables the determination of activation energy with no prior assumptions or the need to determine any form of the kinetic model. The approach implies that at a given value of α , the reaction rate is solely dependent on temperature, thereby allowing the assessment of the activation energy dependence on the degree of conversion for experiments performed using different heating rates (Vyazovkin et al., 2011).

One of the most widely used iso-conversional kinetic methods for the calculation of activation energy and assessment of activation energy dependence on reaction progression for TGA output is the Kissinger-Akahiro-Sunose method (KAS) (Vyazovkin et al., 2011). This was expressed by Jankovic et al (2009) as:

$$\ln\left(\frac{\beta}{T^2}\right) \cong \ln\left(\frac{AR}{E_a g(\alpha)}\right) - \frac{E_a}{RT} \quad (1.16)$$

Where $g(\alpha)$ is the integral form of reaction model. The plot of the left hand side of the equation vs $1/T$ for a given degree of conversion (α) for the different heating rates employed (Eq.4) yields a linear relationship, the slope of which is equal to $-E_a/R$.

1.7 Differential Scanning Calorimetry (DSC)

Physical and chemical reactions are associated with heat exchange or a change in energy. In principle, the change in the heat (ΔQ) of a system is proportional to change in temperature (T). Hence, when a system is subjected to heat, its temperature increases. This increase in temperature is dependent on the heat capacity of the system at a constant pressure (C_p). The heat capacity is defined as the heat required to raise the temperature of a system by 1K. The relationship between heat, temperature and heat capacity is expressed as;

$$\Delta T = \frac{\Delta Q}{C_P} \quad (1.17)$$

DSC measures the differences in the flow between a sample and inert reference (usually empty pan) when subjected to controlled heating. Heat flowing into and out of a sample is governed by heat capacity, by some endothermic process (i.e. melting, evaporation, decomposition, protein denaturation etc.) or by some exothermic processes (i.e. crystallization). The heat flow signal for the DSC output is given by:

$$\frac{dQ}{dt} = C_P \frac{dT}{dt} + f(T, t) \quad (1.18)$$

Where dQ/dt is the heat flow rate, dT/dt is the heating rate (β) and $f(T, t)$ is the kinetic component of the heat flow at absolute temperature. A typical DSC output is presented in Fig.1. 8.

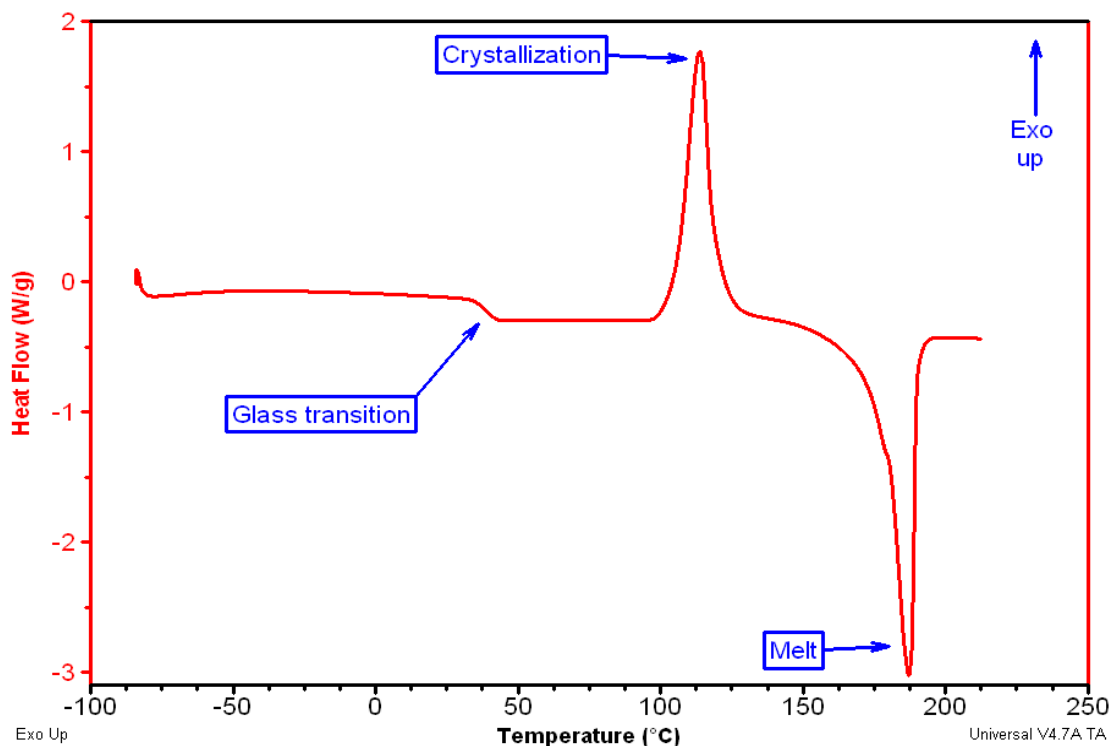


Fig. 1.8 A typical DSC output of the main thermal transitions of pharmaceutical interest during a heating scan.

T_g in DSC studies is defined as the temperature at the midpoint of the step change in baseline of the heat flow signal (Gabbott, 2008, Schick, 2009), while a first order transition, i.e. crystallization and melting temperatures, can be reported as the extrapolated onset temperature or the temperature of the peak maximum (Braga et al., 2011).

The integration of these first order transitions yields the enthalpy change (ΔH), which is a measure of the energy difference of the transition from the initial to the final state. In addition to determining the changes in thermodynamic quantities (under constant pressure) during thermal transitions, kinetic studies can also be performed using DSC (Lu et al., 2010, Vyazovkin et al., 2011). In this case α is calculated as follows (Khawam and Flanagan, 2006):

$$\alpha = \frac{AUC_0^{T,t}}{AUC_0^{\infty}} \quad (1.19)$$

Where, $AUC_0^{T,t}$ is the area under the curve from the starting temperature (θ) to a specified temperature (T) or time (t). The α values for the different heating rates can then be used to calculate the activation energies. The most common differential isothermal computational method is that of Friedman (Vyazovkin et al., 2011), which can be expressed as (Keuleers et al., 2002):

$$\ln\left(\beta \frac{d\alpha}{dT}\right) = \ln(Af(\alpha)) - \frac{E_a}{RT} \quad (1.20)$$

The activation energy is obtained from a plot of $\ln\left(\beta \frac{d\alpha}{dT}\right)$ vs $1/T$ for a given degree of conversion (α) for the different heating rates employed.

1.8 Aims of Project

The significance of the impact of molecular mobility on solid-state physical and chemical stability is not always clear. To further current understanding, investigational efforts need to be directed to the intrinsic mobility of molecules. TSDC provides a means to probe intrinsic and subtle molecular motions in the solid-state that may have stability implications. The overall purpose of the research reported herein is to contribute to the understanding of the influence of solid-state molecular mobility on the stability of materials. To this end biologically significant molecules, which present some of the most challenging stability issues, are examined in terms of:

- (1) How critical attributes of molecules, namely positional isomerism, increasing carbon chain length and molecular size of classes of molecules influences mobility in the solid-state.
- (2) Whether it is possible to relate the parameters of molecular mobility to the relative thermal stability of the materials under investigation.

Chapter 2 : Materials and Instrumentation

2.1 Materials

2.1.1 Aminobutyric Acids

DL- α -aminobutyric acid (99%), DL- β -aminobutyric acid (97%) and γ -aminobutyric acid (99%) were purchased from Sigma-Aldrich, CAS numbers [2835-81-6], [541-48-0] and [56-12-2] and Lot numbers are (1209508 51109193), (S53067-438) and (1420305 12009278), respectively. The chemical formula is $C_4H_9NO_2$ for the three substances and the molecular weight $MW= 103.12 \text{ g.mol}^{-1}$.

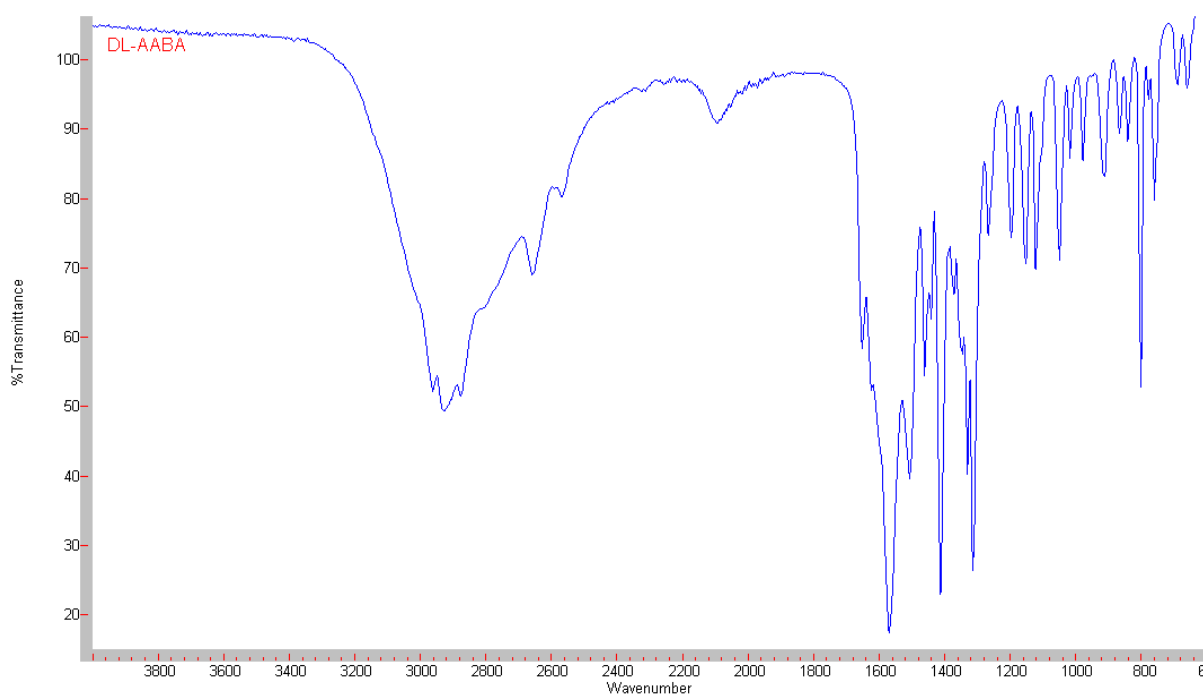
The percentage mass fractions (g.mol^{-1}) observed in elemental analysis using FLASHEA 112 series CHN analyzer (Thermo Electron Corporation) are presented in Table 2.1.

Table 2.1 CHN composition analysis of the aminobutyric acids (n=3).

Compound	% Atomic composition			
		C	H	N
DL-AABA	Experimental	48.49 ± 0.07	9.14 ± 0.06	13.99 ± 0.07
	Theoretical	46.66	8.73	13.58
DL-BABA	Experimental	48.14 ± 0.14	9.40 ± 0.12	13.62 ± 0.01
	Theoretical	46.66	8.73	13.58
GABA	Experimental	48.11 ± 0.05	8.91 ± 0.03	13.99 ± 0.02
	Theoretical	46.66	8.73	13.58

Specific rotation measurements for AABA and BABA were undertaken using a type AA-(6)5 polarimeter (Optical Activity Ltd). Analyses were undertaken in deionized water for both compounds using D- and L-sucrose as calibrants. The α_D^{20} values were found to be 0° for both compounds ($c = 2$) indicating that there was no experimentally significant enantiomeric excess of the D or L forms of either of the compounds.

The FT-IR spectra (Fig.2. 1) acquired using MK11 golden gate (Specac) in the range 4000 to 600 cm^{-1} and the solution $^1\text{H-NMR}$ spectra (Fig.2. 2) obtained at 400 MHz (JEOL) for the three substances are in good agreement with data reported in Spectral Database for Organic Compounds (SDBS), SDBS number = 1076, 1078 and 1075 for DL- α -aminobutyric acid, DL- β -aminobutyric acid and γ -aminobutyric acid, respectively.



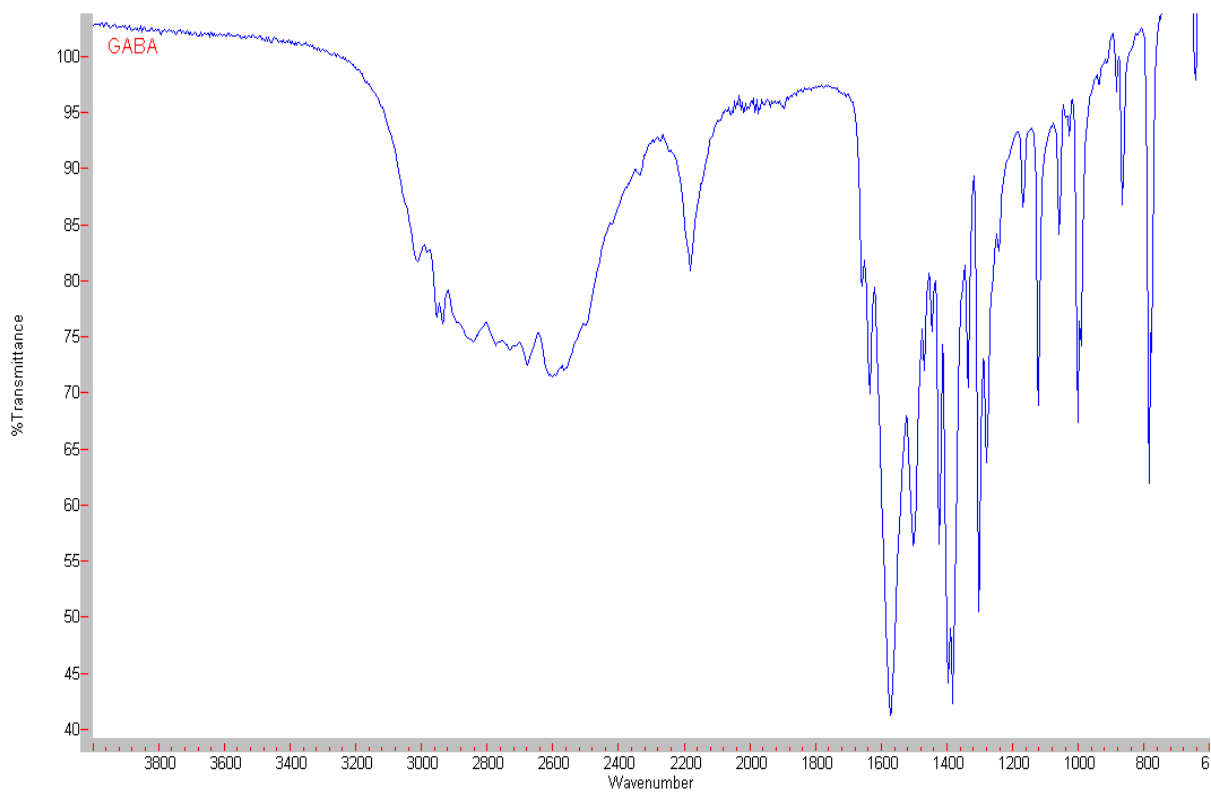
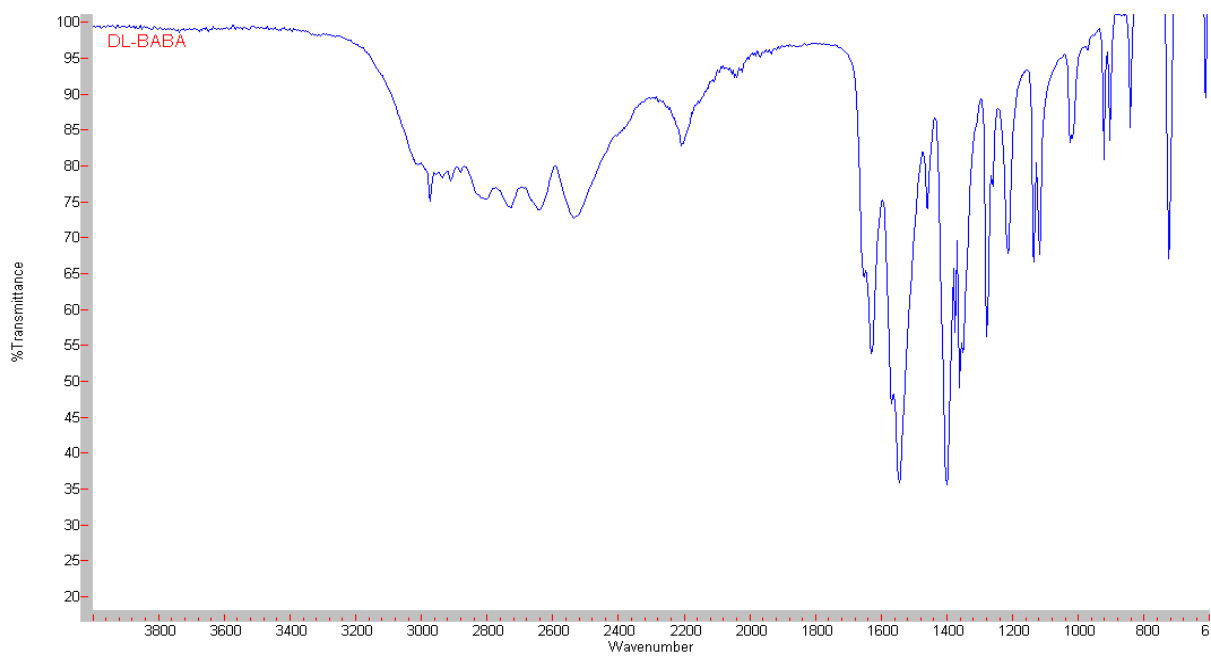
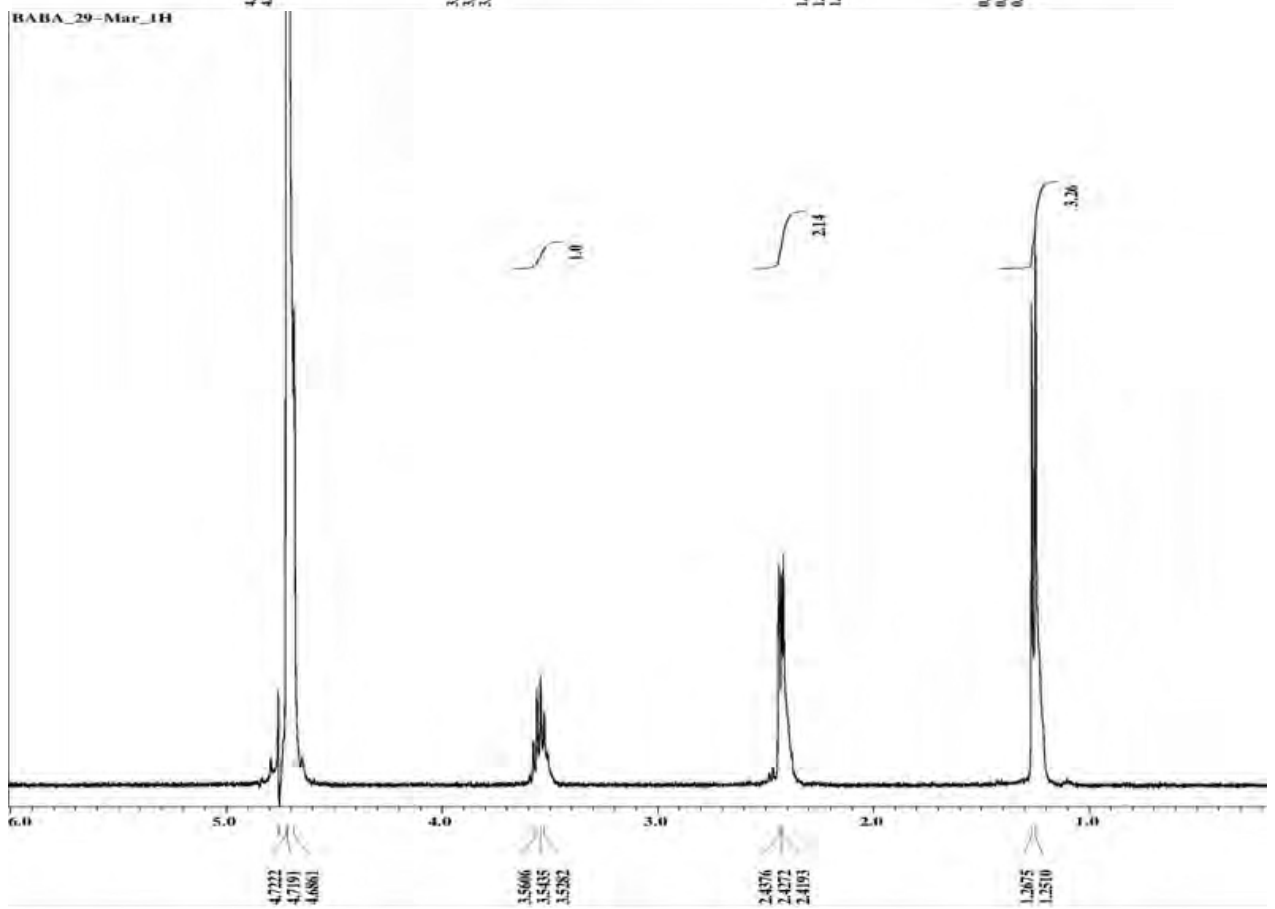
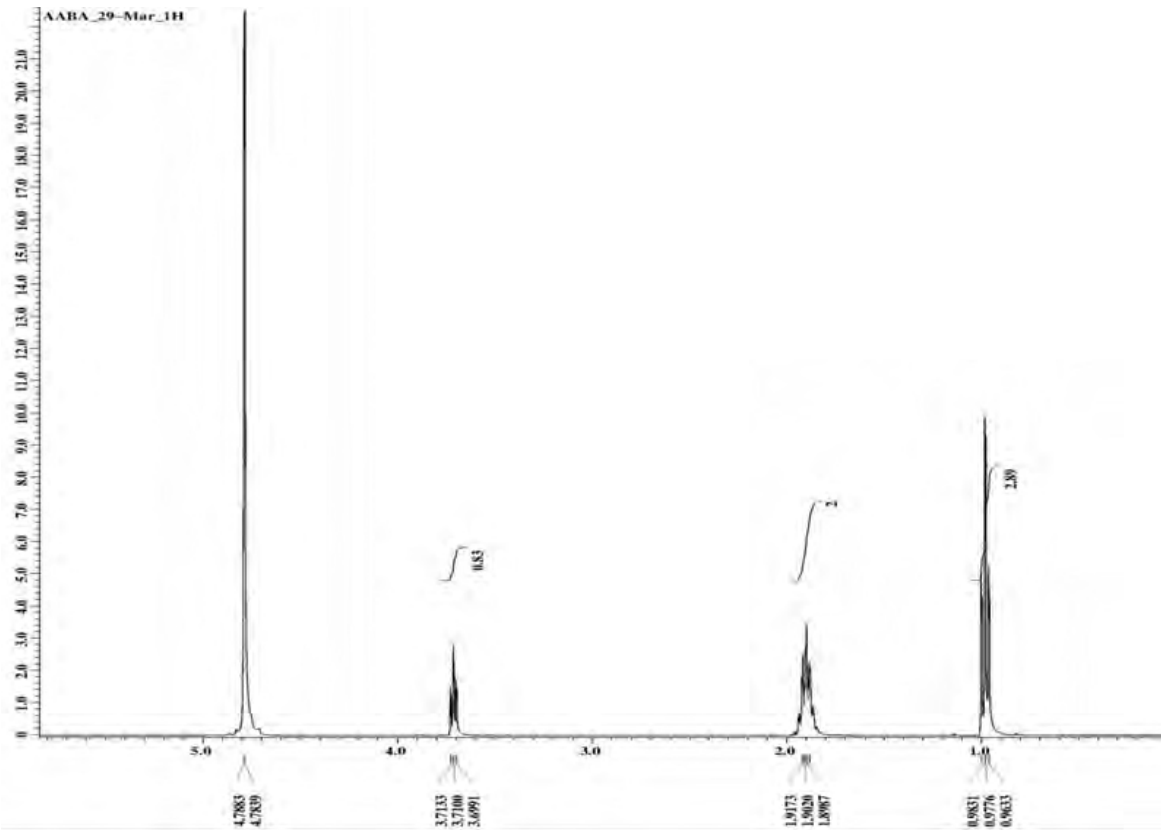


Fig. 2.1 FTIR spectra obtained for DL-AABA, DL-BABA and GABA.



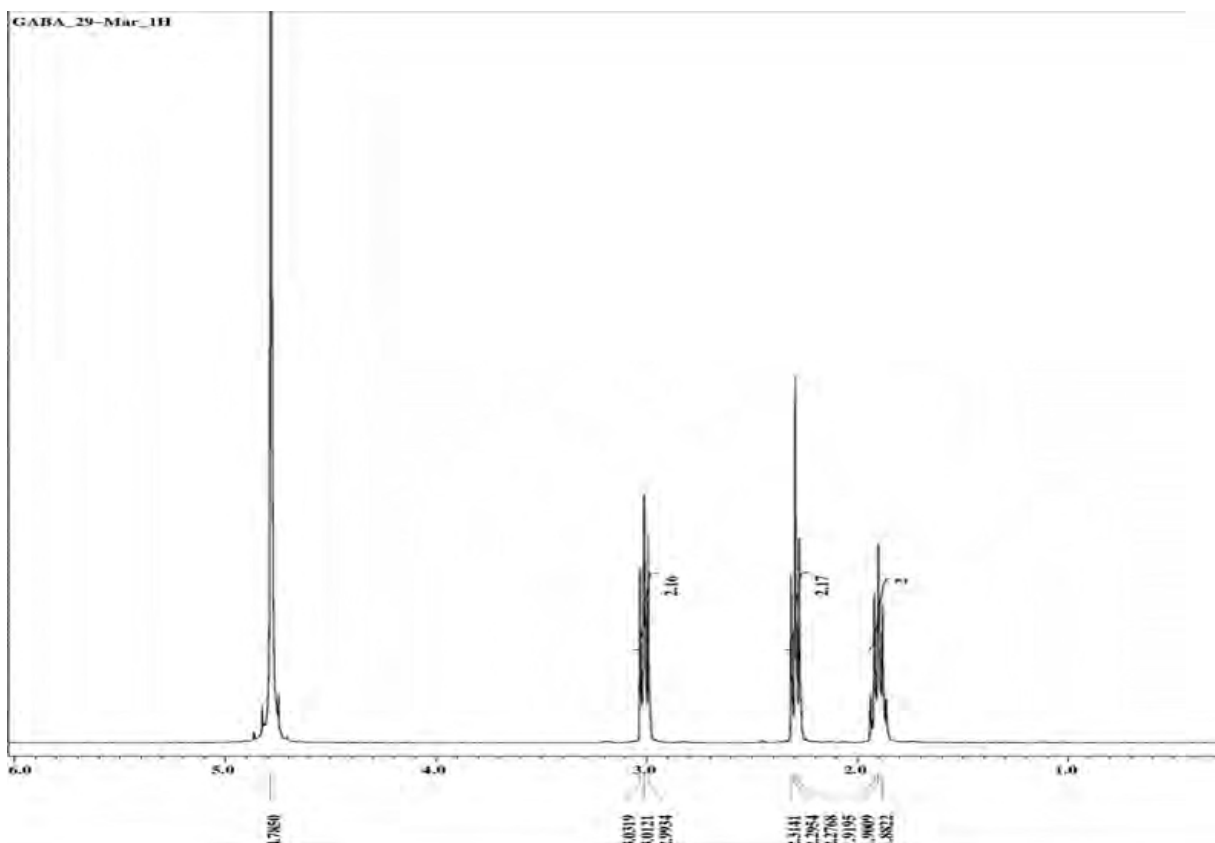
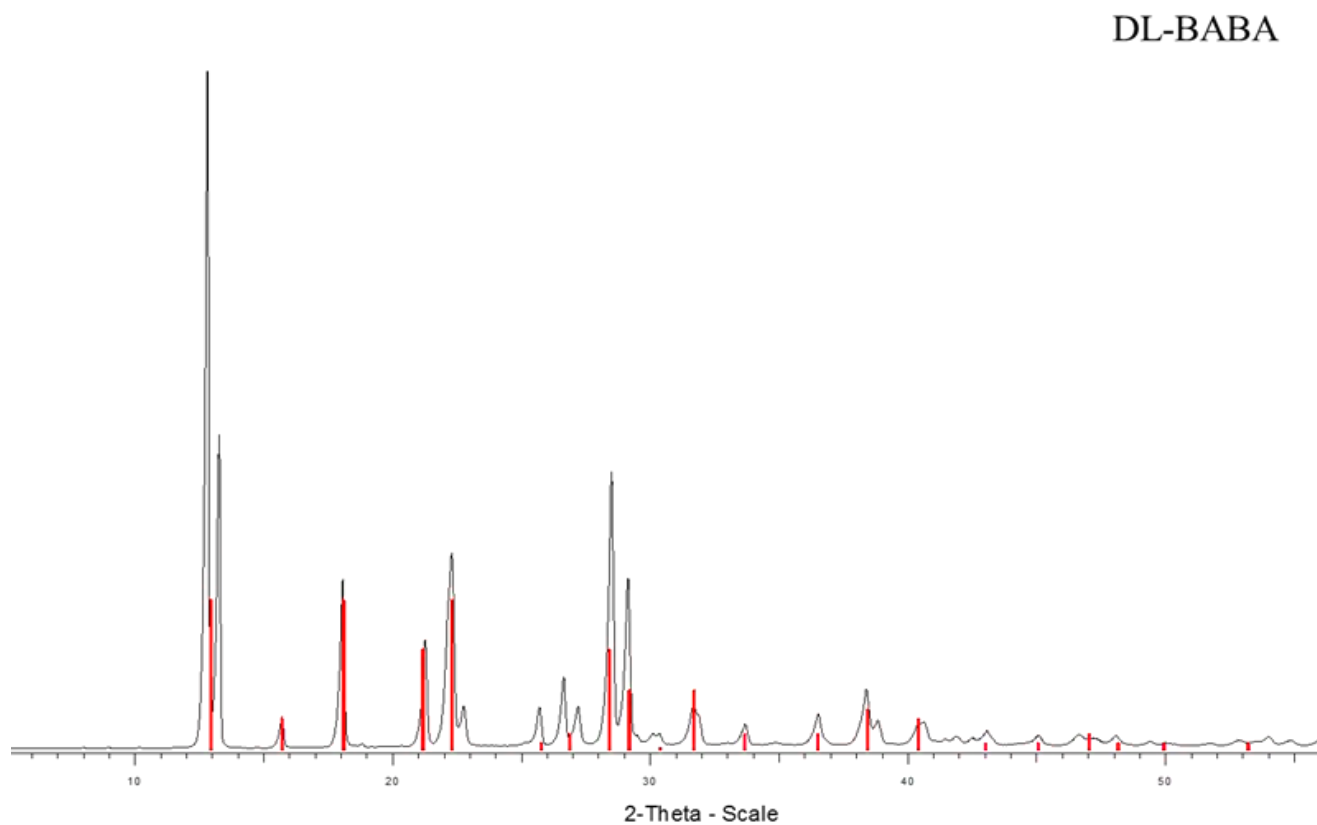
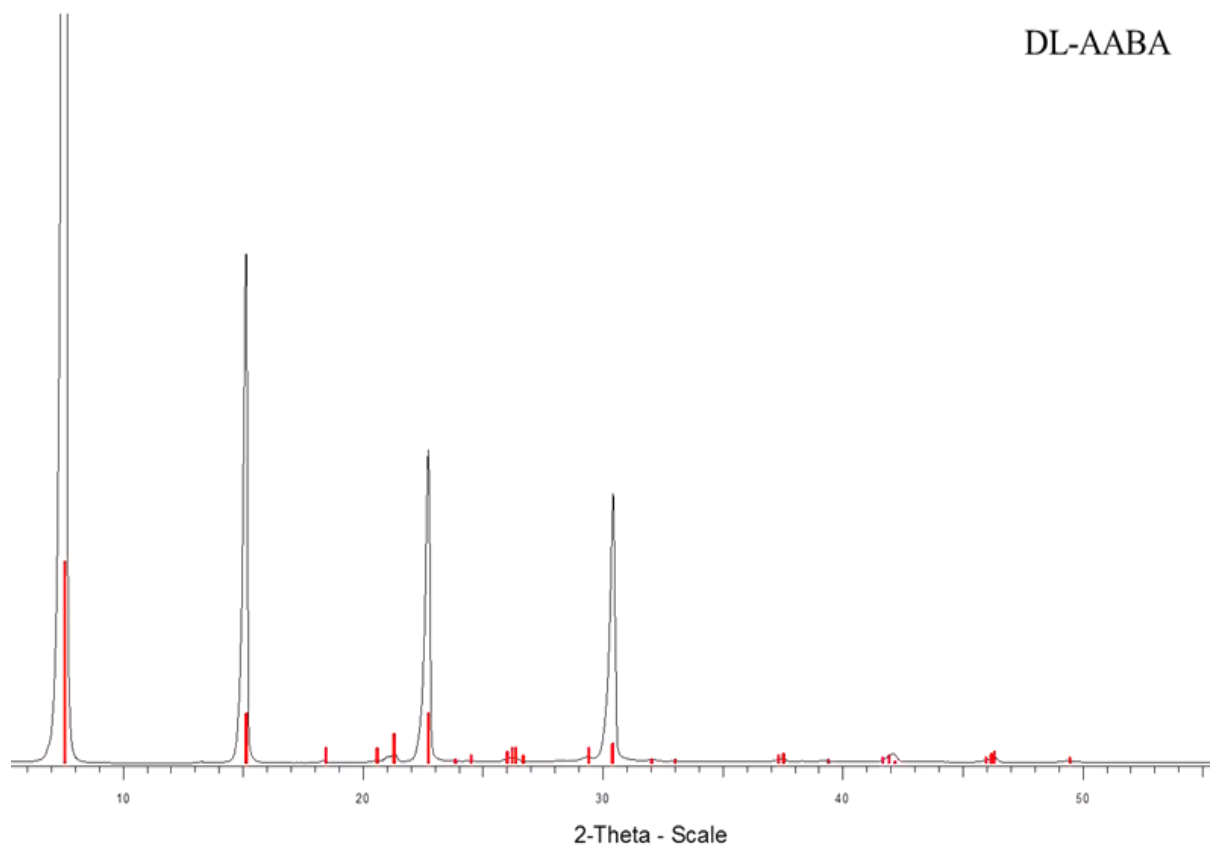


Fig. 2.2 NMR spectra of DL-AABA, DL-BABA and GABA acid obtained at 400 MHz.

X-ray powder diffraction (XRPD) analysis of the samples was carried out at ambient temperature over the range 4 to 60° 2θ using steps of 0.02 2θ counting 30 s per point, performed on D8 Bruker employing CuKα-radiation. The XRPD patterns obtained confirm the samples to be crystalline (Fig.2.3). The structure of DL-α-aminobutyric acid was found to be monoclinic with space group P21/a (14) and lattice parameters are a = 11.988 Å, b = 4.822 Å, c = 9.877 Å, β = 101.170° Z' = 4 which is in good agreement with those previously obtained by single crystal (Ichikawa and Iitaka, 1968, Voogd and Derissen, 1980). The structure for γ-aminobutyric acid was also found to be monoclinic with a space group of P21/a (14) and lattice parameters are a = 4.285 Å, b = 10.224 Å, c = 7.203 Å, β = 110.7° which also compares well with previous single crystal data (Steward et al., 1973). A preliminary prediction of DL-BABA X-RPD patterns shows a triclinic crystal system, with the space group P1 and lattice parameter, a = 5.786 Å, b = 6.709 Å, c = 7.092 Å, α = 91.6°, β = 102.1°,

$\gamma = 93.4^\circ$. However, it must be stated that the prediction yielded low correlation co-efficient and more work is required to fully determine the crystal system.



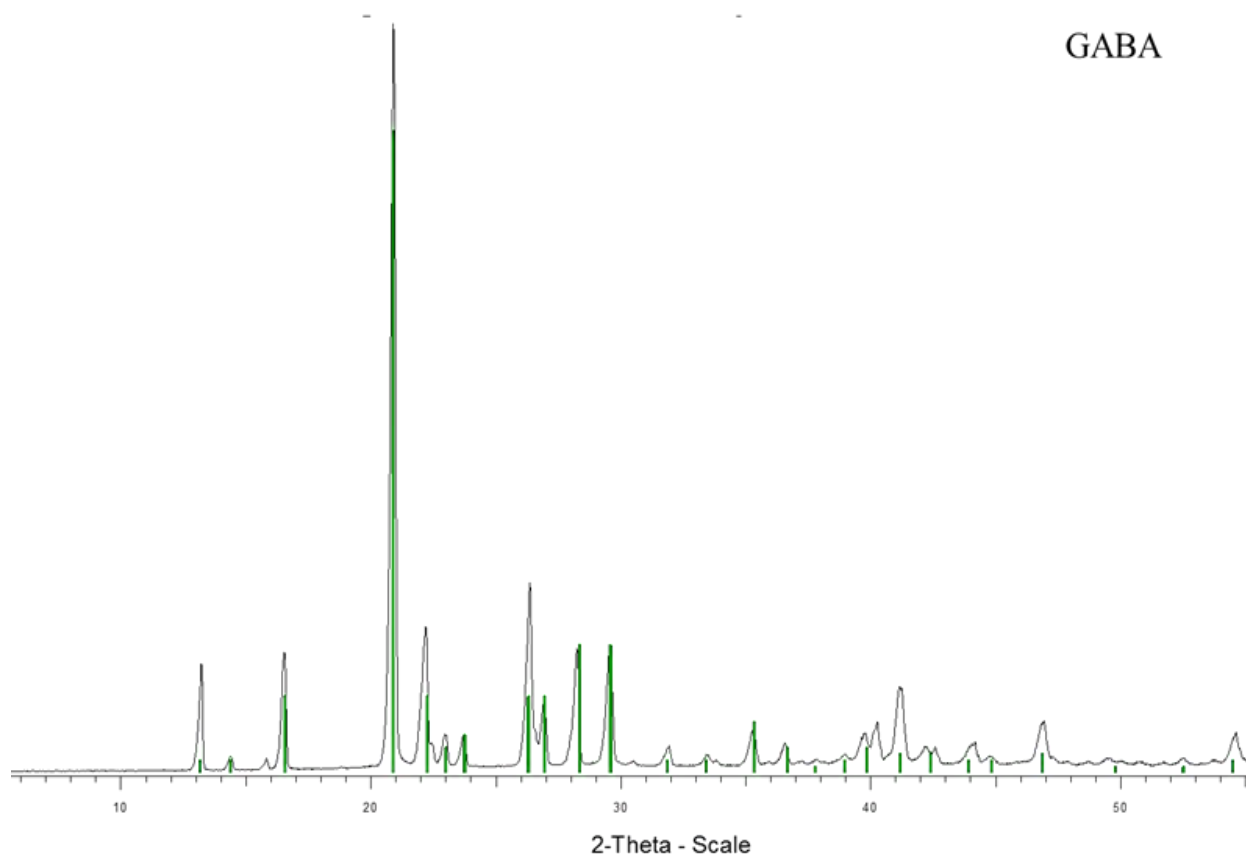


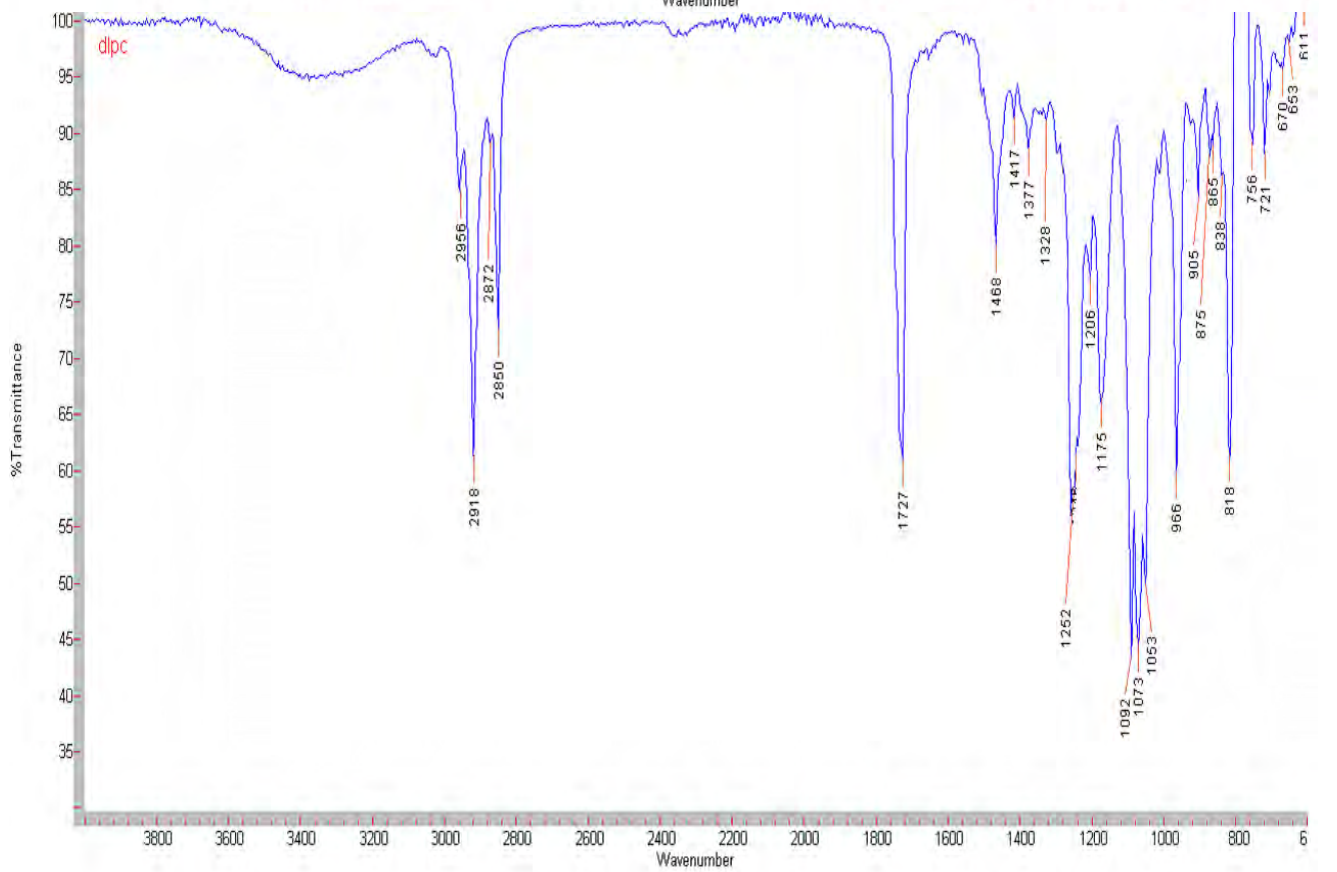
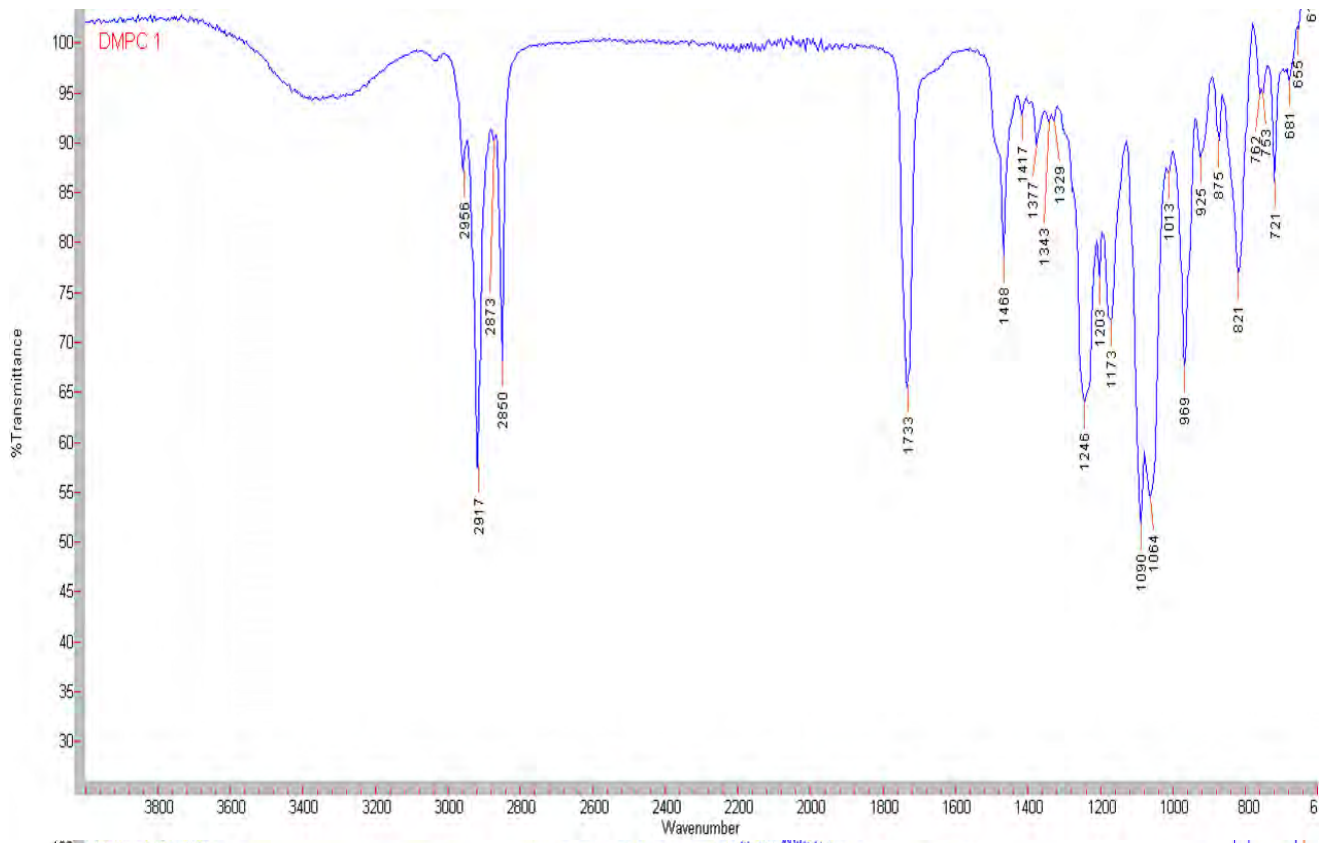
Fig. 2.3 X-ray powder diffractogram of DL-AABA, DL-BABA and GABA.

2.1.2 Phosphatidylcholines

1,2-dilauryl-sn-glycero-3-phosphocholine (DLPC), 1,2-dimyristol-sn-glycero-3-phosphocholine (DMPC), 1,2-dipalmitoyl-sn-glycero-3-phosphocholine (DPPC) and 1,2-distearoyl-sn-glycero-3-phosphocholine (DSPC) of $\geq 99\%$ were kindly provided by Lipoid (Germany). The chemical formulae for the phospholipids are $C_{32}H_{64}NO_8P$, $C_{36}H_{72}NO_8P$, $C_{40}H_{80}NO_8P$ and $C_{44}H_{88}NO_8P$ for DLPC, DMPC DPPC and DSPC, respectively. Their purity and identity were confirmed by elemental CHN analysis (Table 2.1) using a FLASHEA 112 series CHN analyzer (Thermo electron corporation). The FT-IR spectra (Fig.8. 1) acquired using MK11 golden gate (Specac) in the range 4000 to 600 cm^{-1} agrees with previously reported FTIR data of the materials (Fringeli, 1981, Chapman et al., 1967).

Table 2.2 CHN elemental composition analysis of the phosphatidylcholines ($n=3$).

Compound	Carbon chain length	Molecular weight (g mol^{-1})	% Atomic composition			
				C	H	N
DLPC	12:12	621.8	Experimental	61.09 ± 0.51	10.46 ± 0.30	2.14 ± 0.20
			Theoretical	61.81	10.37	2.25
DMPC	14:14	677.9	Experimental	62.25 ± 0.60	10.94 ± 0.45	2.00 ± 0.07
			Theoretical	63.78	10.70	2.07
DPPC	16:16	734.0	Experimental	64.79 ± 0.4	11.18 ± 0.10	1.83 ± 0.15
			Theoretical	65.45	10.99	1.91
DSPC	18:18	790.1	Experimental	66.38 ± 0.39	11.48 ± 0.09	1.84 ± 0.12
			Theoretical	66.88	11.23	1.77



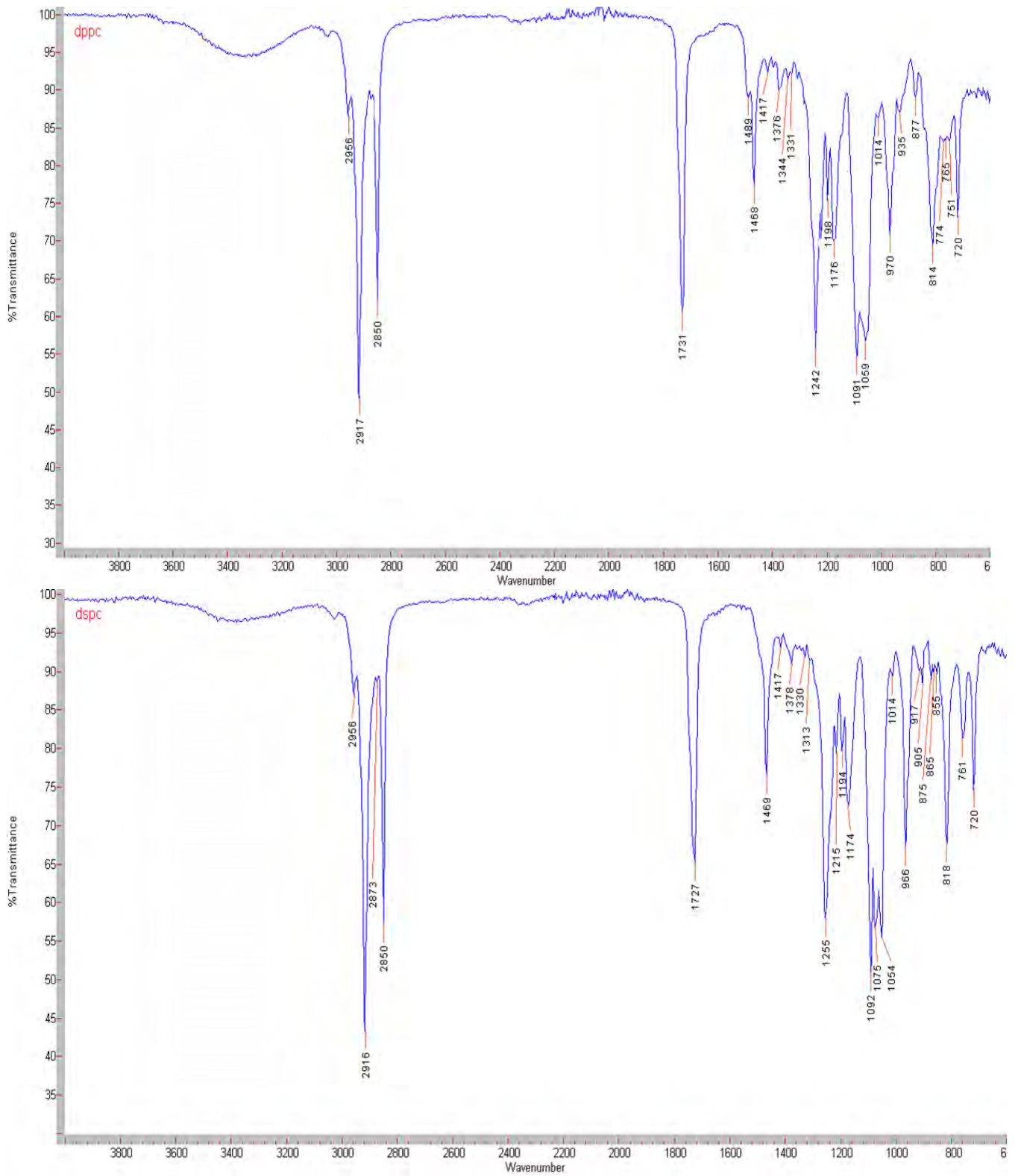


Fig. 2.4 FT-IR spectra of DLPC, DMPC, DPPC and DSPC.

2.1.3 Proteins

Insulin: Lyophilized recombinant human insulin was purchased from Biocon, Bangalore, Karnataka 560099, India.

Lysozyme: Dialyzed, lyophilized lysozyme from chicken egg white was purchased from Sigma-Aldrich St Louis, USA (Product number: 62970-F, Catalogue number: 12650-88-3, Lot number: BCBD9010V).

Myoglobin: Lyophilized myoglobin powder from Equine skeletal muscle of >95% purity, essentially salt-free lyophilized powder was purchased from Sigma-Aldrich St Louis, USA (Product number: M0630, Catalogue number: 100684, Lot number: 039K7004V).

The proteins were analysed using a nano-DSC. The temperatures and enthalpy changes of denaturation were found to be in good agreement with previously reported data when the same pH and heating rate was employed.

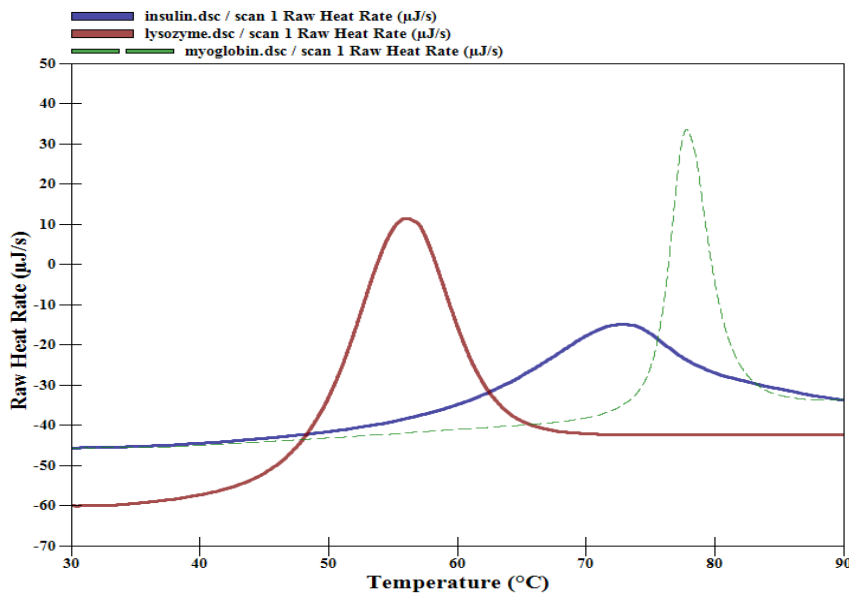


Fig. 2.5 Overlay of HSDSC thermograms for insulin (blue), lysozyme (red) and myoglobin (green) heated from 10°C to 95°C at a heating rate of 1°C/min. Concentrations used: 3, 5 and 3 mg/ml of insulin, lysozyme and myoglobin, respectively. The pH employed was 6.6 for insulin and myoglobin, and 2.4 for lysozyme.

2.2 Instrumentation

2.2.1 Thermogravimetric Analyser (TGA)

Instrument:	Q5000-IR Thermogravimetric Analyser
Manufacturer:	TA Instruments, UK
Cooling system (internal):	Compressed air cooling/water circulator
Software (control):	TA Q Series (TA Instruments, UK)
Software (analysis):	TA Universal Analysis (TA Instruments, UK)

2.2.1.1 Calibration

Temperature calibrations were performed using the Curie point of a ferromagnetic metal as described by the ASTM E1582 method. For this calibration, a magnet is placed beneath the furnace to increase the apparent weight of the certified reference materials, which in this case are alumel and nickel. When the apparent weight stabilises under the influence of the magnet, the sample is subjected to a heating programme, usually 5 and 10°C/min. The sample loses magnetism at the Curie point resulting in a sharp drop in the loss of the apparent weight. The extrapolated end point temperature is calculated. The expected Curie point for the certified alumel and nickel materials is 152.26 and 358.28°C respectively. The instrumental software automatically computes the offset between the experimental and reference Curie point temperatures and stores the value in a calibration temperature table.

Weight calibrations were performed using known calibration weights provided by the manufacturer. For this calibration an empty sample pan and 100 mg standard weight are weighed and automatic adjustments of the balance is performed until the weight reading matches that of the standard weight.

Unless otherwise stated, samples are introduced into the furnace in a Tzero hermetically sealed aluminium sample pan with a single pinhole in the lid. Samples were heated under a

nitrogen atmosphere at a flow rate of 25 ml/min from ambient to a maximum of 600°C at various heating rates.

2.2.2 Differential scanning calorimetry (DSC)

Instrument:	DSC Q2000
Manufacturer:	TA Instruments, UK
Cooling system (internal):	Refrigerated cooling system (RCS)
Software (control):	TA Q Series (TA Instruments, UK)
Software (analysis):	TA Universal Analysis (TA Instruments, UK)

2.2.2.1 Calibration

The calibration of the TA Instruments Q2000 instrument is performed in two parts. The first part is the determination of the cell resistance and capacitance. For this calibration two experiments are performed. The first experiment is the determination of the cell resistance and it is performed with an empty cell. During this experiment the cell is equilibrated at -90°C and held isothermal for 5 minutes, followed by a heating ramp from -90 to 400°C at 20°C/min. Important to note that a preheating experiment using the same parameter is usually performed. The second part of the calibration is to determine the cell capacitance, which involves the same experimental method as the cell resistance but with sapphire discs of known weight and heat capacity on the reference and sample cell.

The next calibration involves the determination of the cell constant and temperature calibration, which are obtained from a single experiment.

In this experiment 1-5 mg of indium standard is pre-heated to above the melting transition temperature i.e. 180°C and held isothermally. The sample is then cooled to 100°C held isothermal and subjected to a heating ramp (usually 10°C/min) to a temperature above the melting transition. The enthalpy of fusion is determined by integration and compared with the known value (28.71 J/g). The cell constant is the ratio between the experimentally determined

and expected value and should be between 1 and 1.2. The melting temperature is determined using the extrapolated onset, and this is also compared with the known value (56.6°C) and the difference is calculated for temperature calibration.

2.2.3 Thermally Stimulated Current (TSC) spectroscopy

Instrument:	TSCII, Thermally Stimulated Current spectrometer
Manufacturer:	SETARAM Instrumentation, France
Electrometer (internal):	6517A electrometer/high-resistance meter (Keithley, UK)
Cooling system (external):	900 series LN2 microdosing system (Norhof, Netherlands)
Software:	TSC/RMA software (SETARAM Instrumentation, France)

2.2.3.1 Calibration

The only calibration that needs to be carried out before analysis is a temperature calibration using indium (In) standard. The objective of the calibration is to compensate for the temperature difference between the temperature sensor and the sample area. The instrument comes with a special calibration kit (Fig. 2.6) that consists of a calibration electrode probe which holds the indium sample firmly in place against the PTFE cup. The dimple in the electrode absorbs the molten indium upon heating to prevent it from flowing out to the edge of the electrode. This is important as it lowers the noise generated during the melting of indium.

Fig. 2.6 SETARAM TSC II calibration kit set up (SETARAM TSC II manual).

In the calibration experiment the indium sample is firstly heated to 190°C, which is about 40°C above the melting point. This preheating process removes any internal stress. A

polarisation voltage of 1V/mm is applied as the sample is kept at 190°C for 3 mins. The response of the indium sample is recorded as the sample is being cooled and heated at the same rate, allowing the determination of the temperature onsets for crystallisation (T_c) and melting (T_m) processes (Fig. 2.7).



Fig. 2.7 Calibration results showing the onsets of crystallisation and melting processes (SETERAM TSC II manual).

The offset is calculated by comparing the experimentally determined onsets with expected values ($T_m = 156.6^\circ\text{C}$ and $T_c = 155.0^\circ\text{C}$) i.e. the offset is given by the subtraction of the experimental onsets from the expected values.

Chapter 3 : Influence of Positional Isomerism on Solid-state Molecular Mobility and Thermal Stability of Aminobutyric Acids

3.1 Introduction

Positional isomers of aminobutyric acid are an interesting group of molecules to study as they exhibit very different functional roles in nature. α -Aminobutyric acid (AABA; Fig.3.1(a)) is a key intermediate in the biosynthesis of ophthalmic acid (first isolated from calf lens) which is a tri-amino acid peptide analogue of glutathione; ophthalmic acid has been proposed as a biomarker for oxidative stress (Soga et al., 2006). AABA has also been investigated as a measure of hepatic injury in sepsis (Effros, 2011). The importance of the chemical synthesis of optically pure non-proteinogenic amino acids, such as AABA and DL- β -aminobutyric acid (BABA; Fig.3.1(b)), as building blocks for pharmaceutical compounds have been highlighted (Shin and Kim, 2009). BABA has been shown to be effective in enhancing resistance to TMV in tobacco plants (Siegrist et al., 2000) and in this respect exhibited isomeric specificity compared to AABA (very little activity) and γ -aminobutyric acid (GABA; no activity). GABA (Fig.3.1(c)) is found in plants (Park et al., 2010) where it is the most abundant amino acid in the apoplast of tomatoes; it may also have a role in cell signalling in plants (Roberts, 2007). GABA is the chief inhibitory neurotransmitter in the mature mammalian central nervous system. It plays a central role in regulating neuronal excitability throughout the nervous system (Owens and Kriegstein, 2002). In humans, GABA is also directly responsible for the regulation of muscle tone (Watanabe et al., 2002).

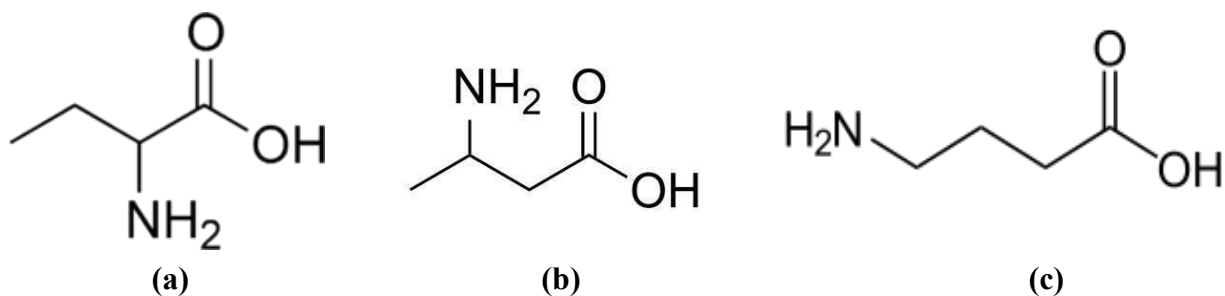


Fig. 3.1 Chemical structures of (a) α -aminobutyric acid (AABA), (b) β -aminobutyric acid (BABA) and (c) γ -aminobutyric acid (GABA).

Studies of relaxation process in small molecular compounds using TSC spectroscopy are limited, especially for small molecular crystalline materials such as butyric acids. This is attributed, in part, to the perceived difficulty in understanding the origin of the relaxation processes detected. Furthermore, the significance of molecular relaxations in small molecular crystalline compounds in relation to stability is not well understood.

The purpose of the research reported herein is to assess solid-state relaxation processes of butyric acids that differ only by the position of the amine group, in an attempt to understand the influence of positional isomerism on molecular mobility. The focus is to elucidate the relationship between the parameters of molecular mobility measured by TSDC at lower temperatures and the relative thermal stability of the butyric acids, as observed by TGA and DSC. The positional isomers of aminobutyric acids are good model compounds for this study because of their “simple” molecular structure and the small change in atomic arrangement is expected to cause significant differences in thermal behaviour.

3.2 Methods

3.2.1 TGA

A sample mass of 2.00 ± 0.06 mg was used for all compounds. Samples were heated to 350°C in hermetically sealed aluminium pans with a single pin hole in the lid, at a heating rate of $2^\circ\text{C}/\text{min}$.

3.2.2 DSC

DSC studies were performed using hermetically sealed Tzero aluminium pans with a pin hole in the lid from TA instruments (UK). Sample mass of 0.57 ± 0.05 mg was equilibrated at 50°C , held isothermal for 5 min and heated to 350°C .

3.2.3 TSDC

Experiments were performed using 60 ± 1 mg samples compressed to ~ 1.3 mm thickness and 8 mm diameter tablets (using a pressure of 500 psi). Tablets were placed between the parallel electrodes (with an effective surface area of 38.5 mm^2) of the TSC instrument. Prior to an experiment, the TSC analysis chamber, containing the sample, was evacuated to 10^{-4} mbar and flushed several times with high purity helium (1.1 bar). The global TSDC spectra were obtained by polarising the sample at 100°C ($T_p = 100^\circ\text{C}$) with a polarisation field (E_p) of 20, 40, 60, 80, 100, 120 and 160 V/mm for 2 min (t_p). The sample was then rapidly cooled to a temperature (T_o) -20°C , where all dipole mobility in the system was assumed to be frozen. The polarisation field was then switched off and the sample is held at T_o for a short time (t_o). The depolarisation current was measured as the sample was heated at a controlled rate of $10^\circ\text{C}/\text{min}$ to a final temperature (T_f) of 170°C which is above the T_p (temperature of polarisation). In the case of thermal windowing experiments, samples were polarised with $E_p = 160$ V/mm at T_p of 40 to 130°C in increments of 3°C for DL- β -aminobutyric acid and γ -aminobutyric acid ($T_w = 3^\circ\text{C}$) and 40 to 168°C increasing by 4°C increments for DL- α -aminobutyric acid ($T_w = 4^\circ\text{C}$). The values of t_p and t_w were set at 2 min for all three samples and the T_f at 150°C for DL- β -aminobutyric acid and γ -aminobutyric acid and 170°C for DL- α -aminobutyric acid.

3.3 Results and Discussion

3.3.1 TGA and DSC

The results obtained from TGA and DSC studies show that the thermo-physical and thermo-chemical behaviour of aminobutyric acid in the solid-state are significantly influenced

by the positional isomerism. From the TGA results (Fig.3. 2), it can be observed that DL-AABA and GABA undergo a single weight loss (100%) process, when heated from ambient temperature to 350°C. DL-BABA, on the other hand, undergoes a two stage decomposition process with weight changes of 83.9 ± 0.1 and $16.1 \pm 0.1\%$ for the first and second processes, respectively (Table 3. 1).

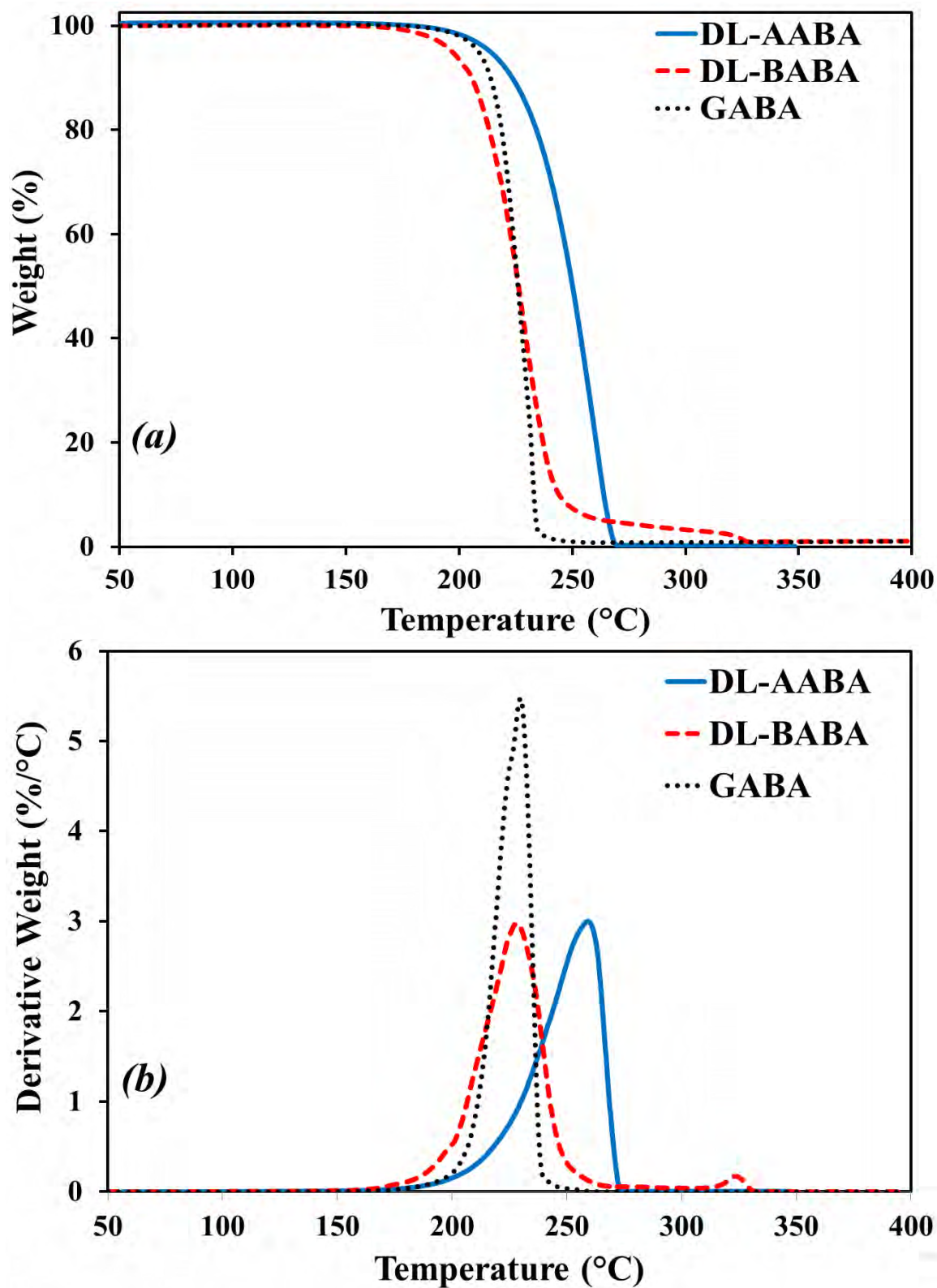


Fig. 3.2 TGA curve overlay of DL-AABA, DL-BABA and GABA heated from ambient temperature to 340°C at 2°C/min. (a) Thermogravimetric (TG) curves and (b) derivative thermogravimetric (DTG) curves.

Table 3.1 The weight changes, onset temperatures and the temperature at the derivative peak maxima associated with the processes observed in TGA studies for the butyric acids.

Compound	Process 1			Process 2	
	Extrapolated onset (°C)	DTG peak (°C)	% Δ Weight	DTG peak (°C)	% Δ Weight
DL-AABA	228 \pm 2	260 \pm 1	99 \pm 1	-	-
DL-BABA	173 \pm 1	193 \pm 1	84 \pm 1	303 \pm 2	16 \pm 1
GABA	179 \pm 1	193 \pm 1	99 \pm 2	-	-

DSC results for DL-AABA, DL-BABA and GABA (Fig.3. 3), with the aid of hot-stage microscopy, show that the single step weight loss process observed for DL-AABA in TGA studies is due to sublimation. DL-BABA undergoes melt-decomposition behaviour and this is detected as a sharp melting endotherm observed at 187°C, which overlaps with the broader decomposition endotherm at 201°C. This is followed by further decomposition at 312°C. GABA also exhibits overlapping melt-decomposition behaviour. The thermodynamic parameters associated with these thermal events are shown in Table 3. 2.

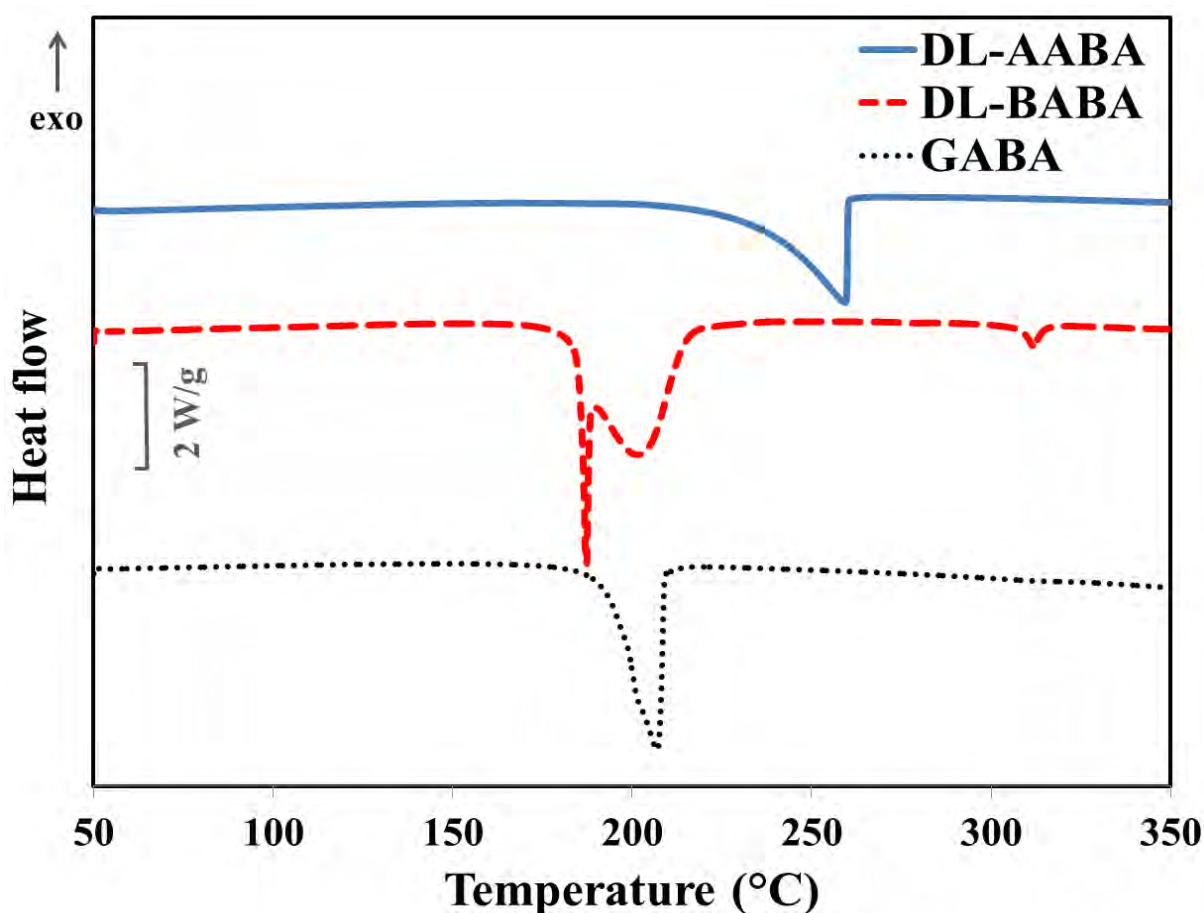


Fig. 3.3 Overlay of the thermograms observed for DL-AABA, DL-BABA and GABA heated from -90 to 350°C at 2°C/min.

Table 3.2 Temperatures and heat changes observed for the endothermic processes observed for DL-AABA, DL-BABA and GABA (n=3).

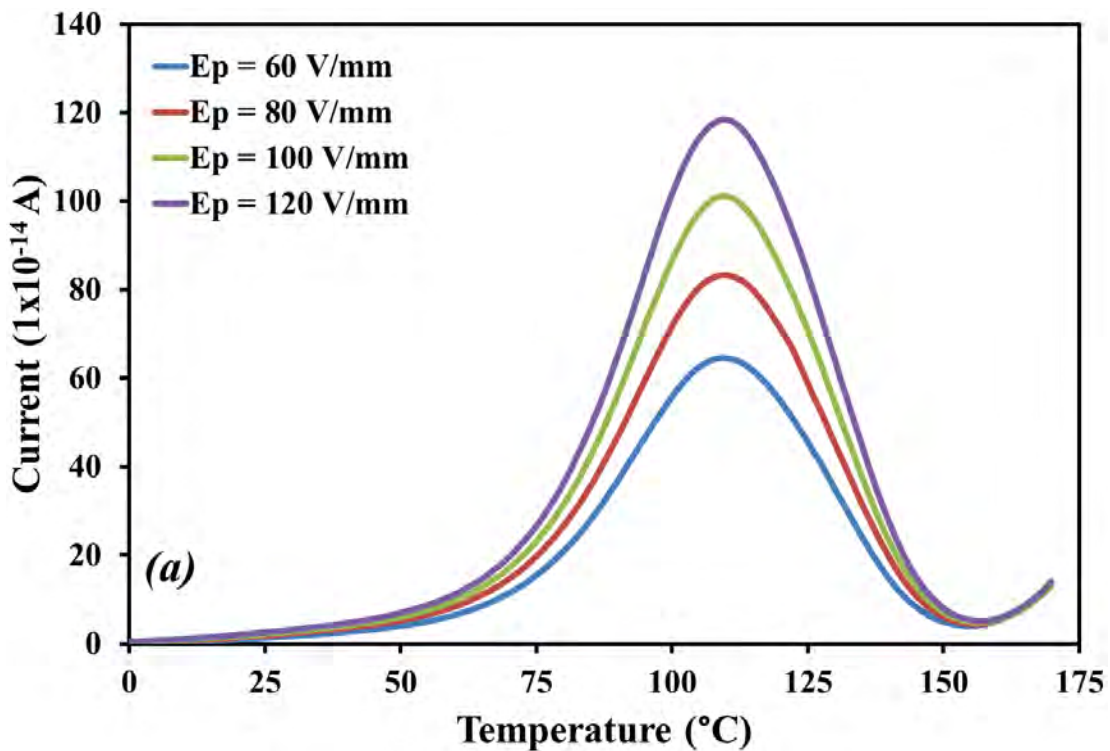
Compound	Process 1				Process 2		
	Onset (°C)	Peak 1 (°C)	Peak 2 (°C)	ΔH (J/g)	Onset (°C)	Peak (°C)	ΔH (J/g)
DL-AABA	234 ± 1	259 ± 1	-	1151 ± 50	-	-	-
DL-BABA	185 ± 1	187 ± 1	201 ± 1	1722 ± 316	308 ± 1	312 ± 1	59 ± 10
GABA	195 ± 1	207 ± 1	-	1121 ± 23	-	-	-

By considering the extrapolated onset temperature obtained from both the TGA and DSC studies (Tables 3.1 and 3.2), it is clear that the DL-AABA is the more thermally stable

positional isomer, followed by GABA. The least thermally stable positional isomer is DL-BABA.

3.3.2 Global TSDC

Fig.3.4 (a-c) shows the depolarisation current profile as a function of temperature for DL-AABA, DL-BABA and GABA obtained after polarising with different electrical field strengths. Increasing the electrical field strength increases the current intensity at the T_{max} . The correlation coefficient for the relationship between current intensity at T_{max} and the strength of the applied electric field were all > 0.999 (Fig.3. 5). This confirms that the processes observed result from dipole orientations i.e. they are an intrinsic property of the materials studied and not artefacts.



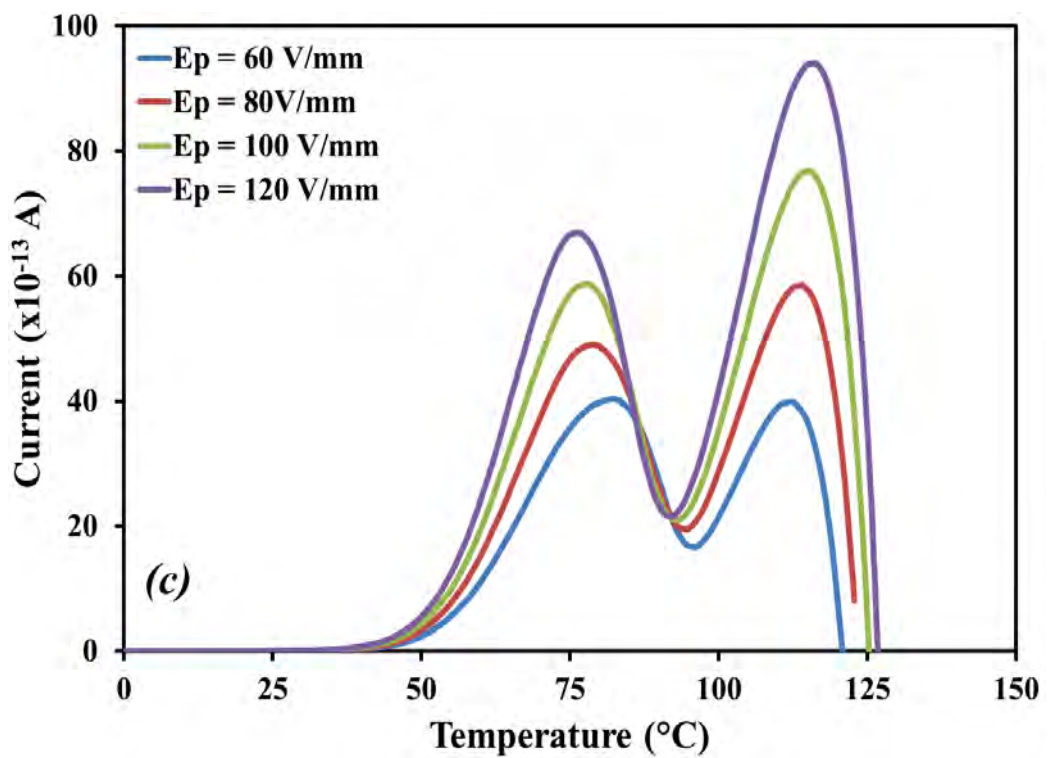
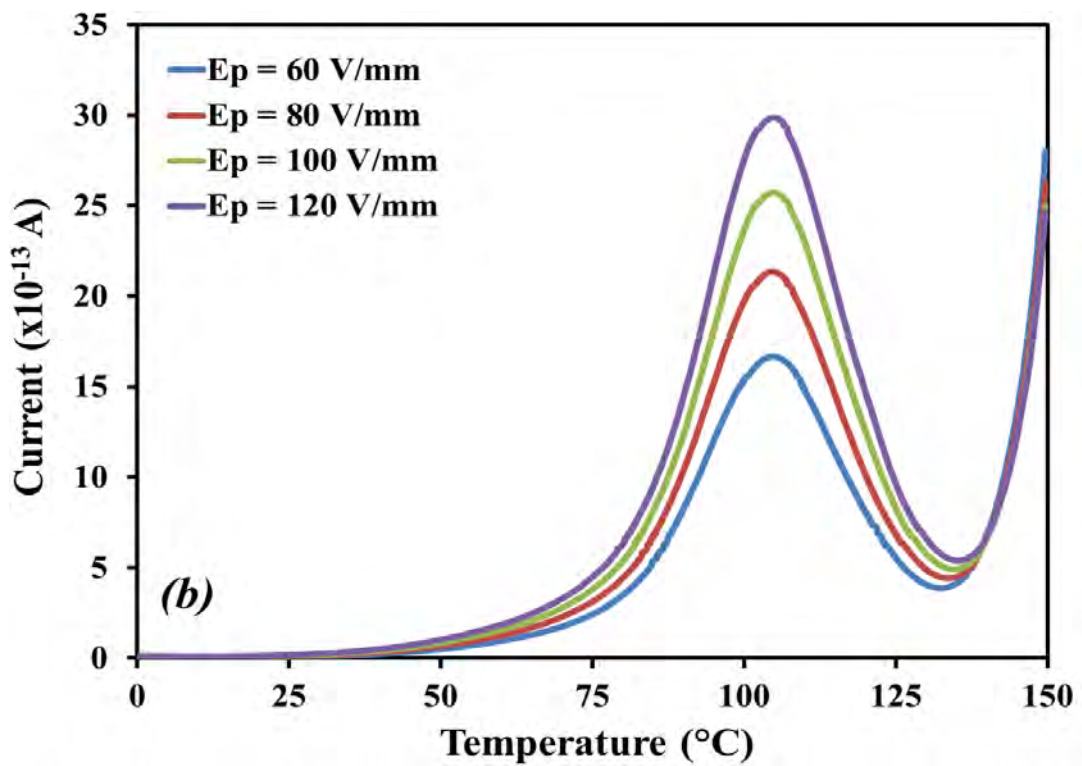


Fig. 3.4 Global TSDC obtained using different electrical field strengths (V/mm) for (a) DL-AABA, (b) DL-BABA and (c) GABA.

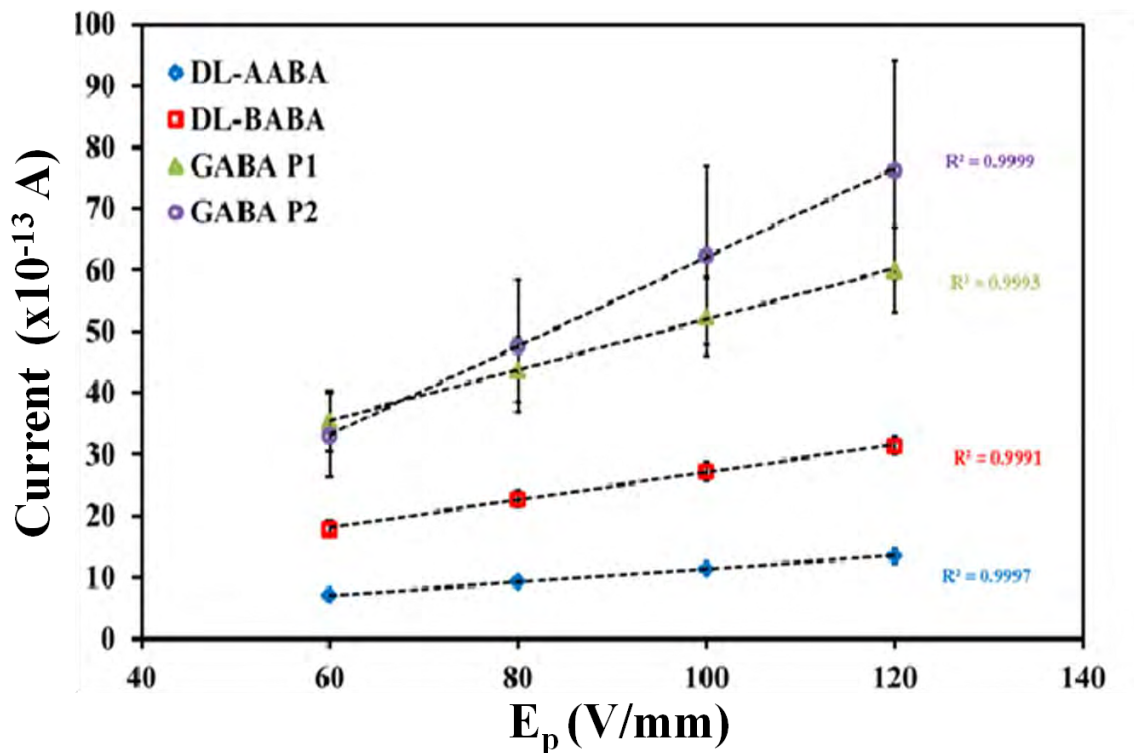


Fig. 3.5 A linear regression plot of current intensity at T_{\max} vs applied electrical field strength (E_p) for the aminobutyric acids.

A comparison of the three aminobutyric acids in the data presented in Fig.3.6 show that changing the position of the amine functional group has a significant influence on the global relaxation curves i.e. increasing the distance between the carboxyl and amino group decreases both the width and T_{\max} of the depolarisation current, while increasing the current intensity at T_{\max} .

GABA exhibits two global depolarisation modes at $77 \pm 2^\circ\text{C}$ and $114 \pm 2^\circ\text{C}$, both with greater current intensity than that observed for DL-AABA at $109 \pm 1^\circ\text{C}$ and DL-BABA at $104 \pm 1^\circ\text{C}$ when polarised at 100°C with a polarising field of 120 V/mm. It should be noted that the second half of the 2nd global relaxation process observed for GABA is characteristic of charge conduction (Turnhout, 1975).

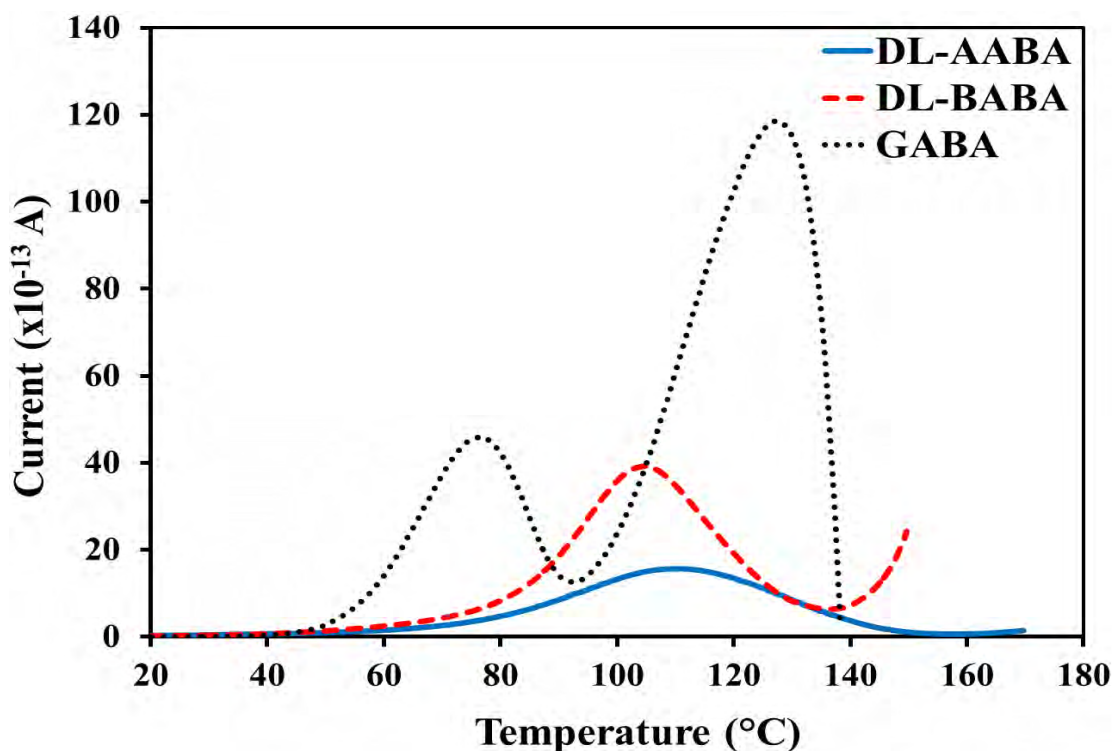


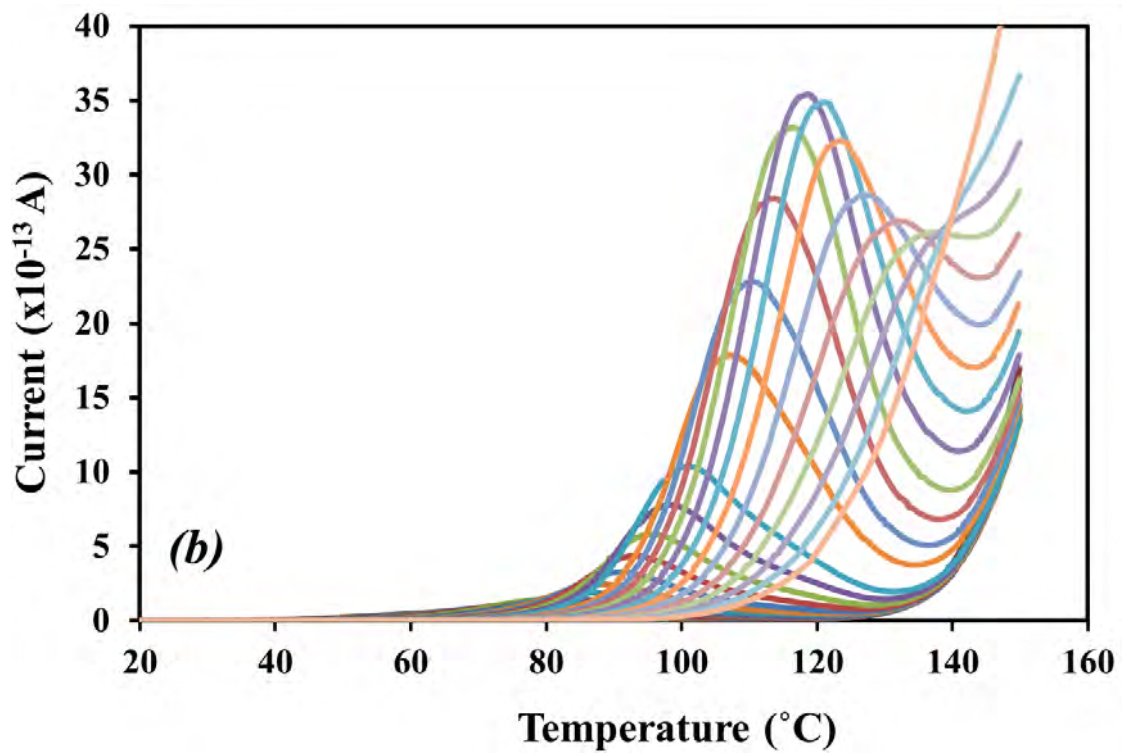
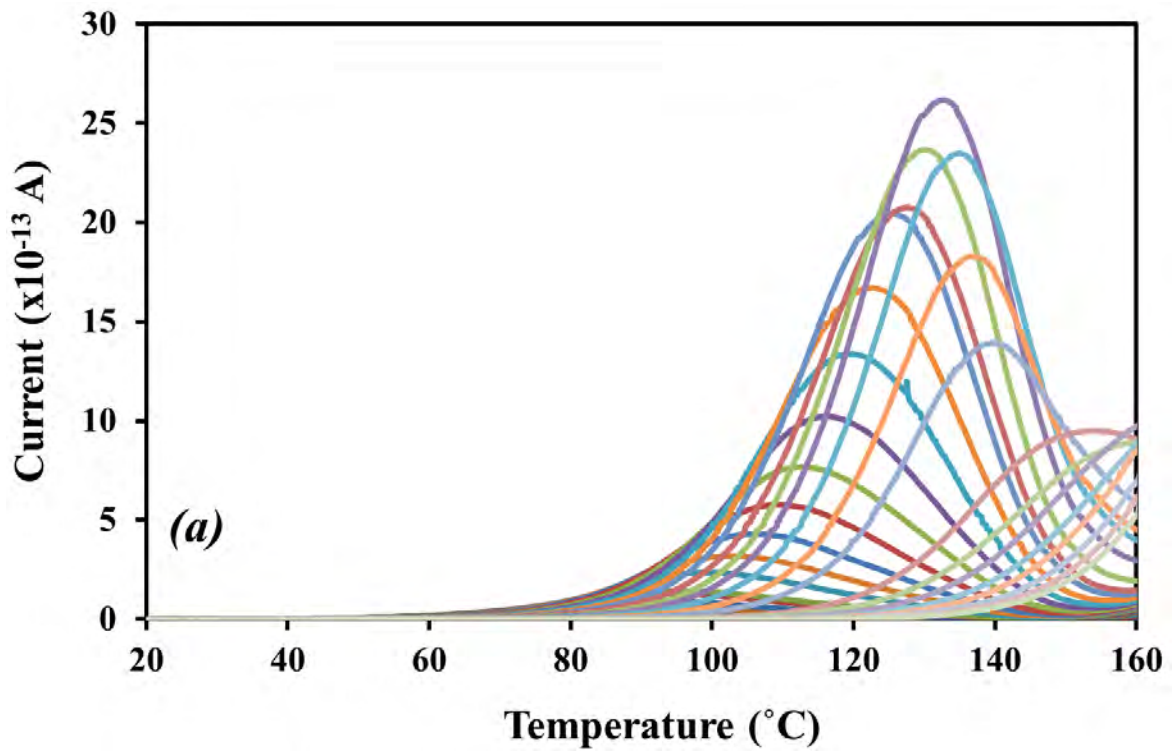
Fig. 3.6 Global TSDC curve overlay of DL-AABA, DL-BABA and GABA polarized at 100°C with a polarizing field of 120 V/mm for GABA and 160 V/mm for DL-AABA and DL-BABA.

The observed differences in the current intensities and T_{\max} for the global dipole relaxation modes of the aminobutyric acid isomers suggest that at lower temperatures the order of dipole mobility is: GABA > DL-BABA > DL-AABA.

Based on these observations, it is concluded that increasing the distance between the amine and carboxyl groups for aminobutyric acid increases motional freedom in the solid-state.

3.3.3 Thermal Windowing

The results obtained for the thermal windowing experiments are presented in Fig. 3. 7. These curves show the “elementary” dipole relaxation modes for the global relaxation processes shown in Figs.3.4 and 3.6.



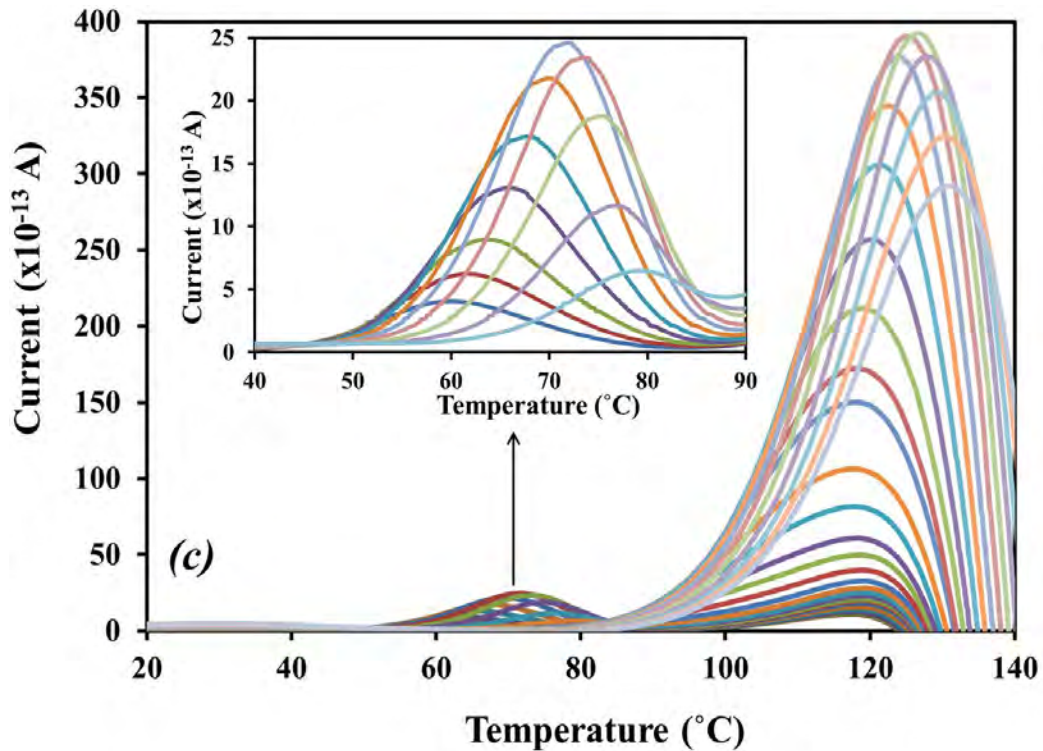


Fig. 3.7 The discrete relaxation modes of the global relaxation processes for (a) DL-AABA, (b) DL-BABA and (c) GABA obtained by the partial polarisation method.

The temperature dependent relaxation time ($\tau(T)$) for these elementary relaxation modes were determined using the Bucci method (Correia, 1997), as explained in Chapter 1. The distributions of relaxation times as a function of temperature for each elementary relaxation process are presented in Fig.3.8.

The distribution of relaxation times obtained for the DL-AABA, DL-BABA and the first relaxation process for GABA all exhibit linear Bucci lines. However, the Bucci lines observed for the second relaxation process for GABA (GABA P2) show significant curvature for the first four lower temperatures of polarisation. The origin of such curvature is not completely clear; however, it is believed that Bucci line curvature may result from a collection of motional modes that are not narrowly distributed, and may encompass several discrete modes (Correia et al., 2000). The Bucci line curvature observed for this process is more likely to be due to space charge contribution and/or overlap of GABA P1 and GABA P2.

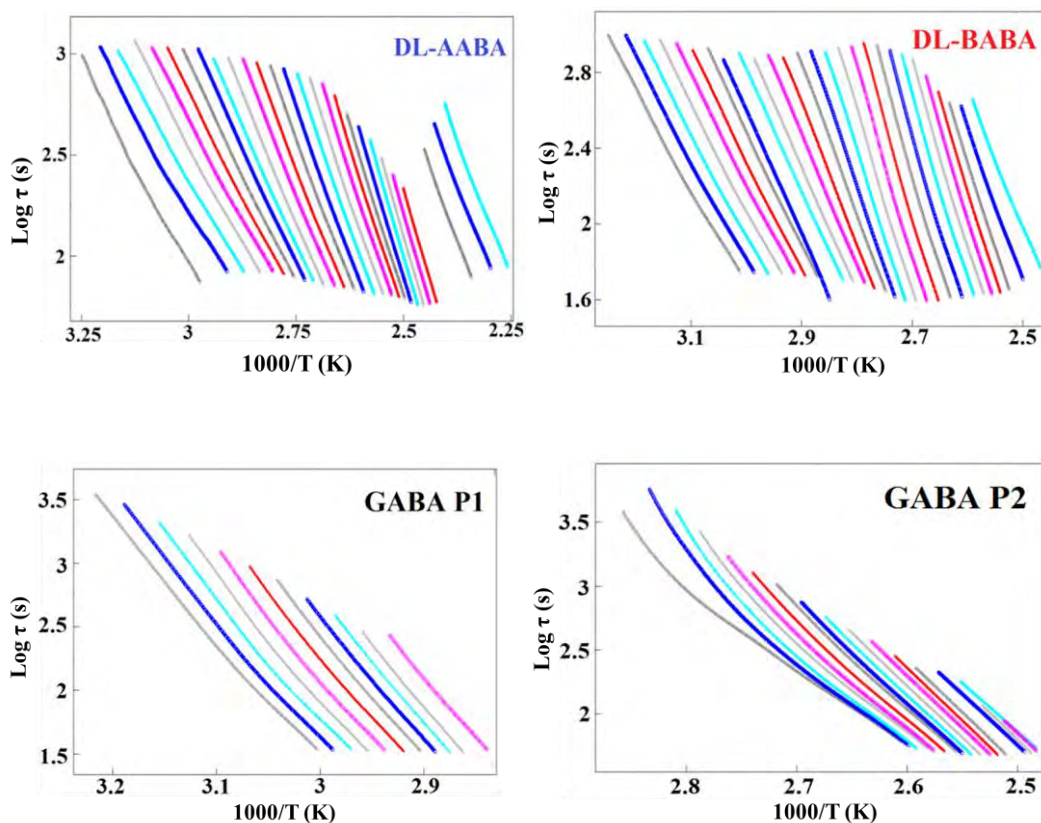


Fig. 3.8 Distribution of relaxation time as a function of temperature determined for each elementary relaxation obtained using the Bucci method.

The fitting of the Bucci lines to appropriate kinetic equations, usually Arrhenius and Eyring, yields kinetic parameters (such as pre-exponential factor/frequency factor (τ_0), activation energy (E_a), enthalpy of activation (ΔH^\ddagger) activation entropy (ΔS^\ddagger)) that characterises each elementary relaxation mode (Neagu and Neagu, 2006).

In general, ΔH^\ddagger is plotted as a function of T_{\max} and the T_{\max} of the elementary relaxation mode with the highest E_a value usually corresponds to the T_{\max} of the global relaxation process. This is also true when ΔS^\ddagger is plotted against T_{\max} when using the Eyring equation. Because E_a changes simultaneously with τ_0 , a plot of $\log \tau_0$ vs T_{\max} also provides the same information. Since these kinetic parameters attained from the Arrhenius and Eyring equations allow similar conclusions to be drawn (Ramos and Mano, 1997), a plot of $\log \tau_0$ vs T_{\max} (as the pre-exponential factor is an indicator of the frequency of relaxation) was used. By considering the $\log \tau_0$ values, obtained from the Arrhenius equation, it is clear that dipole relaxations are more

frequent for GABA P1 in comparison to that observed for AABA, BABA and GABA P2 i.e. the lower the $\log \tau_0$ (s) value the higher the relaxation frequency, hence the faster the elementary relaxation modes.

An interesting observation, using the data displayed in Fig.3. 9, is made when the initial relaxation processes are considered i.e. if only the 1st relaxation process is considered for GABA, it becomes apparent that relaxation frequency increased ($\log \tau_0$ decreased) with increasing distance between the amine and the carboxyl group. For example, the lowest $\log \tau_0$ value is observed for GABA (process 1 (P1), while the highest is observed for DL-AABA (Table 3. 3).

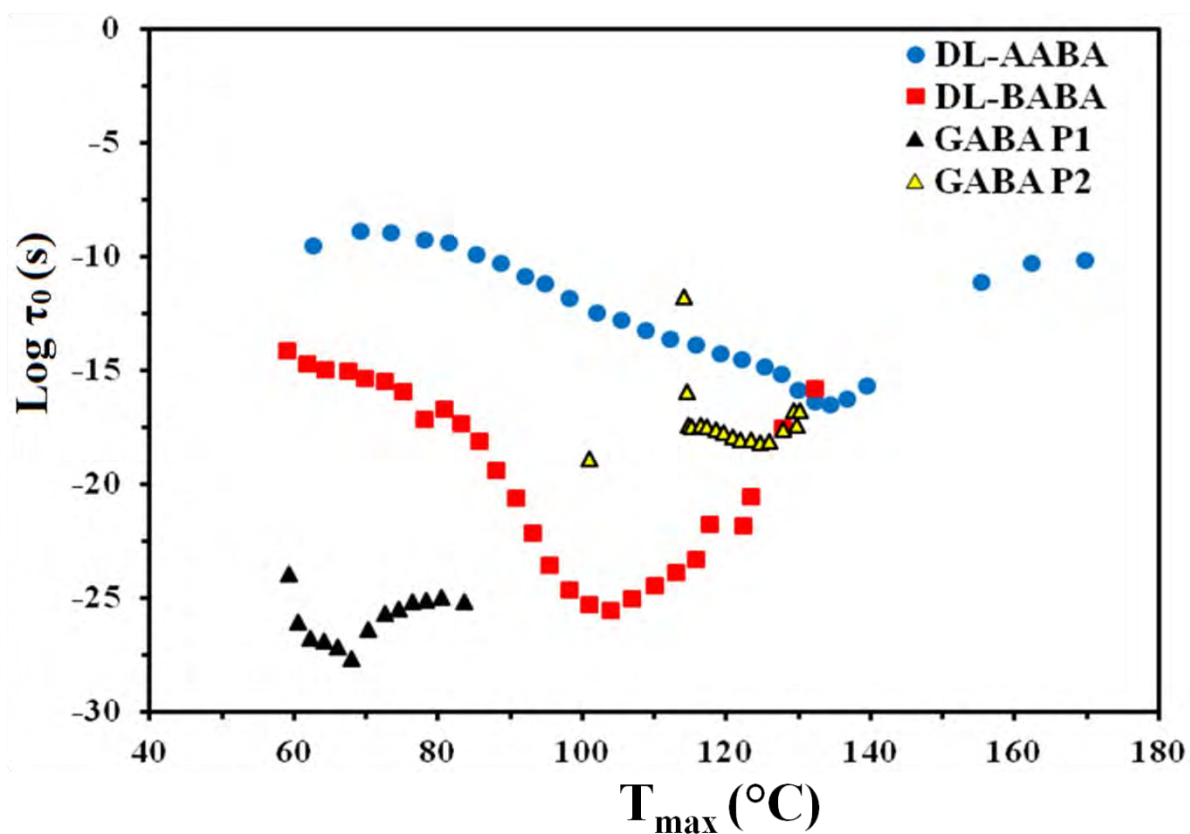


Fig. 3.9 Plot of log pre-exponential factor (τ_0) vs T_m for all processes observed for the amino butyric acids.

Table 3.3 Arrhenius parameters for the aminobutyric acids and the relaxation times observed at the peak maxima.

Sample	Global relaxation process	T_{\max} (°C)	Log τ_0 (s)	E_a (kJ/mol)
DL-AABA	1st	135 ± 1	-16.5 ± 0.2	142 ± 4
DL-BABA	1st	103 ± 1	-25.3 ± 0.2	196 ± 4
GABA	1st	69 ± 1	-27.7 ± 0.5	190 ± 6
	2nd	125 ± 1	-18.2 ± 1.3	152 ± 10

This supports the earlier statement that increasing the distance between the amine and carboxyl group increases motional freedom. However, if consideration is given to the relaxation events on the basis of those that occur just before the higher temperature macroscopic events (melting and decomposition) i.e. if only the 2nd global relaxation process is considered for GABA and inclusive of the processes observed for DL-AABA and DL-BABA, then it becomes quite apparent that the relaxation frequency is in the order DL-AABA > GABA > DL-BABA. This order in relaxation frequency is a reflection of the order of thermal stability observed in DSC and TGA studies (DL-AABA > GABA > DL-BABA). This relationship was also observed for the E_a values presented in Table 3. 3.

These observations demonstrate that there is a relationship between molecular mobility, as detected by TSDC, and the stability of solid crystalline materials. In the case of the butyric acids examined, molecular mobility significantly influences the thermal stability i.e. with increasing motional freedom, as dictated by relaxation frequency, the temperature of the first event observed in TGA and DSC decreases. Furthermore, when comparing the apparent activation energies (E_a) it was found that the relaxation process observed for DL-BABA exhibits the highest values (196 ± 4 kJ/mol) when compared with DL-AABA and GABA. This correlates with the enthalpy changes found using DSC studies, where the two overlapping processes observed for DL-BABA at 187 and 201°C were greater (1722 ± 316 J/g) than DL-AABA and GABA (1151 ± 50 and 1121 ± 23 J/g, respectively). Such an

observation is most probably due to the differences between the crystal lattice properties of the three aminobutyric acids.

3.3.4 Compensation Analysis

DL-AABA and DL-BABA demonstrates compensation behaviour i.e. there exists a linear relationship between $\log\tau_0$ and E_a , which is represented as the intercept and slope of the Arrhenius fitting, respectively (equivalence in Eyring fitting is the linear relationship between ΔS^\ddagger and ΔH^\ddagger). The points displayed in the relaxation map analysis (Fig.3. 10) for DL-AABA and DL-BABA correspond to TW experiments with polarisation temperatures between $T_p = 40$ and 132°C ($T_w = 4^\circ\text{C}$) and $T_p = 43$ and 91°C ($T_w = 3^\circ\text{C}$), respectively.

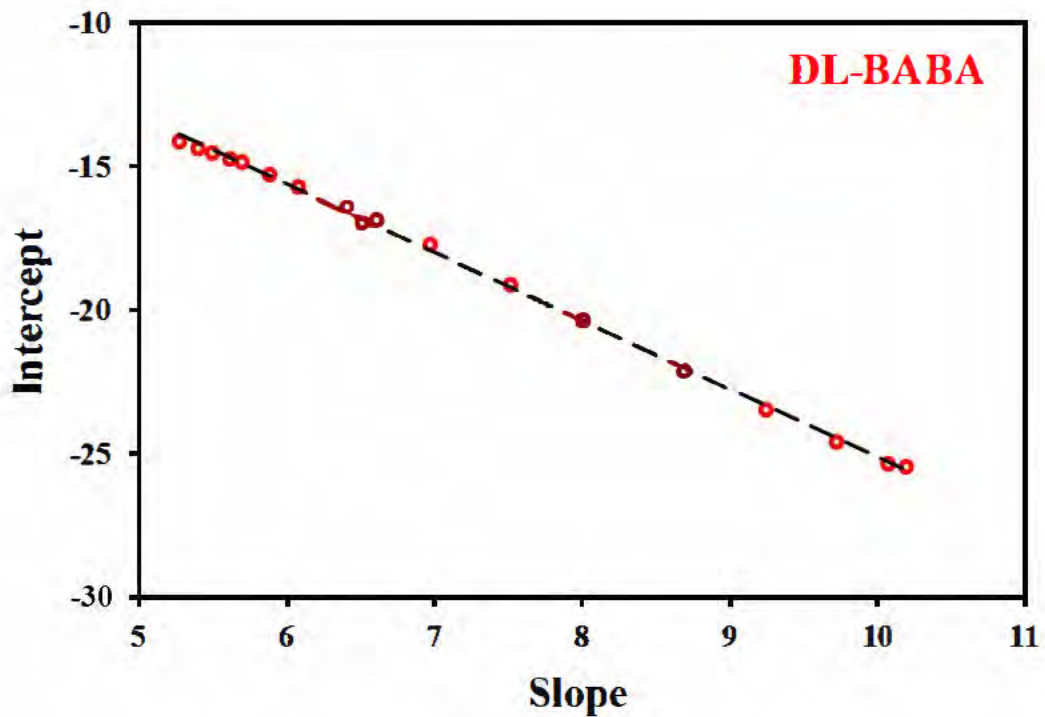
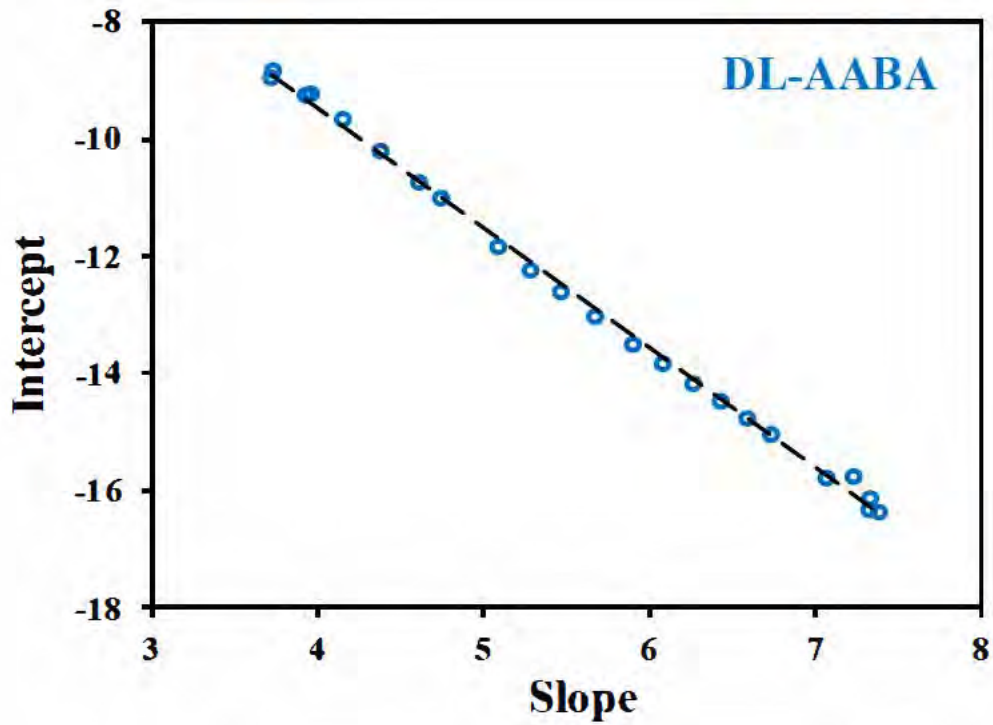


Fig. 3.10 “Compensation search” plots of the intercept vs slope of the Arrhenius plots for the TW experiments performed for DL-AABA and DL-BABA

The compensation point, which is characterised by a coordinate of relaxation time (τ_c) and temperature T_c , is the point at which the Arrhenius or Eyring lines of the elementary relaxation modes converge as shown in Fig.3. 11. The T_c and τ_c values obtained for

DL-AABA are $214 \pm 6^\circ\text{C}$ and 0.051 ($\text{Log } -1.3 \pm 0.2 \text{ s}$) and those for DL-BABA are $153 \pm 3^\circ\text{C}$ and 0.025 ($\text{Log } -1.6 \pm 0.2 \text{ s}$).

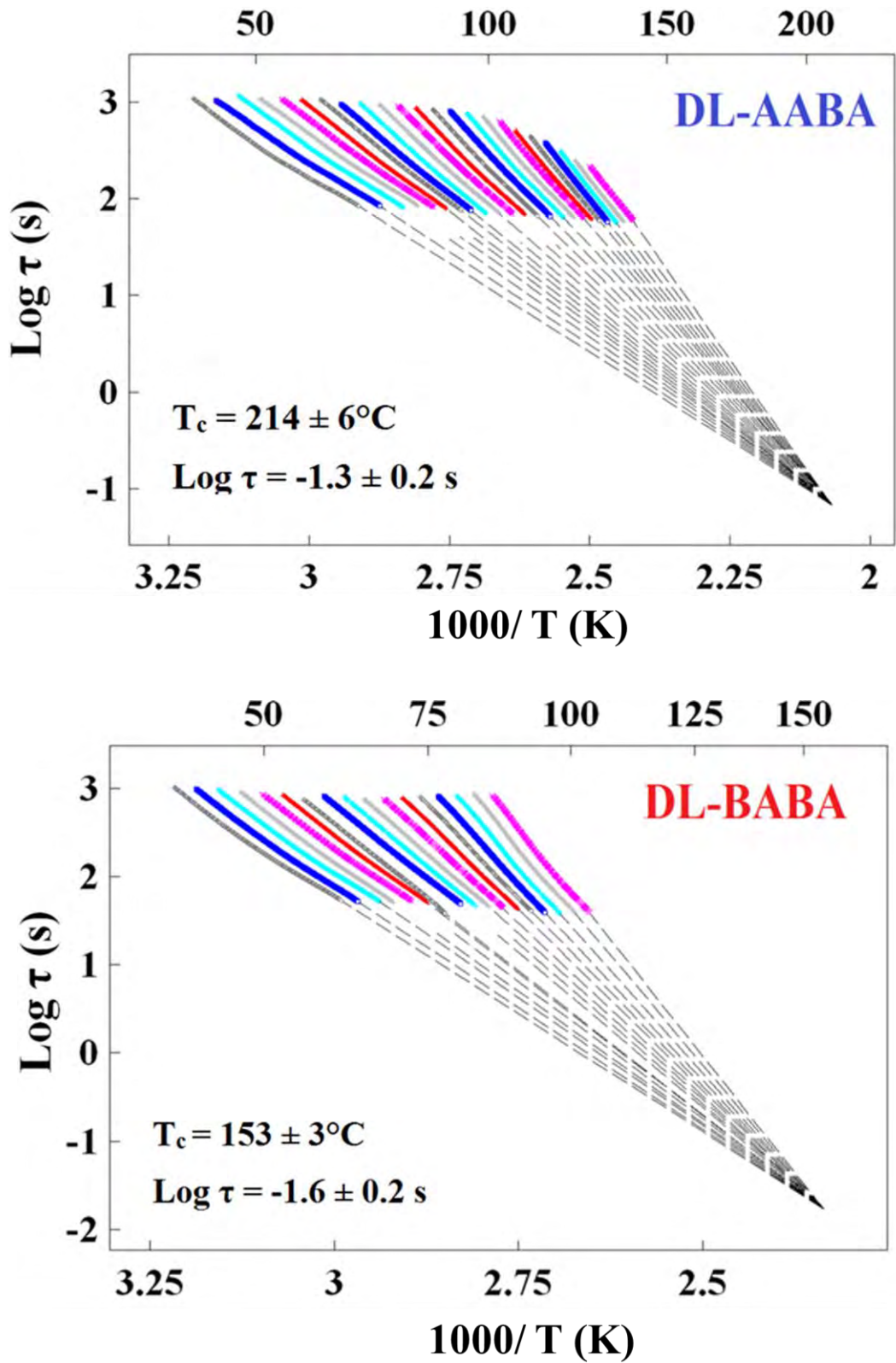


Fig. 3.11 Relaxation map analysis of the compensation point obtained for the lower 23 and 17 polarisation temperatures for DL-AABA and DL-BABA, respectively

As already mentioned, the currents generated in the TSDC studies of aminobutyric acid molecules originate from localised non-cooperative rotational motion from parts of molecule i.e. the amino and/or the carboxyl functional groups, or the rotation of the whole molecule. GABA is uniquely different from DL-AABA and DL-BABA in that it exhibits two dipole relaxation processes prior to high temperature thermal events. Furthermore, the second relaxation process for GABA has a contribution from space charge polarisation. The differences observed in the global TSDC and the relaxation parameters obtained by the Arrhenius equation has been, herein, attributed to the positional isomerism of these materials i.e. the spatial arrangement of the amino group in relation to the molecular backbone and thus the carbon chain length between the amino and the carboxyl functionality is a key contributor. For example, during polarisation-depolarisation processes, several intra- and inter- molecular interactions may occur. As such if only segmental rotations are considered, then the orientation and reorientation may be limited by a possible intra-molecular interaction of the two functional groups (amino and carboxyl). What this implies, in theory, is that the further away the amino and carboxyl group are from each other the less the rotational hindrance and the greater the depolarisation current. On the other hand, the distance between the amino and the carboxyl functional groups strongly influences the flexibility of the molecular backbone and the degrees of orientational freedom of parts of the molecule i.e. GABA will exhibit greater degrees of orientational freedom and DL-AABA will have the lowest degrees of orientational freedom. This could provide the reason why GABA exhibits greater mobility and faster molecular relaxation times, while DL-AABA exhibits the lowest mobility and slowest relaxation time (which is true only when the first relaxation process is considered).

Compensation phenomena, to date, have only been reported for amorphous systems. The physical meaning of compensation behaviour is difficult to interpret and as such, no consistent theory exists that explains the physical origin of compensation phenomena. It has been suggested, however, that the compensation point represents a point (T_c) where all the

characteristic relaxation times (τ_c values) of the different relaxation processes are the same (Neagu and Neagu, 2003) i.e. all relaxation processes in the material behave as a single elementary process. Many have also attributed the compensation behaviour to be indicative of cooperative molecular motions or some other cooperative transitions (Ramos and Mano, 1997). Both these explanations suggest that the motional modes studied at lower temperature are the precursors of the physical process that occur at or near the T_g in amorphous systems. Hence, although not widely accepted, these explanations afford the possibility to correlate TSDC relaxation modes with high temperature physical events (Neagu and Neagu, 2003).

The T_c values obtained for DL-AABA and DL-BABA are both in the vicinity of the sublimation and melt processes observed in TGA and DSC studies, respectively. This, in one respect, suggests that the activated process i.e. the modes of molecular mobility observed in the TSDC may contribute or actually be the precursor to these cooperative high temperature thermal events. When such behaviours are reported in literature, for amorphous systems, the relaxation process studied typically exhibits strong deviation of ΔH^\ddagger from the zero entropy line i.e. the relaxation process results in a significant change in entropy of the environment of the molecule (Correia et al., 2000). However, the ΔH^\ddagger observed for DL-AABA and DL-BABA were found to exhibit negligible deviation from the zero entropy line. This indicates that the relaxation processes are localised rotational motions that have negligible influence on entropy change. The lack of cooperativity associated with the aminobutyric acids is not surprising because of constraints of the crystal lattice and due to the fact that relaxation at higher temperatures, namely melting/degradation and sublimation, are non-cooperative processes. It is important to note that the T_c values for the both DL-AABA and DL-BABA are below the temperature of the high temperature thermal events observed using DSC and TGA, whereas in amorphous systems it is generally found to be 5 to 30°C above the glass transition (Alves et al., 2005). The compensation point observed for the DL-AABA and DL-BABA

could therefore be a point where the cooperative melt, and non-cooperative degradation and sublimation processes begin.

3.4. Conclusions

TSDC spectroscopy can be used to detect previously unreported relaxation processes at $109 \pm 1^\circ\text{C}$ for DL-AABA, $104 \pm 1^\circ\text{C}$ for DL-BABA and at $77 \pm 2^\circ\text{C}$ and $114 \pm 1^\circ\text{C}$ for GABA. These processes have been assigned to dipolar relaxations that are most likely to be precursors of the high temperature events detected by TGA and DSC, leading to the conclusion that in the solid state aminobutyric acids may undergo some structural motions (mobilities of side groups, mobility of the back bone, creation/destruction of intra- and inter-molecular interactions or cooperative mobility of several molecules) which allow them to be “prepared” for the main transition processes (melting, degradation, sublimation). Furthermore, this study has also demonstrated that crystalline materials can demonstrate compensation behaviour, as observed for DL-AABA and DL-BABA. The compensation point (T_c) observed for DL-AABA and DL-BABA are $214 \pm 6^\circ\text{C}$ and $153 \pm 3^\circ\text{C}$, respectively, while the relaxation time at these temperature are 0.051 (log -1.3 ± 0.2 s) and 0.025 (log -1.6 ± 0.2 s), respectively. This is the first time compensation behaviour has been reported for small molecular weight crystalline systems. GABA, which is a naturally occurring neurotransmitter, exhibits distinctly different behaviour when compared to the other two positional isomers. GABA undergoes two relaxation processes with the second showing a contribution from space charge polarisation. Furthermore, both global relaxation modes for GABA have greater current density compared to DL-AABA and DL-BABA when polarised with the same electrical field strength. This indicates the relative ease with which GABA is polarised (greater molecular mobility).

The difference in the dielectric behaviour of the aminobutyric acids has been attributed to the distance between the amino and the carboxyl moieties. The greater the distance between the amino and the carboxyl groups the more flexible the aminobutyric acid back bone and thus

the greater the degree of orientational freedom. This is believed to provide the explanation for the greater dipole mobility and faster relaxation observed for GABA compared to the other two aminobutyric acids. Furthermore, the relatively greater flexibility and the ease with which GABA is polarised in comparison to the DL-AABA and DL-BABA may be a contributing factor to the differences observed in the roles of these aminobutyric acids in biological systems.

Finally, the study has demonstrated the existence of a relationship between molecular mobility and higher temperature thermal events for the aminobutyric acids. In this study the lower the relaxation frequency the more stable the material i.e. DL-AABA exhibits the lowest relaxation frequency and it is the most thermally stable (highest temperature onset in TGA and DSC studies) of the three positional isomers, while DL-BABA demonstrates the greatest relaxation frequency and has the lowest onset temperature.

Chapter 4 : Influence of Carbon Chain Length on Solid-State Mobility and Thermal Stability of Phosphatidylcholines

4.1 Introduction

Phospholipids are amphiphilic molecules which consist structurally of a diglyceride composed of one glycerol (1, 2, 3-propantriol) moiety bonded with two fatty acids at the *sn*-1 and *sn*-2 positions on the glycerol via an ester bond. The third hydroxyl group of glycerol is attached to a phosphoric acid via a phosphate ester bond. Furthermore the phosphate moiety is bonded with a complex amino alcohol by a second phosphate ester bond. These complex amino alcohols can be choline, ethanolamine or an amino acid e.g. serine. Phosphatidylcholines, are phospholipids with a choline as the molecular moiety attached to the phosphate; they are the major phospholipids found in animals, accounting for ~50 % of membrane lipids in eukaryotic cells (Aktas et al., 2010). In addition to contributing to the structural integrity of cellular membranes, phosphatidylcholines are the major constituents of lung surfactants (Bernhard et al., 2001) and have also been shown clinically to protect against liver damage (Kidd, 1996). Furthermore, ingested phosphatidylcholines are the body's main source of choline, which is an important precursor of acetylcholine, a major neurotransmitter (Chung et al., 1995, Zhao et al., 2001).

The functional properties of phospholipids are governed by their ability to undergo lyotropic and thermotropic transitions. Arguably, the most important thermotropic transition in aqueous colloidal suspensions of phosphatidylcholines is the gel phase to liquid-crystalline phase transition which is attributed to the “melting” of the hydrocarbon (i.e. acyl) chains and the temperature at which this occurs is denoted the T_m (Ulrich, 2002, Stark et al., 2010). These transitions influence the fluidity of the bilayer structures formed by phospholipids in aqueous media and therefore the stability and the structural integrity of both model (e.g. liposome formulations and cellular membranes). Hence, understanding the phase behaviour of

phospholipids is of significant importance from a biological perspective. The need to gain greater understanding of pure phospholipids and their phase behaviour was well expressed by Gruner (2004). It was suggested that the existence of the many mesomorphic transitions of phospholipids is, by and large, a structural manifestation of the constraints on intermolecular forces that exist in bio-membranes. Therefore, understanding the structural dynamics of anhydrous phospholipids can shed light on their intrinsic behaviour in living systems and in pharmaceutical applications. Popova and Hinch (2011) also highlighted the importance of understanding the phase behaviour of phospholipids without the interfering effect of water i.e. studies of the non-hydrated state of phospholipids may provide insight into the molecular interactions and properties that govern the phase behaviour of these molecules.

For saturated phospholipids, in particular phosphatidylcholines, the carbon chain length has a significant influence on the T_m values both in the colloidal state and in the solid-state (Popova and Hinch, 2011, Koynova and Caffrey, 1998). Increasing the acyl chain length of saturated phospholipids results in an increase in the T_m (Popova and Hinch, 2003, Popova and Hinch, 2007). The fact that the physico-chemical properties of these materials changes as a result of a change in acyl chain length makes them good models to study in an attempt to elucidate the relationship between molecular mobility and thermal stability of molecules.

The phospholipids used in the studies reported herein are a homologous series of saturated phosphatidylcholines. These compounds are composed of a phosphocholine group attached to the *sn*-3 position of a glycerol moiety and two acyl fatty acids attached to the *sn*-1 and *sn*-2 positions (Fig. 4.1).

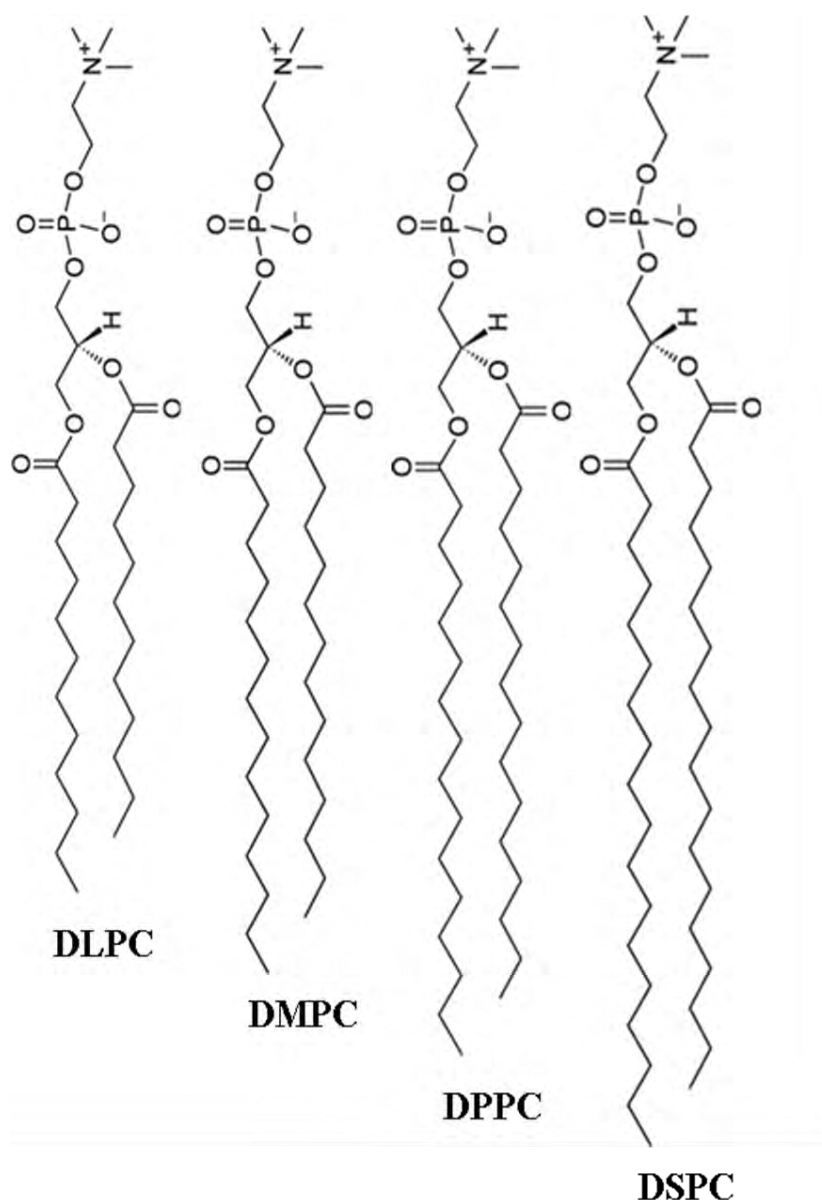


Fig. 4.1 Homologous series of phosphatidylcholines: 1,2-dilauryl-sn-glycero-3-phosphocholine (DLPC), 1,2-dimyristoyl-sn-glycero-3-phosphocholine (DMPC), 1,2-dipalmitoyl-sn-glycero-3-phosphocholine (DPPC) and 1,2-distearoyl-sn-glycero-3-phosphocholine (DSPC) with carbon chain lengths of 12, 14, 16 and 18, respectively.

Previous studies have demonstrated that saturated anhydrous phosphatidylcholines undergo several thermotropic transitions above their T_m values and below the isotropic melts, which occurs at 230°C (Chapman et al., 1966, Chapman et al., 1967). Chapman and colleagues (1967) were able to identify the existence of three liquid crystalline phases at temperatures below the isotropic melt. The thermotropic phase behaviour of the phosphatidylcholines has

been observed to show similarities in the aqueous colloidal state and in the solid state, differing only by the temperatures at which the processes occur. However, the pre-transition process (an endothermic transition, with a small change in heat capacity compared to the gel to liquid crystalline transition) that occurs prior to the acyl chain melting transition in DLPC, DMPC, DPPC and DSPC liposomes has not, to date, been reported in the anhydrous state.

Attempts to understand the molecular dynamics of phosphatidylcholines at temperatures below the T_m is an area of significant contemporary scientific interest. As a result techniques such as dielectric spectroscopy (Bernsten et al., 2011), NMR (Bar-Adon and Gilboa, 1981, Auger, 2000) and quasi-electron neutron scattering (QENS) (Doxastakis et al., 2007) have been employed to understand molecular mobility of partially hydrated phosphatidylcholines. TSDC spectroscopy is an important technique that can be used to obtain additional information relating to molecular relaxation processes at temperatures below the T_m in the absence of any water molecules.

The aim of the work reported in this Chapter, is to understand the influence of hydrocarbon chain length on molecular mobility, as determined by TSDC spectroscopy, and ascertain how this relates to the thermal stability, as determined by TGA and DSC, of a homologous series of phosphatidylcholines.

4.2 Methods

4.2.1 DSC

DSC studies were performed using a Q2000 (TA Instruments) calorimeter. A nitrogen atmosphere at a flow of 50 mL/min was employed, using hermetically sealed Tzero aluminium pans with a single pin-hole in the lid. Sample weights of 2.5 ± 0.3 mg and heating programmes were employed to study the polymorphic behaviour of each material. Prior to data collection each sample is initially cooled to -90°C and heated to 140°C three times. This

was to ensure that all moisture in the systems was removed, thereby allowing the behaviour of the pure anhydrous material to be studied without the interference of water molecules.

Temperature modulated DSC (TMDSC) was performed using a sample size of 8.5 ± 0.4 mg. An underlying heating rate of $2^\circ\text{C}/\text{min}$ with temperature amplitude of 1.5°C every 60 s was employed.

4.2.2 XRPD

X-ray powder diffraction (XRPD) analysis of the samples was carried out at ambient temperature over the 0.5 to $40^\circ 2\theta$ range using steps of $0.02 2\theta$; counting 30 s per point. Experiments were conducted using a D8 Bruker instrument employing $\text{Cu K}\alpha$ -radiation.

4.2.3 TSDC

TSDC studies, covering the range -50 to 110°C (it is important to note that no TSDC transitions could be observed at lower temperatures after removal of moisture), were conducted using a TSCII/RMA spectrometer (SETARAM, France) equipped with a 900 series LN2 micro-dosing cooling system (Norhof, Netherlands) and 6517A electrometer (Keithley, UK). Experiments were performed using a customised sample holder (Fig 4. 2). Sample size used was 40.9 ± 0.4 mg of DLPC, 44.7 ± 0.6 mg of DMPC, 52.8 ± 1.4 mg of DPPC and 56.1 ± 1.0 mg of DSPC (equates to 0.069 ± 0.003 mol dm^{-3} for each phospholipid).

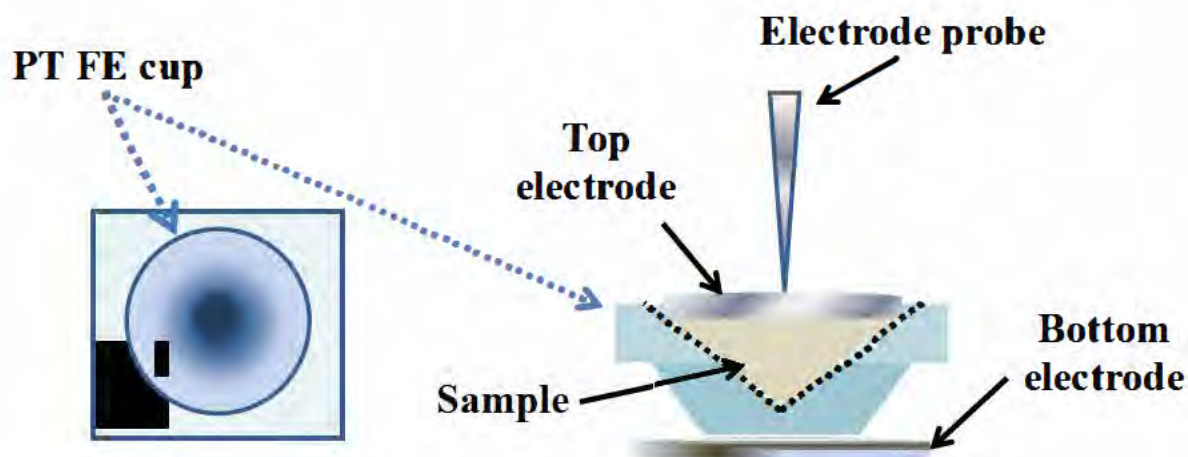


Fig. 4.2 Illustration of custom made sample holder and electrode arrangement employed to study the phosphatidylcholines.

Prior to the experiments, the analysis chamber containing the sample was evacuated to 10^{-4} mbar and flushed several times with high purity helium (1.1 bars). The sample was initially heated from 0 to 140°C at 10°C/min and held isothermally for 2 min. The temperature was then allowed to decrease to ~15°C and the analysis chamber evacuated again, to remove moisture, and refilled with helium (1.1 bars); this procedure was repeated twice. Fig 4.3 shows the appearance of a sample before and after undergoing the aforementioned heat treatment. The sample is uniform in its waxy translucent appearance.



Fig. 4.3 Schematic of the change in the appearance of a phosphatidylcholine samples after the initial heat treatment and after all TSDC experiments were performed.

The global TSDC spectra were obtained by polarising the sample at 90°C with electrical polarisation fields (E_p) of 50, 150, 250 and 350 V/mm for 2 min (t_p). The sample was then rapidly cooled to a temperature (T_o) -50°C, where all dipolar mobilities in the system were assumed to be frozen. The polarisation field was then switched off and the sample held at T_o for a short time (t_o). The depolarisation current was measured as the sample was heated at a controlled rate of 10°C/min to a final temperature (T_f) of 110°C.

In the case of thermal windowing experiments, samples were polarised with $E_p = 400$ V/mm at T_p of -20 to 60°C in increments of 3°C ($T_w = 3^\circ\text{C}$, $t_w = 2$ min).

4.3 Results and Discussion

4.3.1 DSC

DSC results have shown that all of the phosphatidylcholines examined undergo several thermotropic transitions prior to the isotropic melt (at 230°C) (Fig. 4.4). The temperatures and enthalpies of these transitions are presented in Table 4.1. In general, the series of phosphatidylcholines studied undergo a similar number of reversible endothermic processes. DLPC and DMPC undergo additional endothermic processes at $215 \pm 1^\circ\text{C}$ (8th transition) for DLPC and at $122 \pm 1^\circ\text{C}$ (3rd transition) and $209 \pm 1^\circ\text{C}$ (8th transition) for DMPC. Furthermore, the 3rd transition observed for the DMPC was absent in DLPC, DPPC and DSPC.

It is well documented that in the absence of water or other solvents, the chain-melting transition is raised to higher temperatures. For example, the chain-melting transition of DPPC is observed at 41°C in water, whilst the same transition is generally reported at ~100°C in the anhydrous state (Crowe et al., 1996). In this study, the chain-melting transitions were observed at 91 ± 1 , 101 ± 1 , 106 ± 1 and $109 \pm 1^\circ\text{C}$ for DLPC, DMPC, DPPC and DSPC, respectively, which agrees with previously reported values (Chapman, 1966, Chapman et al., 1966, Chapman et al., 1967). The increase in the chain melting transition temperature, when

the sample is in the dehydrated state, results from an increase in the strength of molecular interactions due to the shorter distances between molecules in the solid-state.

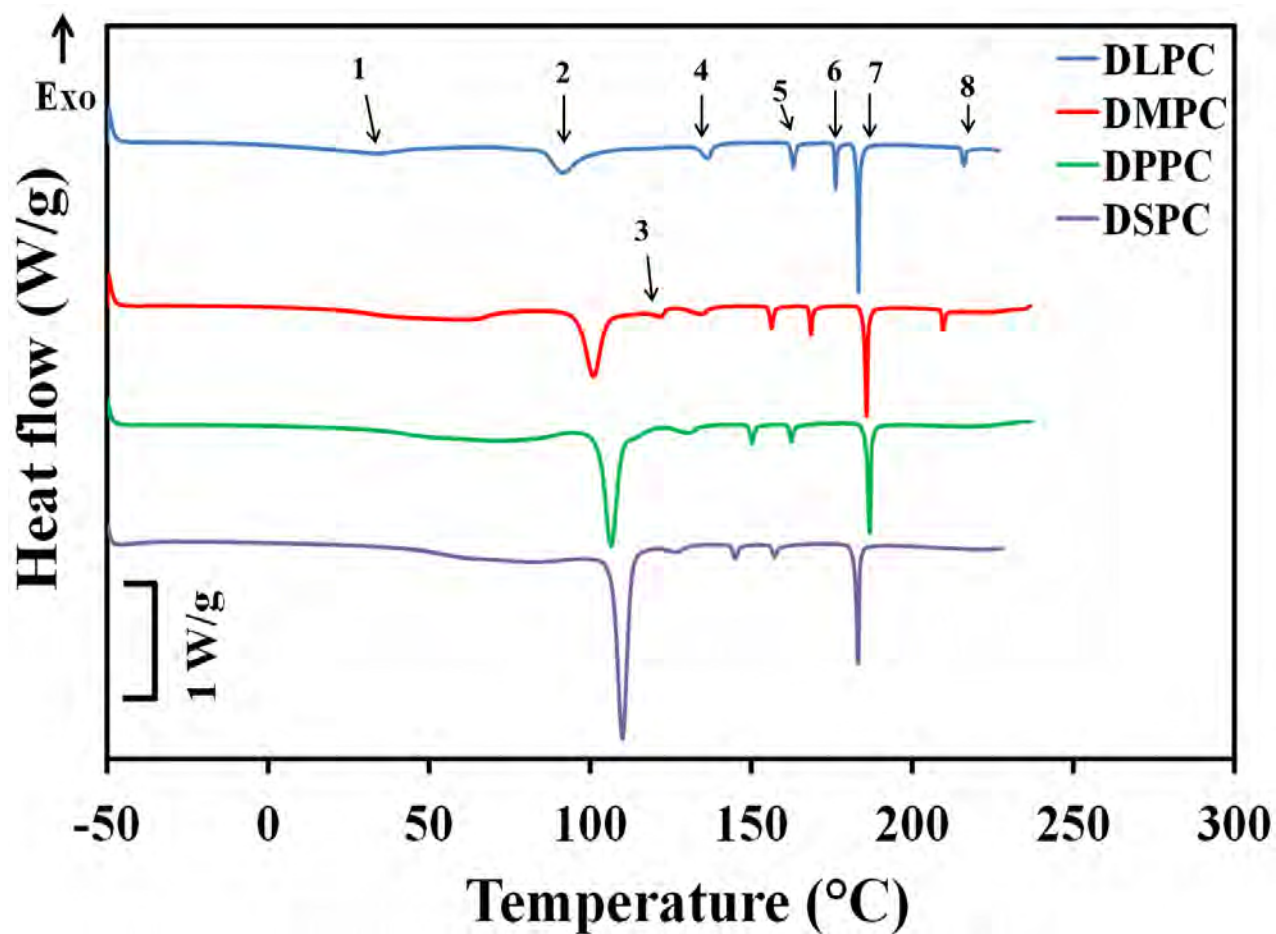


Fig. 4.4 Overlay of the thermograms observed for DLPC, DMPC, DPPC and DSPC heated from -50 to 240°C at 10°C/min after removal of moisture from the samples.

Table 4. 1. Mean temperatures at the peak maxima and enthalpies associated with the mesomorphic transitions of the homologous series of phosphatidylcholines (n =3).

Processes	1 “ re-t nsition”		2 Chain melting		Liquid crystalline transitions											
	3		4		5		6		7		8					
Compound	Peak Temp (°C)	ΔH (J/g)	Peak Temp (°C)	ΔH (J/g)	Peak Temp (°C)	ΔH (J/g)	Peak Temp (°C)	ΔH (J/g)	Peak Temp (°C)	ΔH (J/g)	Peak Temp (°C)	ΔH (J/g)	Peak Temp (°C)	ΔH (J/g)	Peak Temp (°C)	ΔH (J/g)
DLPC (12:12)	34 ± 1	12.4 ± 0.5	91 ± 1	17.0 ± 0.9	-	-	137 ± 1	2.5 ± 0.2	163 ± 1	2.1 ± 0.2	176 ± 1	1.9 ± 0.1	183 ± 1	7.4 ± 0.3	216 ± 1	1.4 ± 0.2
DMPC (14:14)	57 ± 1	19.2 ± 0.8	101 ± 1	20.1 ± 0.8	122 ± 1	1.2 ± 0.2	134 ± 1	1.9 ± 0.1	156 ± 1	1.7 ± 0.3	168 ± 1	1.7 ± 0.4	185 ± 1	7.2 ± 0.3	209 ± 1	1.3 ± 0.2
DPPC (16:16)	70 ± 1	20.4 ± 0.6	106 ± 1	31.0 ± 0.4	-	-	131 ± 1	1.8 ± 0.1	150 ± 1	1.6 ± 0.2	162 ± 1	1.5 ± 0.1	186 ± 1	8.2 ± 0.4	-	-
DSPC (18:18)	78 ± 1	10.8 ± 0.7	109 ± 1	35.9 ± 0.9	-	-	127 ± 1	1.2 ± 0.1	145 ± 1	1.4 ± 0.1	157 ± 1	1.4 ± 0.1	183 ± 1	7.8 ± 0.5	-	-

For anhydrous phospholipids chain-melting transitions are attributed to the transformation from a crystalline to a liquid-crystalline phase (L_α). As such, when the sample is heated above the T_m molecules arrange into a multi-layered structure, in which the interface was at the phosphatidylcholine headgroups. A representation of the possible structure formed (Fig. 4.5) has been reported by Doxastakis et al (2007). With respect to the highly ordered crystalline form, the liquid-crystalline phase exhibits a greater degree of motional freedom, whilst it maintains some degree of order i.e. orientational and/or positional order.

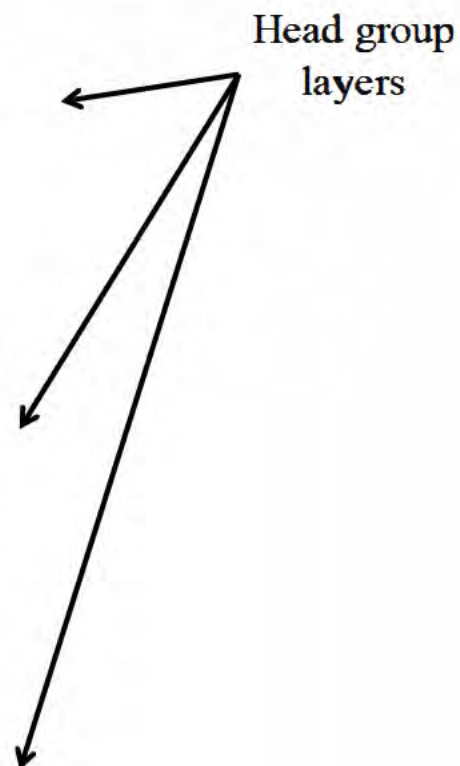


Fig. 4.5 Representation of a typical multi-layered arrangement of phospholipids (reproduced from Doxastakis et al., 2007).

4.3.1.1 “ e -t n sition”

The existence of the endothermic process prior to the chain-melting transition during a heating scan has only been reported for fully hydrated phospholipids and is usually referred to as the pre-transition (Koynova and Caffrey, 1998). In this study, a pre-transition process was observed for all four materials studied. This is the first time this process has been reported for the anhydrous saturated phosphatidylcholines studied on a DSC heating scan. The characteristics of the pre-transitions observed in solution are generally broad and are usually associated with a lower enthalpy change, when compared with the chain melting transition (Koynova and Caffrey, 1998). Furthermore, it has been demonstrated that the temperature difference between this pre-transition process and the chain melting transition decreases with increasing diacyl chain length. The same behaviour was observed in the current study i.e. the “pre-transition” processes were broad and, as shown in Table 4.2, the temperature difference between the two processes decreased with increasing diacyl chain length. It can therefore be postulated that the pre-transition processes observed in this study are similar to those observed in the fully hydrated phosphotidylcholines.

Table 4.2 The temperatures at the peak maxima of the pre-transition and chain melting transition processes observed for DLPC, DMPC DPPC and DSPC.

Compound	Pre-transition (°C)	T_m (°C)	Temperature difference (°C) between the two transitions
DLPC (12)	34	91	57
DMPC (14)	57	101	44
DPPC (16)	70	106	36
DSPC (18)	78	109	31

The nature of these transitions in the anhydrous materials is very complex and difficult to explain. A previous study of DHPC (1, 2-di-n-heptadecanoyl phosphatidylcholine) suggests that the broad initial endothermic process observed during a heating scan is a glass transition, which is then followed by the chain-melting transition (Wang and Tan, 1997) . The authors attributed this behaviour to the “glassy crystal” or semi-crystalline nature of the material, even though it was accepted that below these transitions the sample exist in a crystalline form.

On closer inspection of the pre-transition processes detected by DSC (Fig. 4.4), the heat flow baselines appear to remains the same before and after the pre-transition, which implies that there is no step change in heat capacity for these process to be attributed to glass transitions alone. However, the semi-crystalline nature of the material at temperature below the pre-transition cannot be dismissed. XRPD analysis shows the phosphatidylcholines to exhibit very weak diffraction patterns at high 2θ values (Fig. 4.6 (a)). Weak diffractions are typical of semi-crystalline materials. It is well known that the weak high angle diffractions relate to the chain order, while long-range order are observed only at very low 2θ angles as shown in Fig. 4.6 (b) (Marsh, 1991). Furthermore, the temperature modulated DSC (TMDSC) results (Fig. 4.7 (a-d)) show the samples to undergo transitions that are typical of semi-crystalline materials (Sauer et al., 2000, Sauer et al., 2003, Qui et al., 2003, El-Taweel et al., 2004). From the TMDSC results it was observed that in the reversing heat flow signals, the sample undergoes a step-change in baseline of the heat flow signal (R-1), which is indicative of a glass transition in the amorphous regions. However, it can also be seen that overlapping with this signal is a small but broad endothermic process (R-2). This first order transition in the reversing heat flow is not uncommon, and has been attributed previously to the partial melting of lamellae of some semi-crystalline polymers (Sauer et al., 2000). The observation of melting in the reversing heat flow signal is due to the fact the melting process is in phase

with the modulated temperature i.e. decreasing heating rate decrease the rate of melting and *vice-versa* (Sauer et al., 2003). The observation of an exothermic process in the reversing heat (R-3), however, is not common. Exothermic processes are typically due to crystallisation processes and commonly appear in the non-reversing heat flow signal of TMDSC results. The reason is that they are usually slow processes and typically out of phase with the modulated temperatures (Sauer et al., 2003). What is interesting is that the crystallisation process occurs simultaneously with the chain melting process (NR-3). It is not overly surprising, for a crystallisation process that is in phase with temperature modulation to occur in the chain-melting transition region. The melting of the hydrocarbon carbon chain can be quickly followed by some degree of positional and/or orientational order, a process that is fast and most likely to be heating rate dependent.

In the non-reversing heat flow signal, each sample undergoes three melting transitions (NR-1, NR-2 and NR-3) without any clear signs of re-crystallisation. This can be interpreted to result from the existence of heterogeneity in the morphology of samples. From these observations, it can be confirmed that the phosphatidylcholine samples undergo complex molecular processes/changes as a function of temperature. In addition, the carbon chain length dependence of these processes means that they are related to the hydrophobic regions of the multi-lamellar structures as illustrated in Fig.4.5.

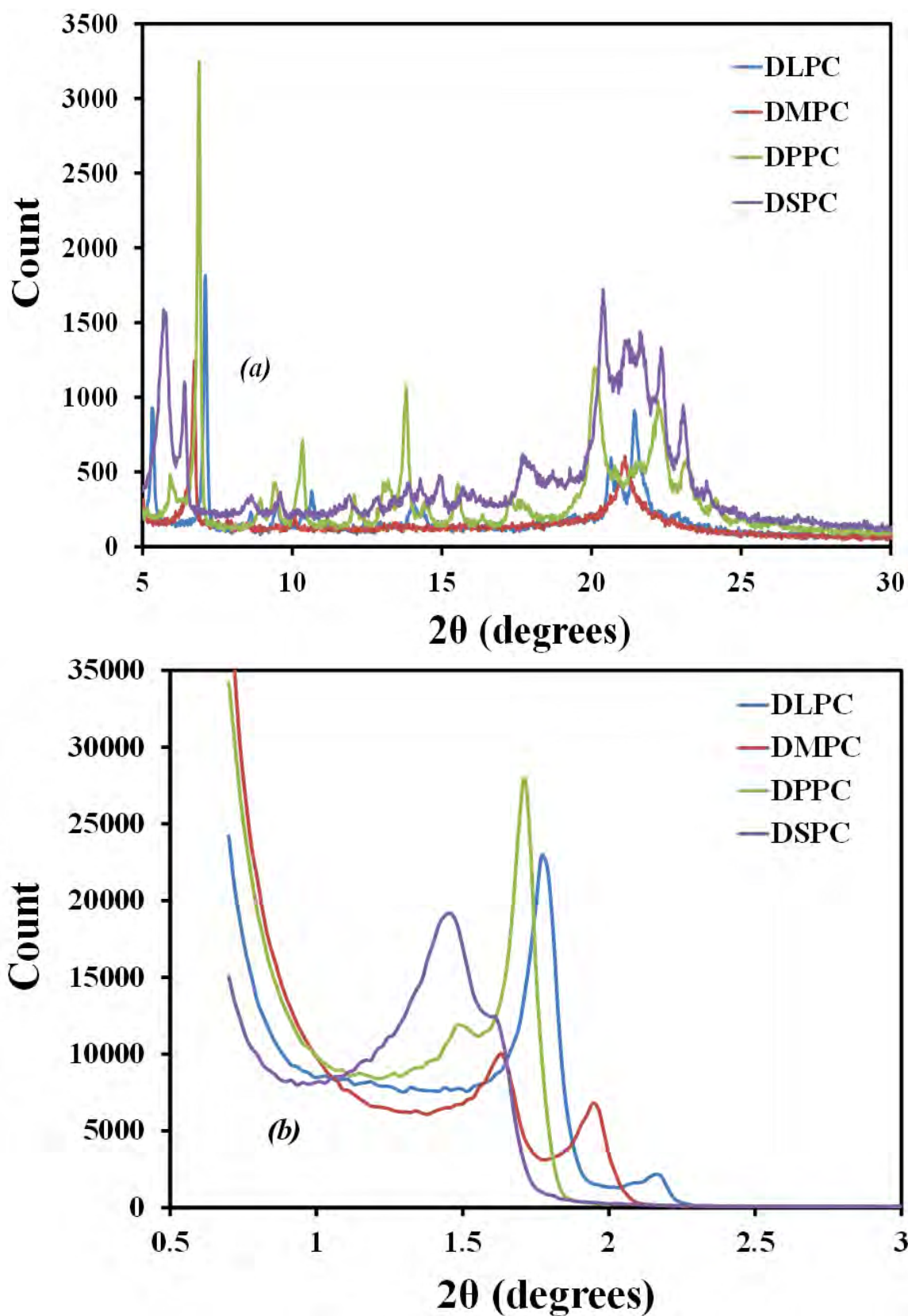
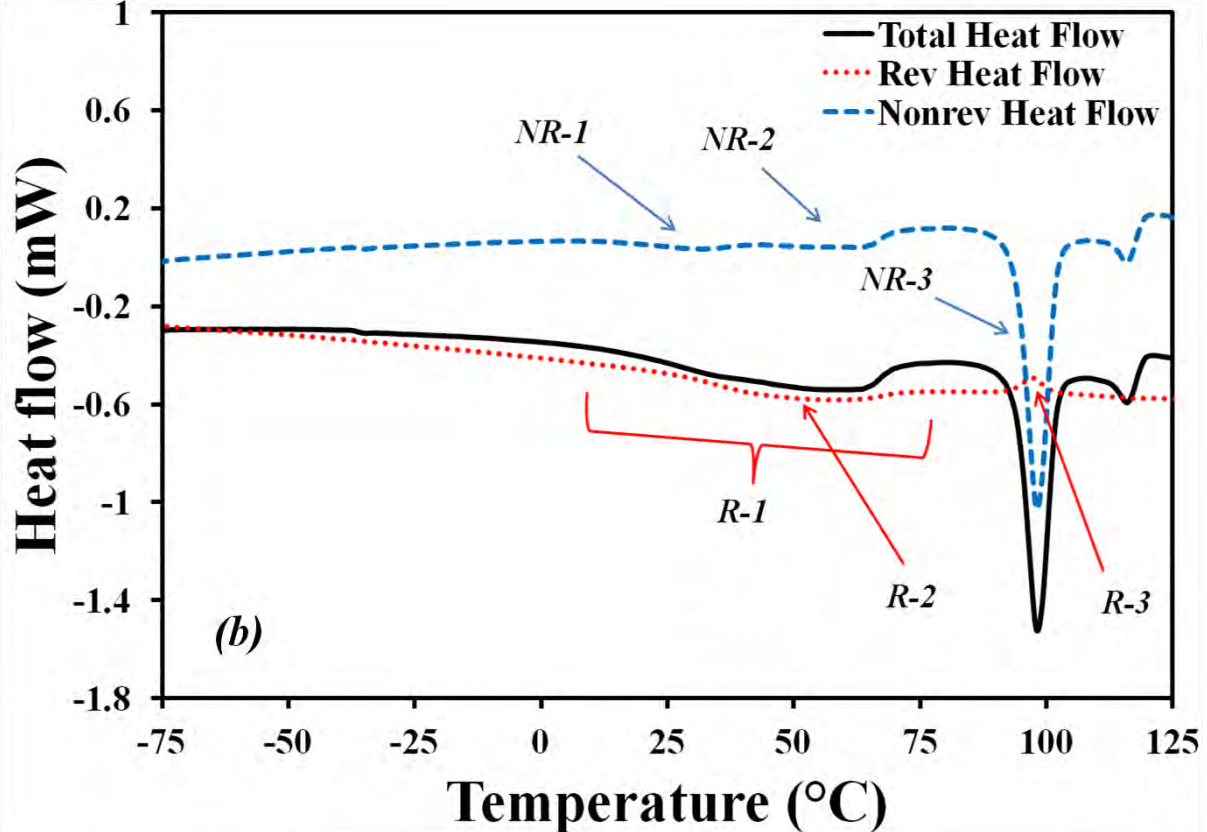
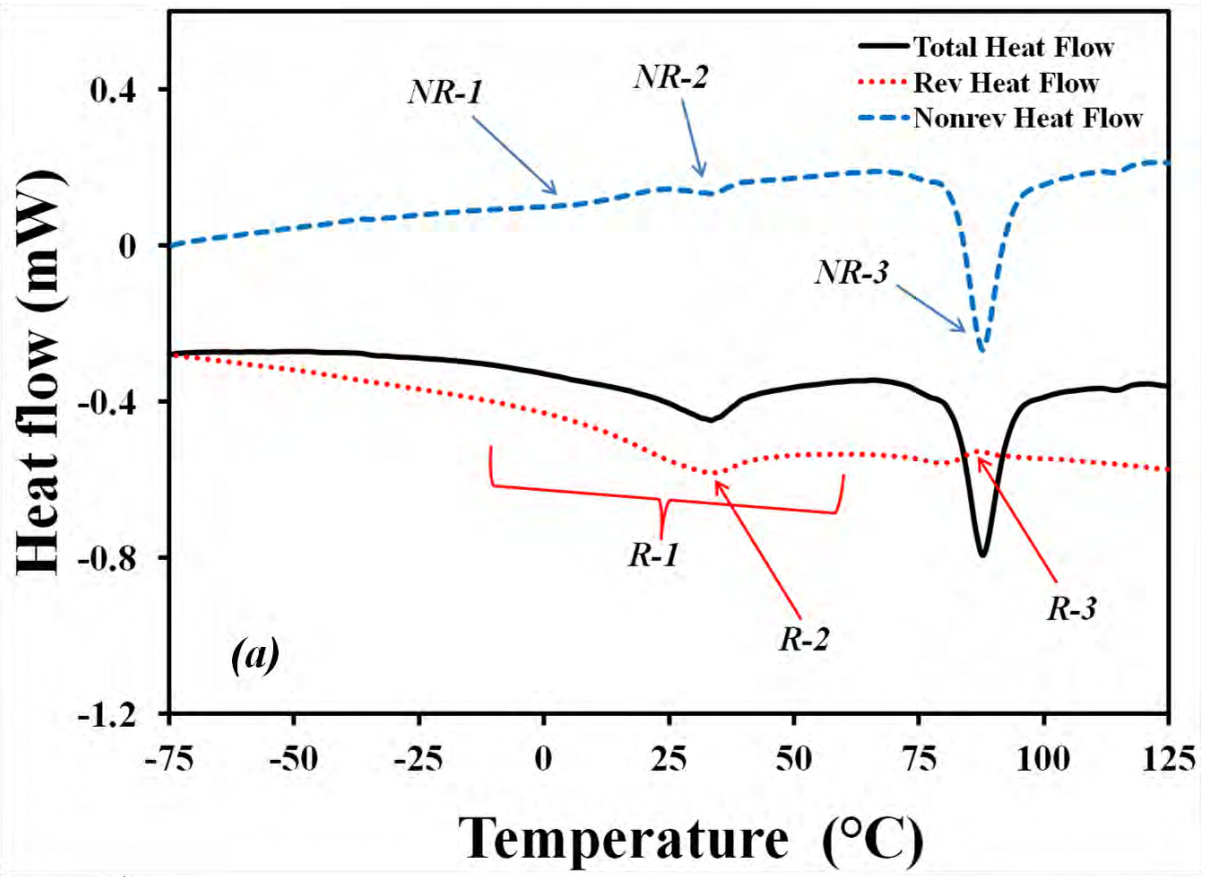


Fig. 4.6 XRPD results for the phosphatidylcholines after heating to 140°C and cooling to ambient temperature (3 times) for each sample.



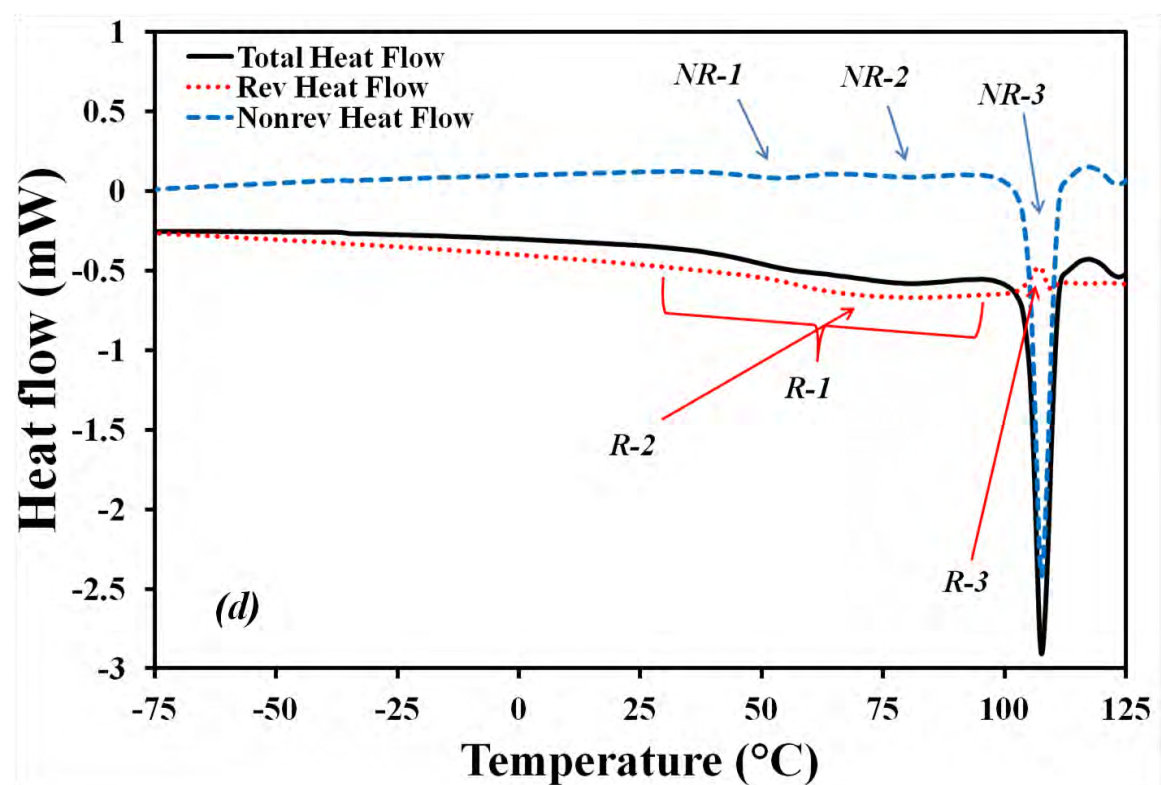
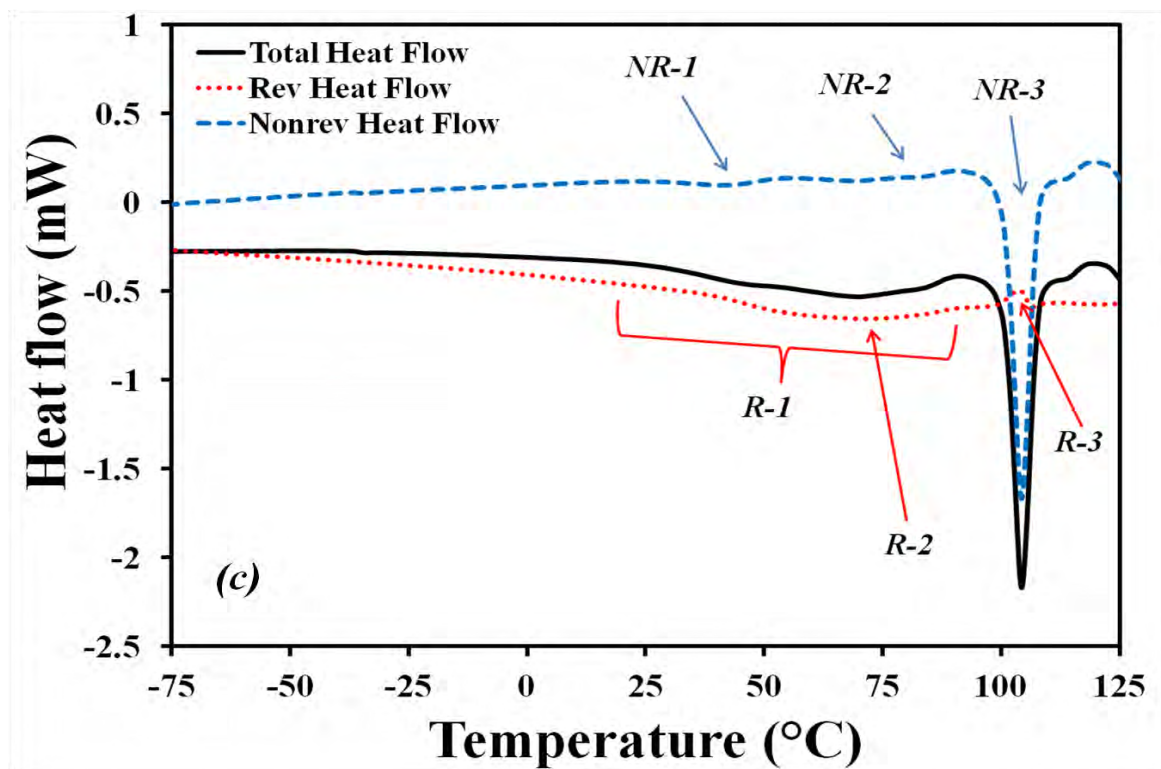


Fig. 4.7 Total, reversing and non-reversing TMDSC curves obtained for (a) DLPC, (b) DMPC, (c) DPPC and (d) DSPC. Data were obtained at an underlying heating rate of 2°C/min and temperature amplitude of 1.5°C every 60 s, using a sample size of 8.5 ± 0.4 mg.

4.3.1.2 Activation Energy

An attempt was made to assess the temperature dependent activation energy of both the pre-transition and the chain melting transitions. However, the pre-transition did not show temperature dependence i.e. increasing the heating rate from 5 to 20°C/min in increments of 5°C/min did not result in a significant shift in the transition temperature. For this reason kinetic studies were not performed on the pre-transition. The chain melting transition, on the other hand, exhibits significant temperature dependence and thus kinetic studies were performed. It is also worth noting that the chain melting transition is considered the most important transition for the functional properties of phospholipids in biological membranes and pharmaceutical liposomal formulations, as this transition changes bilayer integrity (Leekumjorn and Sum, 2007). Hence it is of significant importance to understand the activation barrier that must be overcome for this process to proceed and how this varies with increasing chain length for the phosphatidylcholines.

The computational method employed to attain the apparent activation energies is described in Chapter 1, section 1.3.3. The R^2 values of the Arrhenius plots were ≥ 0.95 . The dependence of the apparent activation energies on the degree of conversion (α) for the phosphatidylcholines is presented in Fig.4.8.

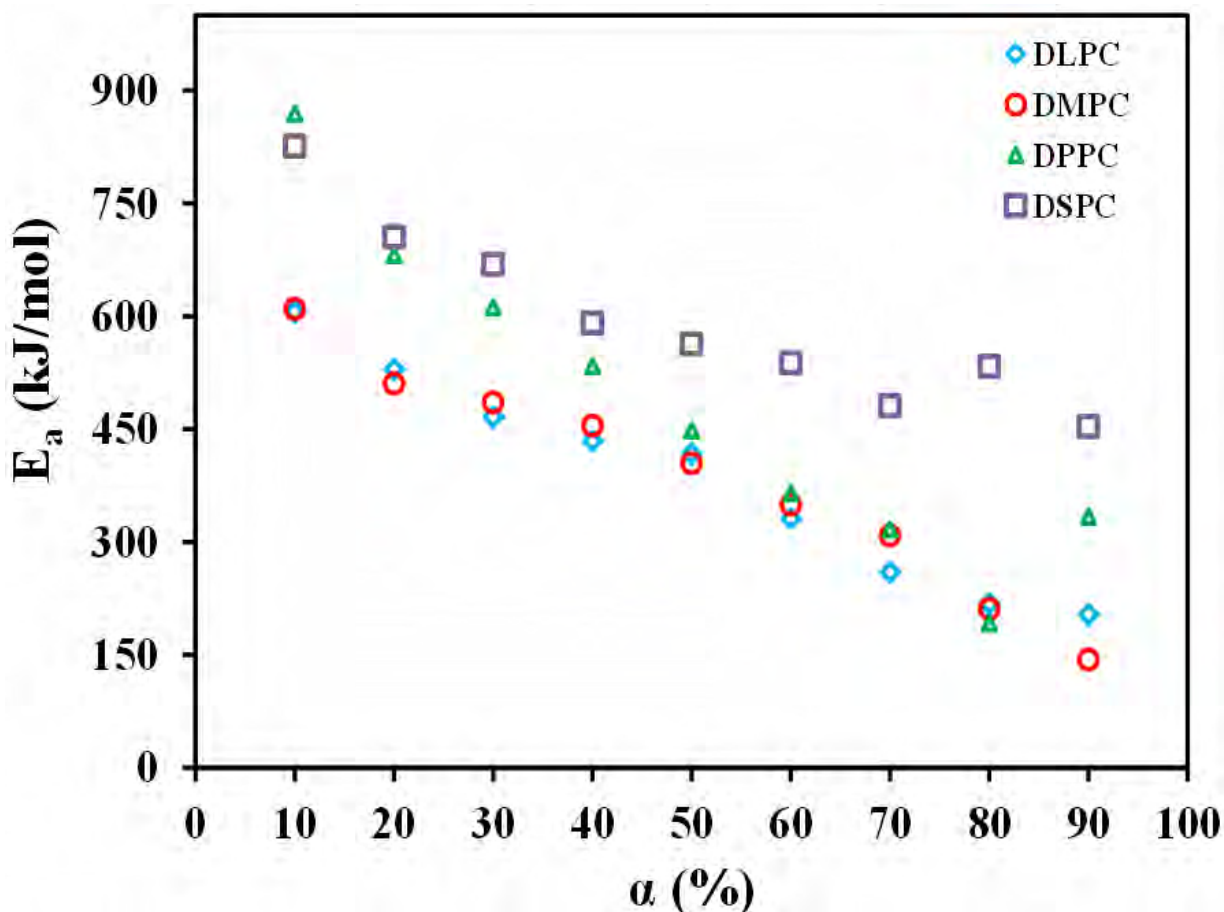


Fig. 4.8 Plots of activation energy (E_a) vs the degree of conversion (α) for the chain melting transition (T_m) of DLPC, DMPC, DPPC and DSPC.

The data acquired shows the existence of a strong dependence of the apparent activation energy on the degree of conversion (α) for chain melting transition of all four phosphatidylcholines studied. In all four samples, the activation energy decreased as the reaction progressed (Fig.4.7 and Table 4.3). The observed behaviour in apparent activation energy could explain/support the cooperative nature of the chain melting transitions. In this case, a relatively high apparent activation energy is required initially for the transition to begin i.e. at this initial stage a high degree of cooperation is required for molecules to move about their local environments, hence greater energy is required. As the molecules gain greater heat energy, the volume of the sample increases, increasing the intermolecular

distances and thus reducing the degree of intermolecular interactions. This in turn reduces the degree of intermolecular cooperation.

Table 4.3 Calculated mean apparent activation energies of the chain melting transition (T_m) at each α for DLPC, DMPC, DPPC and DSPC (n=3).

α (%)	Ea (kJ/mol)			
	DLPC (12:12)	DMPC (14:14)	DPPC (16:16)	DSPC (16:16)
10	606 ± 50	610 ± 24	869 ± 90	826 ± 45
20	530 ± 43	511 ± 45	682 ± 31	705 ± 38
30	466 ± 51	486 ± 19	612 ± 28	669 ± 55
40	434 ± 23	455 ± 18	534 ± 42	591 ± 31
50	418 ± 34	405 ± 36	448 ± 20	563 ± 62
60	331 ± 18	350 ± 20	365 ± 29	538 ± 44
70	260 ± 21	309 ± 27	317 ± 17	481 ± 26
80	218 ± 24	211 ± 18	192 ± 10	534 ± 43
90	204 ± 22	144 ± 8	334 ± 27	453 ± 25

Comparison of the apparent activation energy obtained for the phosphatidylcholine homologues show, in general, that energy required for the chain melting transition increased with increasing carbon chain length (Table 4.3). This is only true if DLPC is ignored and can, again, be attributed to the ability of phospholipids with longer acyl chain lengths to undergo greater hydrophobic interactions.

4.3.2 Global TSDC Results

TSDC studies were initially performed at various polarising temperatures (from -150°C to a temperature past the DSC chain-melting transition temperature of DSPC, 109 ± 1°C), to

identify the temperature regions where samples display observable and reproducible depolarisation currents. Reproducible global depolarisation processes could only be observed when the samples are polarised at temperatures $> -25^{\circ}\text{C}$ and $< 100^{\circ}\text{C}$. Maximum depolarisation current was obtained at T_p of 90°C in all samples.

Fig. 4.9(a-d) shows the depolarisation current profile as a function of temperature for DLPC, DMPC, DPPC and DSPC obtained after polarising with different electrical field strengths. As observed, increasing the electrical field strength increased the current intensity at the T_{max} . The correlation coefficients for the relationship between current intensity at T_{max} and the strength of the applied electric field were all > 0.99 (Fig. 4.10). This confirms that the processes observed result from dipole orientations.

(a)

-10 7
-2

(b)

PTFE signal



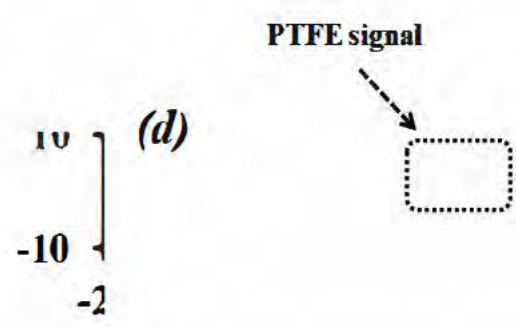
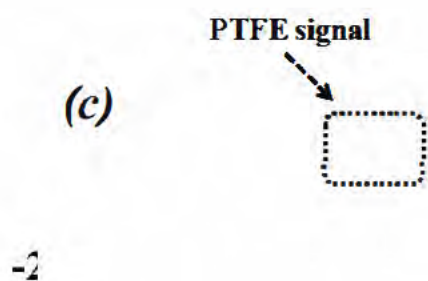


Fig. 4.9 Global depolarisation current as a function of temperature observed for (a) DLPC, (b) DMPC, (c) DPPC and (d) DSPC, obtained using different E_p strength at a T_p of 90°C .

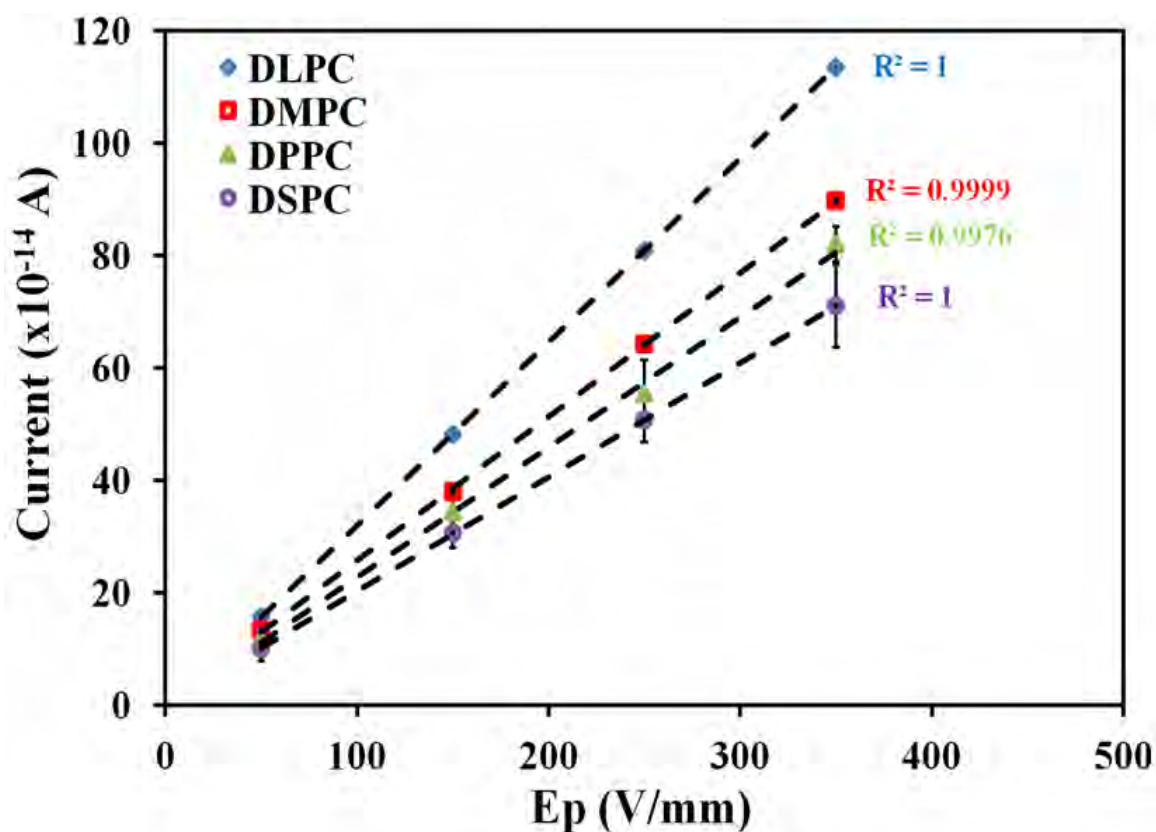


Fig. 4.10 A plot of current intensity at T_{\max} vs applied electrical field strength (E_p) for the phospholipids.

A comparison of the four phospholipids (Fig. 4.11) shows that changing the carbon chain length has a significant influence on the global relaxation curves i.e. increasing the carbon chain length increased the T_{\max} of the depolarisation current, while decreasing the current intensity at the T_{\max} . The temperatures at which the depolarisation processes are observed are indicative of the relative ease with which molecular motion occurs in the materials. Hence the observed increase in T_{\max} with acyl chain length is expected, since the greater acyl chain length of the phospholipid backbone can hinder molecular mobility. The data in Fig. 4.12 shows that the relationship between the T_{\max} and the acyl chain length is linear ($R^2 = 0.97$). The plot also shows that an increase in chain length by a CH_2 unit will result in a $\sim 2.7^\circ\text{C}$ increase in T_{\max} .

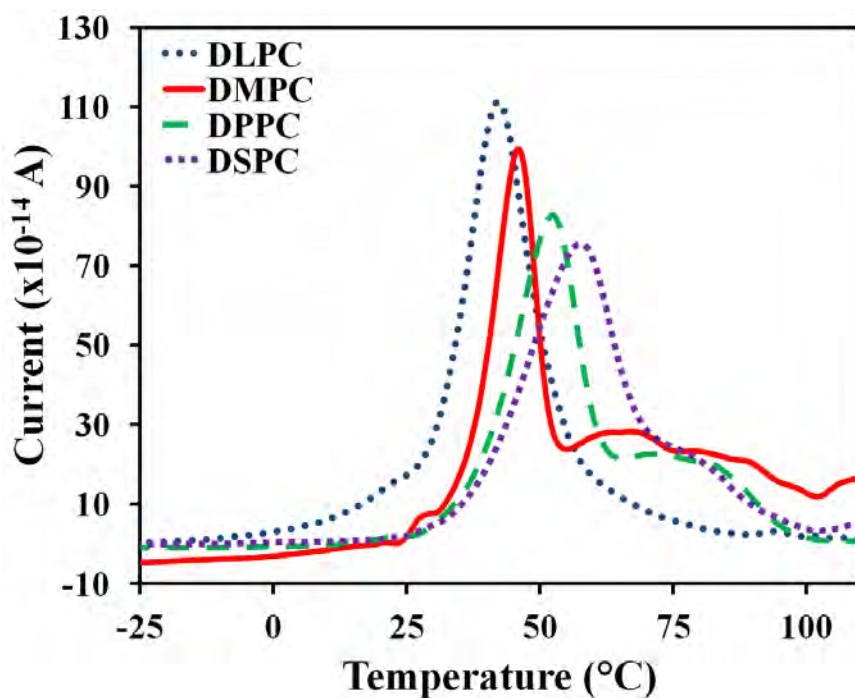


Fig. 4.11 Global TSDC curve overlay for the phosphatidylcholines polarized at 90°C with a polarizing field of 350 V/mm.

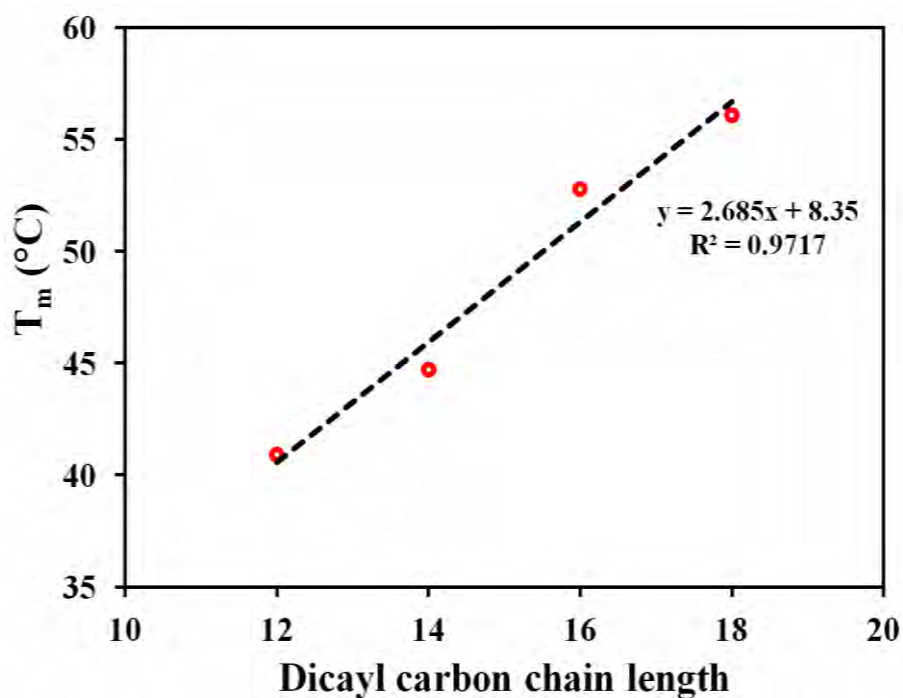
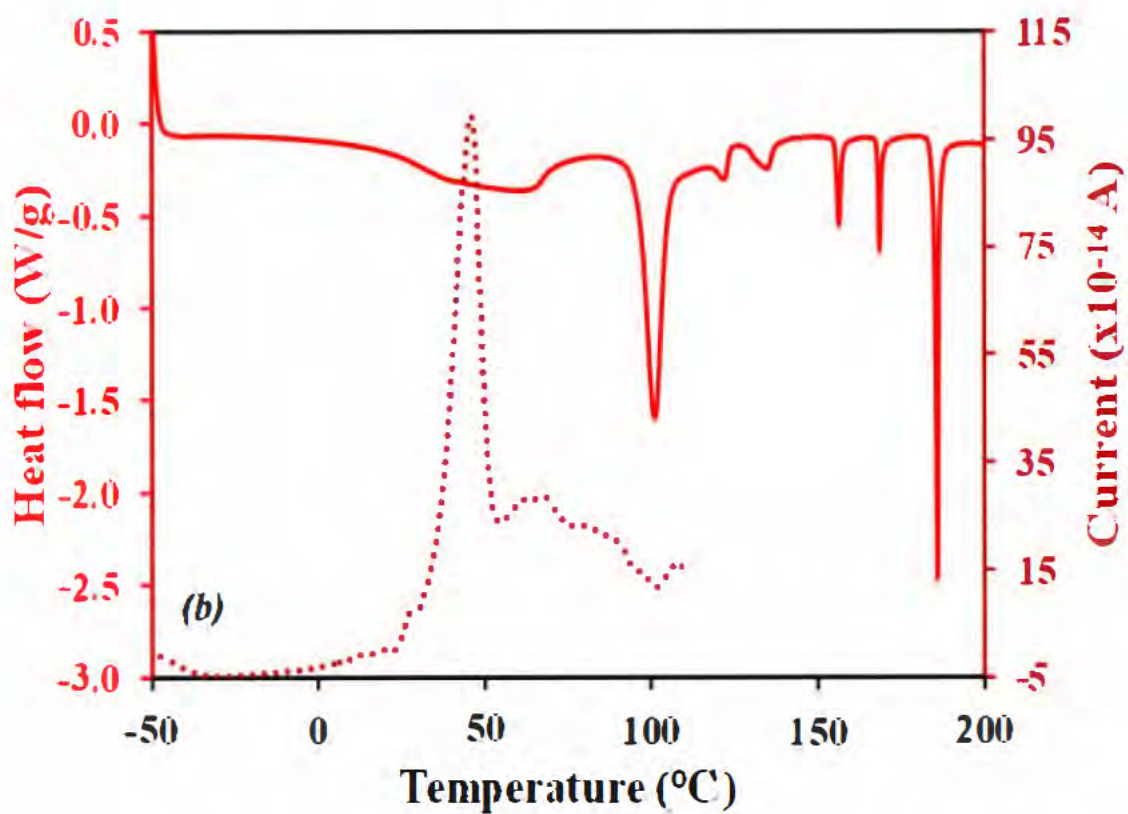
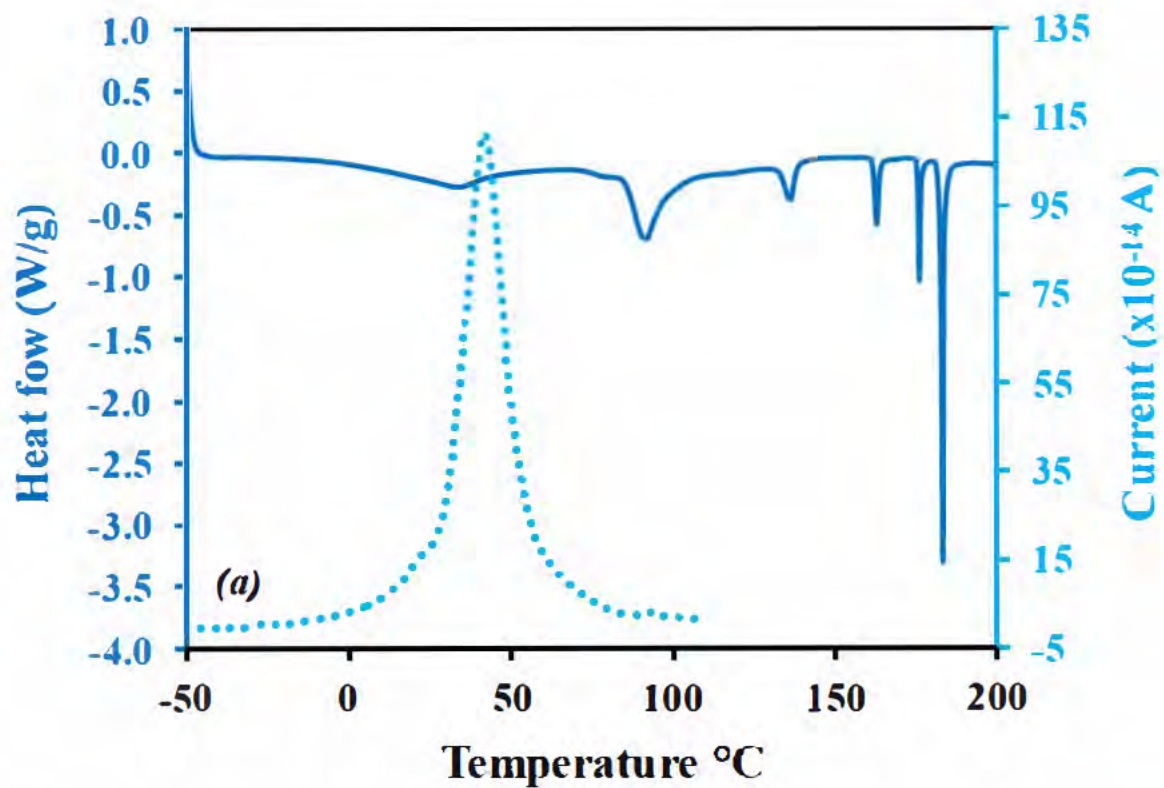


Fig. 4.12 A regression plot showing the relationship between T_m and acyl chain length for the phosphatidylcholines.

The data in Fig. 4.13 indicates that dipole relaxation occurs in the same temperature region as the pre-transition process observed in DSC studies. It is also apparent that the phosphatidylcholines which exhibit broad DSC transitions (DMPC, DPPC and DSPC), exhibit broad higher temperature dipole relaxation shoulders. These observations support the deductions from the DSC studies that the pre-transition process is complex, possibly involving several secondary and primary molecular relaxation processes.

Based on the T_{\max} and the depolarisation current intensity at T_{\max} of the global relaxation processes, it is clear that increasing acyl chain length significantly hinders molecular motion. This maybe the reason for the increase in the temperatures of both the pre-transition and the chain melting transitions observed in DSC studies.



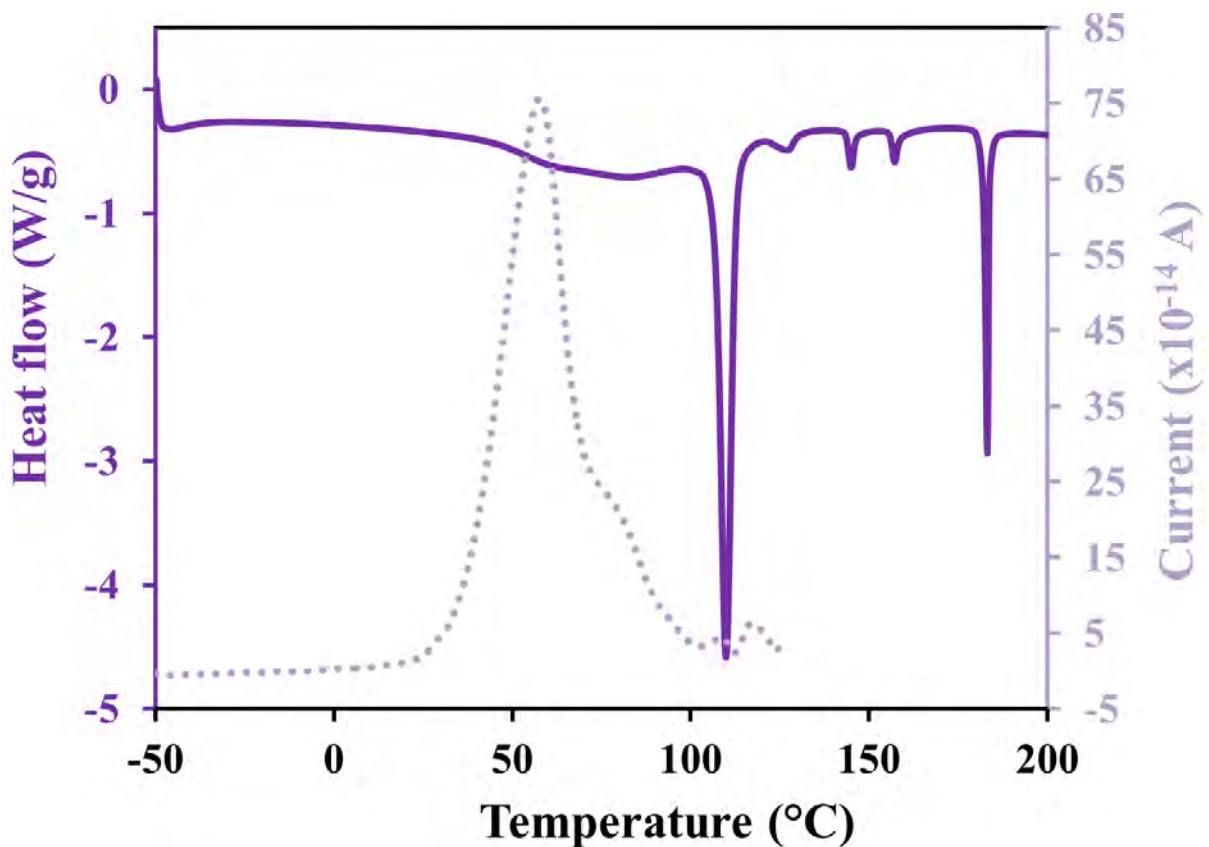
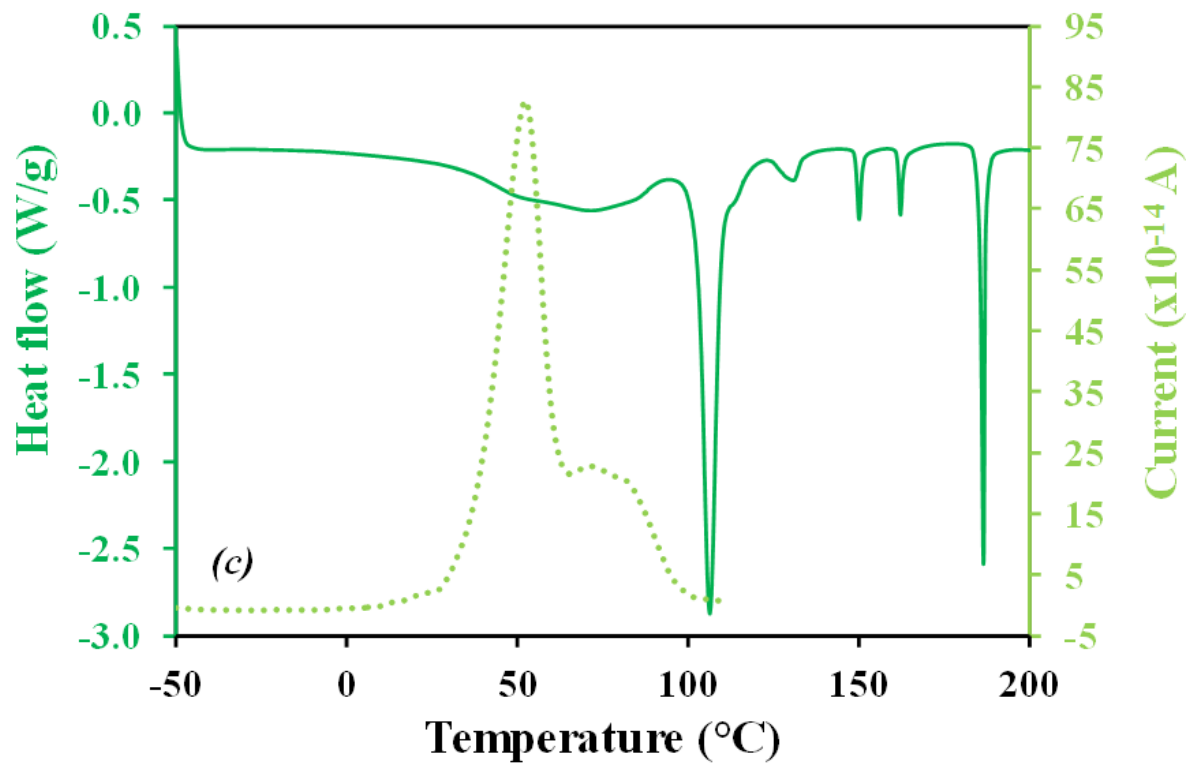


Fig. 4.13 Overlay of DSC curve (solid lines) and TSDCS profiles (dashed lines) obtained after polarising the sample at 90°C using electrical field strength of 350 V/mm for (a) DLPC, (b) DMPC, (c) DPPC and (d) DSPC.

4.3.3 Thermal Windowing Results

The discrete depolarisation modes/components observed from the thermal windowing experiments are presented in Fig. 4.14(a-d). It is important to note that due to the influence of the PTFE signal between 20 and 30°C it was not possible to analyse the distribution of relaxation times for the thermal windowing curves obtained for DMPC, DPPC and DSPC in this temperature region. The influence of the PTFE signal on discrete relaxation processes observed for DLPC appears to be negligible. In addition, the reproducibility of the discrete relaxation profiles could not be achieved at temperatures above 75°C. This behaviour is due to the fact that at temperatures above the T_{\max} the molecules exhibit significant natural mobility, hence at higher temperatures it is difficult to retain the polarisation induced by the electric field (Vicioso et al., 2010).

Global TSDC



DLPC

(a)

Global TSDC



DMPC

Global TSDC →

DPPC

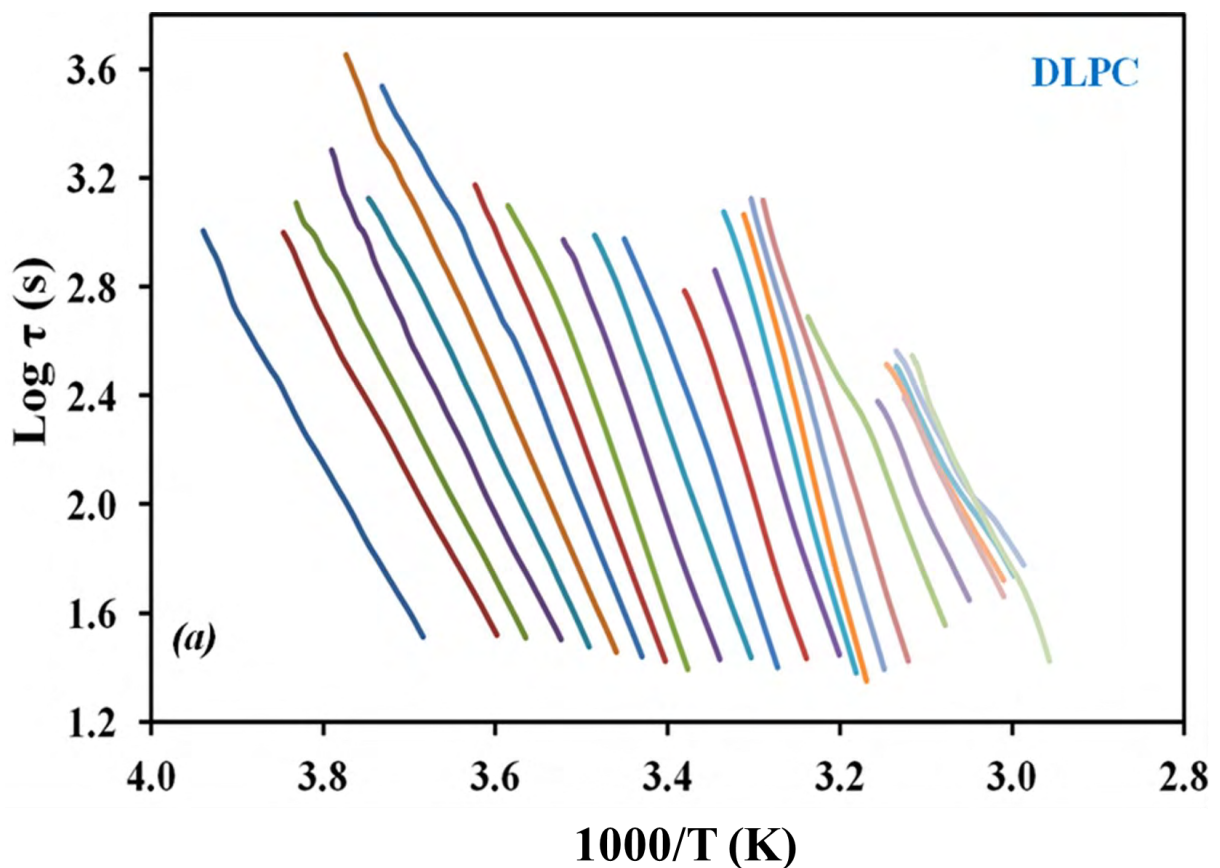
Global TSDC →

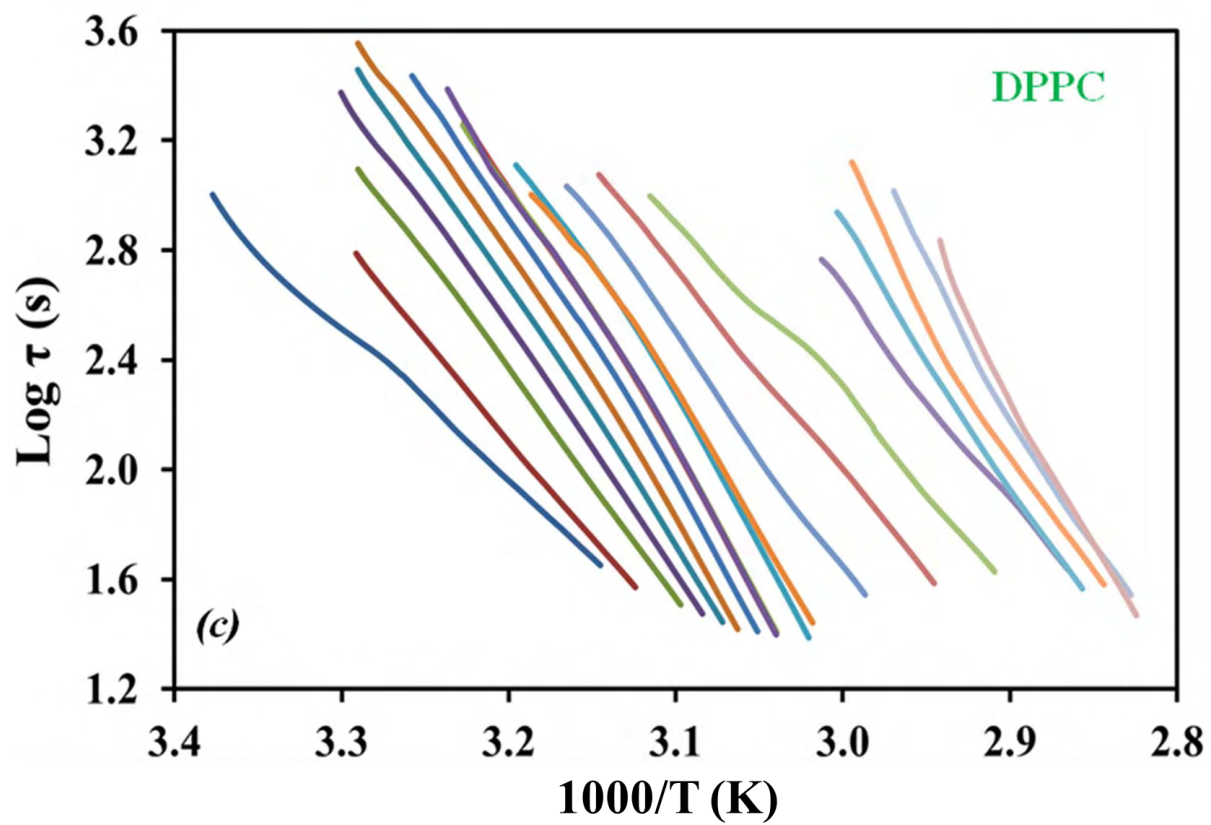
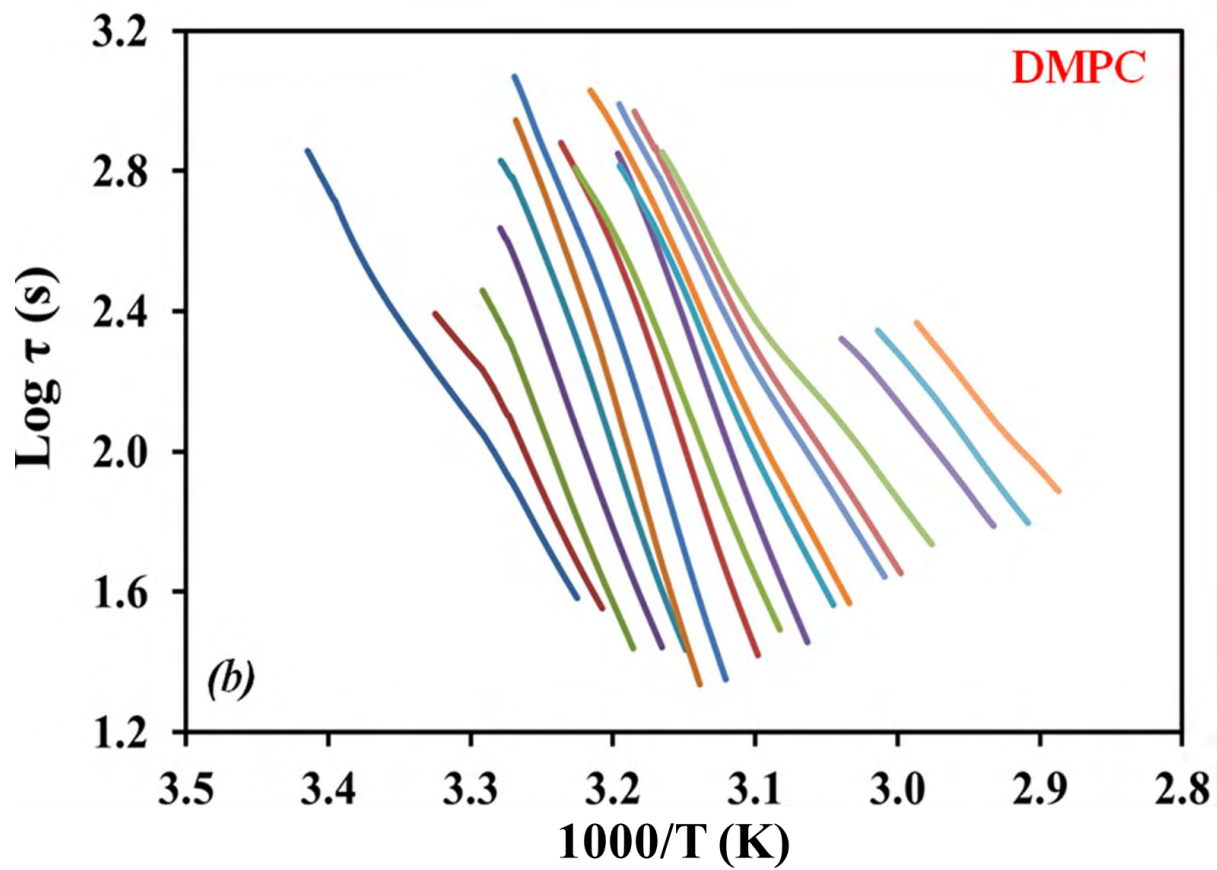
DSPC

-2

Fig. 4.14 The discrete relaxation modes observed under the global relaxation processes for (a) DLPC, (b) DMPC, (c) DPPC and (d) DSPC.

The distributions of relaxation times as a function of temperature for the discrete relaxation components obtained using the Bucci method is presented in Fig. 4.15. It is observed that the lower temperature relaxation components exhibit near linear Bucci lines, whilst significant curvature is observed for the higher temperature components. As mentioned previously, Bucci line curvature results from the polarisation of a collection of molecular motions whose activation energies are not narrowly distributed (Alvarez et al., 2000). In addition, it can be observed that in all samples the discrete components that exhibit relatively linear Bucci lines are those that relate to the sharp portion of the global relaxation process. These observations indicate that greater numbers of motional modes were activated at higher temperatures for all samples, indicating the complexity of molecular mobility at higher temperatures.





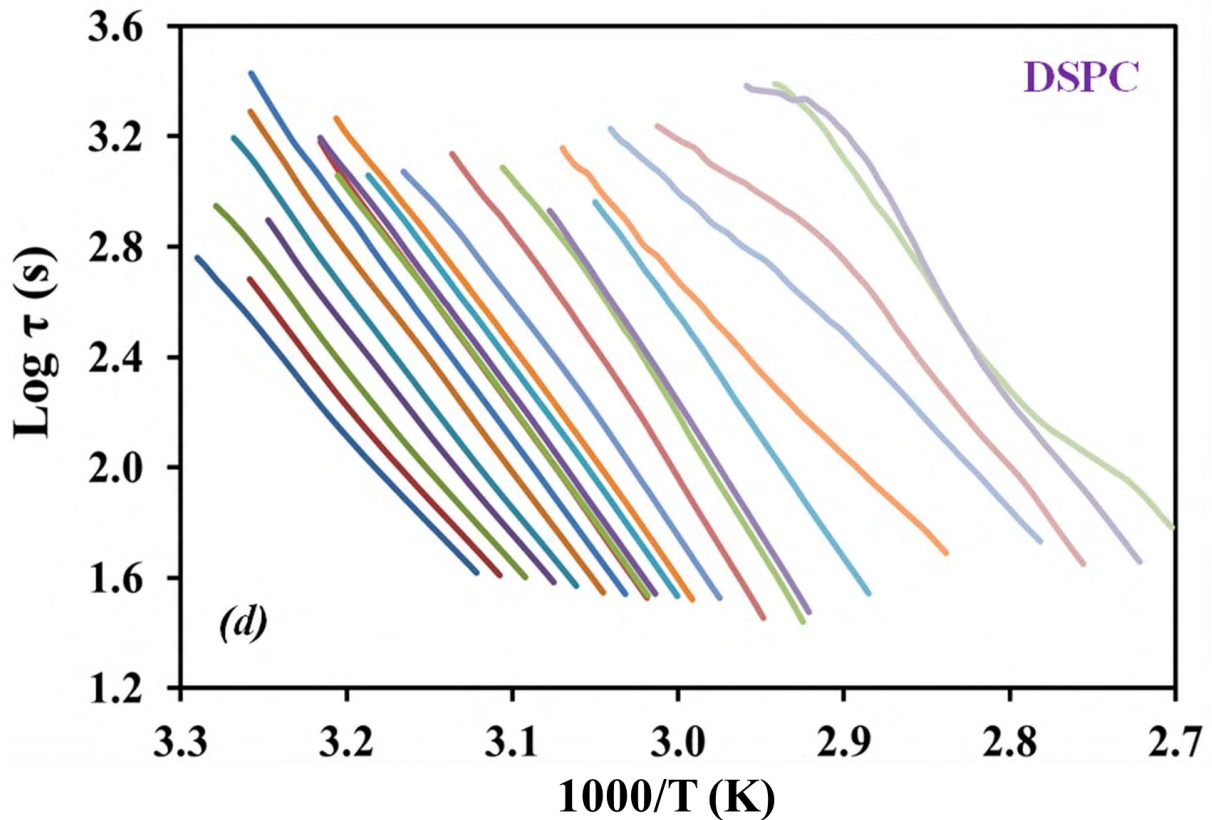
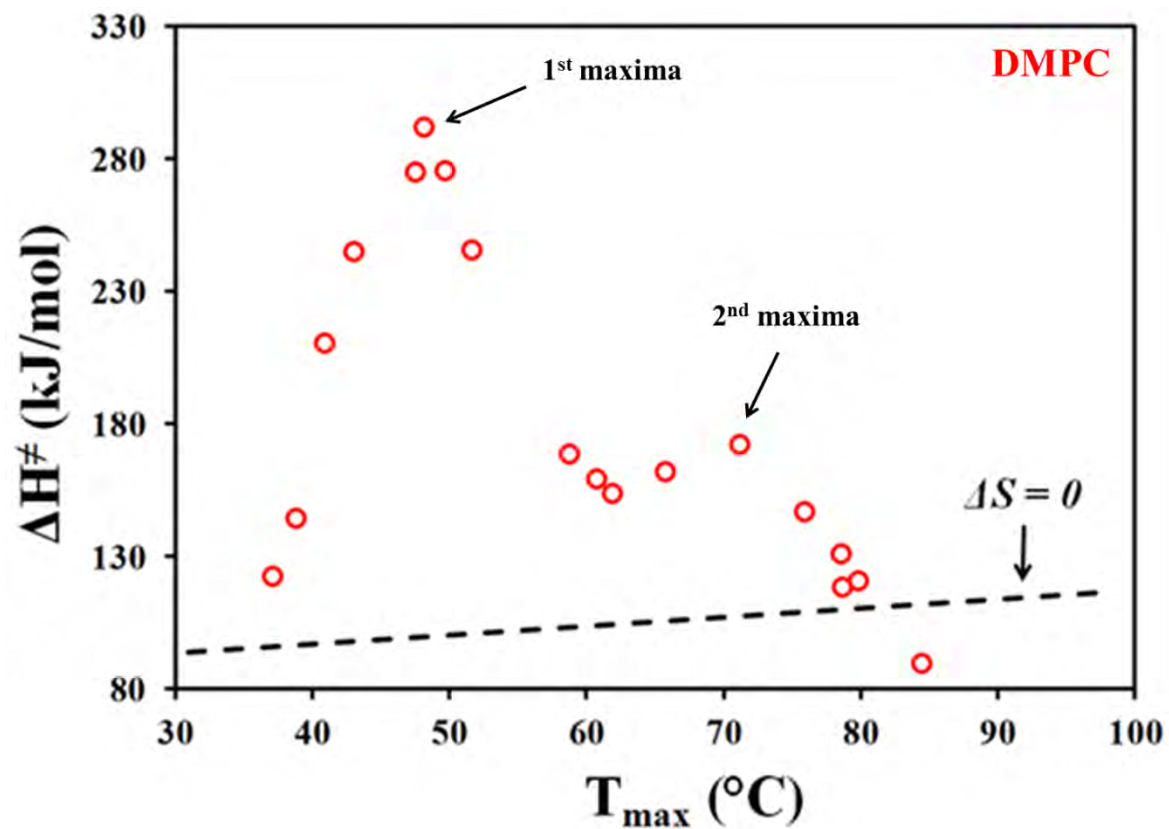
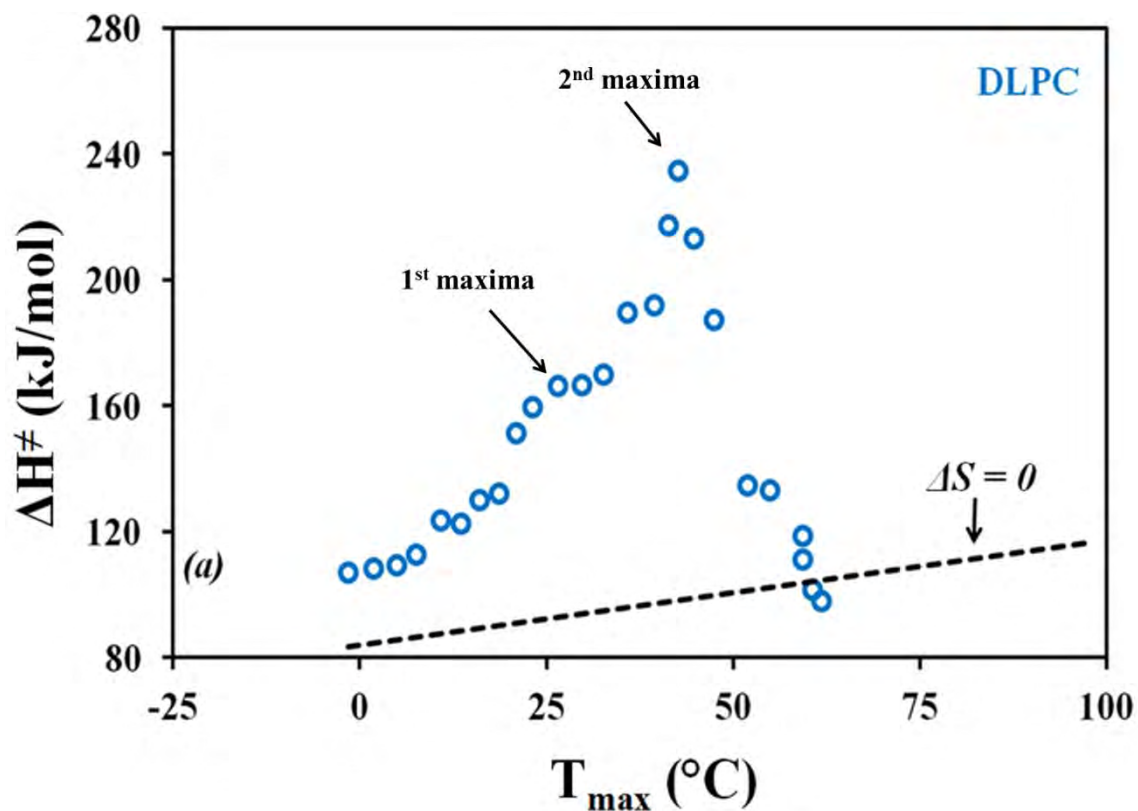


Fig. 4.15 Plot of distribution of relaxation time as a function of temperature (relaxation map analysis) for each elementary relaxation obtained using the Bucci method.

The activation enthalpies (ΔH^\ddagger) obtained by fitting the Bucci lines using the Eyring equation are plotted against the T_{\max} of the discrete depolarisation processes in Fig. 4.16. It can be clearly observed that the activation enthalpies deviate from the zero entropy line, which is typical of molecular motions in the glass transition regions. This supports the statement made by Wang and Tan (1997) that, in the solid state, the pre-transition process involves a glass transition. Deviation of ΔH^\ddagger from the zero entropy line is generally attributed to the cooperative nature of the molecular mobility during glass transitions i.e. increasing T_p activate, on a larger scale, the same type of molecular motions that require greater intra- and/or inter-molecular cooperation. This implies that the depolarisation currents observed results from primary relaxation processes.

The observation of a finite increase in activation enthalpy followed by the sharp descent towards the zero entropy line appears to be typical of semi-crystalline materials (Sauer et al., 1996, Sauer et al., 1997, Dargent et al., 1999, Correia et al., 2000). This further supports previous statement regarding the semi-crystalline nature of the phosphatidylcholines studied. Previous studies have demonstrated that when thermal windowing experiments are performed above the T_g of a pure amorphous system i.e. in the rubbery amorphous phase, ΔH^\ddagger decreased towards the zero entropy line (Vicioso et al., 2010, Sauer et al., 1990). A clear explanation for this behaviour has not been elucidated. However, it has been suggested that the sharp decent of ΔH^\ddagger after the maxima is attributed to the change in the tangent of the slope (decrease in the slope) of broadly distributed relaxation times, due to activation of different types of molecular motions even when undertaking the thermal windowing experiments using a narrow temperature window (Sauer et al., 1990). The constraining influence of the crystalline segments on the non-crystalline regions has also been considered to be a contributor to the observed behaviour (Sauer et al., 1996). It is therefore logical to infer that the processes observed may not originate from primary relaxation processes alone, but a combination of both primary and secondary relaxation processes.



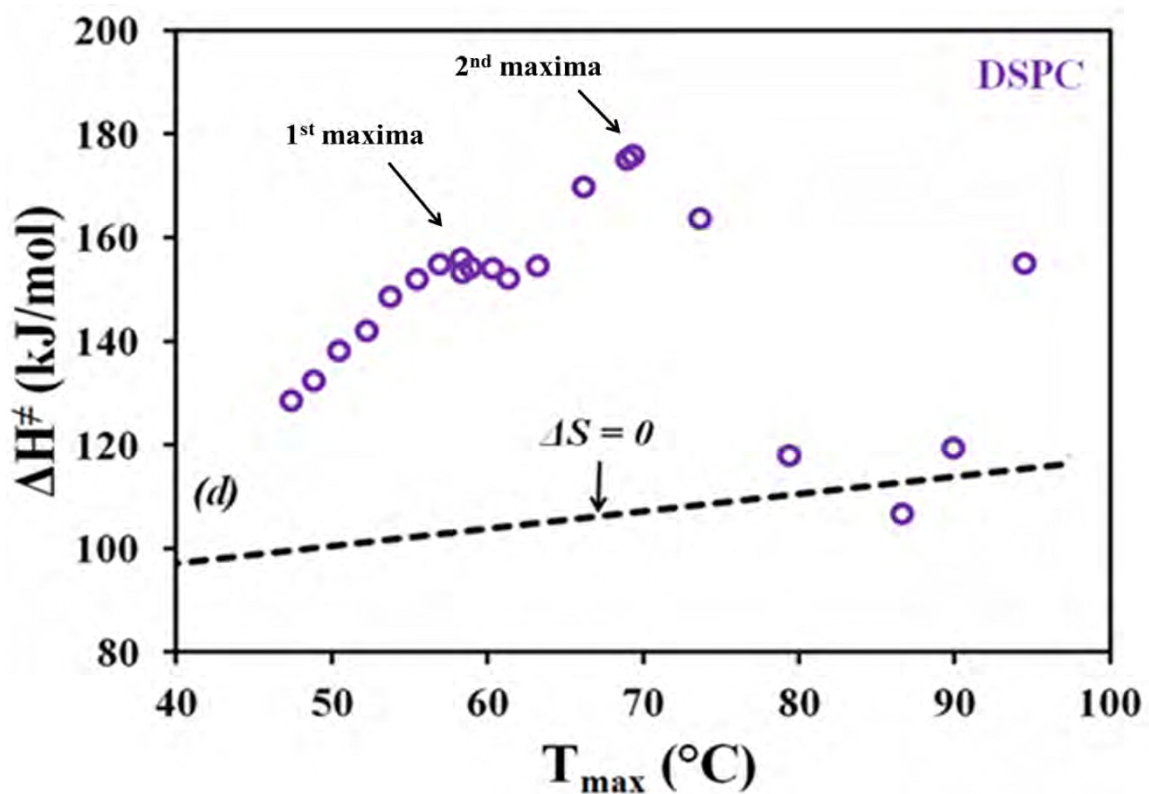
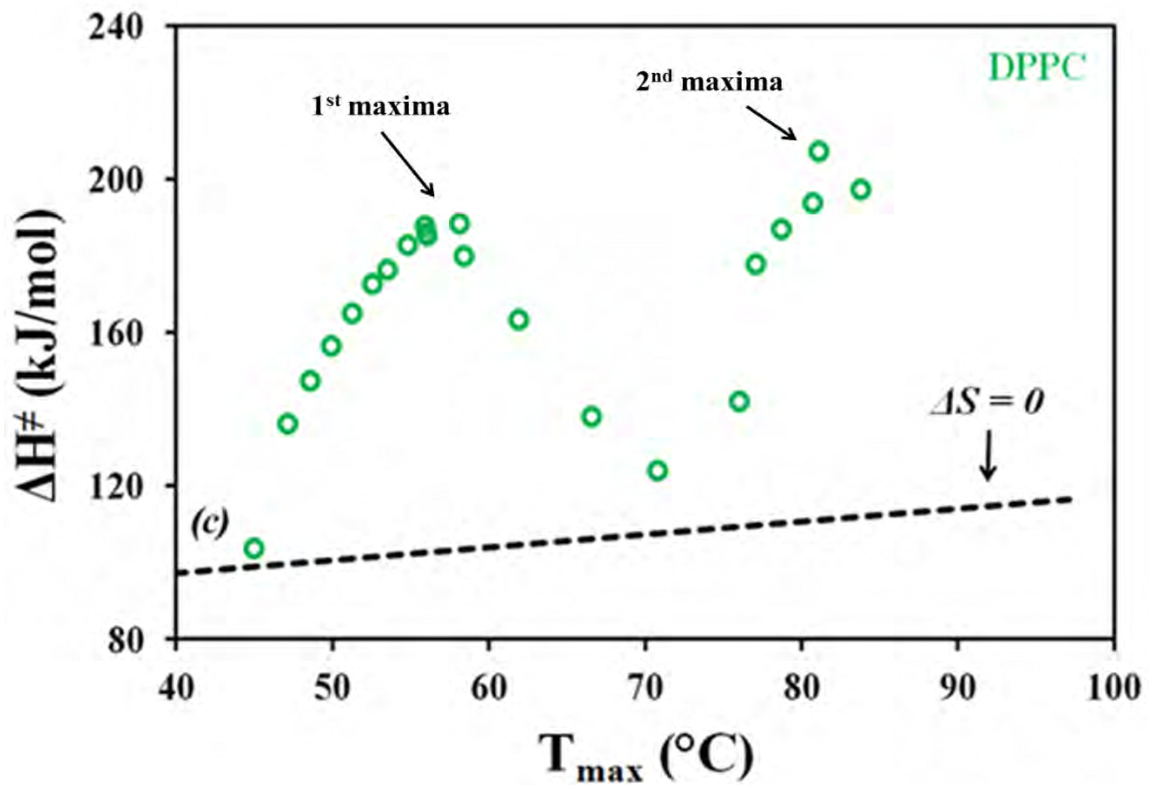


Fig. 4.16 Plot of activation enthalpy vs T_m of the discrete relaxation components for (a) DLPC, (b) DMPC, (c) DPPC and (d) DSPC.

The detection of global ΔH^\ddagger maxima (Fig 4.16) are indicative of different groups of molecular relaxation processes (Sauer and Avakian, 1992). The ΔH^\ddagger maxima observed in this study are presented in Table 4.4. The number of maxima is indicative of the number of relaxation processes occurring. Hence the observation of at least 2 maxima further indicates the phase heterogeneity in the materials studied. As shown in Fig. 4.14, DLPC, DMPC and DPPC have two ΔH^\ddagger maxima in the temperature range analysed, indicating two groups of cooperative molecular motion. DSPC exhibits two ΔH^\ddagger maxima with a potential 3rd ΔH^\ddagger maximum. This 3rd ΔH^\ddagger maximum is not within the temperature range analysed. These findings agree well with the complex behaviour observed in modulated DSC i.e. the two first order transitions (non-reversing heat flow) are overlapped with the glass transition for DLPC, DMPC, DPPC and DSPC. However, due to significant overlapping of the difference process observed in the DSC study, it is not possible to ascertain whether the relaxation process observed is due to a glass transition or melting, since both processes require significant intra- and inter-molecular cooperation.

Table 4.4 Temperatures and activation enthalpy values obtained at the enthalpy maxima for DLPC, DMPC, DPPC and DSPC

Sample		Temperature maxima (°C)	T _p (°C)	ΔH [‡] (kJ/mol)
DLPC (12:12)	1	27 ± 1	12	193 ± 38
	2	41 ± 2	27	250 ± 22
DMPC (14:14)	1	47 ± 2	33	265 ± 33
	2	70 ± 1	54	170 ± 20
DPPC (16:16)	1	57 ± 2	42	193 ± 8
	2	81 ± 3	69	207 ± 15
DSPC (18:18)	1	58 ± 2	42	152 ± 8
	2	67 ± 3	57	163 ± 21

The data obtained from the study of the thermal windowing experiments have so far demonstrated that molecular motions in the pre-transition region is a complex mixture of cooperative large scale reorientation processes and localised molecular orientations and/or intra-molecular rotations. The carbon chain length dependence of these processes indicates that molecular motions are related to the (hydrophobic) acyl chains of the phosphatidylcholines. Hence the motional modes detected are likely to arise from the segmental mobility of the acyl chains. However, it is possible that these cooperative processes do not only occur within and between the hydrophobic layers but may also require significant cooperation from the hydrophilic head groups. Hence, there may be elements of the reorientation processes that are due to the movement of the whole molecule. Furthermore, it is logical to consider that the head group regions may impose constraints on the progressive cooperative orientations of molecules, which could be a contributing factor to the descent in the ΔH[‡] maxima towards the zero entropy line.

In order to understand the influence of acyl chain length on the relaxation times a comparison can be made between the relaxation times obtained at the T_{\max} of the most intense discrete relaxation process (Table 4.5). Fig. 4.17 illustrates the relationship between diacyl chain length and molecular relaxation time. Whilst the differences in relaxation times are not large, it can be clearly observed that a linear relationship exists between the relaxation time and carbon chain length, if the relaxation time observed for DLPC is ignored. It is important to note that DLPC behaves quite different to its expected behaviour both in DSC studies and in the global TSDC results, hence it is not surprising that its relaxation characteristics deviates from the “norm”. It is clearly observed, from the data in Fig. 4.17, that increasing the acyl chain length increases the relaxation time. This means that molecular mobility is slower in saturated phosphatidylcholines with longer diacyl chains and therefore greater molecular weight. This behaviour relates well with the observed influence of acyl chain length on the pre-transition and chain melting processes.

These observations demonstrate that there is a relationship between molecular mobility, as observed by TSDC, and the stability of homologous phosphatidylcholine. In this particular study, molecular mobility appears to influence the physical stability of the phosphatidylcholines i.e. with decreasing relaxation time (τ), the temperature of the pre-transition and chain-melting transition observed in DSC increases. The reason for the observed increase in relaxation time as a function of acyl chain length may be attributed to increase in molecular size which hinders mobility, and Van Der Waals interactions, which increase structural stability.

Table 4.5 Relaxation times obtained at the T_{\max} of the discrete components corresponding to the main relaxation process observed for homologous series of the phosphatidylcholine studied ($n=3$).

Compound	Diacyl chain length	T_p (°C)	T_{\max} (°C)	τ (s)
DLPC	12	27	41 ± 2	21.1 ± 2.0
DMPC	14	33	47 ± 2	19.3 ± 3.5
DPPC	16	42	57 ± 2	25.0 ± 0.8
DSPC	18	57	67 ± 3	32.8 ± 4.1

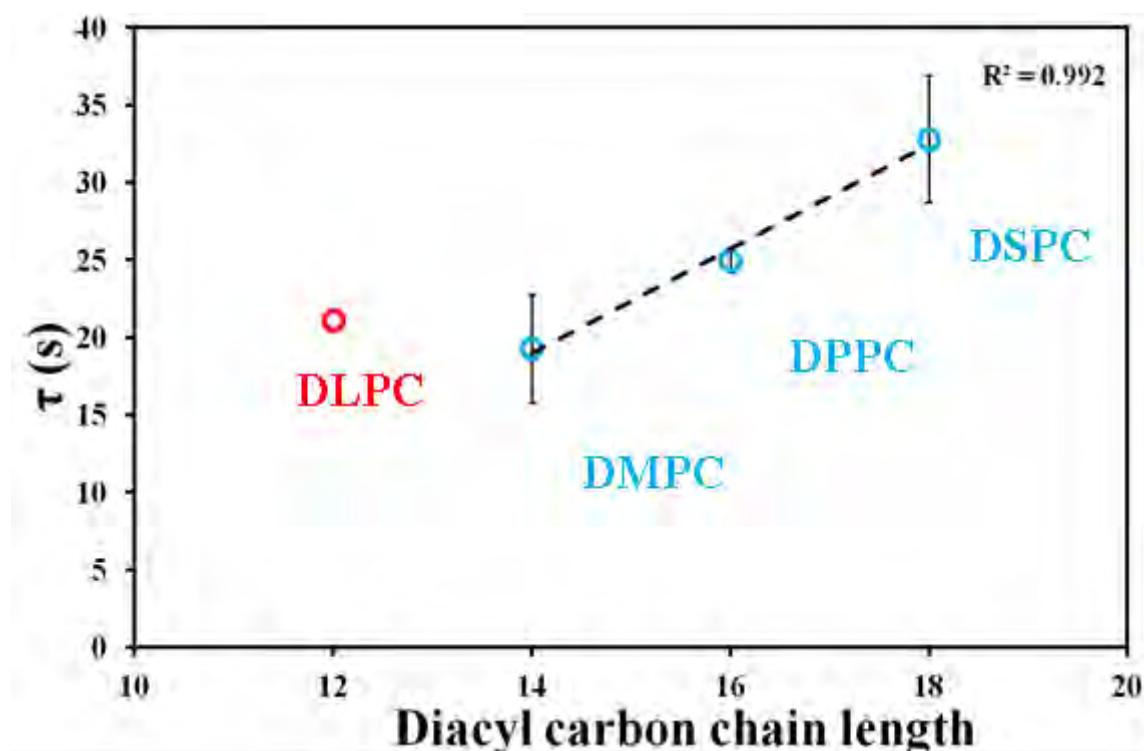


Fig. 4.17 Plots of relaxation times (τ) at the T_{\max} of the discrete relaxation component with the highest current intensity against carbon chain length.

As already stated the molecular motions observed in TSDC studies are due to complex mixtures of large scale reorientations and localised intermolecular and intra-molecular motions within the hydrophobic tail region of multilayered phosphatidylcholines. However, it is possible that these molecular orientations in the hydrophobic regions of the multilayered systems will require significant cooperation from the more rigid hydrophilic head regions. This may be the sections in the materials where significant constraints are imposed on cooperative molecular motions and therefore the possible cause of the descent of activation enthalpy. Previous studies demonstrate that transitions below the T_m involves rearrangements in the hydrophobic and hydrophilic regions of the multilayered structure of the phosphatidylcholines (Fringeli, 1981).

The results show that the molecular relaxation time for the main depolarisation process increases with increasing diacyl carbon chain length. DLPC appears to be an exception to this rule i.e. the relaxation time observed for DLPC is equal to or greater than that observed for DMPC. It is also important to point out, that the similarities in the relaxation time between DLPC and DMPC were also observed with the activation energies in the scanning rate dependent kinetic study of the chain-melting transition i.e. at $\leq 50\%$ (α) little difference in activation energy is observed between DLPC and DMPC, when the activation energy observed for the T_m in DLPC was expected to be lower than that attained for DMPC. In addition to the positive correlation between relaxation time and diacyl chain length, a positive correlation also exists between molecular relaxation time, the peak temperature and the apparent activation energies observed for the chain melting transition in DSC studies (Fig. 4.18). This demonstrates that the rate of molecular mobility, as observed by TSDC, is related to the thermal physical stability of the phospholipids studied.

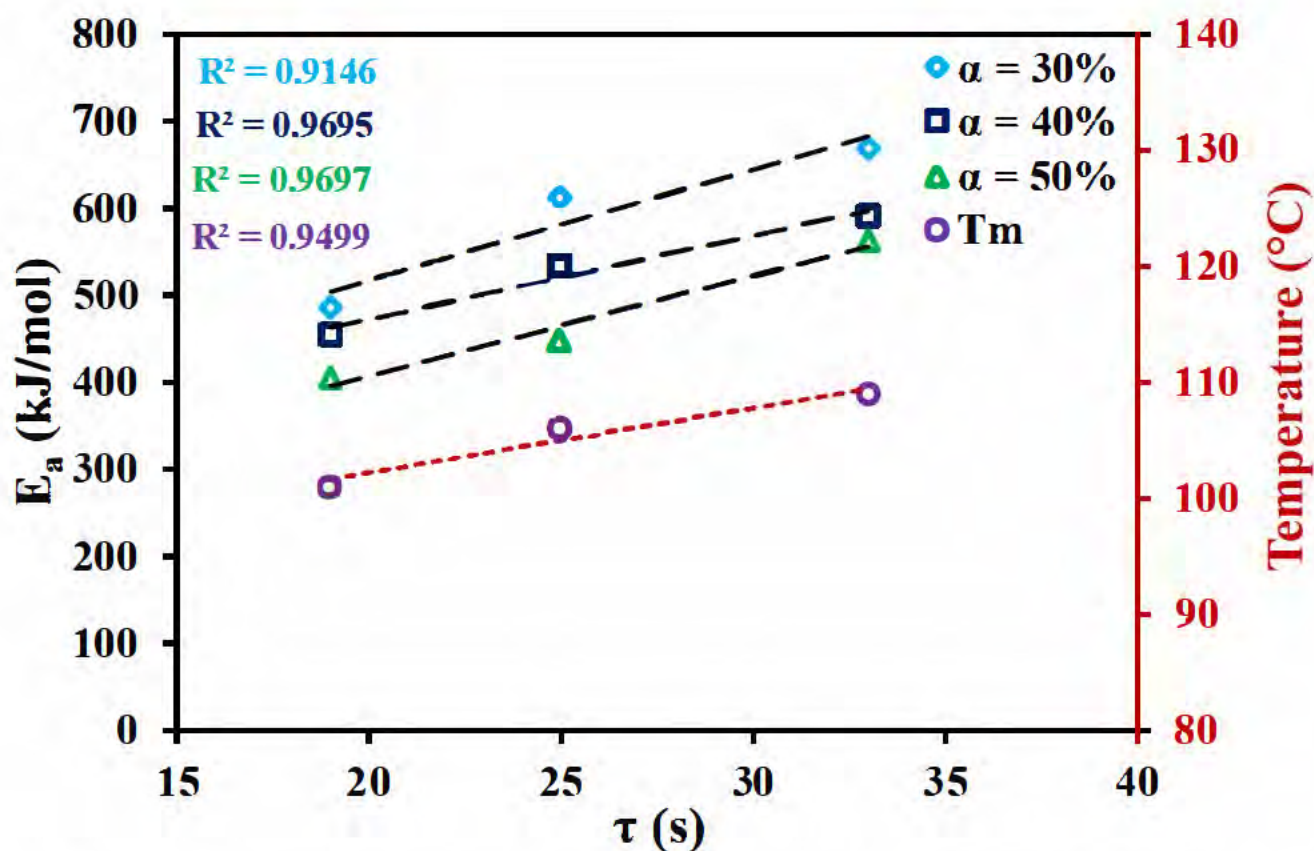


Fig. 4.18 Plots of the relaxation times (τ) obtained at the T_{\max} of the main depolarisation processes observed for DMPC, DPPC and DSPC versus the apparent activation energies obtained at 30, 40 and 50% α of the chain melting transition observed in DSC and the peak temperatures of the chain melting transition (T_m).

4.4 Conclusions

The results from DSC studies have shown for the first time, the existence of 6-8 transitions (including the chain melting transition) prior to the isotropic melt for saturated phosphatidylcholines (Table 4.1). In addition, it is the first time that a pre-transition process has been reported for anhydrous DLPC, DMPC, DPPC and DSPC (at 34 ± 1 , 57 ± 1 , 70 ± 1 , $78 \pm 1^\circ\text{C}$, respectively).

Temperature modulated DSC revealed that the broad pre-transition is composed of complex overlapping 1st and 2nd order transitions. It was found that DLPC, DMPC, DPPC and DSPC

undergo two crystal melting transitions in the non-reversing heat flow signal. Another melting process was identified in the reversing heat flow signal, which is attributed to the partial melting of the phosphatidylcholine lamellae. Within the same temperature region, a glass transition is observed. These observations are the first to be made for the saturated phosphatidylcholines. The peak temperature at which the overall pre-transition process occur was found to be carbon chain length dependent i.e. increasing carbon chain length increases the peak temperature of the transition. Kinetic studies of the chain-melting transitions show the activation energy of this process to decrease as the transition progresses. This behaviour has been attributed to the decrease in the degree of cooperation required for molecular orientations to occur. Furthermore, it was found that increasing the carbon chain length from 14 to 18 (DMPC–DSPC) results in the increase of the apparent activation energy. DLPC does not exhibit significant difference in apparent activation energy when compared with DMPC.

For the first time, the molecular mobility of the pre-melting transition observed for the anhydrous phosphatidylcholines have been characterised by TSDC. It was found that DLPC, DMPC, DPPC and DSPC undergo similar dipole relaxation processes. The ease at which these relaxation processes occur is carbon chain length dependent i.e. T_{\max} of the depolarisation process increases with increasing carbon chain length. The relaxation processes observed are cooperative and have been proposed to originate from the segmental mobility, mainly from the hydrophobic region of the multi-lamellar structure. It has also been recognized that head group orientation are also at play in the mobility states. These mobility states are suspected to require both inter- and intra-molecular cooperation from the hydrophobic tail and also the polar head groups. In general, molecular relaxation time increases with increasing diacyl carbon chain length i.e. the τ values obtained are 21 ± 2 , 19 ± 3 , 25 ± 1 and 32 ± 4 s for DLPC, DMPC, DPPC and DSPC, respectively. This shows that increasing carbon chain length hinders mobility. Molecular mobility of the saturated

phosphatidylcholines is limited by degree of hydrophobic interactions and the size of the hydrophobic chains.

Finally, in addition to demonstrating that a relationship exists between carbon chain length and molecular mobility, this study has also shown also that a relationship exists between the rate of molecular mobility and thermal physical stability. It can be concluded that the longer the carbon chain length of saturated diacyl phosphatidylcholines, the slower the molecular relaxation time and therefore the greater the thermal stability in the anhydrous state.

Chapter 5 : Influence of Molecular Size on Solid-State Mobility and Thermal Stability of a Peptide and Proteins

5.1 Introduction

Peptides and proteins are directional polymers constituted of structurally modified or unmodified α -amino acid monomers. The complex three dimensional structures of these macromolecules originate - in part - from their primary amino acid sequence. The primary amino acid structure of proteins is defined as the number, identity and linear sequence of amino acids. The primary structure organises into several secondary structures such as α -helices, β -sheets, turns and random coils that in turn fold into the overall specific three-dimensional tertiary or quaternary structure (if the peptide/protein consists of more than one polypeptide chain). The resultant native structure determines the specific function of proteins. Peptides/proteins are polyelectrolytes, unless of course their primary sequence consists solely of hydrophobic amino acids. In addition to their specific structure, the surrounding solvent provides the necessary milieu for the internal motions required for protein function (Rupley and Careri, 1991). Internal motions of a peptide/protein in the solution state involve various processes occurring over very broad timescales (Fig 5.1).

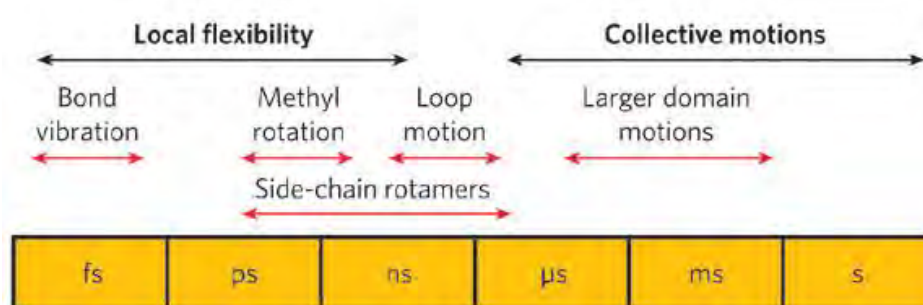


Fig. 5. 1 Timescale of dynamic processes observed in hydrated proteins (reproduced from: Henzler-Wildman and Kern, 2007).

Various techniques have been employed to understand protein dynamics over wide temperature range and hydration levels. Techniques such as Mössbauer spectroscopy (Parak et al., 2007) infrared spectroscopy, x-ray crystallography (Rasmussen et al., 1992, Tilton et al., 1992), DSC (Jansson and Swenson, 2010), neutron scattering (Doster, 2010, Doster et al., 1989), NMR (Henzler-Wildman and Kern, 2007) and dielectric spectroscopy (Jansson and Swenson, 2010) have been employed in order to interrogate the dynamic behaviour of proteins. The applications of these techniques have collectively demonstrated that the dynamic processes and flexibility of hydrated proteins changes drastically between -100 and -50°C for a number of proteins. The temperature dependent molecular relaxations below the transition point follow Arrhenius type behaviour, whilst above the transition point non-Arrhenius behaviour is detected (Jansson and Swenson, 2010, Jansson et al., 2011). This change in protein dynamic processes is described as a “glass transition” due to the increase in slow collective and large domain motions, resulting in a change in heat capacity. In addition, relaxation times as slow as 100 s have been observed for some proteins (Doster, 2010). These changes in dynamic processes have also been demonstrated to be highly sensitive to the hydration state of the proteins (Fitter, 1999) i.e. increasing hydration level decreases the temperature of the dynamic transition, whilst increasing protein flexibility .

The importance of large domain motions to protein function was demonstrated by Rasmussen et al, 1992. Ribonuclease A does not bind to its substrate or inhibitor at temperatures below -53°C, where only localised rotational motions exists, but it is active at temperatures above -53°C, where large amplitude, collective motions exists. This was attributed to the fact that above the dynamic transition temperature, large amplitude motions allows proteins to undergo fluctuating conformational states that enables them to interact with their substrates.

Whilst internal molecular mobility is important for the function of proteins, it is also the major problem with regard to the stability of proteins (Chang and Pikal, 2009). The common practice in the attempt to improve the stability of these macromolecules is to formulate them in the solid-state. This provides better storage stability in comparison to the solution state. However, it is understood that even at very low levels of hydration, proteins exhibit similar physical and chemical instabilities (Lai and Topp, 1999). Due to the poor packing ability of peptides and proteins in the solid-state, enough free volume exists for these macromolecules to undergo rotational and possibly large domain or segmental motions that makes proteins susceptible to irreversible denaturation and chemical deterioration (Parkins and Lashmar, 2000; Strickley and Anderson, 1996; Flores-Fernandez et al., 2010).

The aim of the work reported in this Chapter is to probe the internal mobility of freeze-dried proteins in an attempt to understand the influence, if any, of molecular size of peptides/proteins on internal motions. In addition, an attempt is made to understand how molecular mobility differences relate to the thermal stability of the materials under investigation.

The model peptides/proteins used were insulin, lysozyme and myoglobin. Insulin is a peptide hormone synthesized by the β -cells of the islets of Langerhan in the pancreas. Its primary function is the regulation of blood glucose levels. The insulin molecule consists of 51 amino acid residues split into two helical chains, one contains 21 amino acid residues and the other 30 amino acid residues; denoted A and B chains, respectively. The two chains are joined by two inter-chain disulphide bonds, a 3rd disulphide bond is found in the A chain.

Lysozyme has a molecular weight of 14.3 kD and consists of 129 amino acid units and 4 intra-molecular disulphide bonds. It has 5 helical regions, five regions of β -sheet, β -turns and

a large amount of random coil. Lysozyme is an enzyme found in tears, nasal secretions and bacterial cell walls.

Myoglobin is a globular protein found, predominantly, in skeletal muscles; where it functions as the primary oxygen-carrying pigment of muscle tissues. It consists of 154 amino acid residues with a molecular weight of 17.0 kDa (Ochiai et al., 2010). The globular structure of myoglobin consists of 8 α -helices and a centred heme group. The heme group consists of an organic protoporphyrin component and an iron atom located in its centre.

5.2 Methods

5.2.1 TGA

A sample mass of 3.20 ± 0.40 mg was used for all compounds. Samples were heated under a nitrogen atmosphere at a flow rate of 25 ml/min from ambient temperature to 600°C in hermetically sealed aluminium pans with a single pin hole in the lid, at a heating rate of 10°C/min.

5.2.2 DSC

DSC studies were performed under a nitrogen atmosphere at a flow of 50 mL/min, using hermetically sealed Tzero aluminium pans with a pin hole in the lid. Sample mass of 2.60 ± 0.24 mg was heated to 140°C to remove moisture, equilibrated at -90°C, held isothermal for 5 minutes and heated to 240°C at 10°C/min.

5.2.3 TSDC

TSDC studies, covering the range -150 to -20°C for “as received” samples and between -25 to 150°C for dehydrated samples were conducted using a TSCII/RMA spectrometer (SETARAM, France) equipped with a 900 series LN2 micro-dosing cooling system (Norhof, Netherlands) and 6517A electrometer (Keithley, UK). Experiments were performed using a sample holder that consists of bottom and upper electrodes with a PTFE ring spacer, the

sample in this arrangement had an effective surface area of 38.5 mm^2 . Sample size used was $30 \pm 1 \text{ mg}$. Prior to the experiments, the analysis chamber containing the sample, was evacuated to 10^{-4} mbar and flushed several times with high purity helium (1.1 bars). The global TSDC spectra were obtained by polarising the sample at various temperatures with a polarisation field (E_p) ranging from 100 to 450 V/mm for 2 min (t_p).

In the case of thermal windowing experiments, samples were polarised with $E_p = 400 \text{ V/mm}$ at T_p of -150 to -50°C and from -25 to 120°C in increments of 5°C for the as received samples and after dehydrating the samples, respectively. T_w was set at 5°C , whilst t_p and t_w were set at 2 min for all three samples.

5.3 Results and Discussions

5.3.1 TGA and DSC

The results obtained from TGA and DSC studies show the thermo-physical and thermo-chemical behaviour of the investigated peptide and proteins to be similar. TGA results (Fig. 5.2) suggest that insulin, lysozyme and myoglobin undergo two major weight loss processes when heated from ambient temperature to 600°C . The initial weight loss results from the removal of moisture, whilst the second process is due to decomposition (confirmed using HSM). Myoglobin contains the greatest amount of moisture (Table 5.1), whilst insulin and lysozyme have similar moisture content ($5 \pm 1\%$). Furthermore, the temperature at which dehydration occurs is lowest for myoglobin, whilst lysozyme has the highest temperature of dehydration. This implies that hydrogen bonding between amino acid residues and water molecules are strongest in lysozyme and weakest in myoglobin. No significant differences are observed in the fractional weight change associated with the decomposition processes. The extrapolated onset of the decomposition process was found to be the same for insulin and lysozyme ($268 \pm 1^\circ\text{C}$), whilst that observed for myoglobin is $282 \pm 1^\circ\text{C}$. Furthermore,

derivative peak temperatures for the decomposition process is in the order myoglobin > insulin > lysozyme.

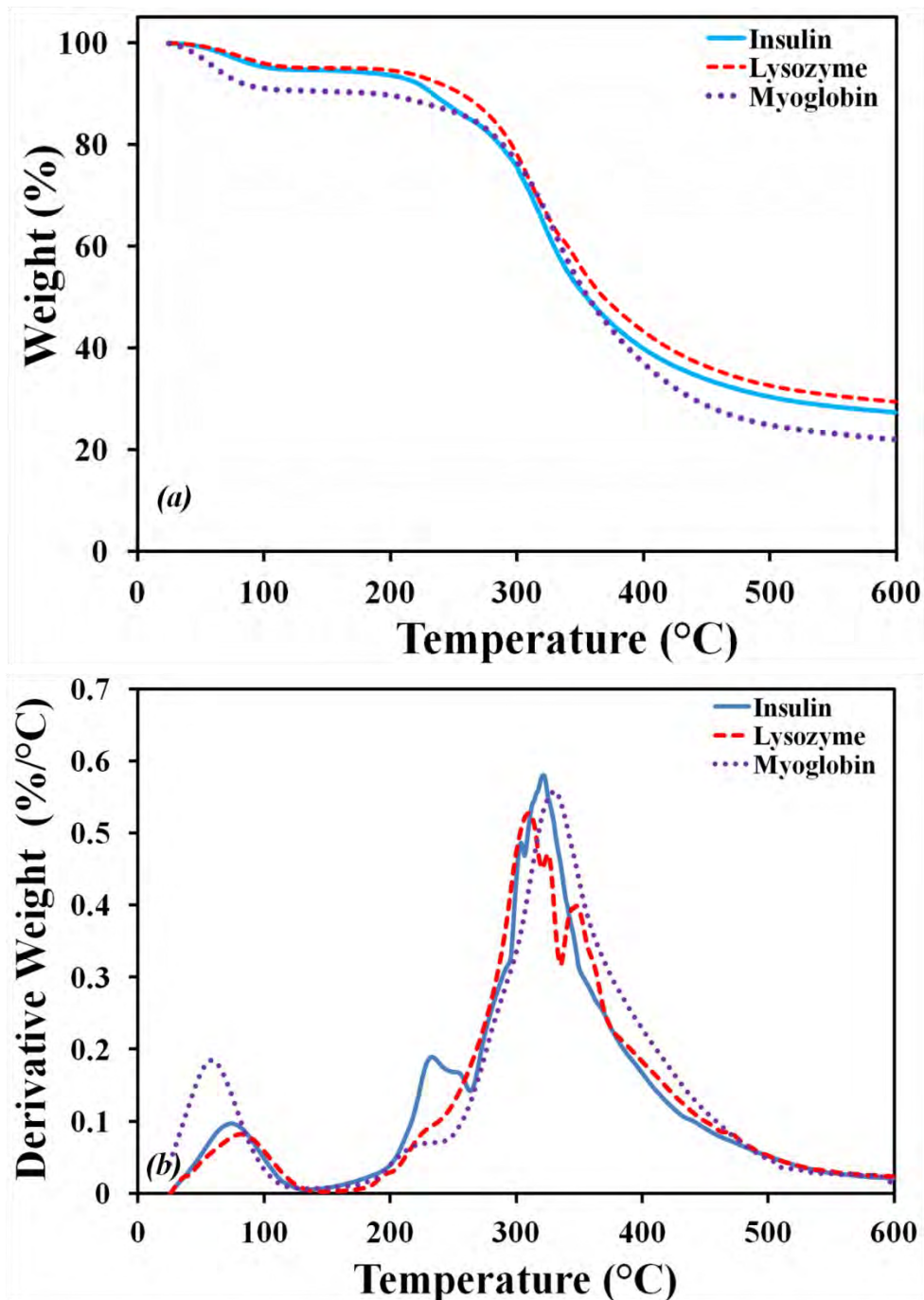


Fig. 5.2 TGA curve overlay of the proteins heated from ambient temperature to 600°C at 10°C/min. (a) Thermogravimetric (TG) curves and (b) derivative thermogravimetric (DTG) curves.

Table 5.1 The temperatures and weight changes associated with the processes observed in TGA studies for the proteins.

Compound	Dehydration			Decomposition	
	Extrapolated onset (°C)	DTG peak (°C)	% Δ Weight	DTG peak (°C)	% Δ Weight
Insulin	49 ± 1	74 ± 1	5.0 ± 0.2	321 ± 2	67.2 ± 0.2
Lysozyme	53 ± 1	82 ± 1	5.0 ± 0.1	309 ± 1	66.0 ± 0.6
Myoglobin	35 ± 1	59 ± 1	9.9 ± 0.2	330 ± 2	68.0 ± 0.9

DSC results show that no thermal transitions occur after the removal of moisture when insulin, lysozyme and myoglobin samples are heated from -90°C to temperatures below the decomposition processes. Overlapping with the decomposition processes is a second order transition. This second order transition is the heat capacity change associated with the denaturation of the peptide and proteins. This means that the proteins unfold before decomposing to release volatile products as observed in the TGA study. From the temperature of denaturation (Table 5.2) the thermal stability is in the order insulin > myoglobin > lysozyme. This order of thermal stability was not observed in the TGA results when the extrapolated onset was considered.

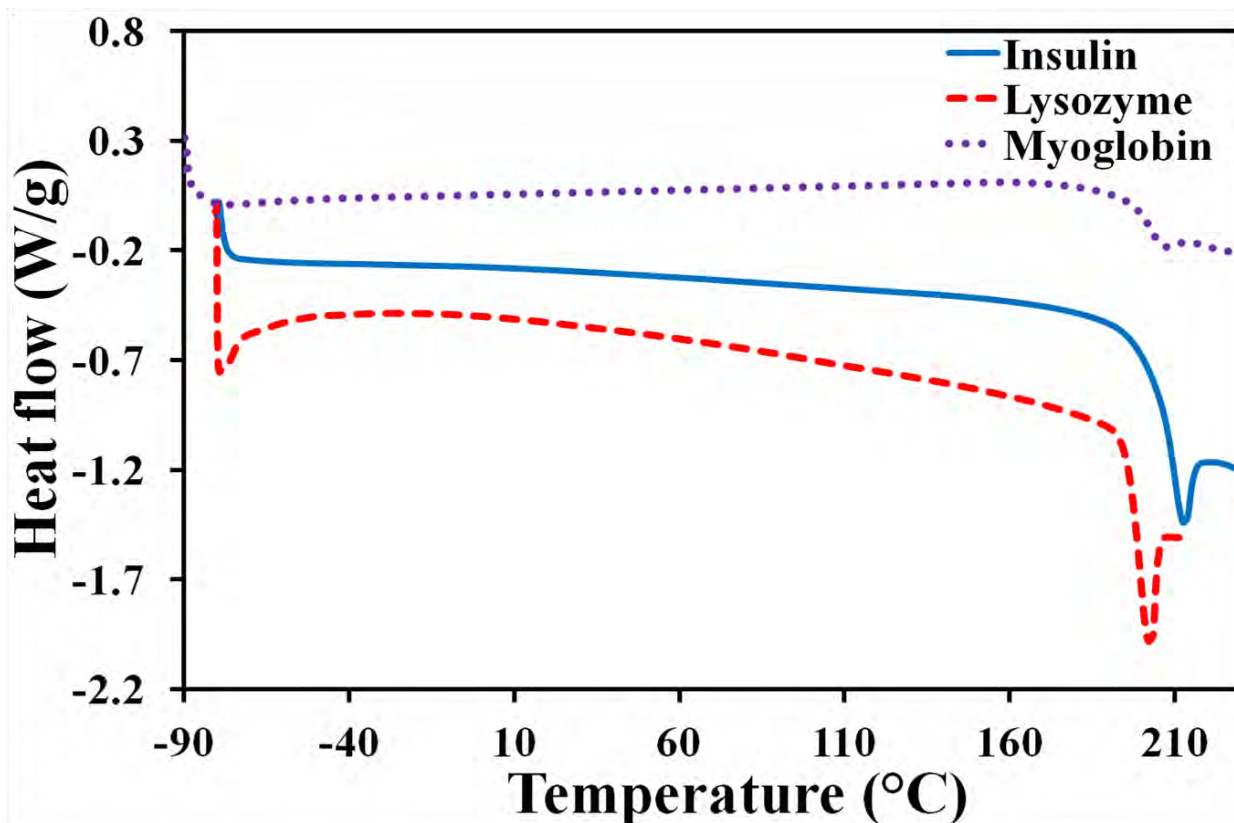


Fig. 5.3 Overlay of DSC thermograms observed for the proteins obtained using a heating rate of 10°C/min.

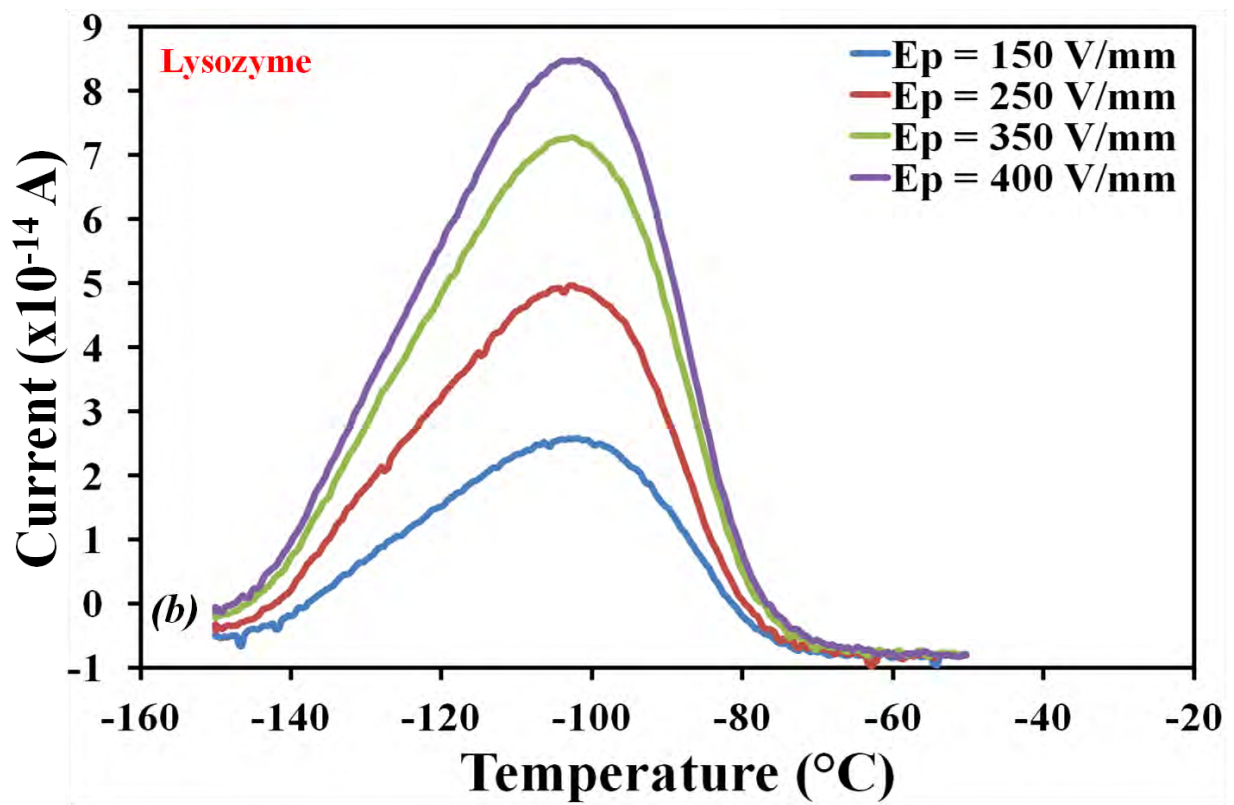
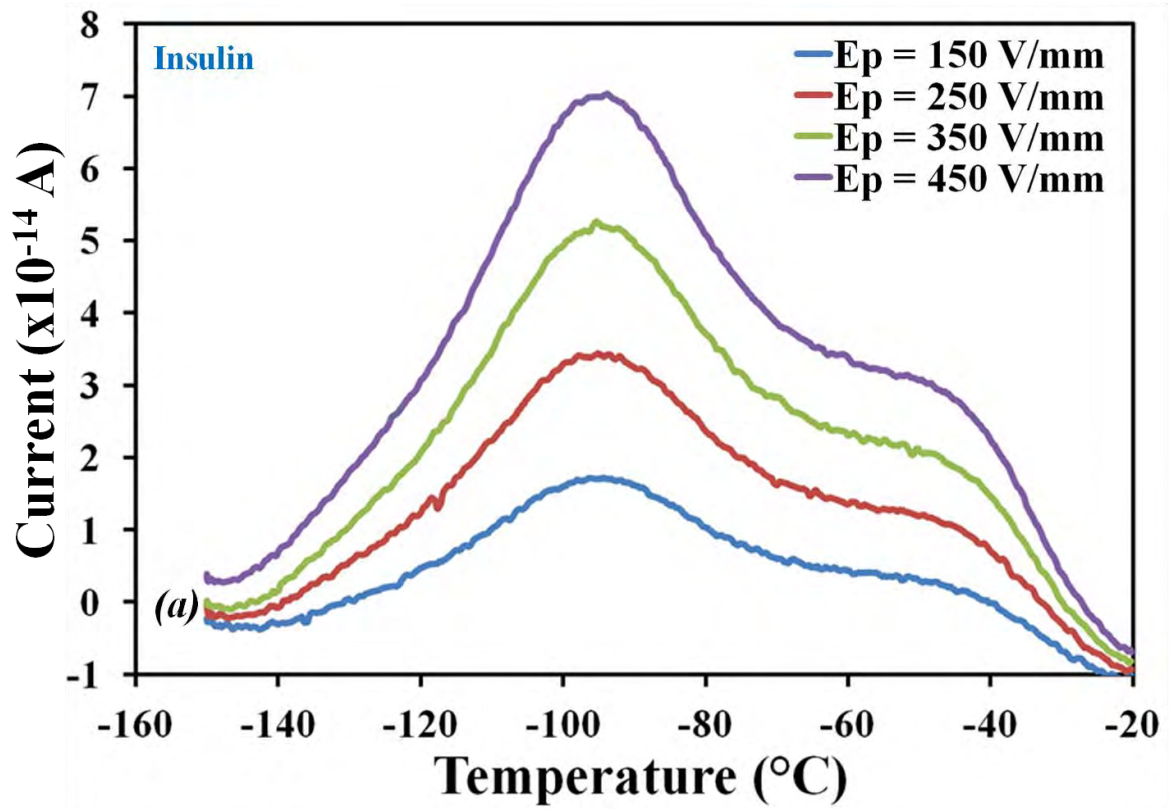
Table 5.2 The “glass transition” temperatures observed for the proteins investigated.

Sample	“T _d ” (°C)
Insulin	205 ± 1
Lysozyme	197 ± 1
Myoglobin	202 ± 1

5.3.2 Hydrated States

5.3.2.1 Global TSDC

The global depolarisation processes were assessed between -150 and -20°C. The depolarisation profiles obtained for each protein, at the polarisation temperature which generated the greatest current intensity at the T_{\max} are presented in Fig. 5.4(a-c). Also, the temperature locations of the depolarisation current maxima observed for each protein are presented in Table 5.3. The T_{\max} obtained for each protein (first process for myoglobin) corresponds to the temperature region where the “protein-water glass transition” is typically observed (Jansson et al., 2011, Panagopoulou et al., 2011). The data in Table 5.3 shows a decrease in T_{\max} from insulin (the smaller protein) to myoglobin (the larger protein). Neither moisture content nor the protein molecular weight exhibits linear relationship with the observed increase in T_{\max} . However, when the number of amino acid units is considered, a linear relationship is observed with an R^2 value of >0.98 (Fig. 5.5). This implies that molecular mobility in the temperature range analysed is easier for proteins containing more amino acid units at lower temperatures in the presence of adsorbed water. In addition to the aforementioned observations, the current intensity was observed to be significantly greater for myoglobin when compared with the other proteins studied. Furthermore, insulin and lysozyme exhibit no significant differences in depolarisation current intensity. These observations correlate well with the differences in moisture content observed in the TGA study i.e. myoglobin has twice the amount of moisture content ($\sim 10\%$) when compared to insulin and lysozyme ($\sim 5\%$). This in turn suggests that water plays an important role in the mobility of the proteins in the temperature range of analysis.



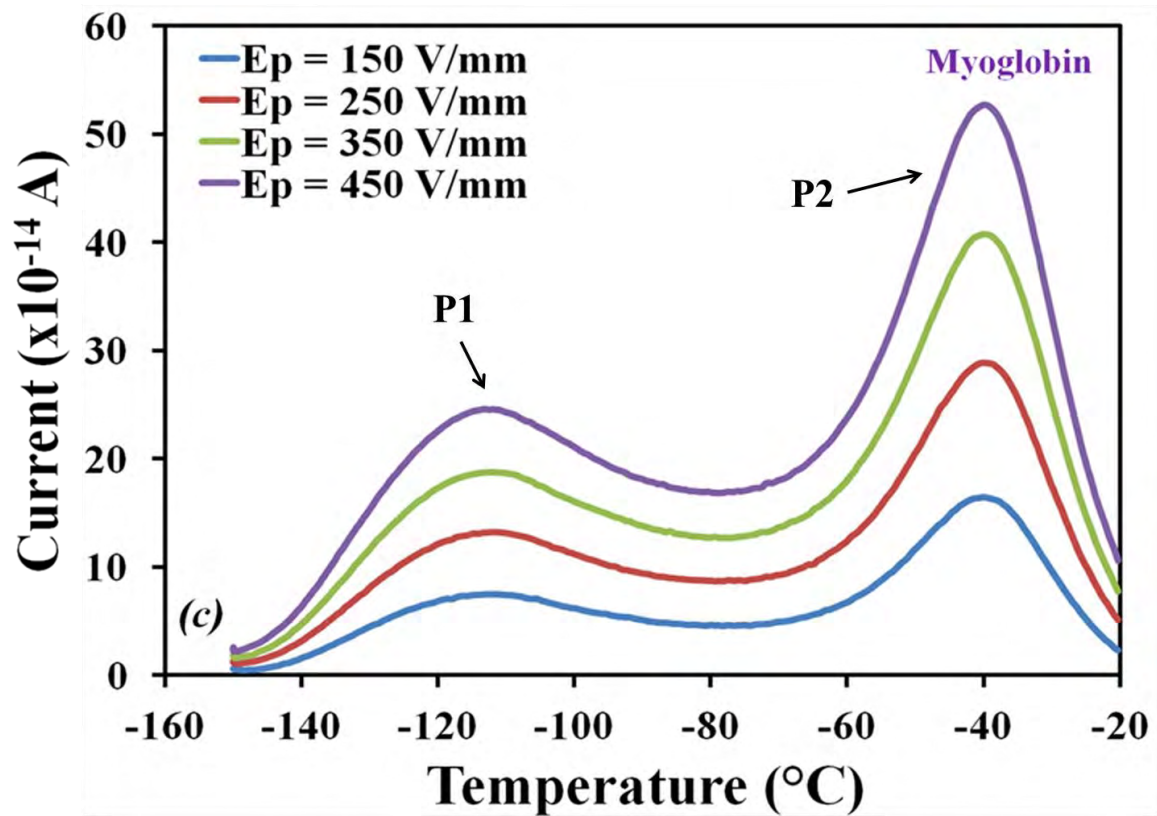


Fig. 5.4 Global depolarisation current as a function of temperature observed using varying polarising field strength for (a) insulin polarised at -50°C , (b) lysozyme polarised at -100°C and (c) myoglobin polarised at -50°C showing two processes (P1 and P2).

Table 5.3 Global depolarisation temperature maxima observed for the proteins and the moisture contents observed in TGA studies.

Sample	Amino acid units	Molecular weight (kDa)	Moisture content (%)	Depolarisation process	T_{\max} (°C)
Insulin	51	5.8	5.0 ± 0.2	1	-95 ± 3
Lysozyme	129	14.3	5.0 ± 0.1	1	-102 ± 3
Myoglobin	154	17.0	9.9 ± 0.2	1	-111 ± 2
				2	-41 ± 2

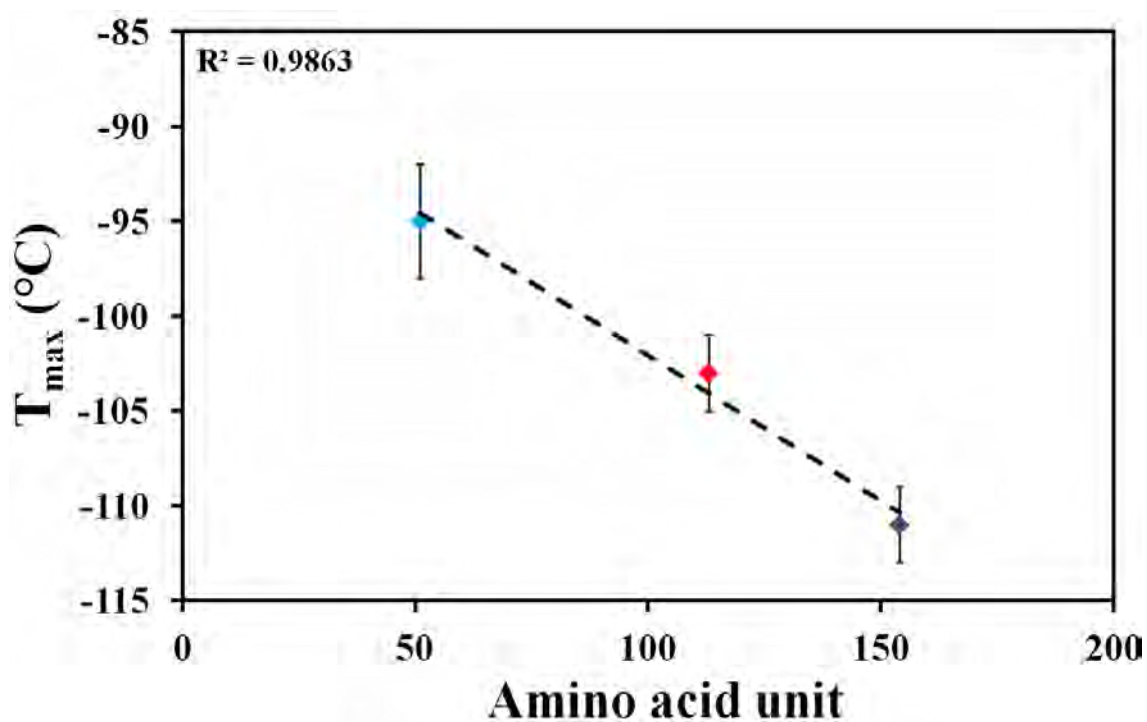
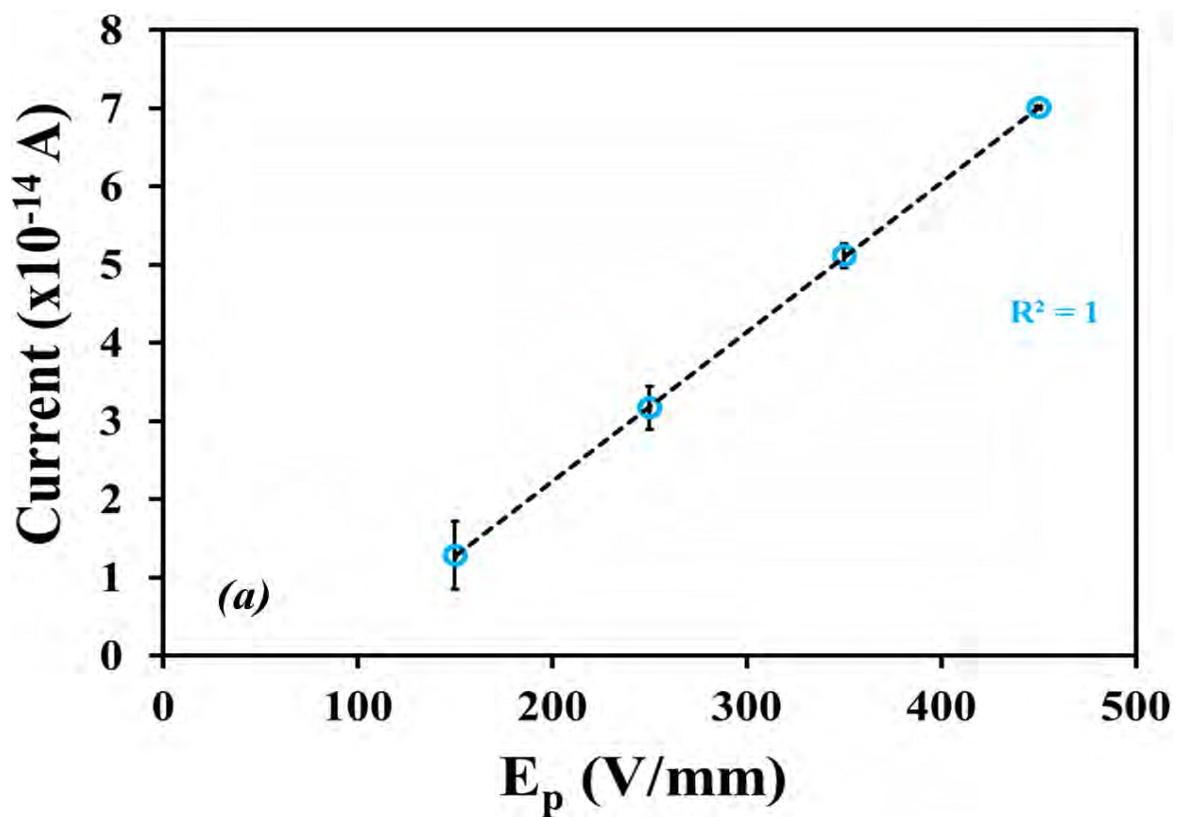


Fig. 5.5 Plot of global depolarisation T_{\max} against amino acid unit of the proteins studied.

The depolarisation processes observed are due to the orientations of molecular dipoles. As shown in Fig. 5.3, the current intensity at the T_{\max} increased with increase in the applied

electrical field strength. This is further supported by the regression plot (Fig. 5.6) which shows positive correlation between current intensity at T_{\max} and strength of applied electrical field with an R^2 value of >0.999 . In the absence of moisture (after dehydration) the relaxation processes observed has drastically been reduced (Fig. 5.7). It was not possible to conduct further studies between -150 and -20°C after dehydration due to the low depolarisation currents generated i.e. the current observed is $< 4 \times 10^{-14}$ A (which is a typical baseline signal), when E_p of 400 V/mm is applied.



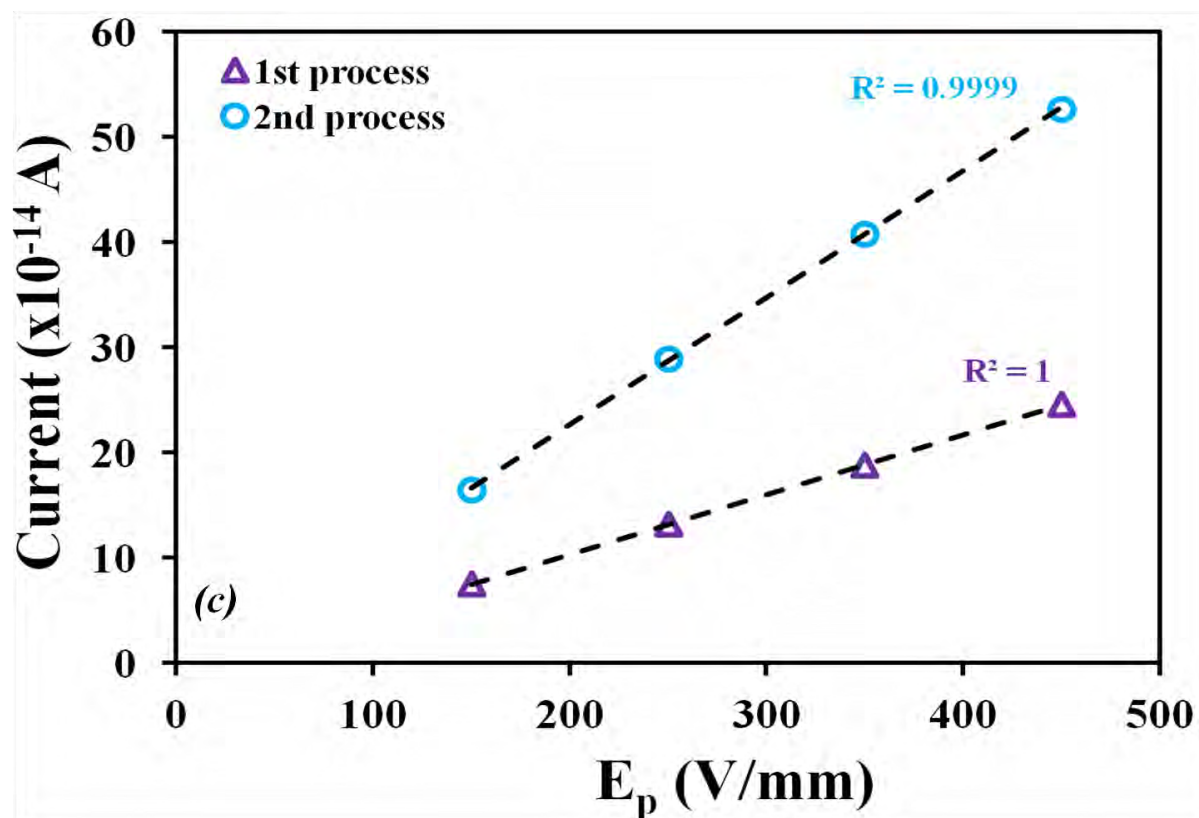
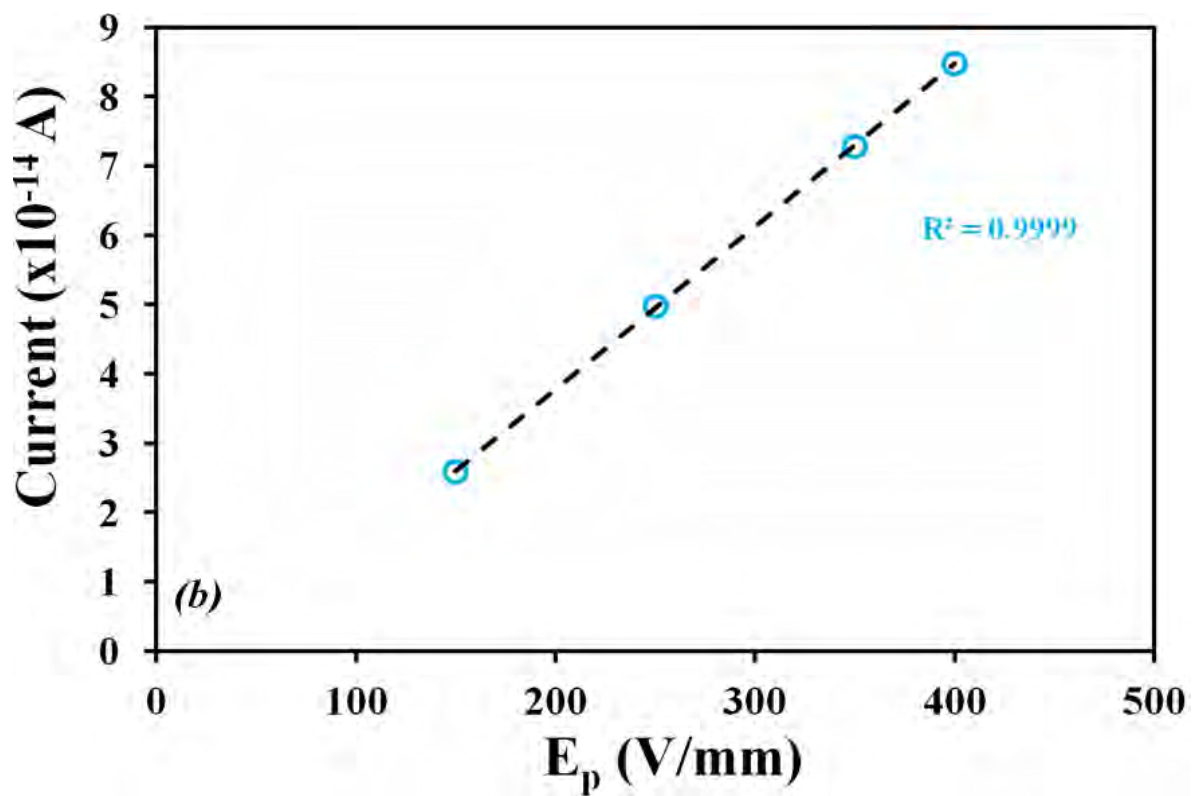
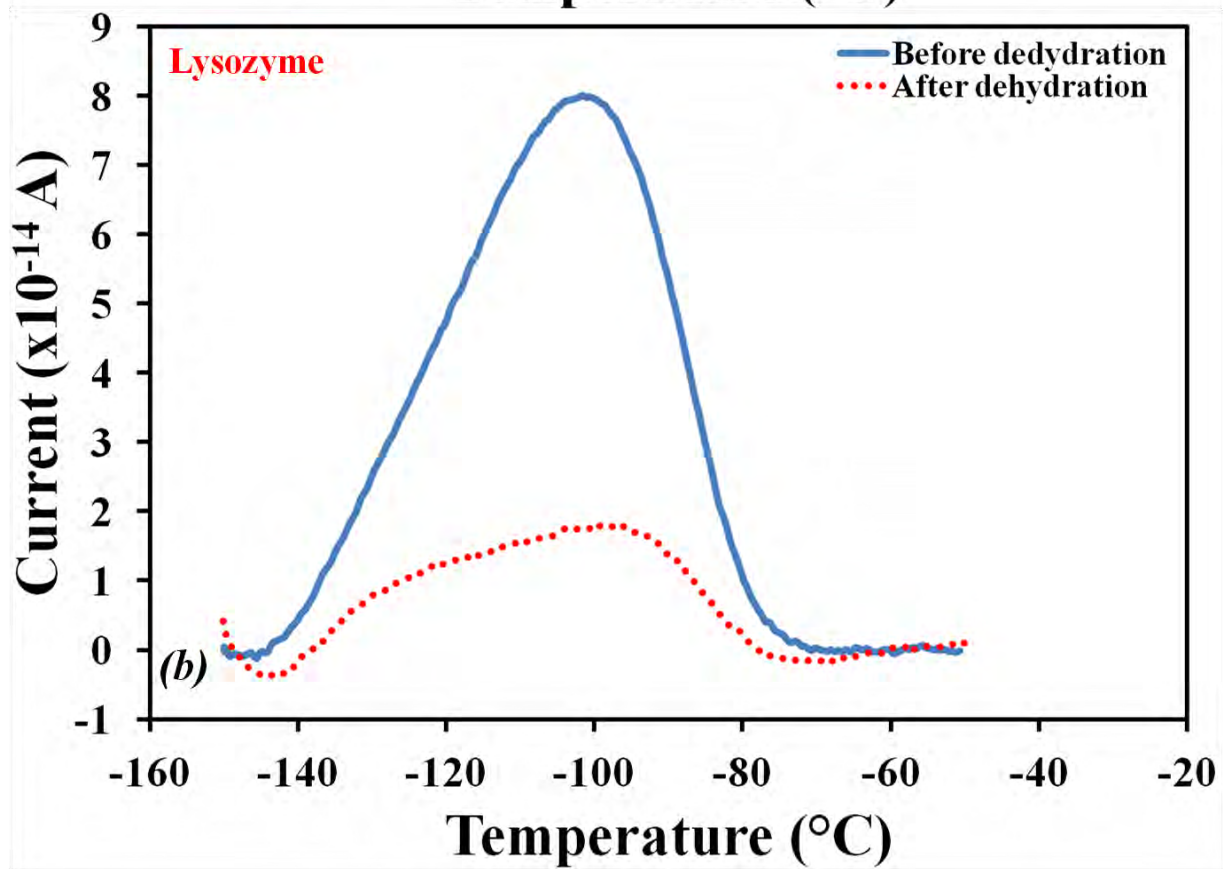
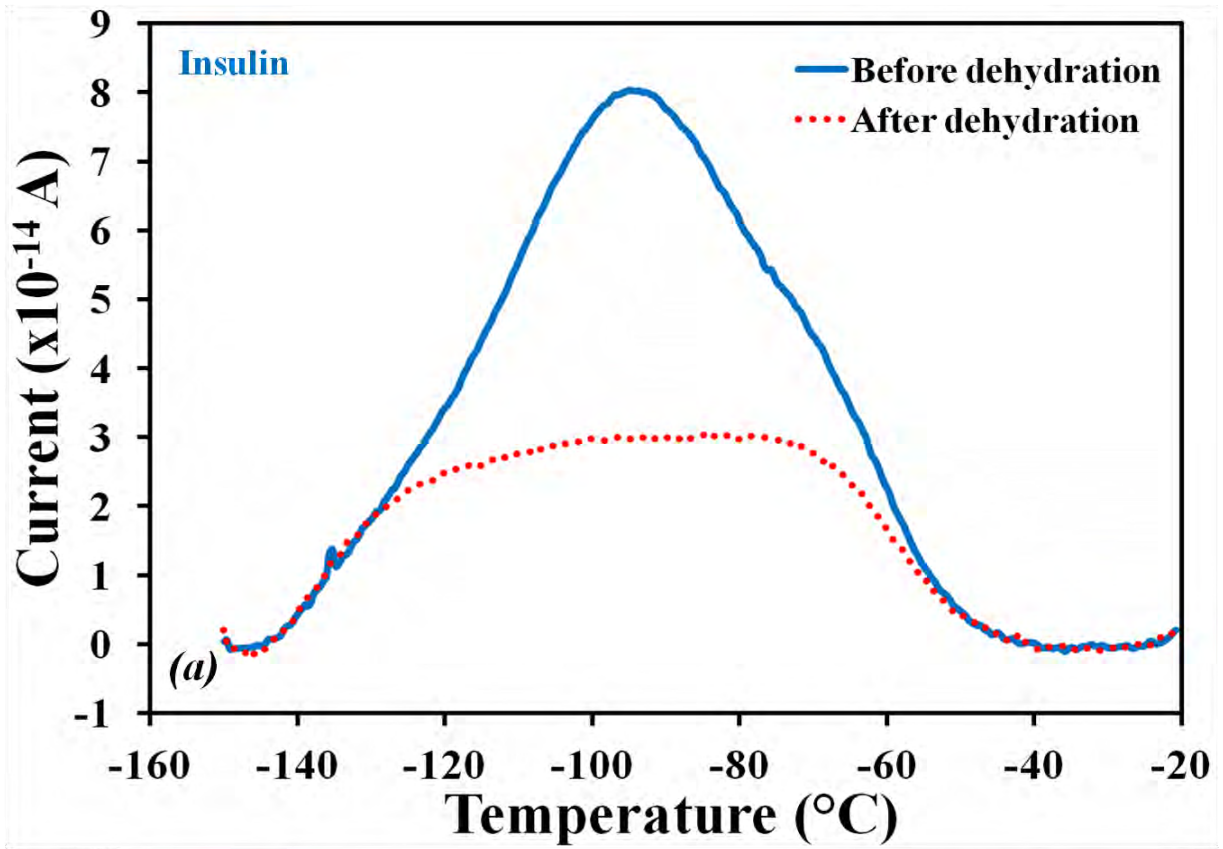


Fig. 5.5 Plots of current intensity at T_{max} against applied electrical field strength (E_p) for (a) insulin, (b) lysozyme and (c) myoglobin.



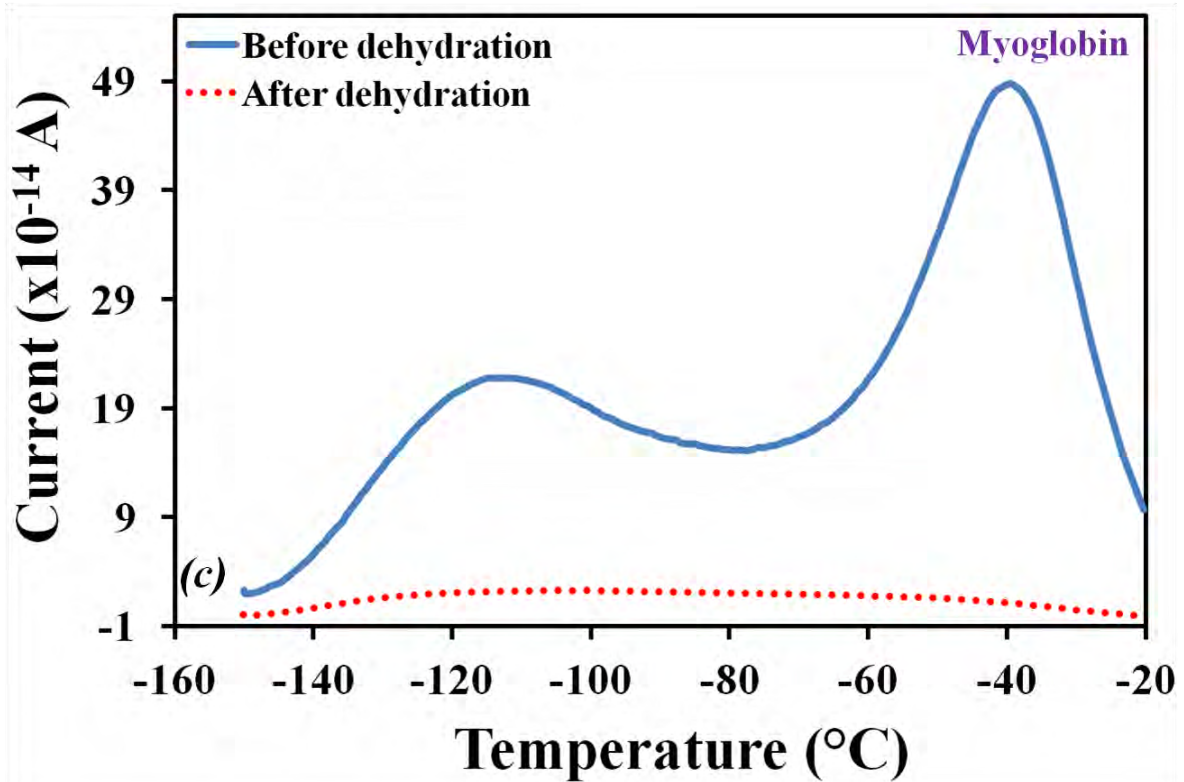
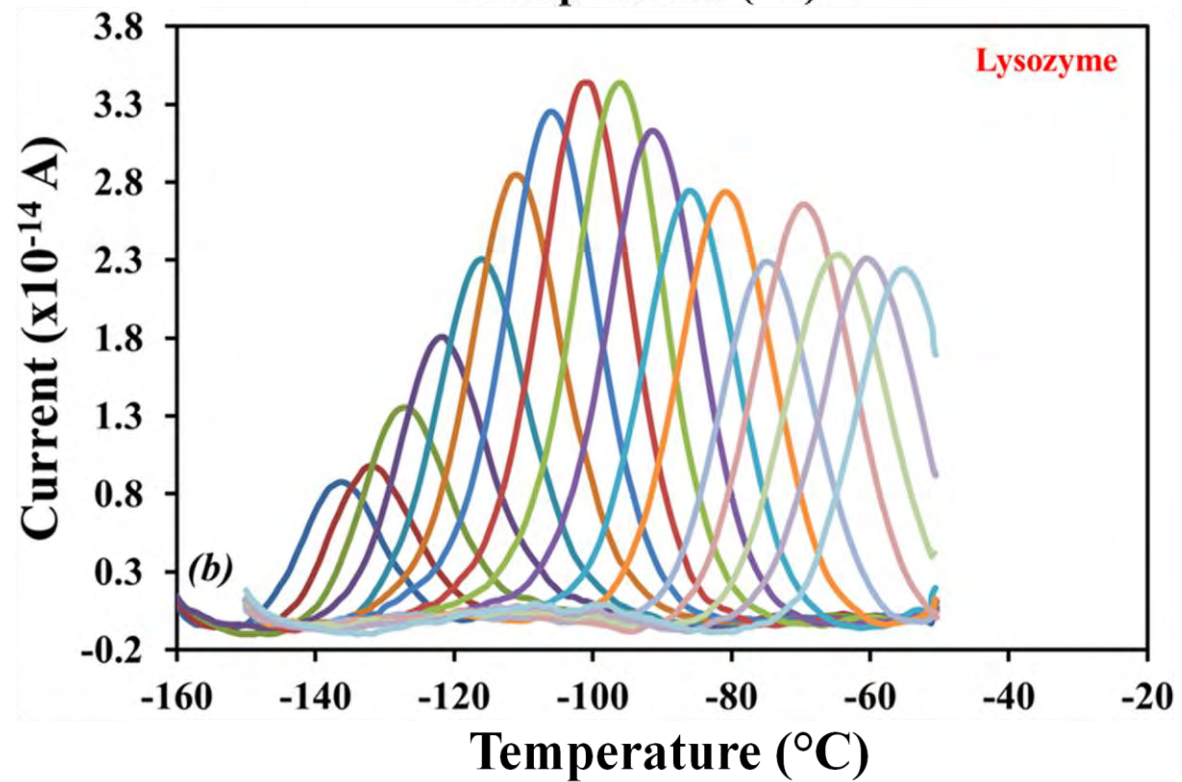
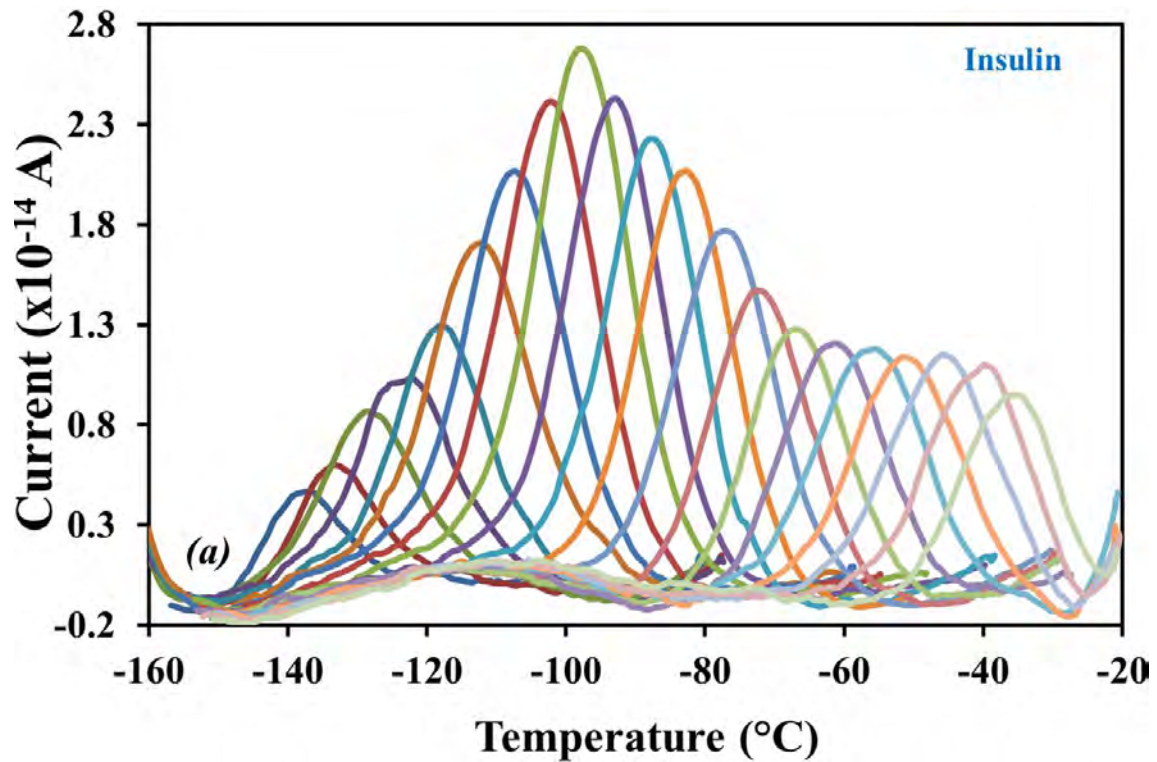


Fig. 5.6 Global depolarisation current observed for the proteins when polarised with an E_p of 400 V/mm before and after dehydration, (a) insulin polarised at -75°C , (b) lysozyme polarised at -100°C and (c) myoglobin polarised at -50°C .

The fact that the relaxation processes observed for the proteins disappears upon dehydration, suggests that these motions are related to water molecules. It has been stated that thermally stimulated mobility in protein molecules are not governed by the increase in thermal energy during heating, but by the increase in the mobility of the surrounding water/solvent molecules (Samouillan et al., 2011, Jansson et al., 2011). The data acquired with the TSDC technique supports this idea that mobility is governed by protein-solvent interactions. Hence, even with the low hydration level, water molecules are still able to provide the flexibility required for internal motions to occur.

5.3.2.2 Thermal Windowing

The elementary dipole depolarisation components observed from the thermal windowing experiments are presented in Fig.5.8.



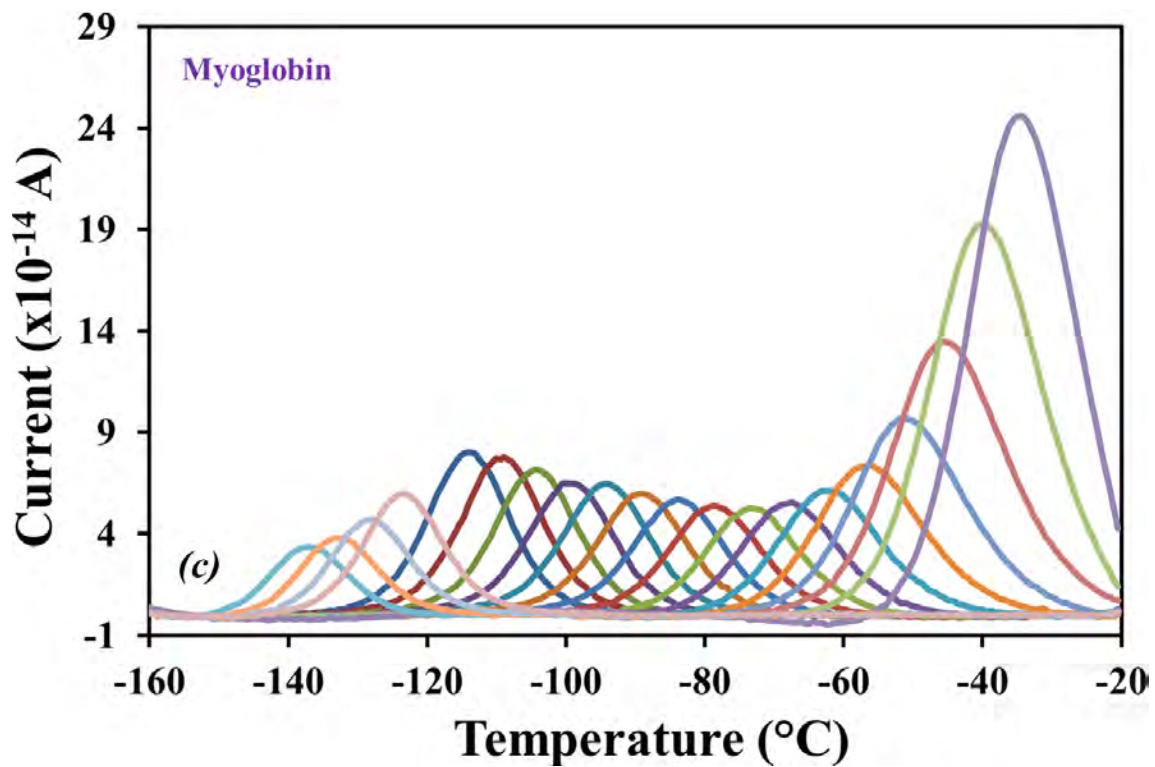
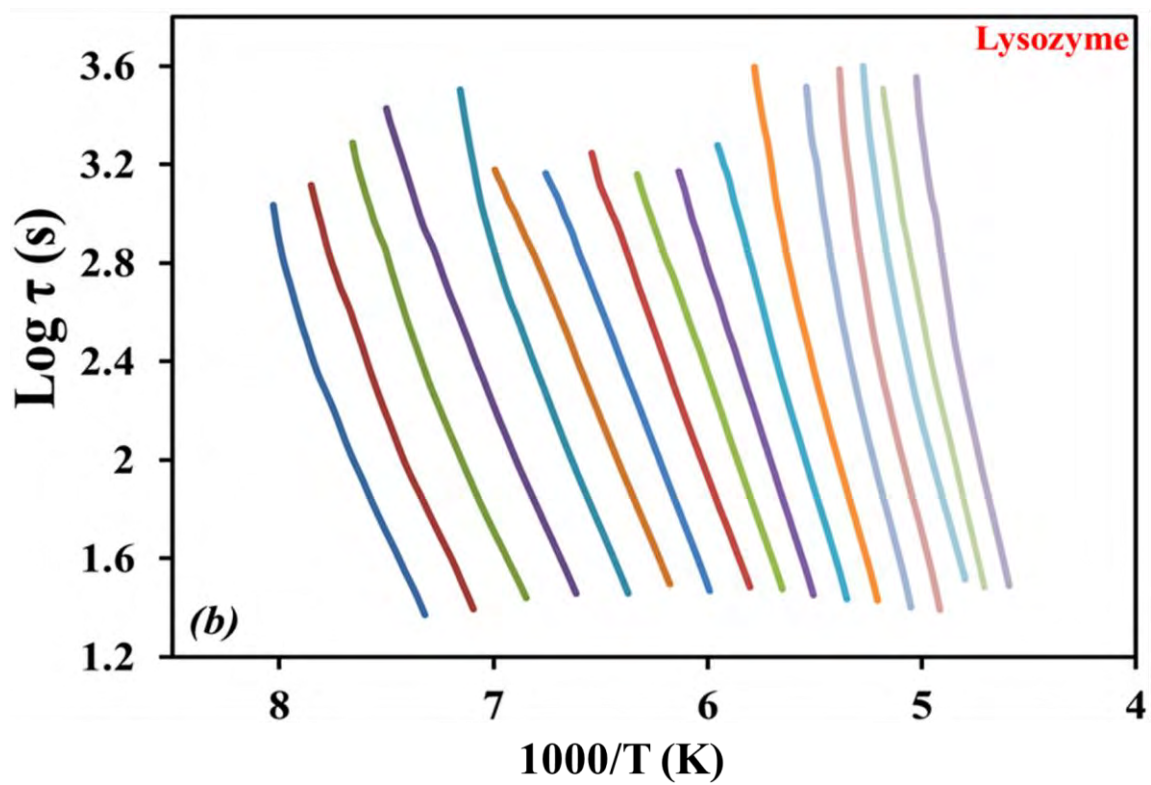
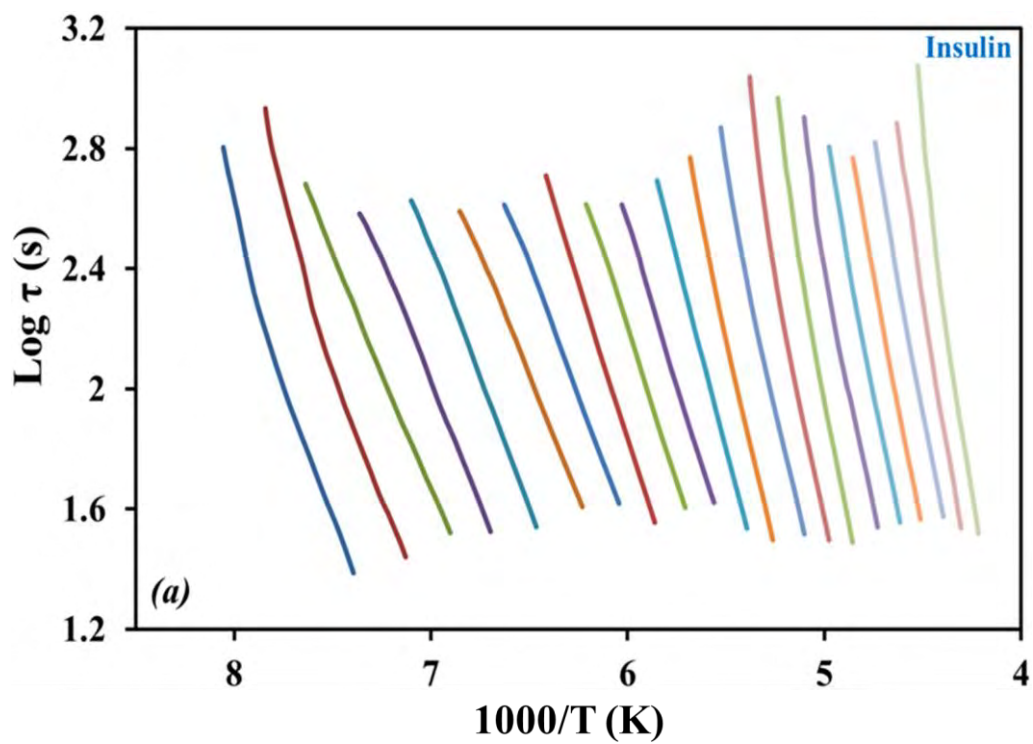


Fig. 5.7 The discrete relaxation mode observed under the global relaxation processes for (a) insulin, (b) lysozyme and (d) myoglobin obtained with a polarising field of 400 V/mm.

The distribution of relaxation times obtained for discrete relaxation components for the proteins exhibits near straight Bucci lines (Fig. 5.9). The relaxation processes therefore have narrowly distributed activation energies and obey the Arrhenius behaviour.



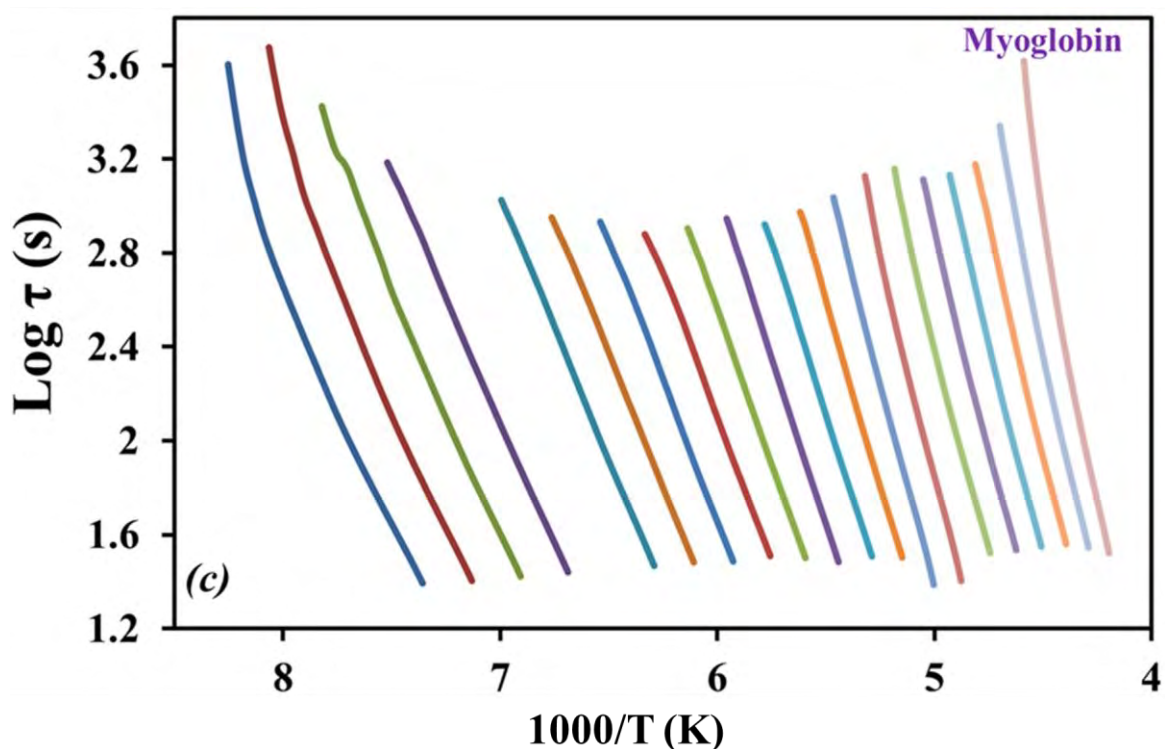


Fig. 5.8 Plots of the distribution of relaxation time as a function of temperature obtained for each elementary relaxation process for (a) insulin, (b) lysozyme and (c) myoglobin.

Fig. 5.10 shows that the activation enthalpy values obtained for the discrete components, observed under the global relaxations processes follow the zero entropy line. Based on these finding, it is postulated that the dipolar relaxations processes observed are non-cooperative processes that result from localised secondary relaxations. These relaxation processes are likely to originate from localised rotations and/or orientations of water molecules, and rotations of amino acid side chains and possible amino acids in the random coil regions of the proteins. It is further postulated that the relaxation processes observed are of the same type/modes i.e. from Fig. 5.10, it is clear that all three proteins have their activation enthalpy maxima at similar temperatures ($-69 \pm 3^\circ\text{C}$). The activation enthalpy values obtained for insulin and myoglobin are essentially the same (ΔH^\ddagger value of 69 ± 6 kJ/mol for insulin and myoglobin). Lysozyme, on the other hand, exhibits slightly greater activation enthalpy (ΔH^\ddagger 77 ± 4 kJ/mol) at the maxima when compared with insulin and myoglobin. This difference in

apparent activation enthalpy of the molecular relaxation processes could be a contributing factor in the observed differences in the dehydration temperatures observed in TGA analysis i.e. dehydration peak temperature for lysozyme is the highest temperature ($82 \pm 1^\circ\text{C}$) of the proteins investigated.

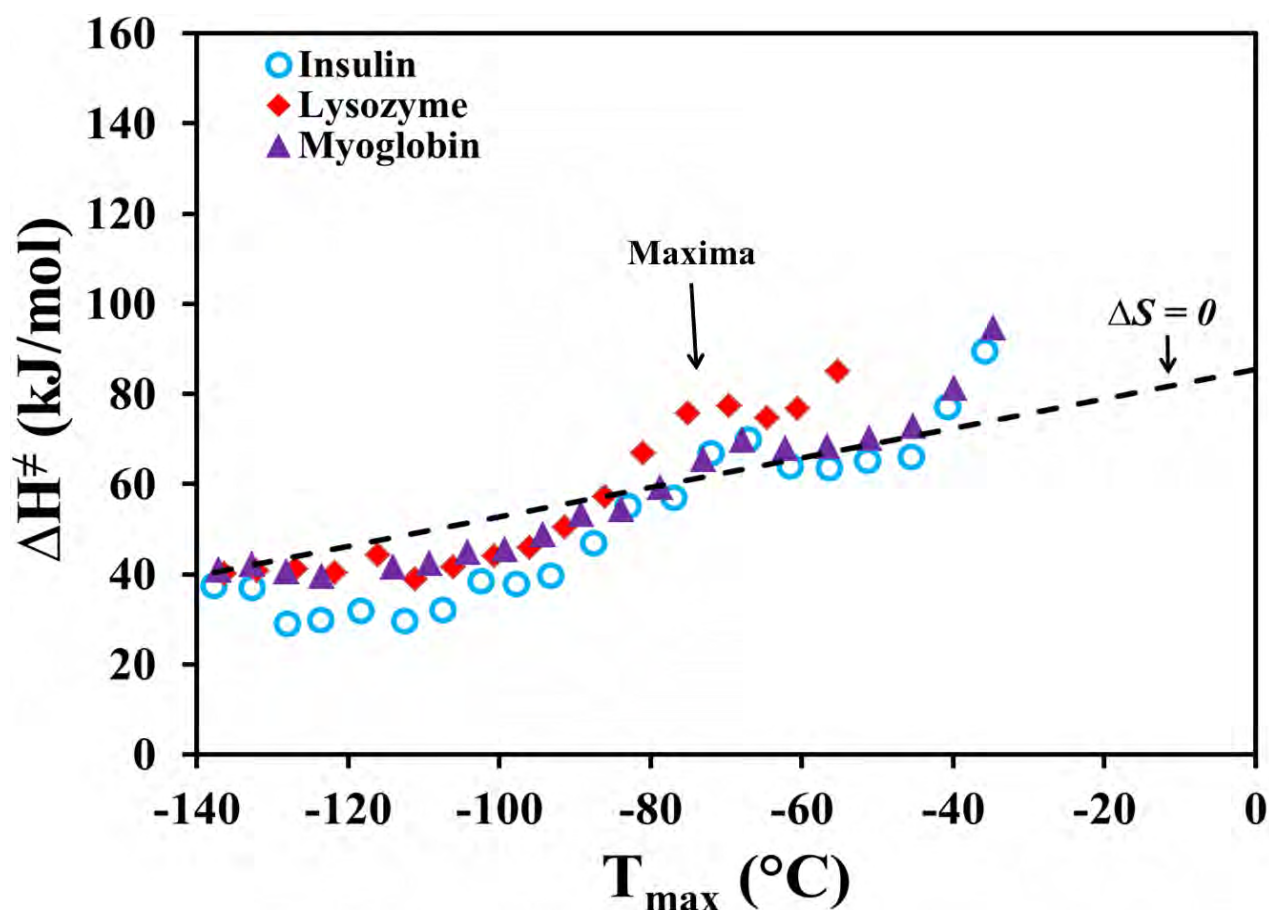


Fig. 5.9 Plot of activation enthalpies vs T_{\max} of the discrete relaxation components for proteins containing water molecules.

In this study the temperature of the enthalpy maxima observed for all three proteins do not correspond to the T_{\max} of the discrete relaxation component with the highest current intensity. No explanation can be suggested for such behaviour. Interestingly, the ΔH^\ddagger maxima observed for all three proteins are at similar temperatures to the glass transition point reported for myoglobin $\sim -73^\circ\text{C}$ (Jansson et al., 2011), and as observed the experimental ΔH^\ddagger begin to

deviate from the zero entropy line after this temperature. It is therefore possible that the proteins are now accessing the larger scale domain or segmental motions. The reason for the non-cooperative nature of these relaxation processes, as shown in the data in Fig. 5.10, is due to the small amount of water molecules involved in the relaxation processes. As such, negligible influence is imposed on entropy i.e. the scale of the glass transition is not big enough to cause a change in entropy of the system.

A major concern in relation to protein-water mobility, when samples are cooled to sub-zero temperatures, is the existence of mobility states that may cause crystallization of the bulk water, as this can cause stresses capable of denaturing proteins (Chang et al., 2005a, Abdul-Fattah et al., 2007c, Chang and Pikal, 2009, Samouillan et al., 2011,). Furthermore, the mobility in the super-cooled regions could facilitate denaturation of proteins molecules via bond transfers and exchange, even though the large scale conformational freedom of the proteins are now reduced to, predominantly, rotational degrees of freedom in very low water contents (Chang et al., 2005a, Kawai et al., 2006). The observations made in this study demonstrate that significant mobility begin to develop from small rotational mobility of water molecules and associated amino acid side-chains, to mobility of larger segment of the protein molecules, below -20° even with water content of $\leq 10\%$. Hence, when lyophilized proteins with moisture content $< 10\%$ are kept at the recommended storage conditions (-20°C for myoglobin and insulin and $2-8^{\circ}$ for lysozyme) they may still undergo significant cooperative molecular orientations, facilitated by the mobility of the adsorbed water molecules, that are of the appropriate scale to cause crystallization or even denaturation of protein molecules.

When considering both the τ values obtained for the thermal windowing component with the highest current intensity and that obtained for the component corresponding to ΔH^{\ddagger} maxima, no significant differences are observed between lysozyme and myoglobin (Table 5.4). However in both cases, insulin exhibits significantly slower relaxation times. Furthermore, it

is observed that the polarisation temperature at which the highest current intensity is observed is greatest for insulin. These observations suggest that the hydrogen bonding networks in insulin are stronger than those in lysozyme or myoglobin.

Table 5.4 The relaxation times obtained at the T_{\max} of the discrete component with the highest depolarisation current intensity and at the T_{\max} of the discrete component with the highest ΔH^\ddagger .

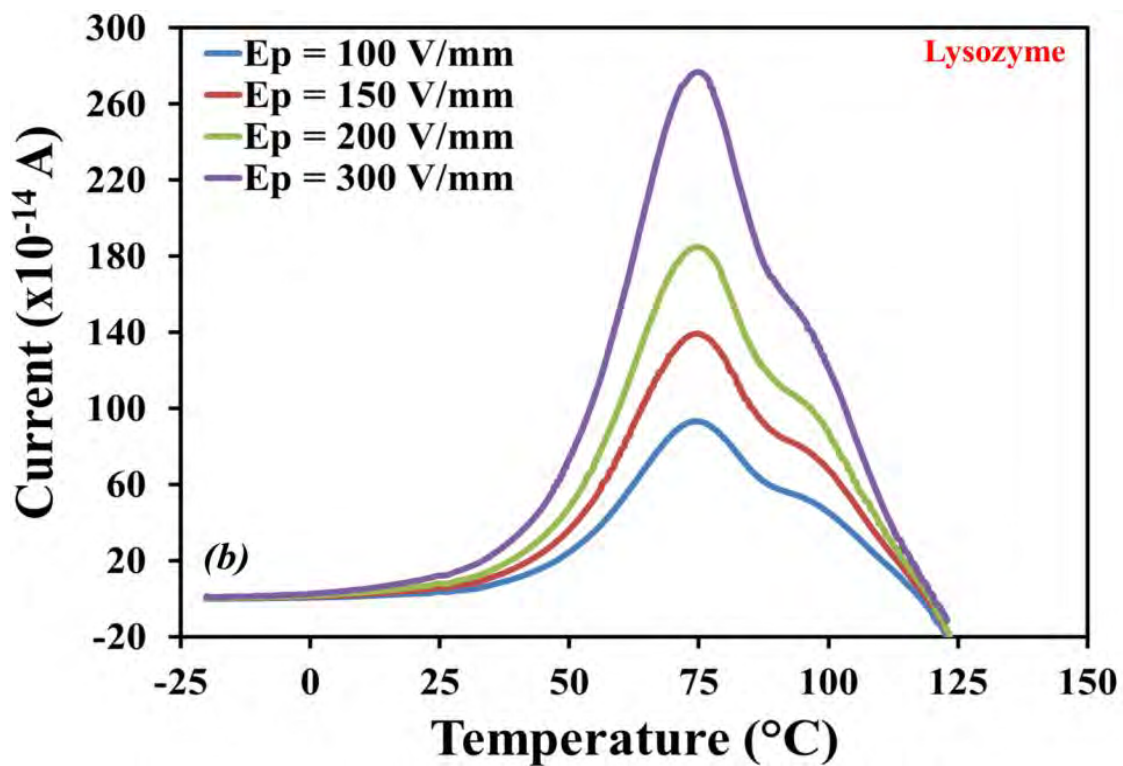
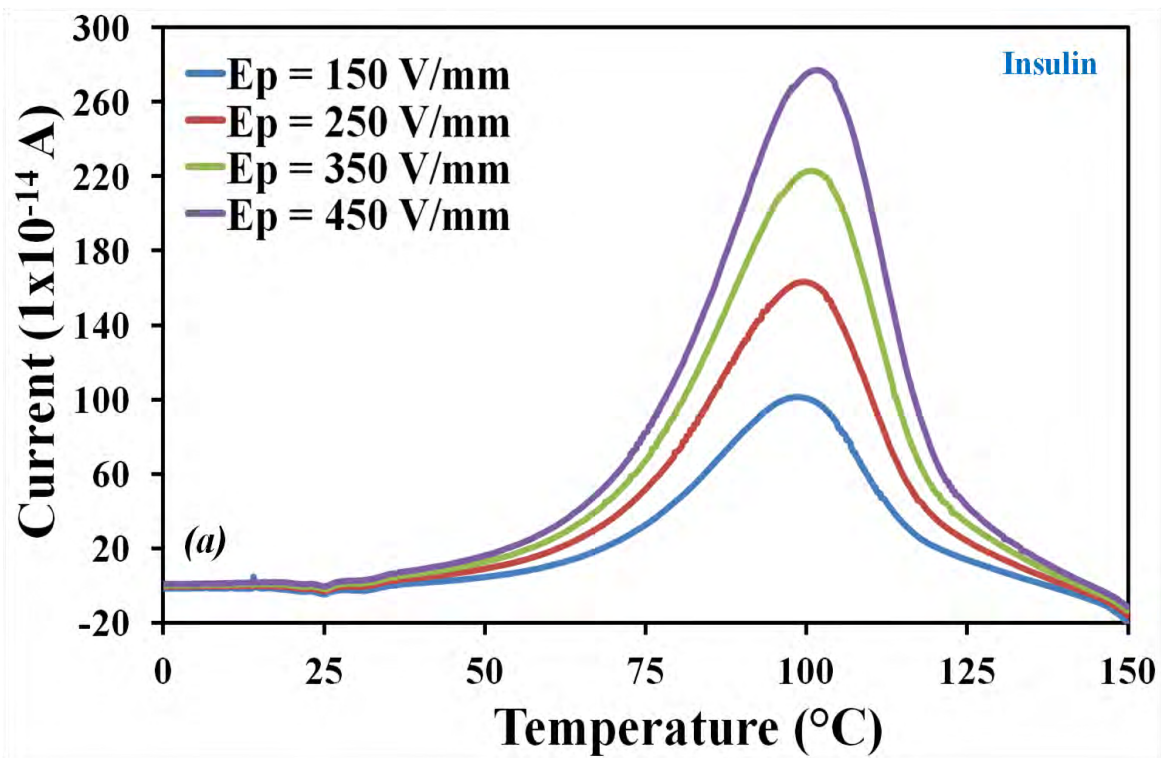
Sample	N° of amino acids	Component with the highest intensity			Component with ΔH^\ddagger maxima		
		T_p (°C)	T_{\max} (°C)	τ (s)	T_p (°C)	T_{\max} (°C)	τ (s)
Insulin	51	-110	-98 ± 2	40.3 ± 1.2	-80	-67 ± 1	30.8 ± 3.1
Lysozyme	129	-115	-101 ± 2	30.4 ± 2.6	-85	-69 ± 1	24.7 ± 2.5
Myoglobin	154	-125	-114	29.3 ± 3.3	-80	-67 ± 2	25.3 ± 2.0

The TSDC results obtained has so far demonstrated moisture content to be the dominating factor in the molecular mobility of the proteins investigated. Whilst no relationship is observed between molecular relaxation times and activation enthalpy and molecular size of the proteins, a relationship is observed between the number of amino acids units and the temperature at which mobility occurs i.e. increasing amino acid units decreases the temperature at which mobility is observed. The molecular motions observed are localised secondary relaxation resulting from orientations of water molecules and the rotations of amino acid side-chains.

5.3.3 Dehydrated Samples

5.3.3.1 Global TSDCS

After dehydration, only a single global depolarisation process is observed for the proteins, when probed from -150 to 150°C. The depolarisation processes are dipolar i.e. the depolarisation currents generated increase in intensity with increase in the applied electrical field strength (Fig. 5.11), exhibiting linear relationship with R^2 value ≥ 0.999 (Fig. 5.12). The T_{\max} at the polarisation temperature that generates the greatest depolarisation current intensity occurs at $96 \pm 3^\circ\text{C}$, $72 \pm 4^\circ\text{C}$ and $82 \pm 3^\circ\text{C}$ for insulin, lysozyme and myoglobin, respectively. These relaxation processes are the first to be reported for totally dehydrated proteins prior to the denaturation/decomposition process. Whilst not a linear relationship, it is observed that the current intensity at T_{\max} observed for the global depolarisation processes increase with molecular size (Table 5.5). This is explained in terms of increase in the number of rotational units as the number of amino acids increase. Furthermore, the order of the T_{\max} depolarisation processes observed correlates with the temperature order of the “ T_g ” of the denaturation process observed for the proteins i.e. T_{\max} of depolarisation occurs in the order insulin > myoglobin > lysozyme which is the same as that observed for the “ T_g ”.



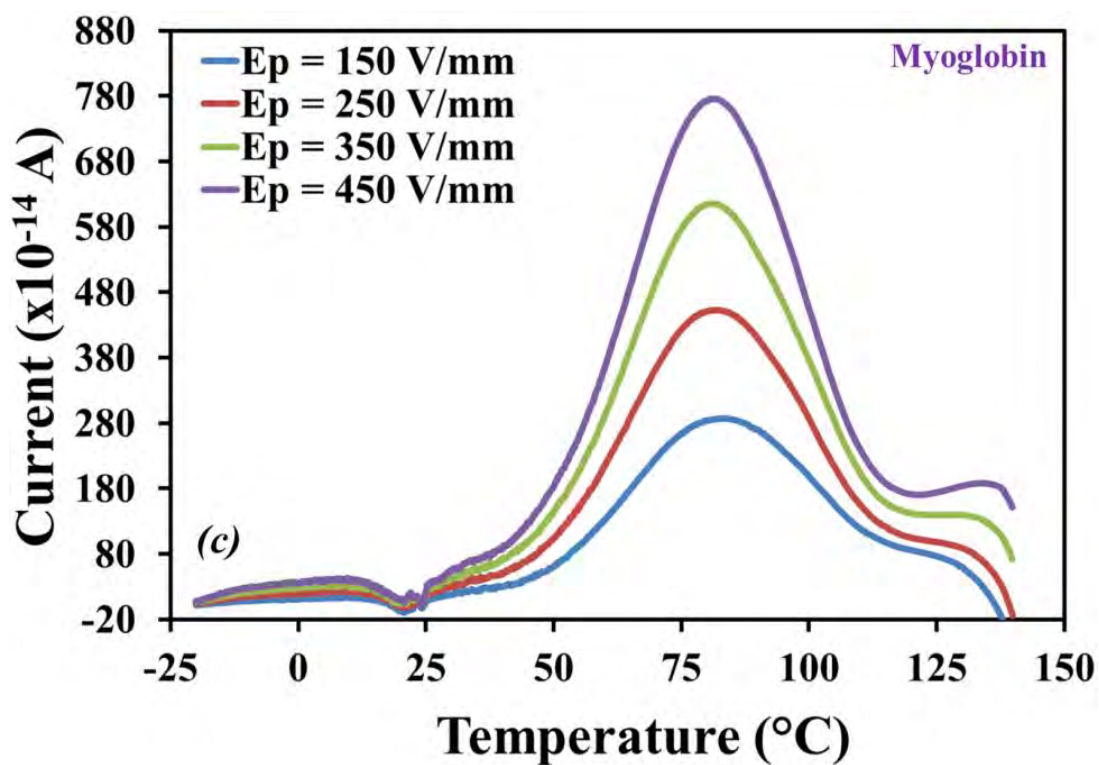
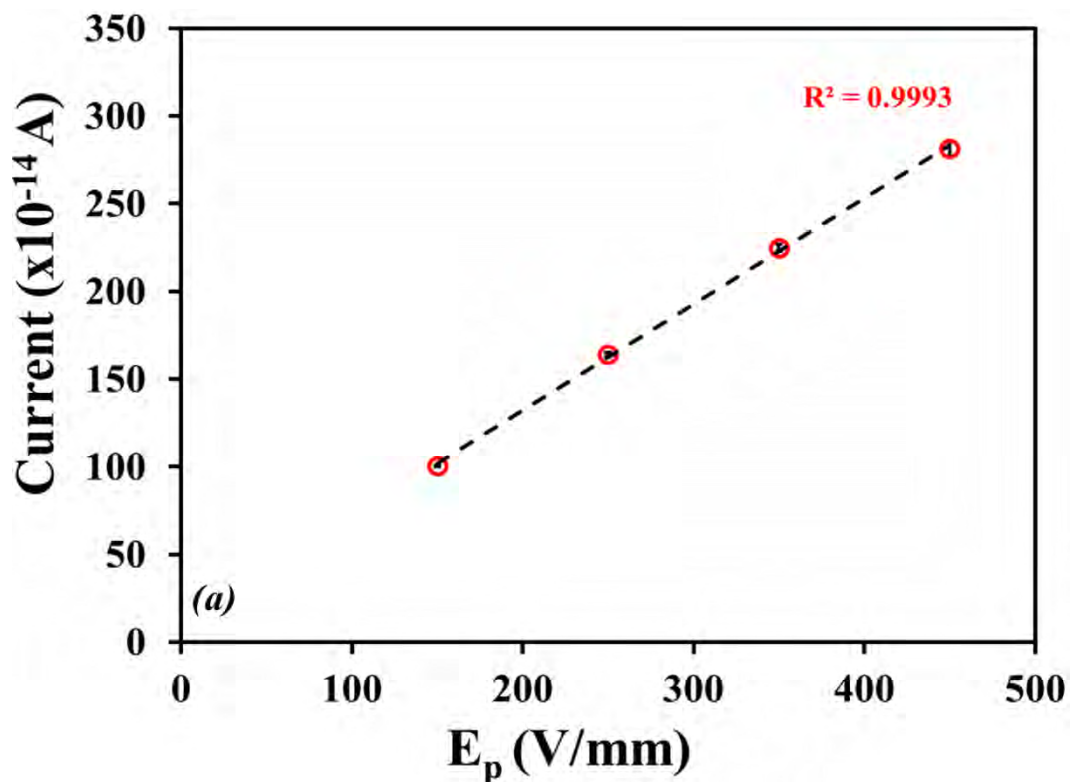


Fig. 5.10 Global depolarisation current as a function of temperature observed using varying polarising field strength for (a) insulin, (b) lysozyme, and (c) myoglobin, all polarised at 100 $^{\circ}$ C.



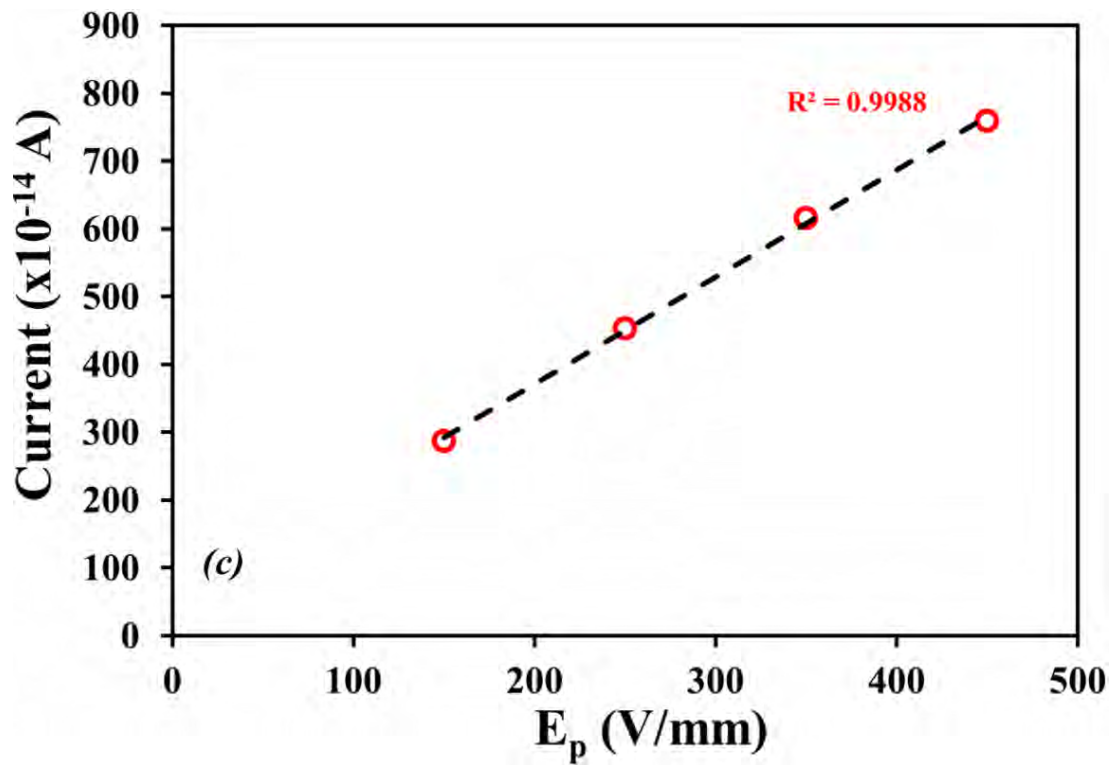
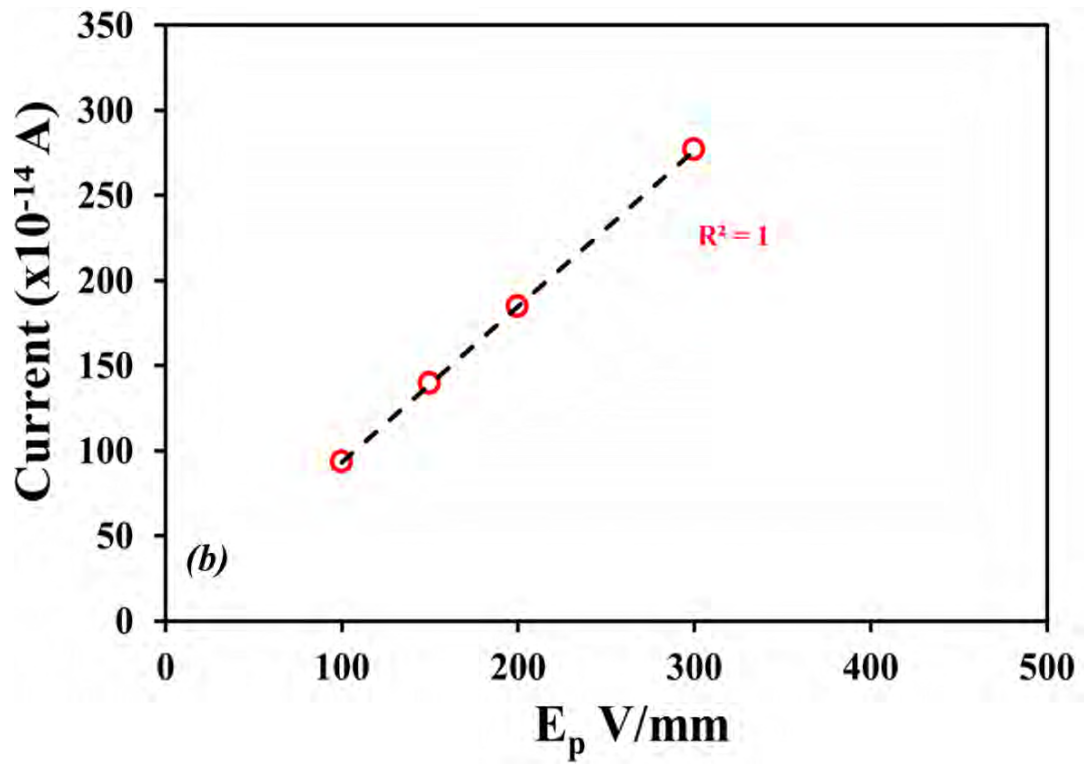


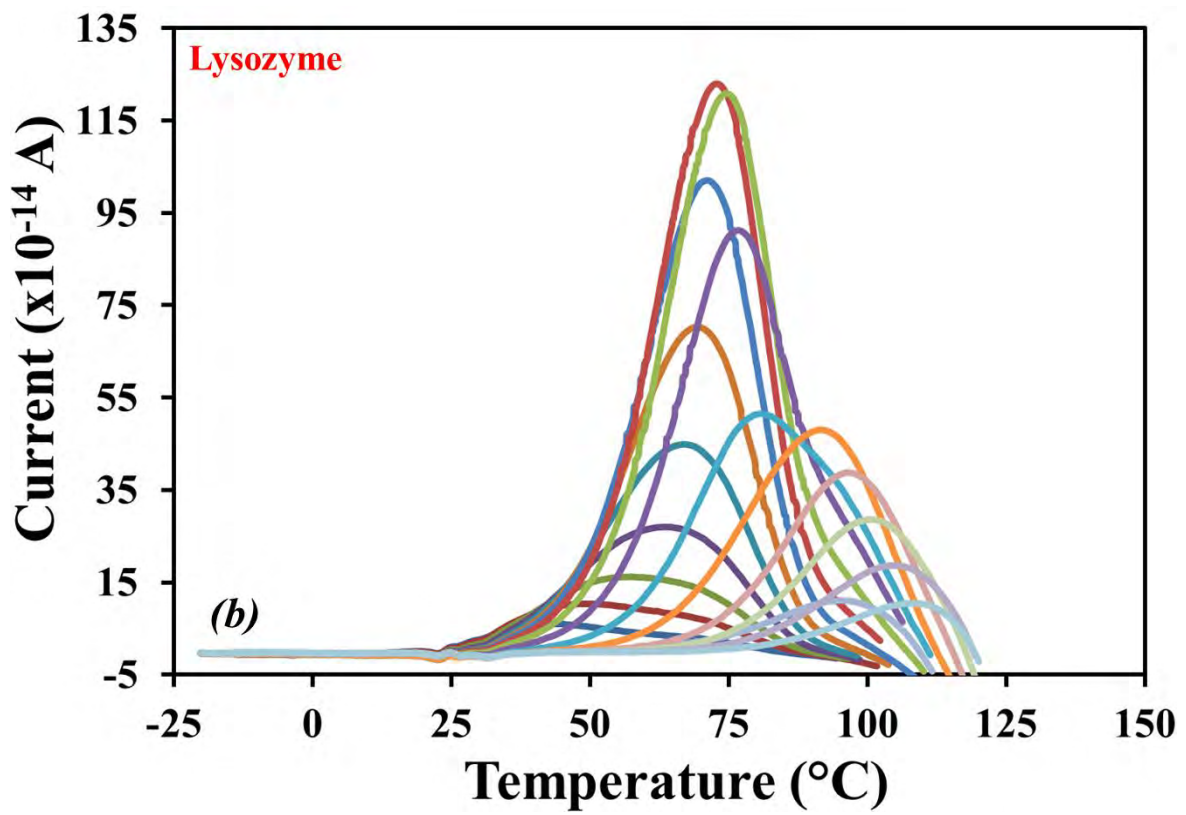
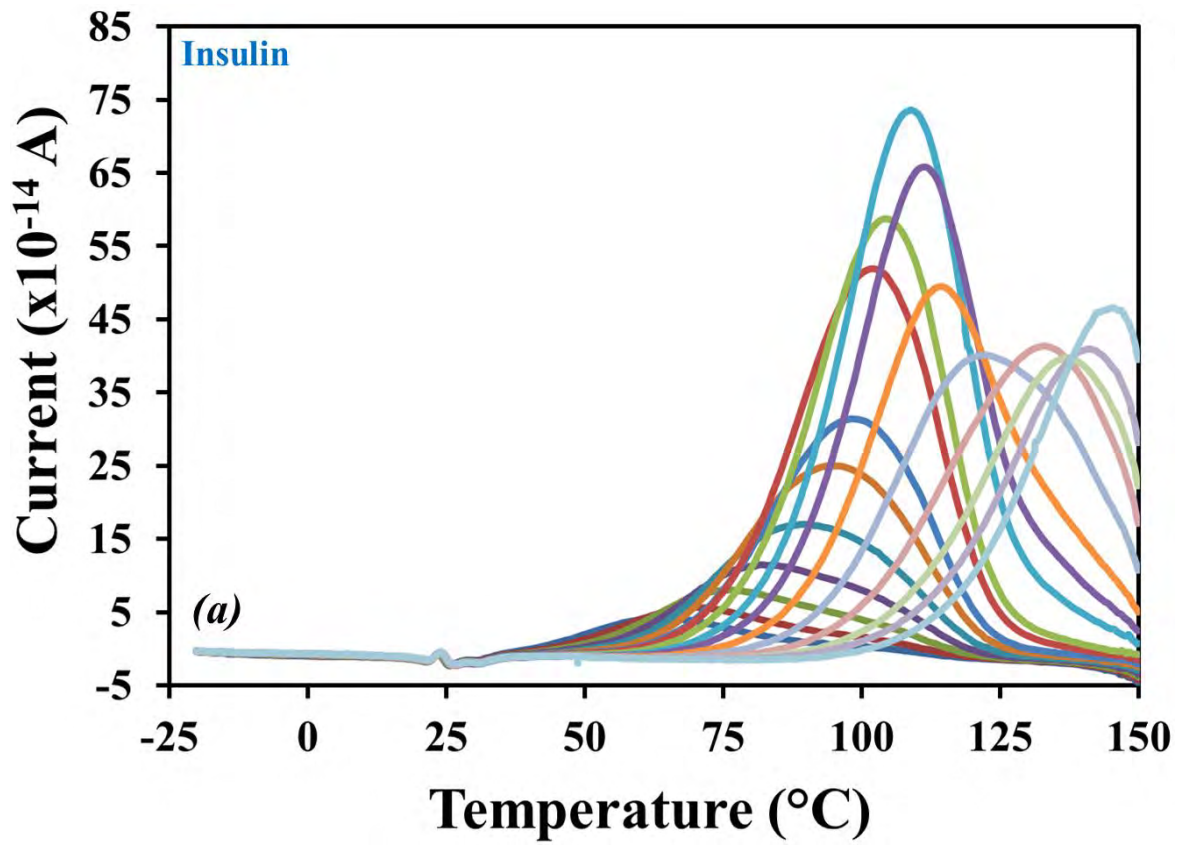
Fig. 5.11 Plots of current intensity at T_{\max} against applied electrical field strength (E_p) for (a) insulin, (b) lysozyme, and (c) myoglobin.

Table 5. 5 The current intensity observed for the protein samples when polarised at 100°C using polarising electrical field strength of 350 V/mm

Sample	N° of amino acids	Molecular weight (kDa)	T_{max} (°C)	Depolarisation current at T_{max} (x10⁻¹⁴ A)
Insulin	51	5.8	96 ± 3	225 ± 11
Lysozyme	113	14.3	72 ± 4	317 ± 16
Myoglobin	154	17.0	82 ± 3	578 ± 54

5.3.3.2 Thermal Windowing

The elementary dipole depolarisation components observed from the thermal windowing experiments are presented in Fig. 5.13. With the exception of the first 2 and 4 components observed for insulin and lysozyme, respectively, the distribution of relaxation times for each component exhibits near linear Bucci lines. Hence as observed for the mobility in the hydrated proteins, these high temperature dipole relaxation processes have narrowly distributed activation energies (Fig. 5.14).



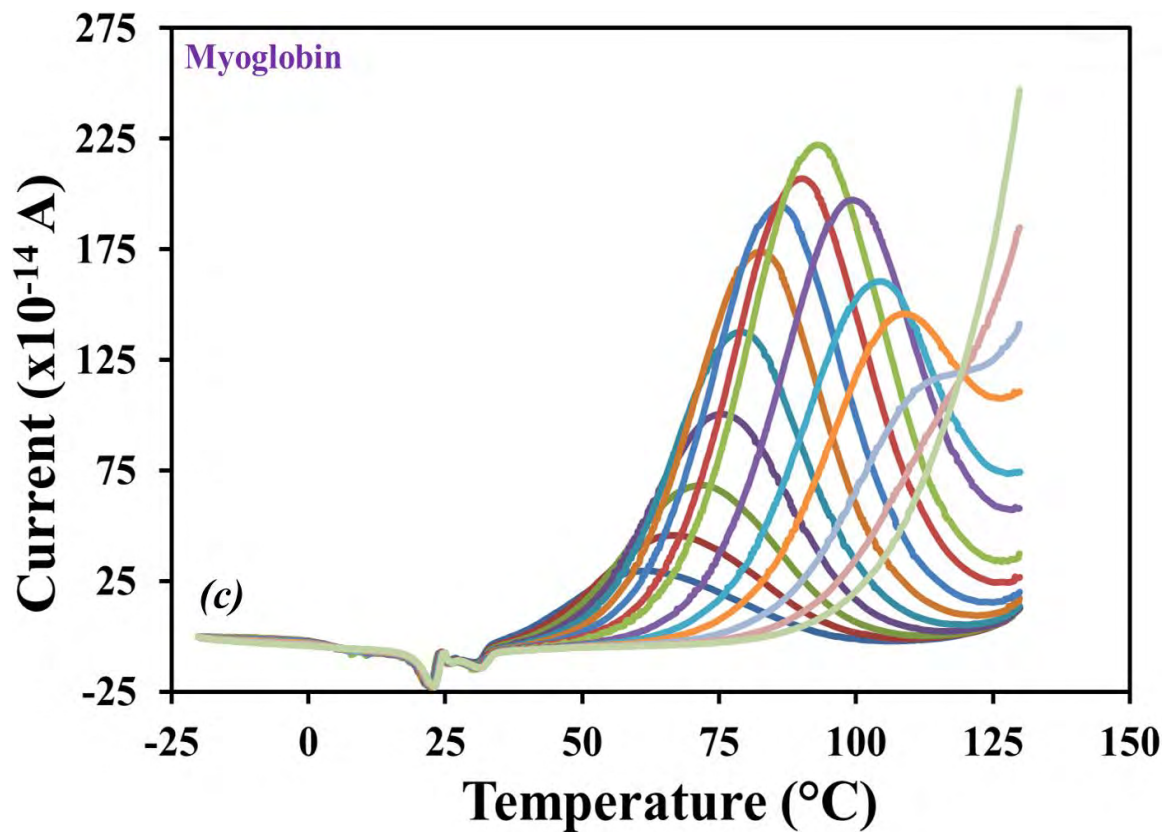
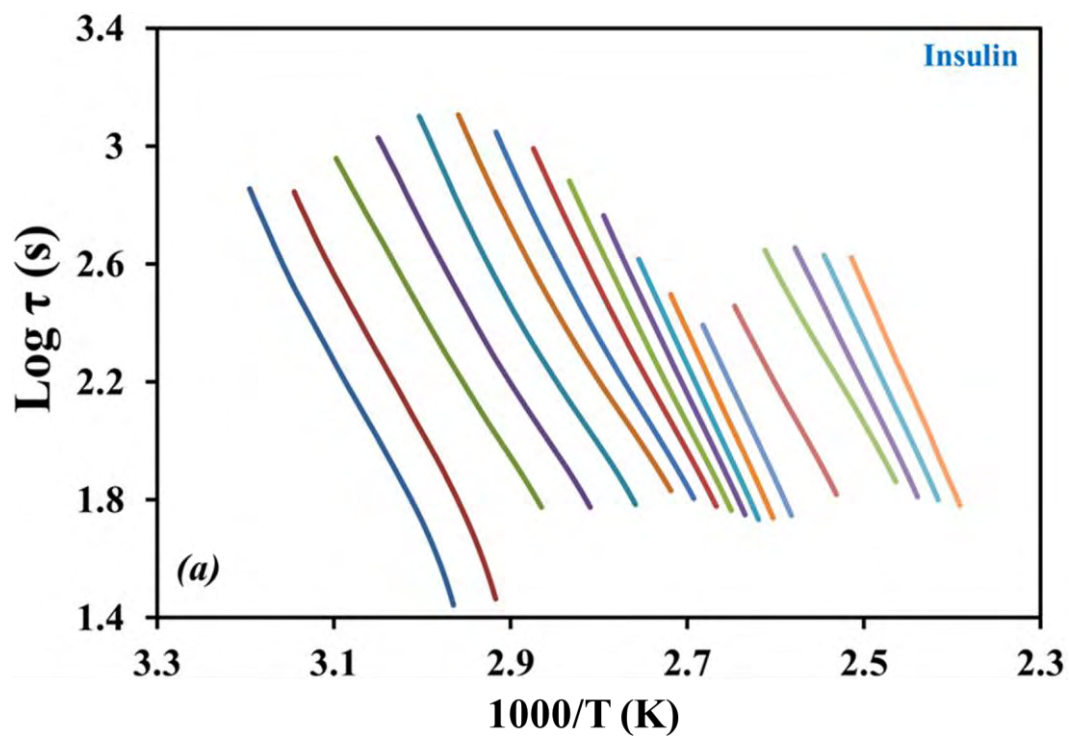


Fig. 5.12 The discrete relaxation mode observed under the global relaxation processes for (a) insulin, (b) lysozyme and (c) myoglobin obtained with a polarising field of 400 V/mm.



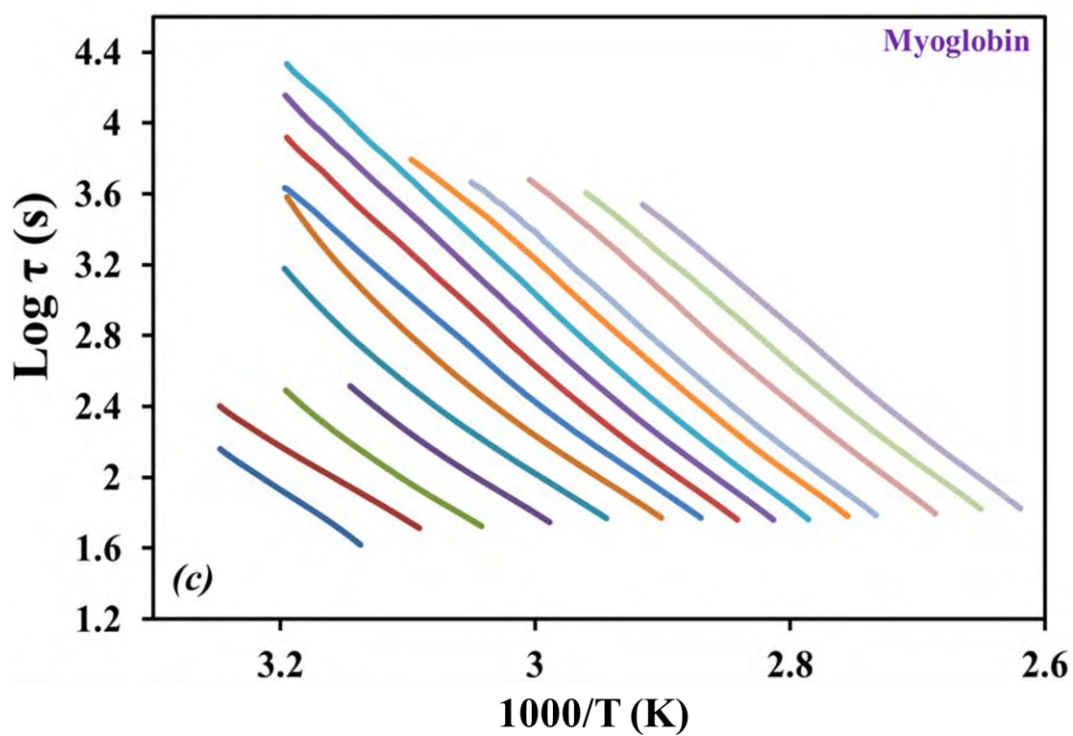
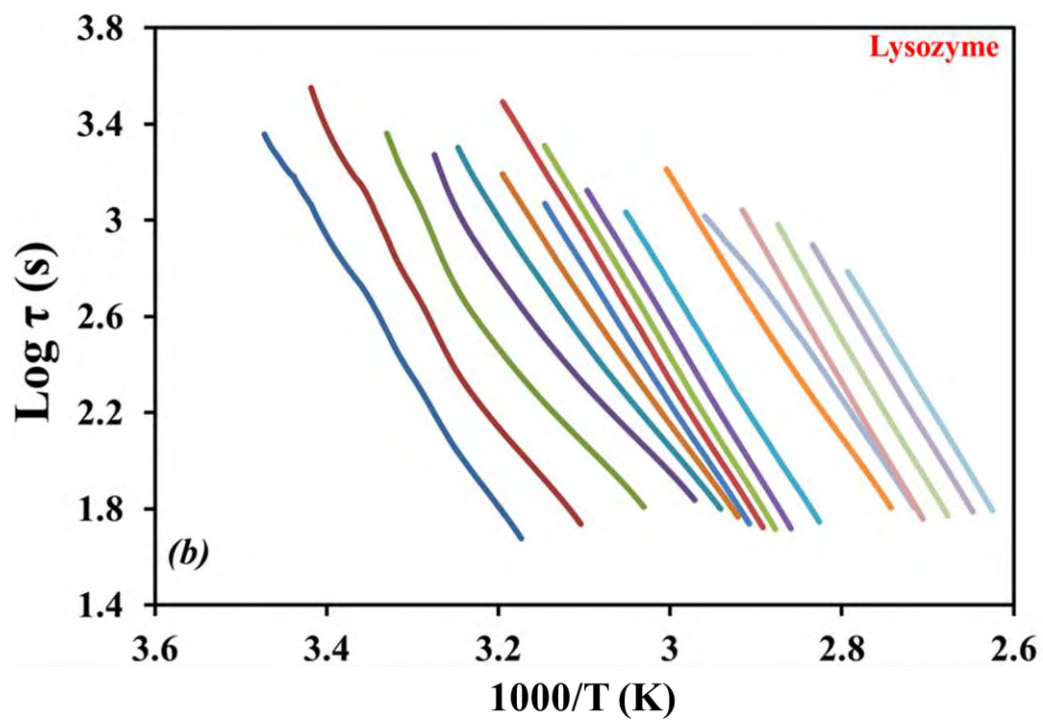


Fig. 5.13 Plots of the distribution of relaxation time as a function of temperature obtained for each elementary relaxation process for (a) insulin, (b) lysozyme, and (c) myoglobin.

The data in Fig. 5.15 demonstrates the dipole relaxations observed in the absence of water molecules to be non-cooperative i.e. the activation enthalpies follow the zero entropy line. These relaxation processes are therefore localised secondary relaxations. Since the samples are dehydrated, the observed mobility states can only be attributed to the rotations of side chains in the amino acid sequences of the protein molecules. Hence the relatively high depolarisation current intensity observed at T_{\max} (Table 5.5), and therefore the greater mobility observed in dehydrated myoglobin, can be attributed to the greater number of amino acid units in the protein sequence. This is because proteins with greater number of amino acid residues possess greater number of sites with rotational freedom.

It is also concluded, from the data in Table 5.6, that no significant differences exist in the activation enthalpy between the proteins investigated. However, albeit small, there are differences in the relaxation times observed. Rotational mobility of the side-chain amino acids seems to be fastest in lysozyme, which is followed closely by insulin. Myoglobin, which is the biggest molecular weight protein, is the slowest.

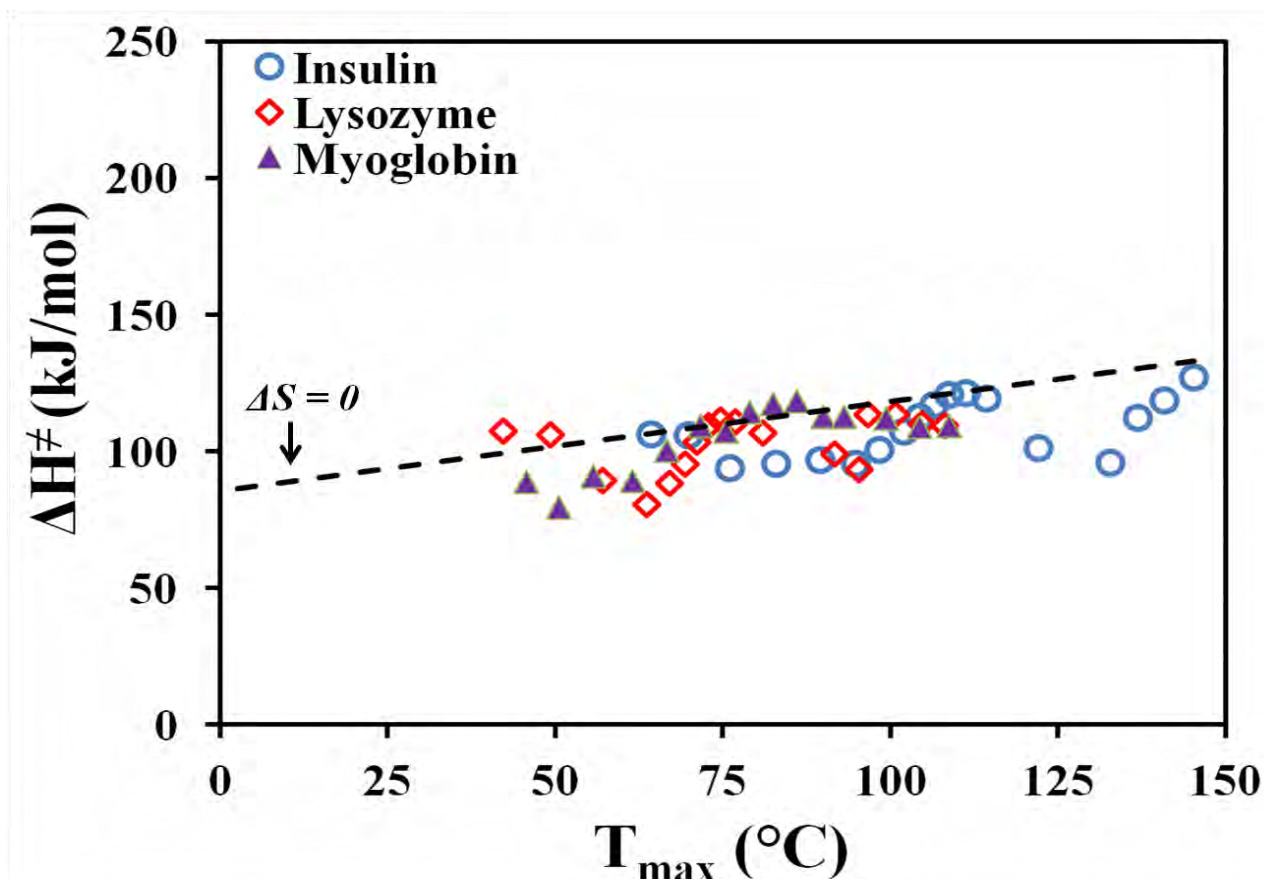


Fig. 5.14 Plot of activation enthalpies against T_{\max} of the discrete relaxation components for dehydrated protein samples.

Table 5.6 Activation enthalpies and the relaxation times obtained at the T_{\max} of the discrete relaxation components with the greatest current intensity.

Sample	N° of amino acids	T_p (°C)	T_{\max} (°C)	ΔH^\ddagger (kJ/mol)	τ (s)
Insulin	51	95	110 ± 2	118 ± 15	54.1 ± 1.0
Lysozyme	113	60	74 ± 3	111 ± 21	51.9 ± 0.7
Myoglobin	154	70	86 ± 2	121 ± 9	58.1 ± 2.1

The results obtained demonstrate that in the absence of moisture the proteins undergo localised secondary relaxation processes prior to the denaturation-decomposition processes. Whilst the temperature order with which these processes occur is the same as the temperature order of the denaturation/decomposition processes, no relationship could be ascertained between molecular relaxation times and the thermal chemical stability of the proteins. However, the fact that the temperature order in which mobility occurs correlates with the temperature order of denaturation-decomposition is a clear indication that molecular mobility is related to thermal stability. It has also been clearly observed that greater mobility occurs in proteins with larger number of amino acids. This has been attributed to the greater number of amino acids with side-chain rotational freedom present in protein molecules with higher molecular weight.

5.3.4 Comparison of Hydrated and Dehydrated Samples

The molecular relaxation processes observed in the hydrated and dehydrated proteins investigated are of the same origin. They result from localised rotational motions that exert no significant influence on the entropy of bulk sample. It is important to note that in the hydrated state, mobility is governed by the interaction of water molecules with the proteins.

As already discussed, these molecular motions occur in the temperature range of -150 to -20°C in the hydrated proteins, due to the plasticizing effect of water molecules. As such, these molecular motions are absent when the samples are dehydrated and analysed from -150 to 0°C. Furthermore, it has been established that water content, rather than increase in kinetic energy governs mobility in hydrated proteins (Jansson et al., 2011). However, the mobility in dehydrated sample can only be attributed to increase in kinetic energy.

When considering the relaxation times obtained at the T_{\max} of the discrete relaxation components observed in the hydrated (below 0°C) and dehydrated (above 0°C) protein

samples (Fig. 5.16), the rotational mobilities observed in the dehydrated samples exhibit longer relaxation times. The existence of the relatively slower rates of molecular mobility observed at higher temperatures in the dehydrated samples demonstrates the stabilizing effect of water/solvent removal from these macromolecules i.e. in the absence of water/solvents greater energy is required for molecular mobility, and when activated the rate of molecular motions are significantly slower.

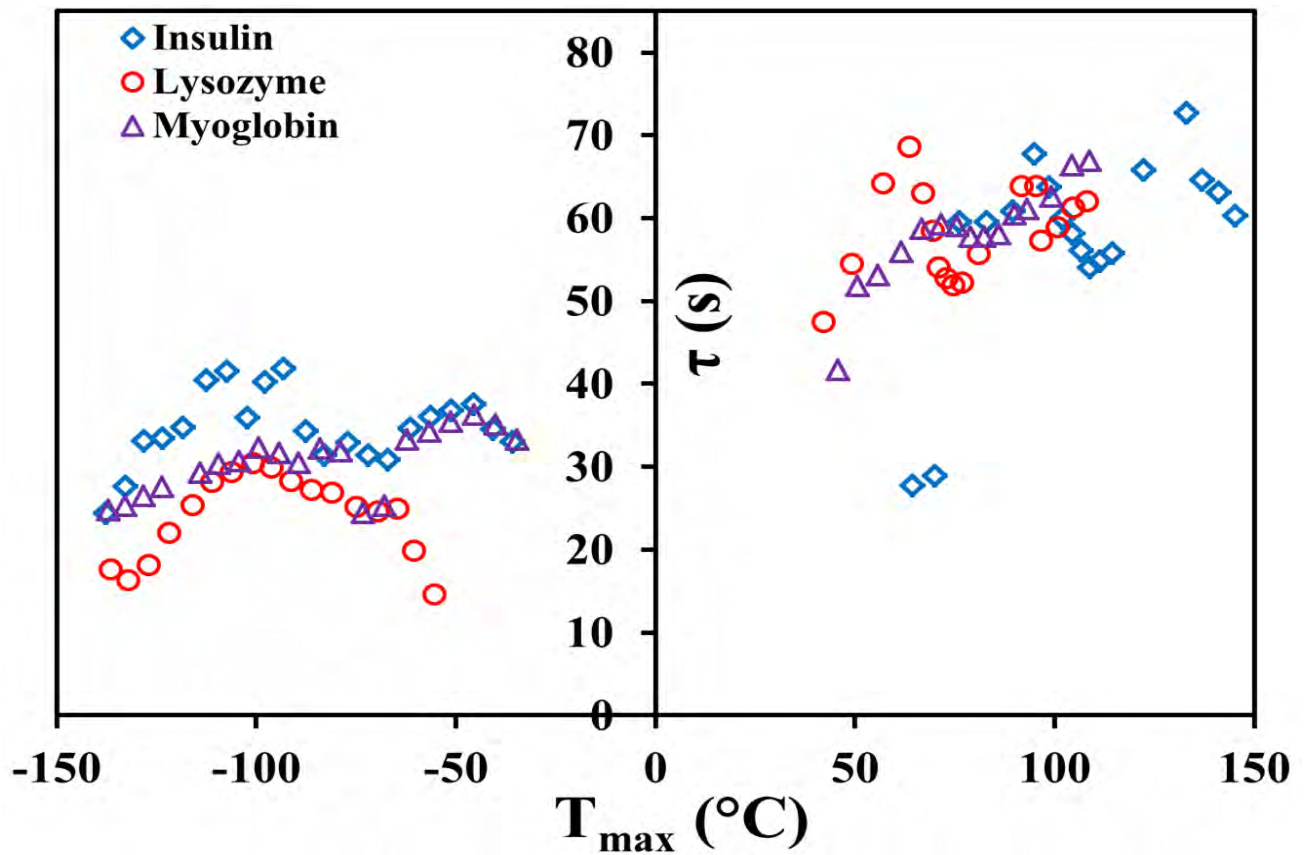


Fig. 5.15 Plots of relaxation times vs T_{max} for the discrete relaxation processes observed for hydrated (below $0^{\circ}C$) and dehydrated (above $0^{\circ}C$) protein samples.

5.4 Conclusions

Application of TSDCS has enabled the observation of localised rotational mobility in hydrated samples at temperatures well below 0°C and dehydrated samples above 0°C. The temperature locations of these processes in the hydrated proteins are -95 ± 3 , -102 ± 3 and $111 \pm 2^\circ\text{C}$ for insulin, lysozyme and myoglobin, respectively. Whilst the temperature location of the processes in the dehydrated protein samples are 96 ± 3 , 72 ± 4 and $82 \pm 3^\circ\text{C}$ for insulin, lysozyme and myoglobin, respectively.

The results presented have demonstrated that very low water content ($< 10\%$) in proteins can cause significant localised molecular mobility at temperature well below 0°C, with the potential of developing into larger scale cooperative motions when heated above -60°C . Therefore, the recommended storage conditions for the proteins investigated, may not be enough to prevent large scale molecular motions and therefore hinder protein deterioration. Hence storing these materials at $\geq -20^\circ\text{C}$ could still present significant stability problems in the solid-state. That said these low temperature molecular motions can be prevented by total dehydration of the proteins, since no significant mobility is observed for these proteins below 0°C after thermal dehydration. Molecular mobility only occurs when the protein samples are heated to temperatures above 25°C.

It is established that in the hydrated state, rotational mobility is governed by the rotational mobility or orientations of water molecules. However, in the absence of moisture mobility is governed by the gain in kinetic energy amongst other factors i.e. the solid form of the protein molecule and the nature of inter- and intra-molecular interactions.

Whilst no relationships were found between molecular mobility and the molecular weight of the proteins after dehydration, it was found that the temperature order in which molecular mobility occurs correlates with the temperature order at which denaturation-decomposition

processes occur. This provides evidence that molecular mobility is associated with thermal stability of proteins. It has also been demonstrated that in the presence of water, there exists a correlation ($R^2 = > 0.98$) between the temperatures at which mobility occurs and number of amino acids in the protein.

The study has, therefore, demonstrated that no relationship exists between molecular mobility and the molecular weight in the absence of water. However, it has demonstrated that mobility can be correlated with the thermal stability of the proteins studied.

Chapter 6 : Summary and General Conclusions

It is evident from the work presented that TSDCS is a powerful technique for the detection and characterisation of secondary relaxation processes in solid materials. The application of the technique to different subsets of solid materials i.e. crystalline (Chapter 3), semi-crystalline (Chapter 4) and amorphous (Chapter 5) solids, has provided valuable information on the characteristics of molecular motions in the different subsets of the solid-state. The studies presented have demonstrated that certain parameters, i.e. molecular relaxation times and the temperatures, associated with secondary relaxation processes can be related to the thermal stability of the materials investigated. It has been further demonstrated that positional isomerism and carbon chain length can influence molecular mobility in the solid state for molecules with molecular weights below 500 Da. However, no relationships could be observed for larger more complex molecules.

Chapter 3 reported the influence of positional isomerism on mobility and thermal stability of crystalline aminobutyric acids. These are interesting set of molecules because they exhibit very different functional roles in nature, even though they differ only by the position of the amine moiety relative to the carboxyl moiety. Positional isomerism of the butyric acids studied was found to influence molecular mobility and thermal stability. TSDCS was used to detect previously unreported relaxation processes at $109 \pm 1^\circ\text{C}$ for AABA, $104 \pm 1^\circ\text{C}$ for BABA and at $77 \pm 2^\circ\text{C}$ and $114 \pm 1^\circ\text{C}$ for GABA. It was also found that the greater the carbon atom distance between the amino and carboxyl groups the greater the molecular mobility, due to the increase in molecular backbone flexibility. The molecular relaxation frequency was found to correlate with the thermal stability, which is observed to be in the order; α -aminobutyric acid (AABA) > γ -aminobutyric acid (GABA) > β -aminobutyric acid (BABA). It was found that the lower the relaxation frequency, the greater the thermal stability, indicating that these relaxation processes bare the precursors of the thermal event.

This is further supported by the observation of a compensation point for AABA and BABA whose compensation temperature (T_c) are in the vicinity of the higher temperature thermal events.

Phospholipids are the chief components of cellular membranes, with phosphatidylcholines accounting for ~50% of membrane phospholipids. The experiments reported in Chapter 4 investigated the influence of carbon chain length on molecular mobility and thermal stability of a semi-crystalline homologous series of phosphatidylcholines. A broad transition (denoted the pre-transition process) was detected and characterised by DSC and TSDCS for the first time for DLPC, DMPC, DPPC and DSPC, prior to the characteristic chain melting transition temperature (T_m). The peak temperature, as revealed by DSC, of the pre-transition processes increases with increasing carbon chain length. TSDCS studies show these transitions to be cooperative in nature and originate from the segmental mobility of the acyl chains. Mobility of the saturated phosphatidylcholines is limited by the degree of hydrophobic interactions and the length of the hydrophobic acyl chains. The molecular relaxation time of this pre-transition process increases with increasing carbon chain length. This order in relaxation time correlates with the order of the T_m i.e. DSPC > DPPC > DMPC > DLPC, and it is therefore concluded that the pre-transition is a precursor of the chain melting transition, in which the material enters into the liquid crystalline phase. This study has demonstrated, as in Chapter 3, that molecular mobility can be related to thermal stability i.e. the slower the molecular relaxation time, the greater the thermal stability of the phospholipids.

An attempt was made to understand the relationship between molecular mobility and thermal stability of larger more complex molecules in the work reported in Chapter 5. In this study three of the most widely studied proteins were investigated. These materials possess some of the most challenging stability issues in the solution state. As such they are usually lyophilized to improve storage stability. The lyophilized proteins examined were found to contain low

levels of moisture (<10%) using TGA. TSDCS results presented in this thesis demonstrated that very low water content in proteins can cause significant localised molecular mobility at temperature well below 0°C, with the potential of developing into larger scale cooperative motions when heated above -60°C. These molecular motions originate from the interaction between water molecules and protein amino acid side-chains. It was found that the greater the moisture content the greater the molecular mobility. When the samples were dehydrated, relaxation processes could only be observed at temperatures above 25°C. Whilst mobility is governed by movement of water molecules, molecular motion in the dehydrated proteins is governed by the gain in kinetic energy. No relationship could be found between molecular weight and mobility of the proteins; however a correlation does exist between the temperature order in which molecular mobility occurs with the temperature order at which denaturation-decomposition processes occur.

Together, these studies have demonstrated that it is possible to relate molecular mobility to thermal stability. In all cases it was found that the temperature of the molecular relaxation maxima provides a good estimation of the thermal stability of the materials studied. In general the lower the temperature of molecular relaxation the less stable the material.

Chapter 7 : Future Work

- **Detection and characterisation of secondary relaxations in empty and drug loaded lyophilized liposomes** - Liposomes have the ability to encapsulate hydrophilic and hydrophobic drugs in their aqueous core and in the membrane layers respectively. This improves solubility of poorly soluble drugs, protect labile drugs from the harsh environment of the body and can also be modified to target release of the drug molecules at specific sites. However, these liposomal delivery systems are plagued by poor stability even in the solid-state (Chang and Yeh, 2012). Currently the most effective methods employed to study and understand stabilization mechanism of lyophilized liposomes is the use of DSC. The aim of this investigation will be to apply TSDC to characterise secondary relaxations in liposomes with varying drug loading concentrations. The application of TSDCS can offer greater advantages in understanding stability of liposome formulations in two ways:
 - It can probe low energy transitions (secondary relaxations) at low temperatures where the lamellar structure of the liposomes are not destroyed.
 - It can provide molecular relaxation times and kinetic parameters of these mobility states and therefore allow predictions of the ease with which drug molecules can leak from the liposomes.

The outcome of this investigation could result in the development of a new technique that allows the confirmation of successful drug loading of liposomes, which can greatly aid the optimisation of liposome formulations.

- **Correlation between molecular relaxation time with aggregation rate of lyophilised proteins at different storage humidity** – Development of protein therapeutics still remains a major challenge. These macromolecules are labile under

various conditions with temperature and humidity being the most important. Previous studies have attempted to correlate molecular mobility with stability of freeze-dried proteins at various storage conditions (Yoshioka et al., 2001, Yoshioka and Aso, 2005, Yoshioka et al., 2007). However, molecular mobility was investigated using DSC, which can only detect primary relaxation processes. The work would utilise TSDCS to characterise molecular relaxations at various storage conditions. The rate of protein aggregation and denaturation at the storage conditions would be assessed using HPLC, FTIR and circular dichroism (CD). The data acquired from such investigations could provide more detailed information that could contribute to current understanding of the relationship between molecular mobility and stability.

- **TDSC method development to understand influence of processing conditions on pharmaceutical solids** – The ability to identify subtle but significant differences in the influence of processing conditions on pharmaceutical materials are fundamental in process analytical technology. The ability of TSDCS to detect and characterise transitions that are inaccessible by other method makes it a good candidate to develop further for this purpose. For such a study TSDCS would be developed to detect different solid-state forms in a pharmaceutical API or product. The TSDCS method would also be developed as a semi-quantitative method to quantify the contents of amorphous and crystalline forms. The influence of tableting conditions on tablet hardness is also another area that could be investigated. Relating the results obtained from such investigations to physical and chemical characteristics could contribute to trouble shooting in manufacturing activities.

REFERENCES

- ABDUL-FATTAH, A. M., KALONIA, D. S. & PIKAL, M. J. 2007. The challenge of drying method selection for protein pharmaceuticals: Product quality implications. *Journal of Pharmaceutical Sciences*, 96, 1886-1916.
- AKTAS, M., WESSEL, M., HACKER, S., KLUSENER, S., GLEICHENHAGEN, J. & NARBERHAUS, F. 2010. Phosphatidylcholine biosynthesis and its significance in bacteria interacting with eukaryotic cells. *European Journal of Cell Biology*, 28, 888-894.
- ALIE, J., MENEGOTTO, J., CARDON, P., DUPLAA, H., CARON, A., LACABANNE, C. & BAUER, M. 2004. Dielectric study of the molecular mobility and the isothermal crystallization kinetics of an amorphous pharmaceutical drug substance. *Journal of Pharmaceutical Sciences*, 93, 218-233.
- ALKHAMIS, K. A., SALEM, M. S. & OBAIDAT, R. M. 2006. Comparison between dehydration and desolvation kinetics of fluconazole monohydrate and fluconazole ethylacetate solvate using three different methods. *Journal of Pharmaceutical Sciences*, 95, 859-870.
- ALVAREZ, C., CORREIA, N. T., RAMOS, J. J. M. & FERNANDES, A. C. 2000. Glass transition relaxation and fragility in a side-chain liquid crystalline polymer: a study by TSDC and DSC. *Polymer*, 41, 2907-2914.
- ALVES, N. M., MANO, J. F. & RIBELLES, J. L. 2002. Molecular mobility in polymers studied with thermally stimulated recovery.II. Study of the glass transition of semicrystalline PET and comparison with DSC and DMA results. *Polymer*, 43, 3627-3633.
- ALVES, N. M., RIBELLES, J. L. & MANO, J. F. 2005. Study of the molecular mobility in polymers with the thermally stimulated recovery technique - A review. *Journal of Macromolecular Science*, 45, 99-124.
- ANDRONIS, V. & ZOGRAFI, G. 1997. Molecular Mobility of Supercooled Amorphous Indomethacin, Determined by Dynamic Mechanical Analysis. *Pharmaceutical Research*, 14, 410-414.
- ANGELL, C. A. 1991. Relaxation in liquids, polymers and plastic crystals - strong/fragile patterns and problems. *Journal of Non-Crystalline Solids*, 131, 13-31.
- ATWOOD, J. L. & STEED, J. W. (eds.) 2004. *Encyclopedia of Supramolecular Chemistry*: Marcel Dekker.
- AUGER, M. 2000. Biological membrane structure by solid-state NMR. *Current Issues in Molecular Biology*, 2, 119-124.
- BAL, T. & MURTHY, P. N. 2012. Studies of drug-polymer interactions of simvastatin with various polymers. *International Journal of Pharmaceutical Science and Research*, 3, 561-563.
- BAR-ADON, R. & GILBOA, H. 1981. Molecular motions and phase transitions. NMR relaxation times studies of several lecithins. *Biophysical Journal*, 33, 419-434.
- BARBAS, R., PROBEN, R. & PULGJANER, C. 2007. A new polymorph of norfloxacin: Complete characterisation and relative stability of its trimorphic system. *Journal of Thermal Analysis and Calorimetry*, 89, 687-692.
- BARKER, S. & ANTONIJEVIC, M. D. 2011. Thermal analysis-Dielectric techniques. In: STOREY, R. A. & YMEN, I. (eds.) *Solid State Characterization of Pharmaceuticals*. United Kingdom: WILEY.
- BERNHARD, W., HOFFMANN, S., DOMBROWSKY, H., RAU, G. A., KAMLAGE, A., KAPPLER, M., HAITSMAN, J. J., FREIHORST, J., VON DER HARDT, H. &

- POETS, C. F. 2001. Phosphatidylcholine Molecular Species in Lung Surfactant: Composition in Relation to Respiratory Rate and Lung Development. *American Journal of Respiratory Cell and Molecular Biology*, 25, 725-731.
- BERNSTEN, P., SVANBERG, C. & SWENSON, J. 2011. Interplay between hydration water and headgroup dynamics in lipid bilayers. *Journal of Physical Chemistry. B*, 115, 1825-1832.
- BHATTACHARYA, S. & SURYANARAYANAN, R. 2009. Local mobility in amorphous pharmaceuticals—characterization and implications on stability. *Journal of Pharmaceutical Sciences*, 98, 2935-2953.
- BRAGA, C. I., REZENDE, M. C. & COSTA, M. L. 2011. Methodology for DSC calibration in high heating rates. *Journal of Aerospace Technology and Management*, 3, 179-192.
- BYRN, S. R., XU, W. & NEWMAN, A. W. 2001. Chemical reactivity in solid-state pharmaceuticals: formulation implications. *Advanced Drug Delivery Reviews*, 48, 115-136.
- CHANG, H. I. & YEH, M. K. 2012. Clinical development of liposome-based drug: formulation, characterisation, and therapeutic efficacy. *International Journal of Nanomedicine*, 7, 49-60.
- CHANG, L. & PIKAL, M. J. 2009. Mechanisms of protein stabilization in the solid state. *Journal of Pharmaceutical Sciences*, 98, 2886-2908.
- CHANG, L., SHEPHERD, D., SUN, J., OUELLETTE, D., GRANT, K. L., TANG, X. & PIKAL, M. J. 2005a. Mechanism of protein stabilization by sugars during freeze-drying and storage: Native structure preservation, specific interaction, and/or immobilization in a glassy matrix? *Journal of Pharmaceutical Sciences*, 94, 1427-1444.
- CHANG, L., SHEPHERD, D., SUN, J., TANG, X. & PIKAL, M. J. 2005b. Effect of sorbitol and residual moisture on the stability of lyophilized antibodies: Implications for the mechanism of protein stabilization in the solid state. *Journal of Pharmaceutical Sciences*, 94, 1445-1455.
- CHAPMAN, D. 1966. LIQUID CRYSTALS AND CELL MEMBRANES. *Annals of the New York Academy of Sciences*, 137, 745-754.
- CHAPMAN, D., BYRNE, P. & SHIPLY, G. G. 1966. The physical properties of phospholipids. I. Solid state and mesomorphic properties of some 2,3-diacyl-DL-phosphatidylethanolamines. *Proceedings of the Royal Society A*, 290, 115-142.
- CHAPMAN, D., WILLIAM, R. M. & LADBROOKE, B. D. 1967. Physical studies of phospholipids. VI. Thermotropic and lyotropic mesomorphism of some 1,2-diacyl-phosphatidylcholines (Lecithins). *Chemistry and Physics of Lipids*, 1, 445-475.
- CHAWLA, G. & BANSAL, A. 2009. Molecular mobility and physical stability of amorphous Irbesartan. *Scientian Pharmaceutica*, 77, 695-709.
- CHEN, W., STITHIT, S., ZHENG, J. Y. & HWANG, R. 2009. Specification Setting and Manufacturing Process Control for Solid Oral Drug Products. In: YIHONG, Q., YISHENG, C., GEOFF, G. Z. Z., LIRONG, L. & WILLIAM, R. P. (eds.) *Developing Solid Oral Dosage Forms*. San Diego: Academic Press.
- CHEN, X., LI, T., MORRIS, K. R. & BYRN, S. R. 2002. Crystal Packing and Chemical Reactivity of Two Polymorphs of Flufenamic Acid with Ammonia. *Molecular Crystals and Liquid Crystals*, 381, 121-131.
- CHIENG, N., RADES, T. & AALTONEN, J. 2011. An overview of recent studies on the analysis of pharmaceutical polymorphs. *Journal of Pharmaceutical and Biomedical Analysis*, 55, 618-644.
- CHUNG, M., MALATESTA, P., BOSQUESI, P., YAMASAKI, P., SANTOS, J. L. D. & VIZIOLI, E. 2012. Advances in Drug Design Based on the Amino Acid Approach:

- Taurine Analogues for the Treatment of CNS Diseases. *Pharmaceuticals*, 5, 1128-1146.
- CHUNG, S.-Y., MORIYAMA, T., UEZU, E., UEZU, K., HIRATA, R., YOHENA, N., MASUDA, Y., KOKUBU, Y. & YAMAMOTO, S. 1995. Administration of Phosphatidylcholine Increases Brain Acetylcholine Concentration and Improves Memory in Mice with Dementia. *The Journal of Nutrition*, 125, 1484-1489.
- CICERONE, M. T. & DOUGLAS, J. F. 2012. [small beta]-Relaxation governs protein stability in sugar-glass matrices. *Soft Matter*, 8, 2983-2991.
- CORREIA, N. T., ALVAREZ, C., RAMOS, J. J. M. & DESCAMPS, M. 2000. Molecular motions in molecular glasses as studied by thermally stimulated depolarization currents (TSDC). *Chemical Physics*, 252, 151-163.
- CORREIA, N. T. C., J.M. MOURA-RAMOS, J.J. 1997. Molecular motions in solid chloropentamethylbenzene: A thermally stimulated depolarisation current study. *Journal of the Chemical Society, Faraday Transaction*, 93, 157-163.
- COSTANTINO, H. R. 1995. *Stability of solid pharmaceutical proteins*. Doctor of Philosophy, Massachusetts Institute of Technology.
- CRAIG, D. Q. M. & READING, M. 2007. *Thermal Analysis of Pharmaceuticals*. United States of America: CRC Press, Taylor & Francis Group.
- CROWE, J. H., HOEKSTRA, F. A., NGUYEN, K. H. N. & CROWE, L. M. 1996. Is vitrification involved in depression of the phase transition temperature in dry phospholipids. *Biochimica et Biophysica Acta*, 1280, 187-196.
- CROWLEY, K. J. & ZOGRAFI, G. 2001. The use of thermal methods for predicting glass-former fragility. *Thermochimica Acta*, 380, 79-93.
- CUI, Y. 2007. A material science perspective of pharmaceutical solids. *International Journal of Pharmaceutics*, 339, 3-18.
- DARGENT, E., KATTAN, M., CABOT, C., LEDRU, J. & GRENET, J. 1999. Compensation Effect Observed in Thermally Stimulated Depolarization Currents Analysis of Polymers. *Journal of Applied Polymer Science*, 74.
- DIOGO, H. P. & RAMOS, J. J. 2008. Slow molecular mobility in the crystalline and amorphous solid states of glucose as studied by thermally stimulated depolarization currents (TSDC). *Carbohydrate Research*, 343, 2797-2803.
- DOSTER, W. 2010. The protein-solvent glass transition. *Biochimica et Biophysica Acta (BBA) - Proteins and Proteomics*, 1804, 3-14.
- DOSTER, W., CUSACK, S. & PETRY, W. 1989. Dynamical transition of myoglobin revealed by inelastic neutron scattering. *Nature*, 337, 754-756.
- DOSTER, W., CUSACK, S. & PETRY, W. 1990. Dynamic instability of liquidlike motions in globular proteins observed by inelastic neutron scattering. *Physical Review Letters*, 65, 1080-1083.
- DOXASTAKIS, M., SAKAI, V. G., OHTAKE, S., MARANAS, J. K. & PABLO, J. J. 2007. A molecular view of melting in anhydrous phospholipidic membranes. *Biophysical Journal*, 92, 147-161.
- DRANCA, I., BHATTACHARYA, S., VYAZOVKIN, S. & SURYANARAYANAN, R. 2009. Implications of Global and Local Mobility in Amorphous Sucrose and Trehalose as Determined by Differential Scanning Calorimetry. *Pharmaceutical Research*, 26, 1064-1072.
- DYRE, J. C. 1998. Source of non-Arrhenius average relaxation time in glass-forming liquids. *Journal of Non-Crystalline Solids*, 235, 142-149.
- EFFROS, R. M. 2011. Alpha aminobutyric acid, an alternative measure of hepatic injury in sepsis? *Translational Research : the Journal of Laboratory and Clinical Medicine*, 158, 326-327.

- EL-TAWEEL, S. H., HOHNE, G. W. H., MANSOUR, A. A., STOLL, B. & SELIGER, H. 2004. Glass transition and the rigid amorphous phase in semicrystalline blends of bacterial polyhydroxybutyrate (PHB) with low molecular mass atactic R,S-PHB-diol. *Polymer*, 45, 983-992.
- FITTER, J. 1999. The Temperature Dependence of Internal Molecular Motions in Hydrated and Dry α -Amylase: The Role of Hydration Water in the Dynamical Transition of Proteins. *Biophysical Journal*, 76, 1034-1042.
- FLORES-FERNANDEZ, G. M., PAPAN, M., ALMENAS, M., SOLA, R. J. & GRIEBENOW, K. 2010. Moisture-induced solid state instabilities in α -chymotrypsin and their reduction through chemical glycosylation. *BMC Biotechnology*, 10, 1-11.
- FRINGELI, U. P. 1981. A new crystalline phase of 1- α -dipalmitoyl phosphatidylcholine monohydrate. *Biophysical Journal*, 34, 173-187.
- GABBOTT, P. (ed.) 2008. *Principles and Applications of Thermal Analysis*: Blackwell Publish.
- GARDNER, C. R., WALSH, C. T. & ALMARSSON, O. 2004. Drug as materials: Valuing physical form in drug discovery. *Nature Reviews*, 3, 926-934.
- GBI 2011. Manufacturing of solid dosage forms-2011.
- GFELLER, D., MICHELIN, O. & ZOETE, V. 2012. SwissSidechain: a molecular and structural database of non-natural sidechains. *Nucleic Acids Research*.
- GREIN, C., BERNREITNER, K. & GAHLEITNER, M. 2004. Potential and Limits of Dynamic Mechanical Analysis as a Tool for Fracture Resistance Evaluation of Isotactic Polypropylenes and Their Polyolefin Blends. *Journal of Applied Polymer Science*, 93, 1854-1867.
- GRUNER, S. M. 2004. *Nonlamellar lipid phases*, USA, CRC Press LLC.
- HENZLER-WILDMAN, K. & KERN, D. 2007. Dynamic personalities of proteins. *Nature*, 450, 964-972.
- HIKIMA, T., HANAYA, M. & OGUNI, M. 1999. Microscopic observation of a peculiar crystallization in the glass transition region and β -process as potentially controlling the growth rate in triphenylethylene. *Journal of Molecular Structure*, 479, 245-250.
- HORNYKIEWICZ, O. 2010. A brief history of levodopa. *Journal of Neurology*, 257, 249-252.
- HULSE, W. L., FORBES, R. T., BONNER, M. C. & GETROST, M. 2009. Influence of protein on mannitol polymorphic form produced during co-spray drying. *International Journal of Pharmaceutics*, 382, 67-72.
- ICHIKAWA, T. & IITAKA, Y. 1968. The Crystal Structures of DL- α -Amino-n-butyric Acid. *Acta Crystallographica, Section B - Structural Crystallography and Crystal Chemistry*, 24, 1488.
- JAIN, D., CHANDRA, L. S. S., BHARADWAJ, S., ANWAR, S., GANESAN, V. & LALLA, N. P. 2010. Thermally stimulated depolarization current studies of relaxation in L-Asparagine monohydrate. *IEEE Transactions on Dielectrics and Electrical Insulation*, 17, 1128-1134.
- JANSSON, H., BERGMAN, R. & SWENSON, J. 2011. Role of solvents for the dynamics and glass transition of proteins. *The Journal of Physical Chemistry B*, 115, 4099-4109.
- JANSSON, H. & SWENSON, J. 2010. The protein glass transition as measured by dielectric spectroscopy and differential scanning calorimetry. *Biochimica et Biophysica Acta (BBA) - Proteins and Proteomics*, 1804, 20-26.

- JIMENEZ-RUIZ, M., GONZALEZ, M. A. & BERMEJO, F. J. 1999. Relaxation dynamics in the glassy, supercooled liquid and orientationally disordered crystal phases of polymeric molecular materials. *Physical Review B*, 59, 9155-9166.
- JOHARI, G. P. & GOLDSTEIN, M. 1970. Viscous Liquids and the Glass Transition. II. Secondary Relaxations in Glasses of Rigid Molecules. *The Journal of Chemical Physics*, 53, 2372-2388.
- KAMINSKA, E., KAMINSKA, K. & PALUCH, M. 2006. Primary and secondary relaxations in supercooled eugenol and isoeugenol at ambient and elevated pressure: Dependence on chemical microstructure. *The Journal of Chemical Physics*, 124, 1-10.
- KAMINSKI, K., KAMINSKA, E., ADRIANOWICZ, K., WOJNAROWSKA, Z., WLODARCZYK, P., GRZYBOWSKA, K., DULSKI, M., WRZALIK, R. & PALUCH, M. 2010. Observation of the dynamics of clusters in d-glucose with the use of dielectric spectroscopy. *Physical Chemistry Chemical Physics*, 12, 723-730.
- KAWAI, K., SUZUKI, T. & OGUNI, M. 2006. Low-temperature glass transitions of quenched cooled and annealed bovine serum albumin aqueous solutions. *Biophysical Journal*, 90.
- KEULEERS, R. R., JANSSENS, J. F. & DESSEYN, H. O. 2002. Comparison of some methods for activation energy determination of thermal decomposition reactions by thermogravimetry. *Thermochimica Acta*, 385, 127-142.
- KHAWAM, A. & FLANAGAN, D. R. 2006. Basics and applications of solid-state kinetics: A pharmaceutical perspective. *Journal of Pharmaceutical Sciences*, 95, 472-498.
- KIDD, P. M. 1996. Phosphatidylcholine: A superior protectant against liver damage. *Alternative Medicine Review*, 1, 258-274.
- KOYNOVA, R. & CAFFREY, M. 1998. Phases and phase transitions of the phosphatidylcholines. *Biochimica et Biophysica Acta*, 1376, 91-145.
- KRIPOTOU, S., PISSIS, P., BERSHTEIN, V. A., SYSEL, P. & HOBZOVA, R. 2003. Dielectric studies of molecular mobility in hybrid polyimide-poly(dimethylsiloxane) networks. *Polymer*, 44, 2781-2791.
- LAI, M. C. & TOPP, E. M. 1999. Solid-state chemical stability of proteins and peptides. *Journal of Pharmaceutical Sciences*, 88, 489-500.
- LEEKUMJORN, S. & SUM, A. K. 2007. Molecular studies of the gel to liquid-crystalline phase transition for fully hydrated DPPC and DPPE bilayers. *Biochimica et Biophysica Acta*, 1768, 354-365.
- LU, S.-F., CHEN, M., SHIH, Y.-C. & CHEN, C. H. 2010. Nonisothermal crystallization kinetics of biodegradable poly(butylene succinate-co-propylene succinate)s. *Journal of Polymer Science Part B: Polymer Physics*, 48, 1299-1308.
- LUCAS, T. I., BISHARA, R. H. & SEEVERS, R. H. 2004. A stability program for the distribution of drug products. *Pharmaceutical Technology*. www.pharmtech.com: ADVANSTAR COMMUNICATIONS.
- LUTHRA, S. A., PIKAL, M. J. & UTZ, M. 2008. Solid state ¹³C NMR investigation of impact of annealing in lyophilized glasses. *Journal of Pharmaceutical Sciences*, 97, 4336-4346.
- MARGULIES, M. M., SIXOU, B., DAVID, L., VIGIER, G., DOLMAZON, R. & ALBRAND, M. 2000. Molecular mobility of sorbitol and maltitol: A ¹³C NMR and molecular dynamics approach. *The European Physical Journal E*, 3, 55-62.
- MARSH, D. 1991. General features of phospholipid phase transitions. *Chemistry and Physics of Lipids*, 57, 109-120.
- MASUDA, K., TABATA, Y., HAYASE, T., YONEMOCHI, E. & TERADA, K. 2005. Comparison of Molecular Mobility in the Glassy state Between Amorphous

- Indomethacin and Salicin Based on Spin-Lattice Relaxation Times. *Pharmaceutical Research*, 22, 797-805.
- MATHESON, A. J., GOLDSTEIN, M., WILLIAMS, G., JOHARI, G. P., WATTS, R. O., WHALLEY, E., ALLEN, G. & WHITE, J. W. 1972. General discussion. *Faraday Symposia of the Chemical Society*, 6, 42-47.
- MIURA, H., KANEBAKO, M., NAKAO, H., INAGI, T. & TERADA, K. 2011. 2-benzyl-5-(4-chlorophenyl)-6-[4-(methylthio)phenyl]-2H-pyridazin-3-one, in silica mesopores and measurement of its molecular mobility by solid-state ¹³C NMR spectroscopy. *International Journal of Pharmaceutics*, 410, 61-67.
- MOHAMMED, A. R., COOMBES, A. G. A. & PERRIE, Y. 2007. Amino acids as cryoprotectants for liposomal drug delivery systems. *European Journal of Pharmaceutical Science*, 30, 406-413.
- MORISSETTE, S. L., ALMARSSON, O., PETERSON, M. L., REMENAR, J. F., READ, M. J., LEMMO, A. V., ELLIS, S., CIMA, M. J. & GARDNER, C. R. 2004. High-throughput crystallization: Polymorphs, salts, co-crystals and solvates of pharmaceutical solids. *Advanced Drug Delivery Reviews*, 56, 275-300.
- NEAGU, E. R. & NEAGU, R. 2003. Comments on the compenstaion effect observed in thermally stimulated depolarization current analysis. *Thermochimica Acta*, 395.
- NEAGU, R. M. & NEAGU, E. R. 2006. The distribution of the relaxation times and the thermally stimulated depolarization currents *Journal of Optoelectronics and Advanced Materials*, 8, 949-955.
- NGAI, K. L. 2003. An extended coupling model description of the evolution of dynamics with time in supercooled liquids and ionic conductors. *Journal of Physics: Condensed Matter*, 15, S1107.
- OCHIAI, Y., WATANABE, Y., OZAWA, H. & IKEGAMI, S. 2010. Thermal denaturation profile of Tuna myoglobin. *Bioscience, Biotechnology and Biochemistry*, 74, 1673-1679.
- OLIYAI, C., PATEL, J. P., CARR, L. & BORCHARDT, R. T. 1994. Chemical Pathways of Peptide Degradation. VII. Solid State Chemical Instability of an Aspartyl Residue in a Model Hexapeptide. *Pharmaceutical Research*, 11, 901-908.
- OTVOS, L. 2008. Peptide-Based Drug Design: Here and Now.
- OWENS, D. F. & KRIEGSTEIN, A. R. 2002. Is there more to gaba than synaptic inhibition? *Nature Review Neuroscience*, 3, 715-727.
- PANAGOPOULOU, A., KYRITSIS, A., SERRA, S., RIBELLES, J. L. G., SHINYASHIKI, N. & PISSIS, P. 2011. Glass transition and dynamics in BSA-water mixtures over a wide range of composition studied by thermal and dielectric techniques. *Biochimica and Biophysica Acta-Proteins and Proteomics*, 1814, 1984-1996.
- PARAK, F. G., ACHTERHOLD, K., CROCI, S. & SCHMIDT, M. 2007. A Physical Picture of Protein Dynamics and Conformational Changes. *Journal of Biological Physics*, 33, 371-387.
- PARK, D. H., MIRABELLA, R., BRONSTEIN, P. A., PRESTON, G. M., HARING, M. A., LIM, C. K., COLLMER, A. & SCHUURINK, R. C. 2010. Mutations in γ -aminobutyric acid (GABA) transaminase genes in plants or *Pseudomonas syringae* reduce bacterial virulence. *The Plant Journal*, 64, 318-330.
- PARKINS, D. A. & LASHMAR, U. T. 2000. The formulation of biopharmaceutical products. *Pharmaceutical Science & Technology Today*, 3, 129-137.
- PIKAL, M. J. & RIGSBEE, D. R. 1997. The Stability of Insulin in Crystalline and Amorphous Solids: Observation of Greater Stability for the Amorphous Form. *Pharmaceutical Research*, 14, 1379-1387.

- PINHEIRO, A. & MANO, J. F. 2009. Study of the glass transition on viscous-forming and powder materials using dynamic mechanical analysis. *Polymer Testing*, 28, 89-95.
- PINTO, S. S., DIOGO, H. P., NUNES, T. G. & MOURA RAMOS, J. J. 2010. Molecular mobility studies on the amorphous state of disaccharides. I--thermally stimulated currents and differential scanning calorimetry. *Carbohydrate Research*, 345, 1802-1807.
- POPOVA, A. V. & HINCHA, D. K. 2003. Intermolecular interactions in dry and rehydrated pure and mixed bilayers of phosphatidylcholine and digalactosyldiacylglycerol: A fourier transform infrared study. *Biophysical Journal*, 85, 1682-1690.
- POPOVA, A. V. & HINCHA, D. K. 2007. Effect of cholesterol on dry bilayers: Interactions between phosphatidylcholine unsaturation and glycolipid or free sugar. *Biophysical Journal*, 93, 1204-1214.
- POPOVA, A. V. & HINCHA, D. K. 2011. Thermotropic phase behavior and headgroup interactions of the nonbilayer lipids phosphatidylethanolamine and monogalactosyldiacylglycerol in the dry state. *BMC Biophysics*, 4 :11.
- QIU, Y., CHEN, Y. & ZHANG, G. G. Z. (eds.) 2009. *Developing Oral Dosage forms*, United States of America: Academic Press.
- QUI, Z., KOMURA, T. & NISHI, T. 2003. DSC and TMDSC study of melting behaviour of poly(butylene succinate) and poly(ethylene succinate). *Polymer*, 44, 7781-7785.
- RAMOS, J. J. M., CORREIA, N. T. & DIOGO, H. P. 2004. Vitrification, nucleation and crystallization in phenyl-2-hydroxybenzoate (salol) studied by Differential Scanning Calorimetry (DSC) and Thermally Stimulated Depolarisation Currents (TSDC). *Physical Chemistry Chemical Physics*, 6, 793-798.
- RAMOS, J. J. M. & MANO, J. F. 1997. Some comments on the significance of the compensation effect observed in thermally stimulated current experiments. *Polymer*, 38, 1081-1089.
- RASMUSSEN, B. F., STOCK, A. M., RINGE, D. & PETSKO, G. A. 1992. Crystalline ribonuclease A loses function below the dynamical transition at 220 K. *Nature*, 357, 423-424.
- RENGARAJAN, G. T., ENKE, D. & BEINER, M. 2007. Crystallization behavior of acetaminophen in nanopores. *The Open Physical Chemistry Journal*, 1, 18-24.
- REYES-LABARTA, J. A., OLAYA, M. M. & MARCILLA, A. 2006. DSC and TGA study of the transitions involved in the thermal treatment of binary mixtures of PE and EVA copolymer with a crosslinking agent. *Polymer*, 47, 8194-8202.
- ROBERTS, M. R. 2007. Does GABA Act as a Signal in Plants? Hints from Molecular Studies. *Plant Signal Behavior*, 2, 408-582.
- ROEDER, J., OLIVEIRA, R. V. B., BECKER, D., GONÇALVES, M. W., SOLDI, V. & PIRES, A. T. N. 2005. Compatibility effect on the thermal degradation behaviour of polypropylene blends with polyamide 6, ethylene propylene diene copolymer and polyurethane. *Polymer Degradation and Stability*, 90, 481-487.
- RUPLEY, J. A. & CARERI, G. 1991. Protein hydration and function. *Advances in Protein Chemistry*, 41, 37-172.
- RUS, L. M., TOMUTA, I., IUGA, C., KACSO, I., BORODI, G., BRATU, I. & BOJITA, M. 2012. Compatibility studies of indapamide/pharmaceutical excipients used in tablet preformulation. *FARMACIA*, 6, 92-101.
- SAFFELL, J. R., MATTHIESEN, A., MCINTYRE, R. & IBAR, J. P. 1991. Comparing thermal stimulated current (TSC) with other thermal analytical methods to characterise the amorphous phase of polymers. *Thermochimica Acta*, 192, 243-264.

- SAMOUILLAN, V., TINTAR, D. & LACABANNE, C. 2011. Hydrated Elastin: Dynamics of water and protein followed by dielectric spectroscopies. *Chemical Physics*, 385, 19-26.
- SAUER, B. B. & AVAKIAN, P. 1992. Cooperative relaxations in amorphous polymers studied by thermally stimulated current depolarization. *Polymer*, 33, 5128-5142.
- SAUER, B. B., AVAKIAN, P., FLEXMAN, E. A., KEATING, M., HSIAO, B. S. & VERMA, R. K. 1997. A.C. Dielectric and TSC Studies of constrained Amorphous Motions in Flexible Polymers Including Poly(OxyMethylene) and Miscible Blends. *Journal of Polymer Science: Part B*, 35, 2121-2132.
- SAUER, B. B., AVAKIAN, P. & STARKWEATHER, H. W. 1996. Cooperative Relaxations in Semicrystalline Fluoropolymers Studied by Thermally Stimulated Currents and ac Dielectric. *Journal of Polymer Science: Part B*, 34, 517-528.
- SAUER, B. B., AVAKIAN, P., STARKWEATHER, H. W. & HSIAO, B. S. 1990. Thermally Stimulated Current and Dielectric Studies of Poly(aryl ether ketone ketone). *Macromolecules*, 23, 5119-5126.
- SAUER, B. B., KAMPERT, W. G., BLANCHARD, E. N., THREEFOOT, S. A. & HSIAO, B. S. 2000. Temperature modulated DSC studies of melting and recrystallization in polymers exhibiting multiple endotherms. *Polymer*, 41, 1099-1108.
- SAUER, B. B., KAMPERT, W. G. & MCLEAN, R. S. 2003. Thermal and morphological properties of main chain liquid crystalline polymers. *Polymer*, 44, 2721-2738.
- SCHICK, C. 2009. Differential scanning calorimetry (DSC) of semicrystalline polymers. *Analytical and Bioanalytical Chemistry*, 395, 1589-1611.
- SHALAEV, E. Y., SHALAEVA, M., BYRN, S. R. & ZOGRAFI, G. 1997. Effects of processing on the solid-state methyl transfer of tetraglycine methyl ester. *International Journal of Pharmaceutics*, 152, 75-88.
- SHIN, J. & KIM, B. 2009. Transaminase-catalysed asymmetric synthesis of L-2-aminobutyric acid from chiral reactants. *Biotechnol Lett*, 31, 1595-1599.
- SIEGRIST, J., OROBER, M. & BUCHENAUER, H. 2000. β -Aminobutyric-mediated enhancement of resistance in tobacco to tobacco mosaic virus depends on the accumulation of salicylic acid. *Physiological and Molecular Plant Pathology*, 56, 95-106.
- SMITH, G. D. & BEDROV, D. 2007. Relationship between the α - and β -relaxation processes in amorphous polymers: Insight from atomistic molecular dynamics simulations of 1,4-polybutadiene melts and blends. *Journal of Polymer Science Part B: Polymer Physics*, 45, 627-643.
- SOGA, T., BARAN, R., SUEMATSU, M., UENO, Y., IKEDA, S., SAKURAKAWA, T., KAKAZU, Y., ISHIKAWA, T., ROBERT, M., NISHIOKA, T. & TOMITA, M. 2006. Differential Metabolomics Reveals Ophthalmic Acid as an Oxidative Stress Biomarker Indicating Hepatic Glutathione Consumption. *Journal of Biological Chemistry*, 281, 16768-16776.
- STARK, B., PABST, G. & PRASSL, R. 2010. Long-term stability of sterically stabilized liposomes by freezing and freeze-drying: Effects of cryoprotectants on structure. *European Journal of Pharmaceutical Science*, 41, 546-555.
- STEWART, E., PLAYER, R. & WARNER, D. 1973. The crystal and molecular structure of β -aminobutyric acid determined at low temperature. *Acta Crystallographica, Section B - Structural Crystallography and Crystal Chemistry*, 29, 2038.
- STOREY, R. A. & YMAN, I. 2011. *Solid State Characterization of Pharmaceuticals*, Wiley.
- STRICKLEY, R. G. & ANDERSON, B. D. 1996. Solid-State Stability of Human Insulin I. Mechanism and the Effect of Water on the Kinetics of Degradation in Lyophiles from pH 2–5 Solutions. *Pharmaceutical Research*, 13, 1142-1153.

- TILTON, R. F., DEWAN, J. C. & PETSKO, G. A. 1992. Effects of temperature on protein structure and dynamics: x-ray crystallographic studies of the protein ribonuclease-A at nine different temperatures from 98 to 320K. *Biochemistry*, 31, 2469-2481.
- TRIPATHY, T. & DE, B. R. 2008. Making sense about dipole moments. *Journal of Physical Science*, 12, 155-172.
- TURNHOUT, J. 1975. *Thermally stimulated discharge of polymer electrets*, Netherland, Elsevier Scientific Publishing Company.
- ULRICH, A. S. 2002. Biophysical aspects of using liposomes as delivery vehicles. *Bioscience Reports*, 22, 129-150.
- VAMECQ, J., FEUTELAIS, Y., MAUROIS, P., SGHAIER, M., DICI, E., GERMAN-FATTAL, M., HERRENKNECHT, C., GRESSENS, P., CECHELLI, R., DEHOUCK, L., STABLES, J., PAGES, N., LEGENDRE, B. & BAC, P. 2009. Engineering a GABA endowed with pharmacological CNS activity when given by an extracerebral route. *Medicinal Chemistry Research*, 18, 255-267.
- VECCHIO, S., CAMPANELLA, L., NUCCILLI, A. & TOMASSETTI, M. 2008. Kinetic study of thermal breakdown of triglycerides contained in extra-virgin olive oil. *Journal of Thermal Analysis and Calorimetry*, 91, 51-56.
- VICIOSA, M. T., RAMOS, J. J. M. & DIOGO, H. P. 2010. Molecular dynamics of an epoxy resin studied by Thermally Stimulated Depolarisation Currents. *Journal of Non-Crystalline Solids*, 356, 2858-2864.
- VIPPAGUNTA, S. R., BRITTAIN, H. G. & GRANT, D. J. W. 2001. Crystalline solids. *Advanced Drug Delivery Reviews*, 48, 3-26.
- VOOGD, J. & DERISSEN, J. 1980. Structure of DL--amino-n-butyric acid (modification A): a reinvestigation. *Acta Crystallographica, Section B - Structural Crystallography and Crystal Chemistry*, 36, 3175.
- VYAZOVKIN, S., BURNHAM, A. K., CRIADO, J. M., PÉREZ-MAQUEDA, L. A., POPESCU, C. & SBIRRAZZUOLI, N. 2011. ICTAC Kinetics Committee recommendations for performing kinetic computations on thermal analysis data. *Thermochimica Acta*, 520, 1-19.
- VYAZOVKIN, S. & DRANCA, I. 2006. Probing Beta Relaxation in Pharmaceutically Relevant Glasses by Using DSC. *Pharmaceutical Research*, 23, 422-428.
- WANG, B. & TAN, F. 1997. DSC study of phase transition of anhydrous phospholipid DHPC and influence of water content. *Science in China B*, 40, 412-418.
- WANG, W. 2000. Lyophilization and development of solid protein pharmaceuticals. *International Journal of Pharmaceutics*, 203, 1-60.
- WATANABE, M., MAEMURA, K., KANBARA, K., TAMAYAMA, T. & HAYASAKI, H. 2002. GABA and GABA receptors in the central nervous system and other organs. In: KWANG, W. J. (ed.) *International Review of Cytology*. Academic Press.
- WU, R. R., KO, H. M., CHIANG, J. C. & WOO, E. M. 2002. Solid-state NMR studies on phase behaviour and motional mobility in binary blends of polystyrene and poly(cyclohexyl methacrylate). *Polymer*, 43, 171-176.
- WUNDERLICH, B. 1999. A classification of molecules, phases, and transitions as recognized by thermal analysis. *Thermochimica Acta*, 340-341, 37-52.
- YOSHIOKA, S. & ASO, Y. 2005. A Quantitative Assessment of the Significance of Molecular Mobility as a Determinant for the Stability of Lyophilized Insulin Formulations. *Pharmaceutical Research*, 22, 1358-1364.
- YOSHIOKA, S. & ASO, Y. 2007. Correlations between molecular mobility and chemical stability during storage of amorphous pharmaceuticals. *Journal of Pharmaceutical Sciences*, 96, 960-981.

- YOSHIOKA, S., ASO, Y. & KOJIMA, S. 2001. Usefulness of the Kohlrausch-Williams-Watts Stretched Exponential Function to Describe Protein Aggregation in Lyophilized Formulations and the Temperature Dependence Near the Glass Transition Temperature. *Pharmaceutical Research*, 18, 256-260.
- YOSHIOKA, S., MIYAZAKI, T., ASO, Y. & KAWANISHI, T. 2007. Significance of Local Mobility in Aggregation of β -Galactosidase Lyophilized with Trehalose, Sucrose or Stachyose. *Pharmaceutical Research*, 24, 1660-1667.
- YOU, Y. & LUDESCHER, R. 2010. The Effect of Molecular Size on Molecular Mobility in Amorphous Oligosaccharides. *Food Biophysics*, 5, 82-93.
- ZHANG, G. G. Z., LAW, D., SCHMITT, E. A. & QIU, Y. 2004. Phase transformation considerations during process development and manufacture of solid dosage forms. *Advanced Drug Delivery Reviews*, 56, 371-390.
- ZHAO, D., FROHMAN, M. A. & BLUSZTAJN, J. K. 2001. Generation of choline for acetylcholine synthesis by phospholipase D isoforms. *BMC Neuroscience*, 2:16.